PREPARATION OF NOVEL FUNCTIONAL POLYMERIC NANOPARTICLES AND VARIOUS APPLICATIONS

By

Elrika Harmzen-Pretorius

Dissertation presented for the degree of Doctor of Philosophy (PhD) in the Faculty Science at Stellenbosch University

at the

UNIVERSITEIT
iYUNIVESITHI
STELLENBOSCH
UNIVERSITY

University of Stellenbosch

Department of Chemistry and Polymer Science

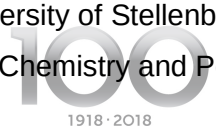

Promotor: Prof. Bert Klumperman

March 2018

DECLARATION

By submitting this thesis electronically, I declare the entirety of the work contained therein is my own, original work, that I am the owner of the copyright thereof (unless to the extent explicitly otherwise stated) and that I have not previously in its entirety or in part submitted it for obtaining any qualification.

Elrika Harmzen-Pretorius September 2017

ABSTRACT

Polymeric nanoparticles (PNPs) with accessible reactive and functional groups on the surface of the particles, commonly known as functional polymeric nanoparticles (FPNPs), provide additional physical and chemical characteristics for a wide range of fields, including biomedical, optical, electronic and environmental technologies. The main aim of this study was to investigate the synthesis of FPNPs and various applications using further modified FPNPs. A facile technique, *i.e*. surfactant-free dispersion polymerization, was used to prepare FPNPs, of controlled and tunable size and morphology, based on the highly-crosslinked terpolymer of styrene, maleic anhydride and divinylbenzene (poly(St-*co*-MAnh-*co*-DVB) also called MAnh-FPNPs). The particle size, varying from 70 nm to 1300 nm, and surface morphology, smooth to popcorn-shaped, were obtained by simply varying the experimental parameters, such as RAFT, monomer and crosslinker (DVB) concentrations, feed rate and reaction time. The highly reactive maleic anhydride and the pendant vinyl groups on the surface of the particles allow for easy modification if additional functionalization is needed for a specific application. The obtained FPNPs interestingly showed auto-fluorescent properties which allowed visualization using confocal fluorescence microscopy. Cytotoxicity assays and cellular uptake studies showed that these particles are benign to cells and are rapidly taken up in the cells.

The surface of these particles was modified with different functional groups including, *N*,*N*-dimethyl-3-aminopropyl-1-amine (DMAPA), boronic acid (BA) and a tetraphenylborate derivative respectively, producing DMAPA-FPNPs and BA-FPNPs respectively that were further used to fabricate Janus nanoparticles (JNPs) and permeable micro-sized capsules, as well as an adsorbent for the extraction of biomolecules. Inverse Pickering emulsions were utilized as template for (a) the synthesis of JNPs and (b) the formation of permeable capsules combined with the encapsulation of viable live bacteria. Rotating DMAPA-FPNPs captured at the interface of an inverse Pickering emulsion droplet, and Au-ions in the aqueous phase, allowed the complementary reaction between the tertiary amine on particles and Au-ions producing JNPs with tunable Au-covered surfaces. Correlative SEM imaging was used to confirm the synthesis of JNPs with varying fractions of surface areas modified through utilizing the rotation of the particles at the interface of the droplets. The BA-FPNPs were also used to synthesize permeable micro-capsules (MCs) via inverse Pickering emulsions, that were stabilized by boronic ester-FPNPs (BE-FPNPs), and the capsule wall fabricated through crosslinking individual FPNPs on the interface using a polydiol, starch, with capsule diameters between 20

μm and 100 μm. Successful fabrication of MCs was proven by LM and SEM analyses. The hollow hybrid starch-FPNP microcapsules (MC) were used to encapsulate constructed *Escherichia coli*. The *E. coli* strain allowed the release of amylase using an inducible GAL10 promotor to express AmyA amylase upon exposure to galactose. The degradation was visualized by confocal fluorescence microscopy (CFM).

Furthermore, the FPNPs were utilized in the extraction of biomolecules from dilute solutions after post-modification of the PNPs. The particle's surface was modified via two different routes, *i.e*. direct surface modification using the reactive maleic anhydride and chain extending from the surface of the particles, to obtain particles able to extract specific biomolecules.

One of the more intriguing and challenging aspects in current material science is the synthesis of functional and anisotropic particles, as theoretical work has shown that such particles could be very useful for controlling molecular recognition, self-assembly processes and various other applications.

OPSOMMING

Polimeriese nanopartikels (PNPs) met toeganklike reaktiewe en funksionele groepe op die oppervlakte van die partikel, algemeen bekend as funksionele polimeriese nanopartikels (FPNPs). Die FPNPs het addisionele fisiese en chemiese eienskappe wat aanwending in `n wye verskeidenheid van velde, insluitend dié van biomedisyne, optiese, elektroniese en omgewingstegnologie moontlik maak. Hierdie studie se hoofoogmerk is om ondersoek in te stel na die sintese van FPNPs en verskeie toepassingsmoontlikhede van verder gemodifiseerde FPNPs. Die FPNPs was voorberei by wyse van `n inskiklike tegniek i.e. benatter vrye verspreidings polimerisasie met n beheerde en manipuleerbare grootte en morfologie, gebaseer op die hoogs kruisverbinde terpolimeer of stireen, maleïensanhidried en diviniel benseen (poli (St-*co*-MAnh-*co*-DVB) ook MAnh-FPNPs).

Die partikels se grootte, wat wissel van 70nm tot 1300 nm, en oppervlak morfologie (glad tot springmielie-vormig) is verkry deur om die eksperimentele beperkings, onder andere die RAFT-, monomeer- and kruisverbinder_konsentrasies, te verander. Weens die hoogs reaktiewe maleïensanhidried en die vryhangende viniel_groepe aanwesig op die oppervlakte van die partikels, is dit maklik om veranderinge aan te bring indien addisionele funksionaliteit vereis word vir `n spesifieke aanwending. Die verkrygde FPNPs het interessant genoeg ook auto-fluoresseerende eienskappe getoon wat visualisering by wyse van konfokale fluoresseerende mikroskopie (KFM) moontlik maak. Sitotoksiese toetse en selulêre opname studies dui daarop dat hierdie partikels goedaardig vir die selle is en vinnig in die selle opgeneem word.

Die oppervlakte van die partikels was aangepas met verskeie funksionele groepe, naamlik *N*,*N*-dimetiel-3-aminopropiel-1-amien (DMAPA), boronsuur (BA) and n tetrafenielboraat afgeleide. Hierdie aangepaste DMAPA-FPNPs en BA-FPNPs was toe gebruik om Janus nanopartikels (JNPs), deurlaatbare mikro-grootte kapsules, sowel as `n funksionele partikel, vir die onttrekking van biomolekules, te vervaardig. Omgekeerde Pickering emulsies was aangewend as templaat vir (a) die sintese van JNPs en (b) die vorming van deurlaatbare mikrokapsules (MKs) gekombineer met die inkapsulering van lewendige bakterië.

Roterende DMAPA-FPNPs, vasgevang op die skeidingsvlak van `n omgekeerde Pickering emulsie druppel, en Au-ione in die waterige fase, het die komplementêre reaksie tussen die tersiêre amien op partikels en die Au-ione, wat JNPs met manipuleerbare Au-bedekte oppervlaktes produseer, moontlik gemaak. Korrelatiewe skandeer elektron mikroskoop (SEM) beelding was gebruik om die sintese van die JNPs met wisselende fraksies op die oppervlak

areas, gemodifiseer deur die aanwending van die rotering van die partikels op die skeidingsvlak van die druppels, vas te stel.

Die FPNPs was ook aangewend om deurlaatbare MKs via omgekeerde Pickering emulsies, wat gestabliseer was deur boron ester-FPNP's (BE-FPNPs), te sintetiseer. Die kapsule-wand was vervaardig deur `n kruisbinding van individuele FPNPs op die skeidingsvlak deur n polidiol, stysel, te gebruik. Kapsules met `n deursnee van tussen 20 µm en 100 µm was vervaardig. Lig mikroskopie en SEM analises was gebruik om suksesvolle vervaardiging van die MKs te bewys. Die hol hibriede stysel-FPNP MKs was gebruik om geneties gemodifiseerde *Escherichia coli* te enkapsuleer. Die tipe *E Coli* het die vrystelling van amilase moontlik gemaak deur die gebruik van `n induseerbare GAL10 promotor om die uitdrukking van *AmyA* amilase te verkry wanneer dit blootgestel word aan galaktose. Die afbreking was uitgebeeld by wyse van KFM.

Die FPNPs was verder ook aangewend in die onttrekking van biomolekules vanuit verdunde oplossings na die modifisering van die PNPs. Die oppervlakte van die partikels was aangepas by wyse van twee verskillende metodes, *i.e.* direkte oppervlak aanpassing deur reaktiewe maleïensanhidried en ketting verlenging van die oppervlakte van die partikels, om sodoende partikels te kry wat spesifieke biomolekules kan onttrek.

Een van die meer belangwekkende en uitdagende aspekte in die huidige materiële wetenskappe is die sintese van funksionele en anisotrope partikels aangesien teoretiese werk daarop dui dat hierdie partikels baie bruikbaar kan wees in onder andere die beheer van molekulêre herkenning, die selfvervaardigingsproses en verskeie ander aanwendings.

Die sintese en vervaardiging van FPNPs is `n voortudrende navorsingsveld wat ontelbare addisionele funksionaliteite kan bied en dien as intelligente instrumente in verskeie aanwendings.

DEDICATED TO

To my loving husband, parents and sister

ACKNOWLEDGEMENTS

I would like to take this time to say thank you to the people that made this research and PhD possible, but firstly, I would like to thank God for blessing me with the opportunity to study.

I would like to acknowledge and thank my promotor, Bert Klumperman, for all his invaluable guidance. Thanks for being the mentor you are and giving me the opportunity to work with you.

I would like to extend my gratitude to all my colleagues, mentors, assistants and friends from the Polymer Science and Chemistry department. A special thank you to the Free radical research group, each one of you, thank you for all the conversations, all the coffees, sometimes tears, sometime laughs and the many ways you aided me during my PhD studies, as well as for the friendships that we made. Without you guys this would not be possible.

I would further like to thank the people that formed part of collaborated work. Especially Prof Carine Smith and Johan Visser from Physiology as well as Prof Pieter Swart and Stefan Hayward from Biochemistry. Without you this would not have been possible.

I would like to say thanks to CAF for support, in particular to the EM unit, Madelaine Frazenburg and Angelique Laurie for all the hours in front of the SE microscopes. A special thank you to Lize Engelbrecht at Fluorescence; you were always there to help and think outside the box, never saying no to an idea. Elsa Malherbe, at the NMR unit, for all the spectra you ran for me, even if I needed a re-run, you would always do it with the biggest heart and smile.

I am eternally grateful for the funding I received from the NRF, NRF Chair Grants and Stellenbosch University.

On a more personal level, I deeply value and appreciate the support and encouragement I received from my family. To my beloved husband, Corné, I cannot thank you enough. You stood with me all the way, gave me all the support and love I needed to be able to do this, especially through the many late nights towards the end of my PhD. To my parents, Pieter and Elize, thanks for all the possibilities and privileges you allowed me. Thanks for the support through all the years, for making me believe all is possible if I work hard. To my sister, Nelmari, it is such a pleasure working with you in the lab, all the coffees and laughs. To all of you, thanks for always believing in me! Friends close to my heart that really made this journey possible, I would like to say a special thank you to Ingrid, Anna, Lehani, Welmarie, Judith, for all the insights, late night talks and even being silly in the lab. When things got tough, you made it easier. Without the help of Leanie, Lisa, Anna, Andy and Waled this would not be possible.

There are not enough thank yous to give to all of you.

TABLE OF CONTENT

LIST OF ACRONYMS

PNPs	Polymeric nanoparticles
FPNPs	Functional polymeric nanoparticles
MAnh-FPNPs	Styrene-co-maleic anhydride-co-divinylbenzene particles
Poly(St-*co*-MAnh-*co*-DVB)	Styrene maleic anhydride and divinylbenzene copolymer
SMA	Poly(St-*alt*-MAnh)
DVB	Divinylbenzene
MAnh	Maleic anhydride
St	Styrene
DMAPA	*N*,*N*-dimethyl-3-aminopropyl-1-amine
BA	Boronic acid
JNPs	Janus nanoparticles
SEM	Scanning electron microscopy
MCs	Micro-capsules
BA-FPNPs	Boronic acid-FPNPs
BE-FPNPs	Boronic ester-FPNPs
LM	Light microscopy
CFM	Confocal fluorescence microscopy
Poly(St-*co*-MAnh-*co*-DVB) FPNPs	Poly(styrene-*co*-maleic anhydride-*co*-divinylbenzene) functional nanoparticles
NPs	Nanoparticles
O/W	Oil-in-water
EPR	Enhanced permeability and retention
PEG	Poly(ethylene glycol)
PLGA	Poly(D,L-lactic acid-*co*-glycolic acid)
PLA	Poly(D,L-lactide)
PCL	Poly(Ɛ-caprolactone)
PDMAEMA	Poly (*N,N*-dimethylaminoethyl-methacrylate)
MLABe	Poly(benzyl malolactonate)
PAMAM	Polyamidoamine

PSMA or P(St-*co*-MAnh)	Poly (styrene-*alt*-maleic anhydride)
EDA	Ethylenediamine
MA	Methyl acrylate
Hept	Heptane
MEK	Methyl ethyl ketone
AIBN	2,2'-Azo-bis(isobutyronitrile)
BPT	Butane-1-phenylethyl trithiocarbonate
RAFT	Reversible addition−fragmentation chain-transfer
FEG-SEM	Field emission gun scanning electron microscope
ATR-FTIR	Fourier transform infrared spectroscopy
K_3PO_4	Potassium phosphate
CS_2	Carbon disulphide
DMF	*N*,*N*-Dimethylformamide
AF	Auto-fluorescence
HUVECs	Human umbilical vein endothelial cells
ACQ	Aggregation-caused quenching
AIE	Aggregation-induced emission
RIR	Restriction of intramolecular rotations
RT	Room temperature
PBS	Phosphate buffered saline
NMR	Nuclear magnetic resonance spectroscopy
ROI	Regions of interest
RMFIs	Relative mean fluorescent intensity
VAc	Vinyl acetate
PMAnh	MAnh homopolymer
THF	Tetrahydrofuran
MEFs	Mouse embryonic fibroblasts
PI3K	Phosphoinositide 3-kinase
GM-CSF	Granulocyte-macrophage colony-stimulating factor
θ	Three-phase contact angle
BA	3-Aminophenylboronic acid monohydrate
DMF	Dimethylformamide
DMAP	4-Dimethylaminopyridine
DCC	N,N'-Dicyclohexylcarbodiimide
YML	Yeast mediated ligation

PCR	Polymerase chain reaction
TB	Terrific Broth
DAPI	4',6-Diamidino-2-phenylindole
PI	Propidium iodide
Au^{3+}	Gold(III)ions
$AuCl_3$	Gold(iii)chloride
HCl	Hydrogen chloride
BSD	Backscatter detector
STEM	Scanning transmission electron microscope
Na-TPB	Sodium tetraphenylborate
TPBD	Tetraphenylborate derivative
NaH	Sodium hydride
Đ	Dispersity
FR	Free radical
TBVE	Lithium triphenyl (4-((2-(2-vinyloxy) ethoxy) ethoxy) methyl)-phenyl) borate
M_n	Number-average molecular weight

CHAPTER 1

General Introduction, Objectives and Outline

This chapter provides a general introduction to polymeric nanoparticles, the synthesis thereof and various possible applications. The main objectives for this study and the layout of the dissertation are explained.

1.1 Introduction

Nanotechnology is a multidisciplinary field, and it has become a bourgeoning research focus around the world, with widespread applications in various fields including bioengineering, biomedical diagnostics, molecular biology and therapeutics.[1–4] In the past few decades, polymeric nanoparticles have, in particular, attracted immense amounts of interest due to the availability of various types of polymers with tunable molecular weights and functionalities.[5–7] This provides the nanoparticles with endless properties leading to a wide range of applications, including electronics, conductivity, catalysis, pollution control, environmental technology, pharmaceuticals and drug delivery, among many other applications.[3,4,8–12] Each individual application is dependent on the unique polymer composition of the nanoparticles, and thus, on the properties inherent to these polymers. Furthermore, the mode of preparation of these nanoparticles plays a significant role in obtaining the desired properties. An additional advancement in nanotechnology research is the inclusion of additional functionality and reactivity through the incorporation, adsorption or covalent coupling of functional groups to the surface of the nanomaterial itself.[13–16] Previous studies have shown that many different compounds, including polymers, carbohydrates, peptides, proteins, nucleic acids, ligands, and small molecules can be attached to the nanoparticles' surfaces.[1,17–19]

PNPs with reactive groups accessible on the surface of the particles, called functional polymeric nanoparticles (FPNPs), possess additional physical and/or chemical characteristics different from the ones originally found on the surface of the particles. Researched functional nanoparticles are often inorganic or PNPs with large size dispersity.[11,12] Additionally, the particles need supplementary chemical treatment, with fabricating NPs limited to various fields.[20–22] However, with the increasing use of FPNPs in advanced fields, some parameters need optimization. Firstly, precise control of particle size and size distribution is needed, and secondly, the ability to reproducibly prepare the particles is also important.[1,7]

Synthesizing particles most often leads to spherical shapes with their surface functionalities arranged in an isotropic fashion.[27] A number of methods to produce FPNPs have been reported, however, the method is highly system and application specific.[25] Most of these methods require expensive equipment and complex post-processing to remove additional surfactants, and are produced in multiple step reactions.[3,6,14]

The applications of FPNPs are predominantly dominated by the chemical and/ or physical properties of the polymers that it is made of. An important physical property to control is the size and size distribution of the final particles. The modification of nanoparticles introduces a wide array of interesting properties, depending on the functionalization agent, that allow modified

nanoparticles to offer unique and system-specific opportunities in various fields. This dissertation focusses on a surfactant-free dispersion polymerization technique that allows fabrication of FPNPs in a controlled and tunable manner. These FPNPs are comprised of highly reactive groups, such as maleic anhydride and pendant vinyl groups, that allow further modification and introduction of additional functional groups, for various highly specific applications.

1.2 Objectives

The main objective of the study was to synthesize novel functional polymeric nanoparticles and obtain more insight into the parameters affecting the obtained particle size and morphology. Several different applications of the FPNPs are also explored. The objectives of this study can be summarized as follows:

1. To synthesize FPNPs via free radical and RAFT mediated polymerization methods.
2. To stabilize Pickering emulsions, to be used as a template, for polymer-based microcapsules synthesis, through the crosslinking the FPNPs at the interface.
3. To investigate the triggered degradation of the microcapsule wall by encapsulating viable micro-organisms.
4. Pickering emulsion droplets were also used as template to obtain novel polymer based functional Janus nanoparticles.
5. To decorate the surface of the FPNPs further using two different approaches. The first approach entails grafting a tetraphenylborate derivative onto the FPNP surface. The second approach focuses on surface modification with a boronic acid moiety. Both surface-decorated FPNPs are investigated for biomolecule extraction from dilute solutions.

1.3 Layout of this thesis

Chapter 2-8 of this thesis are written with the intention to convert them over the coming months into manuscripts that can be submitted for publication in peer-reviewed journals. This thesis is divided into the following chapters:

Chapter 1

The chapter provides a general introduction to the field of nanoparticles, in specific functional polymeric nanoparticles, the synthesis thereof and the objectives for this study.

Chapter 2

A review is provided regarding functional PNPs. After a general introduction into the topic, specific examples of FPNPs, their synthesis and applications will be discussed.

Chapter 3

Chapter 3 contains the results obtained for the synthesis of poly(styrene-*co*-maleic anhydride-*co*-divinylbenzene) nanoparticles (poly(St-*co*-MAnh-*co*-DVB) FPNPs also referred to as MAnh-FPNPs). The influence of various experimental parameters on particle size, size distribution and morphology are discussed.

Chapter 4

Chapter 4 investigate the auto-fluorescent properties of the poly(St-*co*-MAnh-*co*-DVB) FPNPs as well as a preliminary study on their uptake in mammalian cells.

Chapter 5

Chapter 5 contains results regarding the use of poly(St-*co*-MAnh-*co*-DVB) FPNPs and the further modification of these FPNPs for the stabilization of inverse Pickering emulsions. These water-in-oil emulsions will subsequently be used as a template for hybrid permeable polymer-based microcapsules.

Chapter 6

The microcapsules described in Chapter 5 are used to encapsulate live bacteria. The bacteria have genetically been modified to produce amylase upon exposure to a trigger. Due to time constrains the work that should lead to the triggered release of the bacteria from the microcapsules, is still in progress. We show in Chapter 6 that the capsule wall can be degraded, but possible release of the encapsulated material still needs to be explored.

Chapter 7

Chapter 7 contains results on the synthesis of polymer-based Janus nanoparticles (JNPs). The MAnh-FPNPs were modified to be used for stabilizing inverse Pickering emulsions that are used to synthesize the JNPs, where the rotation of the particles at the interface leads to tunable fractions of the particles being surface modified.

Chapter 8

Chapter 8 describes the decoration of the particle surface for the extraction of specific biomolecules. For that purpose, two different modifications of the particle surface are explored.

Chapter 9

In Chapter 9, the overall conclusions of this study are summarized and recommendations are proposed for future work within this field of research.

1.4 References

(1) Nahar, M.; Dutta, T.; Murugesan, S.; Asthana, A.; Mishra, D.; Rajkumar, V.; Tare, M.; Saraf, S.; Functional Polymeric Nanoparticles: An Efficient and Promising Tool for Active Delivery of Bioactives. *Crit. Rev. Ther. Drug Carr. Syst.* **2006**, *23* (4), 259–318.

(2) Hanemann, T.; Szabo, D. V. Polymer-Nanoparticle Composites: From Synthesis to Modern Applications. *Materials*. **2010**, *3* (6), 3468-3517

(3) Nagavarma, B. V. N.; Yadav, H. K. S.; Ayaz, A.; Vasudha, L. S.; Shivakumar, H. G. Different Techniques for Preparation of Polymeric Nanoparticles - A Review. *Asian J Pharm Clin Res.* **2012**, *5* (3), 16–23.

(4) Vauthier, C.; Bouchemal, K. Methods for the Preparation and Manufacture of Polymeric Nanoparticles. *Pharm. Res.* **2009**, *26* (5), 1025–1058.

(5) Murcia, M. J.; Naumann, C. A. Biofunctionalization of Fluorescent Nanoparticles. In N*anotechnologies for the Life Sciences*, 1st Ed; Kumar, CSSR, Ed.; Wiley-VCH: Weinheim, Germany, **2005**, 1, 1–40.

(6) Rao, J. P.; Geckeler, K. E. Polymer Nanoparticles: Preparation Techniques and Size-Control Parameters. *Prog. Polym. Sci.* **2011**, *36* (7), 887–913.

(7) Abd Ellah, N. H.; Abouelmagd, S. A. Surface Functionalization of Polymeric Nanoparticles for Tumor Drug Delivery: Approaches and Challenges. *Expert Opin. Drug Deliv.* **2016**, *5247*, 1–14.

(8) Morris, J. Use of Silver-Coated Polymer Particles in Isotropic Conductive Adhesives for Electronic Applications. *In Isotropic conductive adhesives in electronics.* **2011**; 105–136.

(9) Tungittiplakorn, W.; Lion, L. W.; Cohen, C.; Kim, J. Engineered Polymeric Nanoparticles for Soil Remediation. *Environ. Sci Technol.* **2004**, *38*, 1605-1610.

(10) Twaites, B. R.; de las Heras, C.; Cunliffe, D.; Lavigne, M.; Pennadam, S.; Smith, J. R.; Górecki, D. C.; Alexander, C. Thermo and pH Responsive Polymers as Gene Delivery Vectors: Effect of Polymer Architecture on DNA Complexation in Vitro. *J. Control. Release.* **2004**, *97* (3), 551–5662.

(11) Liong, M.; Lu, J.; Kovochich, M.; Xia, T.; Ruehm, S. G.; Nel, A. E.; Tamanoi, F.; Zink, J. I. Multifunctional Inorganic Nanoparticles for Imaging, Targeting, and Drug Delivery. *ACS Nano*. **2008**, *2* (5), 889–896.

(12) Giner-Casares, J.; Malou Henriksen-Lacey, M. C.P. Inorganic Nanoparticles for Biomedicine: Where Materials Scientists Meet Medical Research. *Mater. Today.* **2015**, *19* (1), 1–10.

(13) Link, C.; Alexis, F.; Pridgen, E.; Molnar, L. K. Factors Affecting the Clearance and Biodistribution of Polymeric Nanoparticles. *Mol. Pharm*. **2015**, *5* (4), 505–515.

(14) Mout, R.; Moyano, D. F.; Rana, S.; Rotello, V. M. Surface Functionalization of Nanoparticles for Nanomedicine. *Chem. Soc. Rev.* **2012**, *41* (7), 2539.

(15) Engelhardt, N.; Ernst, A.; Kampmann, A.-L.; Weberskirch, R. Synthesis and Characterization of Surface Functional Polymer Nanoparticles by a Bottom-Up Approach from Tailor-Made Amphiphilic Block Copolymers. *Macromol. Chem. Phys.* **2013**, *214* (24), 2783–2791.

(16) de Folter, J. W. J.; van Ruijven, M. W. M.; Velikov, K. P. Oil-in-Water Pickering Emulsions Stabilized by Colloidal Particles from the Water-Insoluble Protein Zein. *Soft Matter.* **2012**, *8* (25), 6807–6815.

(17) He, J.; Chen, D.; Fan, X.; Wang, L.; Deng, J.; Yang, W. Reactive Poly(Divinylbenzene- Co -Maleic Anhydride) Nanoparticles: Preparation and Characterization. *Chinese Chem. Lett*. **2013**, *24*, 970–974.

(18) Shim, S. E.; Yang, S.; Choi, H. H.; Choe, S. Fully Crosslinked Poly(Styrene-Co-Divinylbenzene) Microspheres by Precipitation Polymerization. *J. Polym. Sci. Part A Polym. Chem*. **2003**, 835–845.

(19) Perro, A.; Reculusa, S.; Ravaine, S.; Bourgeat-Lami, E.; Duguet, E. Design and Synthesis of Janus Micro- and Nanoparticles. *J. Mater. Chem*. **2005**, *15* (35–36), 3745–3760.

(20) Dobiasch, S.; Szanyi, S.; Kjaev, A.; Werner, J.; Strauss, A.; Weis, C.; Grenacher, L.; Kapilov-Buchman, K.; Israel, L.-L.; Lellouche, J.-P.; Locatelli, E.; Franchini, M. C.; Vandooren, J.; Opdenakker, G.; Felix, K. Synthesis and Functionalization of Protease-Activated Nanoparticles with Tissue Plasminogen Activator Peptides as Targeting Moiety and Diagnostic Tool for Pancreatic Cancer. *J. Nanobiotechnology*. **2016**, *14* (81), 1-18.

(21) Shokeen, M.; Pressly, E. D.; Hagooly, A.; Zheleznyak, A.; Ramos, N.; Fiamengo, A. L.; Welch, M. J.; Hawker, C. J.; Anderson, C. J. Evaluation of Multivalent, Functional Polymeric Nanoparticles for Imaging Applications. *ACS Nano.* **2011**, *5* (2), 738–747.

(22) Yetter, R. A.; Risha, G. A.; Son, S. F. Metal Particle Combustion and Nanotechnology. *Proc. Combust. Inst.* **2009**, *32* (2), 1819–1838.

CHAPTER 2

Functional and reactive polymeric nanoparticles – A Review

This chapter gives an in-depth consideration of the functional polymeric nanoparticles currently available and the techniques to synthesize them.

Functional and reactive polymeric nanoparticles – A Review

Abstract

Polymeric nanoparticles represent smart, multi-functional tools and have become a focal point in modern materials science. The ability to tailor and impart additional functionality to these nanoparticles allows for the design of intelligent and multi-functional tools for use in a large variety of fields. The present review introduces different functional polymeric nanoparticle architectures and discusses drawbacks of the specific synthesis routes followed to obtain them. The functionality and potential applications of these nanoparticles are also discussed.

Introduction

Nanotechnology is a multi-disciplinary field that explores materials and devices with dimensions of less than 1000 nm. It has, in recent years, become a popular research area within fields such as bioengineering, biomedical diagnostics, molecular biology and therapeutics.[1–4] Most nanomaterials commonly exhibit at least one dimension below 100 nm in size, making them an ideal bridge between the bulk state and molecular or atomic structures, the relative scales of which are exemplified in Figure 1.

The physio-chemical properties of nanoparticles are directly dependent on the properties of their individual building blocks, and can generally be controlled by varying parameters in the synthesis technique (reaction time, temperature, solvent, surfactants and precursors), each of which has an impact on the final morphology and size of the material.[5,6] The correct properties

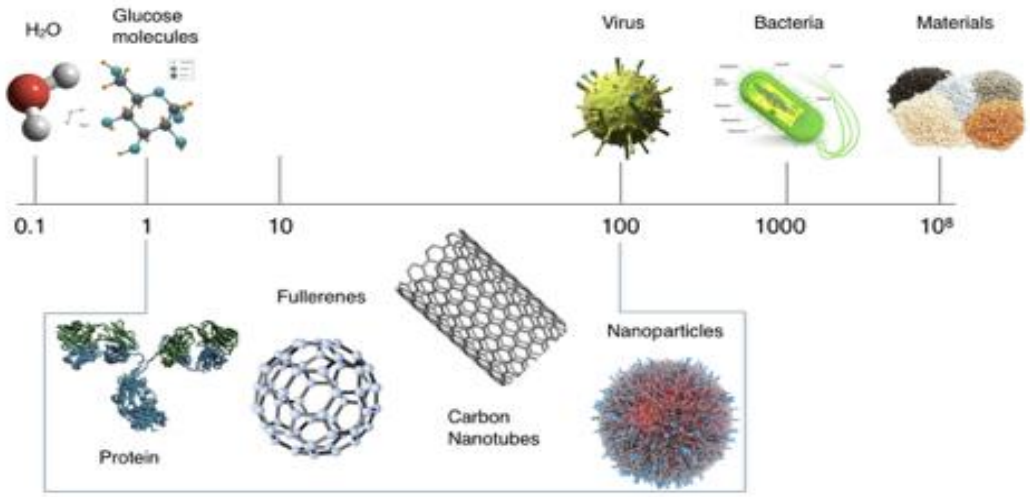

Figure 1: *Relative size of nanomaterials compared to molecules and bulk materials.*[152]

for a specific end-application can therefore be obtained by careful design and selection of individual building blocks.

Nanomaterials can be divided into several classes, *i.e.* incidental nanomaterials, naturally occurring nanomaterials and engineered materials. Naturally occurring nanomaterials include proteins, silk, viruses and the wax crystals covering a lotus leaf. Incidental nanomaterials are the by-products of materials produced by industrial and mechanical processes, such as polluting the air or starting a fire. In contrast, engineered nanomaterials are designed for specific applications and are purposefully synthesized by humans. An interesting example of the latter are nanostructured membranes designed to reduce air pollution by separating CO_2 from industrial plant exhaust streams, or those designed to store energy.[7,8] Another type of engineered nanomaterials are nanoparticles (NPs). NPs are actively used in various fields such as optoelectronics,[9] biomedical fields,[10,11] coatings[12] and solar energy[13].

NPs of inorganic nature include quantum dots,[14–19] ceramic and carbon NPs,[20–23] as well as metal-based NPs such as magnetic NPs,[24] gold,[25,26] silver,[27,28] and metal-oxide NPs.[29,30] While they have shown promising results within various applications, their inorganic or metallic nature has raised concerns within the medical field regarding their toxicity, immunogenicity, and slow excretion kinetics from the body.[31–33]

In the broad spectrum of nanoparticles, polymeric nanoparticles (PNPs) represent only a small part of the nanoparticle class, however, in the last few decades, they have attracted an immense amount of interest as demonstrated by the increasing number of associated publications.[3,34,35] PNPs are submicron-sized, colloidal, polymeric particles defined by their polymer composition consisting of either a homopolymer or a copolymer.[36] The advantages of PNPs include the ability to tune functional groups and design the polymer, the easier synthesis routes, and the potentially biodegradable properties. These properties have rendered PNPs appropriate for a wide range of applications and market-related needs, such as stealth characteristics[37], drug delivery[38–41], UV-protection[42] and special coatings[43] to only name a few.[3,4,]

Fabrication of polymeric nanoparticles

Advanced developments in polymer chemistry, physical chemistry and colloid and interface science allow for the synthesis of PNPs with endless potential characteristics.[4,44–47] The preparation methods of these nanoparticles play an important role in obtaining the desired properties. Traditionally, PNPs have been synthesized using emulsion polymerization, mini- and macro-emulsion polymerization, precipitation polymerization, dispersion polymerization, solvent

evaporation, interfacial polymerization, solvent displacement, spray drying and salting out.[3,34,35,48] Reviews detailing comprehensive information regarding the preparation techniques for these PNPs can be found.[3,49] Each individual application of PNPs is dependent on the unique polymer composition of the nanoparticle. The polymer composition, in turn, is dependent on the properties inherent to the polymer, which are strongly influenced by the polymerization technique.

The development of functional polymeric nanoparticles

A recent advancement in polymeric nanoparticle research is the development of functional polymeric nanoparticles (FPNPs) by introduction, adsorption, or covalent coupling of additional reactive functionalities which allow for interactions of other compounds on the surfaces of the PNPs (Figure 2).[50] Biomedical fields are taking advantage of the new developments within FPNPs. An example of this is derived from the original work of Ringsdorf,[51] where he aimed to design a polymer therapeutic with a drug covalently, yet reversibly, bound to the polymer backbone and upon a trigger, such as pH, temperature, reductive environment or the presence of enzymes, releases the attached drug. From this, the concept of FPNPs for drug delivery was born.

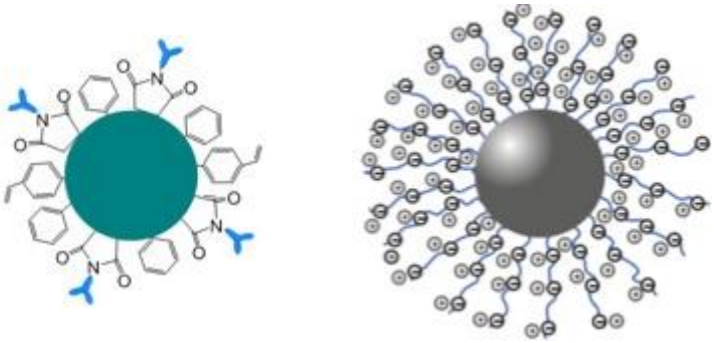

Figure 2: *Images of functional polymeric nanoparticles as seen in literature, for the extraction of biomolecules[52] and drug delivery[40].*

The basic concept of FPNPs is to have functional groups available on the surface of the PNP that are either already reactive, or that allow for the further modification of the reactive groups for the introduction of additional functionalities. FPNPs also possess excellent benefits due to the possibility of biocompatibility and/or biodegradability. Other benefits include the structural versatility,[53,54] which depends on the chosen polymer system, as well the possibility of designing and developing every aspect and functionality by introducing it from the start as a monomer or macromonomer.

Design and fabrication of functional polymeric nanoparticle

Multi-functional PNPs, that is, PNPs having additional functionality, were designed to hold multiple tasks at hand. Although FPNPs are mostly used for drug and gene delivery, the overall idea of FPNPs is to be able to introduced a functionality that is applicable to a specific field. The modification of PNPs introduces a wide array of interesting and system-specific properties. These properties greatly depend on the functionalization agent, and allow nanoparticles to become intelligent tools with multi-functional abilities.[1,47,55] The functionalities can be imparted onto the polymer backbone itself, or onto the surfaces of the PNPs. The surface functionalities can be attached during particle formation or post-particle formation, depending on the desired product and its intended applications.

Generally, there are four design approaches to the synthesis of FPNPs. The first approach is the synthesis of functional block copolymers, triblock copolymers or comb-like polymers (Figure 3A).[56,57] The second approach is through the physical modification of the surface of the particle in the form of an introduced functional surfactant or block copolymer during particle synthesis. These techniques involve the adsorption of the functional materials (e.g. polymer or surfactant) onto the particle surface through non-covalent interactions (Figure 3B).[36,58] The third approach includes chemical methods which involve the attachment of active materials via covalent bonds onto the particle surface (Figure 3C) or the grafting of monomers from the surface of the PNPs.

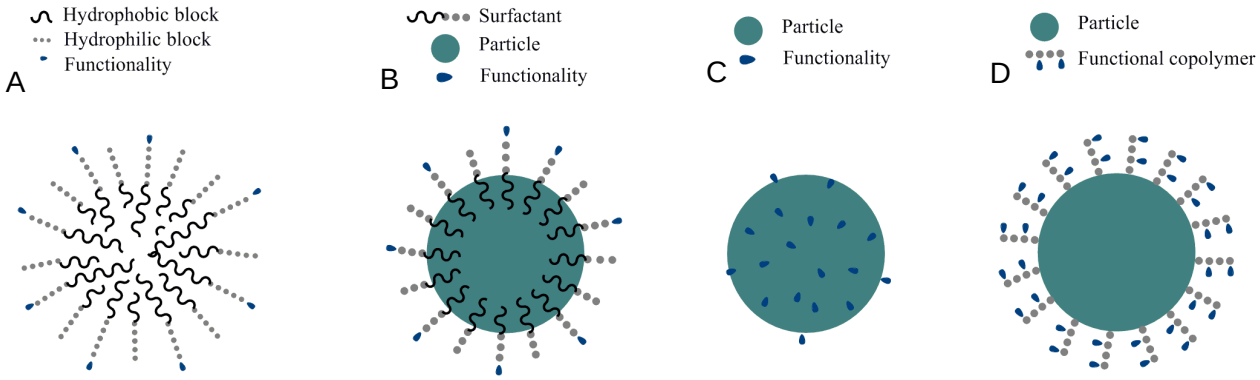

Figure 3: *Illustrations of the three general approaches of A) block copolymers, B) surfactant-based interactions on the particle surface, C) direct surface modification of particles, and D) surface grafting from the surface of particles.*

This results in surface grafted particles resembling a hairy surface layer (Figure 3D).[39,59]

The design of FPNPs is dependent on the requirements associated with a specific application, so, the FPNPs are either fabricated by the self-assembly of functional monomers or polymers,

or by the processing of prefabricated PNPs. These are comprised of the following components: (i) a core component that offers nanoparticle formation, and (ii) a functional group that is either covalently or non-covalently attached to the shell component. The different architectures of FPNPs (Figure 3) have led to only a few synthetic techniques to create FPNPs. A better understanding of the different designs will aid in clarifying these techniques.

Relating to the first design (Figure 3A), block copolymers are synthesized with required functionalities introduced at the polymer end groups. Block copolymers are polymeric chains consisting of two different polymeric segments that are connected at the junction point. In a selective solvent that dissolves only one block, block copolymers tend to self-assemble into various morphologies, including micelles and vesicles (usually in the nanometer range), among others. The advantage of block copolymers is that the functionality can be conjugated to one end of the chain, hence directing such functionalities either to the periphery or core of the micellar structure upon self-assembly. The techniques most frequently employed for the final fabrication of FPNPs are nanoprecipitation and emulsification techniques (Figure 4). Upon careful solvent evaporation or precipitation in the presence of another compound that is soluble in that solvent, the compound can potentially be encapsulated and the structure is locked into their shapes (*i.e.* particles in nanometer size range) producing FPNPs capable of encapsulating certain materials.[45] The use of tailor-made amphiphilic block copolymers that self-assemble in an appropriate solvent, forming micellar aggregates that, when triggered, crosslink the core, can also produce FPNPs. A wide range of methods with different mechanisms have been used to introduce a certain degree of crosslinking required to stabilize polymers of PNPs.

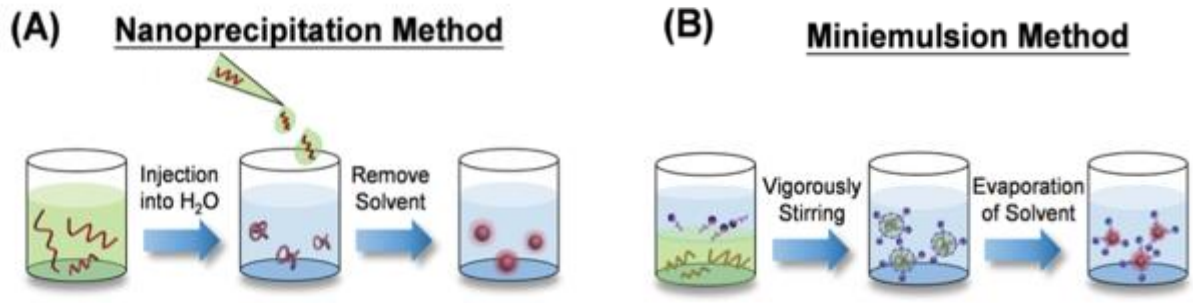

Figure 4: Schematic illustration of nanoprecipitation and mini-emulsion techniques for the synthesis of FPNPs.[153]

Such methods include UV-induced reactions[60–62], radical-based crosslinking (e.g. polymers containing double or triple bonds)[63,64], reversible disulfide-bridge formation[64]. Another method is the reaction of multifunctional polymers with a di- or trifunctional linker (e.g. isocyanate

containing polymers with diamines, click chemistry or Michael addition).[65–67] Although various examples of crosslinking exist, core-stabilized nanoparticles with orthogonal surface functional groups fabricated by the crosslinking of the core are still rare.

The second design entails reactive functional groups on the surface of PNPs introduced via surfactants or block copolymers acting as surfactant, with a desired functional group adhering to the surfactant/block copolymer (Figure 3B). These kinds of FPNPs are mostly fabricated using an oil-in-water (O/W) emulsion method,[39] with dispersed surfactants/block copolymers for the preparation of surfactant/block copolymer particles with the functional moiety physically absorbed onto the particle surface. For these non-covalent interactions, the homopolymer and surfactant must be chosen very carefully to ensure stable interactions with the functional component, otherwise they may readily detach from the PNPs.

The last two design approaches include the surface modification of pristine particles generally synthesized by traditional PNP techniques (section fabrication of PNPs). The surface modification can occur by the direct modification of a relevant reactive group on the surface of the PNP (Figure 3C) or by the addition of functionality on the surface of nanoparticles using functional monomers grafted onto the surface of PNPs, like hairy particles (Figure 3D). It is therefore important that the core particle used for this kind of approach has a well-controlled particle size. This is especially important in the field of drug delivery.

Recent advances in polymer nanoparticle research have led to the development of functional polymeric nanoparticle systems. Other than drug delivery, fields such as the biomedical, pharmaceutical, cosmetic, electronic and food industries have also benefited from their development.[3,5,35,55,68] Imperative to grasp is that the end-application wholly influences the polymer system design and architecture, and the functionality can either be introduced as a block copolymer or as a functional monomer or compound attached to the surface of the PNPs. Although some information regarding the preparation of specific FPNPs is available, it is widely scattered in literature and restricted to only a few applications. To the best of our knowledge, no review exists which considers the different synthetic techniques for FPNPs while considering the fundamentals of polymer architecture, particle size and morphology. Current advances in using functional polymeric nanoparticles for various applications in the biomedical field play a pivotal role, and are duly discussed.

Applications of polymeric nanoparticles

In the following sections, the four approaches, namely block copolymer, surfactant-based, direct surface modification, and surface grafting, are discussed. We will highlight the specific requirements of FPNPs to be used in selected applications.

Drug- and gene-delivery

Most FPNPs are used in drug delivery as these systems represent concurrent candidates for drug/ gene encapsulation and site-specific targeted delivery.[69,70] Traditionally, drugs were delivered through pills or injection among other methods, however, such methods have many drawbacks such as undesirable misdistribution of the drug and poor pharmacokinetics.[71,72] As a result, many approaches have been developed for more efficient systems.[34,72,73] FPNPs provide an attractive solution to overcome the limiting problems of either just drug encapsulation or delivery thereof. Stemming from recent development in nanotechnology that arose as a type of drug and/or gene delivery method, the field was revolutionized. Among the various nano-platforms designed to optimize drug and gene delivery, PNPs show potential mainly because of the versatility and the polymers allowing adjustments of the nano-carriers. Consequently, several different families of polymers have been developed.[58,74–76] However, one needs to keep in mind the role the FPNPs need to fill in drug/gene delivery as well as the different possible methods of fabricating FPNPs (polymer design), and it is therefore necessary to consider the basic design of how FPNPs are built up in conjunction with the various properties which they need to have for drug delivery.

In most cases the FPNPs contain a hydrophobic domain within the FPNPs core to provide surface areas for drug harboring and protection against changing environments. The therapeutic agent (drug/ gene) is dissolved, entrapped, encapsulated within the FPNP or adsorbed onto the FPNP surface, and the PNP itself needs to be non-toxic and biocompatible. Additionally, the PNP needs to have a stealth property to reduce immunogenicity, combined with a functionality to accumulate at specific sites through the incorporation of targeting moieties specific for a receptor or cell surface ligands.[77–79] PNPs decorated with PEG chains have shown to introduce a stealth property to the PNPs that decreases the amount of plasma proteins attaching to the surface of the PNPs and lower the uptake into phagocytes (Figure 5).[80,81] However, total protection against plasma protein adsorption was not obtained. It is expected that the nature of the particle core plays a main role in determining the type and amount of protein adsorbed.[80]

FPNPs utilized for biomedical fields not only carry or encapsulate drug/genes, but contribute to being a selective tool towards the area of delivery and release of the drug. The release mechanism is designed to deliver the drugs at the tumor sites as pathophysiological change occur that trigger drug release.[82–85]

FPNPs are excellent tumor-targeting tools because of the inherent properties of tumors. The enhanced permeability and retention (EPR) effect includes a way by which nanoparticles tend to accumulate in tumor tissue much more than they do in normal tissues due to fast growth, perforation and poor drainage of tumors.[86] PNPs with stealth properties avoid reticuloendothelial uptake and mononuclear phagocytosis, thus allowing longer circulation times of the NPs.[87–89] However, specific targeting seems to be more reliant on the selective adhering of the FPNPs to the surface of the target cell and then the internalization of the FPNP, followed by the release of the encapsulated drugs. The drug should be released in a controlled manner at specific sites to prevent nonspecific drug action on healthy cells and will also be discussed in specific examples later. The drug release can be triggered by either a passive or ligand-targeted mechanisms (Figure 5).[90]

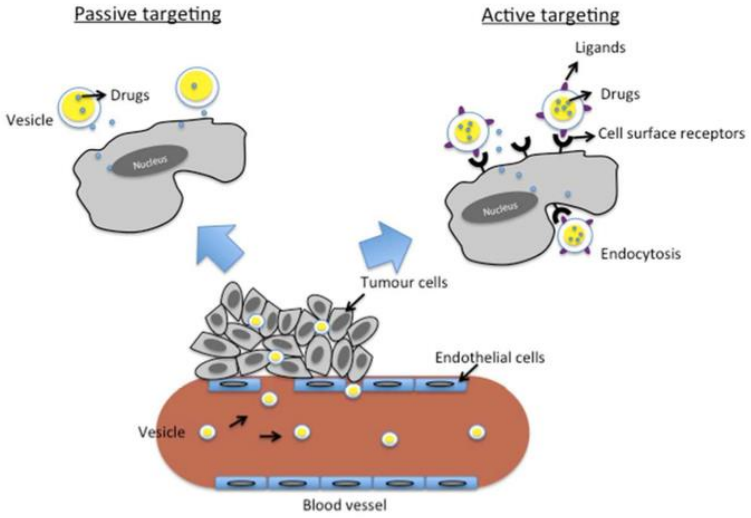

Figure 5: *Schematic presentation of passive vs. active targeting of FPNPs. (A) With passive targeting the PNPs extravasate through leaky vessels and preferentially accumulate through the EPR effect at the tumor cells. In passive targeting the drugs may be released in the extracellular matrix and get released via changes in pathophysiological environments. (B) With active targeting the FPNPs actively bind with receptors on target cells or tissue, resulting in specific cellular uptake through receptor-mediated endocytosis.*[105]

Passive targeting is where FPNPs accumulate in tumor tissue due to the EPR effect through leaky vessels that originate from membrane abnormalities and the lack of pericytes lining the

endothelial cells.[81,86,91] In the case of passive targeting, the drugs can potentially be released in the extracellular matrix and diffuse throughout the tissue, or the FPNPs can be taken up by the cells in a non-specific manner. The drug release can be trigged by changes in pathophysiological conditions, such as pH, ion (e.g. type and concentration) or temperature. For example, the pH of tumor cells were found to be lower than in normal cells, hence, the release mechanism is designed to deliver the drugs at the tumor sites as pH lowers that trigger the drug release.[82–85] Xiao *et al.*, studied the effect of surface charge and hydrophobicity on particle uptake, and found that cellular uptake is highly affected by the surface properties of the nanoparticles, and the drug is released at the affected sites (e.g. tumor) hence allowing high drug concentration. This may enhance the therapeutic efficacy and reduce drug side-effects.[92]

Ligand targeting is based on the conjugations of a ligand to the carrier (*e.g*. FPNPs) that binds with a specific receptor at targeted sites, which generally involves receptors that are overexpressed by tumor cells.[93–95] These ligands include proteins (transferrin)[96–101], nuclei acids (aptamers)[102] or others (peptides, vitamins or carbohydrates)[88,103,104]. Although the drug release of most of these FPNPs fall under the ligand targeting and release, very little is mentioned regarding the actual mechanism allowing the drugs to be released at the targeted site, and this topic deserves more attention. Despite the preferential accumulation of the FPNPs in tumor tissue by the EPR effect, the added functionality to the surface of the PNPs enhances tumor-specific localization of the FPNPs. In addition, it allows targeting of much smaller and earlier stage tumors.[81,105]

Research in targeted drug delivery is based on; firstly, the encapsulation of the drug using micelles that encapsulate the drug within the internal structure and then upon solvent removal FPNPs are fabricated, and secondly the targeting of the encapsulated drug to specific regions, making targeting and encapsulation within the same structure more advanced, thus resulting in more advanced synthesis.

Through using the concept of FPNPs and the synthesis technique appropriate for the application, the encapsulation of drugs or genes are possible through using a nanoprecipitation, emulsion polymerization or micellar formation technique. Combined with the modification of the original polymer to introduce a targeting ligand, for the ability to deliver these FPNPs to a site of interest, the synthesis becomes complex. We wish to show, with the examples that will follow, that the design of a FPNPs system for drug/gene delivery is based on a couple of polymers and synthetic techniques.

Block copolymers

The benefit of block copolymers is that the functionality can be conjugated to one of the chain ends, and in the presence of a drug, upon solvent evaporation, directing such functionalities to the outside of the micellar structure while encapsulating the drug.[45] One of the most widely employed hydrophilic segments is poly(ethylene glycol) (PEG). Hydrophobic segments include, poly(D,L-lactic acid-*co*-glycolic acid) (PLGA)[80,106,107], poly(D,L-lactide) (PLA)[80,108], poly(Ɛ-caprolactone) (PCL)[80], poly (*N,N*-dimethylaminoethyl-methacrylate) (PDMAEMA)[109] and poly(benzyl malolactonate) (MLABe)[41] used to fabricate PNPs.

A very well researched and used approached, is the biotin-avidin interaction for biological conjugation.[46,108,110]

Biotin binds to avidin with extremely high affinity and high rates. Using block copolymers, the functionalization of the free chain-end of the hydrophilic block with a biotin moiety (Figure 6A) allows the further modification using avidin (Figure 6B). Targeting ligands/ enzymes/ antibodies/ proteins can be conjugated to biotin to allow another biotin-avidin interaction onto the surface of particles (Figure 6C). In the section that follows (and Table 1) we show how various groups are employing this approach, varying the hydrophobic block, the encapsulated drug and the targeting ligand attached to biotin.

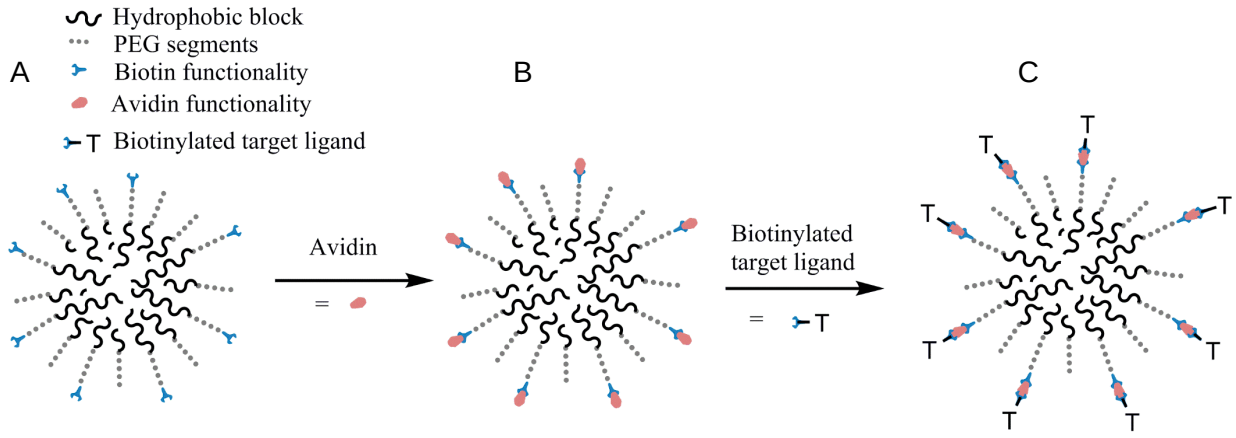

Figure 6: *Illustration of block copolymer system used regularly for drug delivery purposes. The functionality is introduced to the hydrophilic segment as biotin (A), an avidin-biotin interaction is utilized (B). The presence of avidin on the surface of the FPNPs allows the further functionalization of the FPNPs in various ways (C).*

For example, Gref *et al*. have fabricated biotin functionalized PNPs from amphiphilic copolymers through self-assembly.[110] Initially, the amphiphilic copolymer was synthesized using a 1,1'-carbonyldiimidazole (CDI) coupling reacting between diamino-PEG and biotin. The modification of the PEG chain was followed by the polymerization of PCL onto the PEG chain, initiated by the terminal amino group that resulted in a PCL-*b*-PEG-biotin amphiphilic copolymer. Following emulsification, self-assembly of block copolymers and solvent removal, FPNPs with an average particle size of 100 nm were obtained with biotin moieties on the hydrophilic segments orientating to the outside of the particle. Further addition of functionalization occurred via the introduction of an avidin moiety and a biotinylated targeting ligand. The targeting ligand, a biotinylated carbohydrate-recognizing lectin, wheat germ (WGA), was added to the avidin moieties that specifically recognizes carbohydrates located on various cell surfaces and was shown to increase cellular interactions and uptake 12-fold.

In a similar study, to show the versatility of the block copolymer approach, paclitaxel (PTX) were directly encapsulated within biotin-FPNPs.[108] These anticancer, drug-harboring FPNPs were produced through the micellar self-assembly of PCL-*b*-PEG-biotin block copolymer in the presence of the drug. Upon self-assembly into the micelles and subsequent solvent evaporation, nanoparticles with entrapped drug, and biotin moieties orientated on the outside on the FPNPs, were produced with diameters ranging from 88-118 nm. These biotin-FPNPs were incubated with cancer cells. Cancer cells over-express the biotin receptor, that resulted in high cytotoxicity for cancer cells compared to healthy cells.

In addition to the functionality being introduced via a biotin-avidin interaction, covalent attachment of the functionality to the block copolymer is also possible and shown in a study by Yao *et al*.[111] PLGA-*b*-PEG and PLGA-*b*-PEG-maleimide block copolymers were synthesized and an emulsion (O/W) produced using two immiscible solvents. During emulsification, the drug minocycline, used for epithelial cell-targeting leading to the treatment of chronic periodontitis, was encapsulated within the PLGA-*b*-PEG micellar structure, followed by solvent evaporation producing PNPs with the encapsulated drug, and PEG and maleimide-PEG to the outside of the particles (Figure 7A). The maleimide functionality on the surface of the PNPs allows conjugation to a thiol containing cyclic-RGD peptide via a thiol-maleimide click reaction (Figure 7B and Figure 7C). Particle size analysis showed particles to be 98 nm in size that increased to 106 nm after the conjugation to RGD peptide. Cellular uptake was increased 3-fold with the presence of the RGD peptide on the PNP surface and the drug was gradually released, and the effective drug concentration was maintained for 14 days.

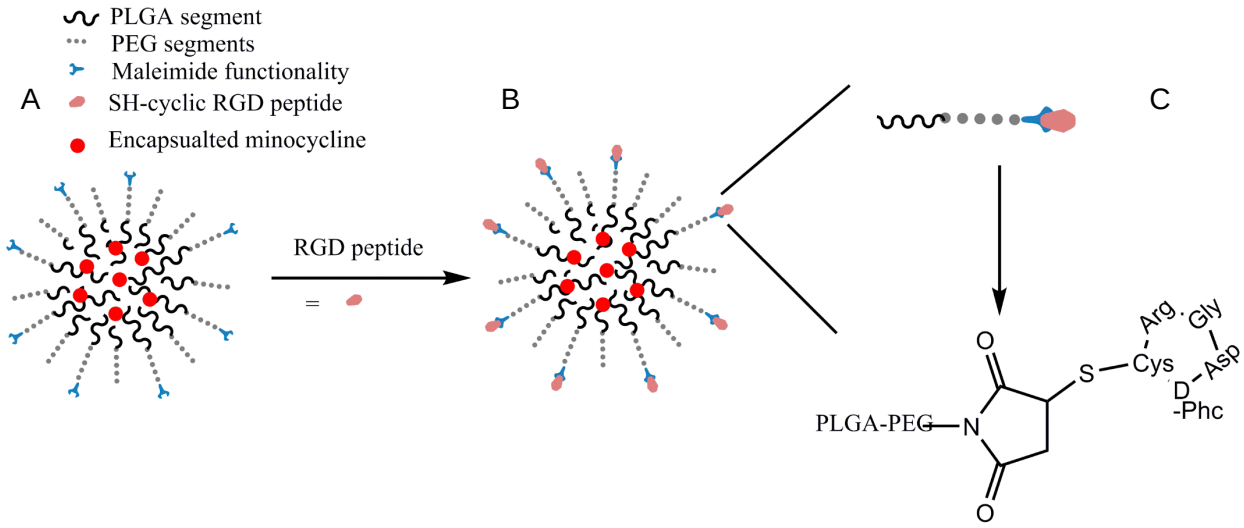

Figure 7: *Illustration of the block copolymer approach with the functionality added covalently. A) Maleimide functionalized-FPNPs habouring encapsulated drug. B) The maleimide moieties allows the introduction of RGD moieties via a thiol-maleimide click reaction. C) The conjugation between the maleimide functionality and the cyclic RGD peptide is shown. Structures are not drawn to scale.*

Hyaluronic acid (HA), a natural occurring anionic polysaccharide, is found in the extracellular constituents of connective tissues and has been extensively studied for biomedical and pharmaceutical applications. HA has been studied as a targeting ligand for drug delivery as various cancer cells overexpress the HA receptor CD44.[112,113] In the work of Han *et al*., HA and PCL were utilized as an amphiphilic block copolymer that was conjugated with 2-(pyridyldithio)-ethylamine (PDA) (Figure 8). The PDA can induce crosslinking in the presence of catalytic amounts of dithiothreitol (DTT) via bioreducible disulfide linkages. HA was reacted with propargylamine to obtain alkyne containing HA (alkyne-HA) and PDA was attached onto the α-alkyne-HA polymer backbone via an EDC coupling reaction (Figure 8, PDA is the red dot). The hydrophobic block, PCL, was synthesized via a ring opening polymerization and at the hydroxyl end, reacted with TosCl, and modified using sodium azide to yield an azide end group (PCL-N_3). A block copolymer was prepared by click chemistry between the alkyne and azide groups. Owing to its amphiphilic nature, the copolymer self-assembled into micelles in an aqueous solution. DOX was loaded into the FPNPs using an emulsification method. DOX was dissolved in chloroform, with equimolar trimethylamine. The solution was added to an aqueous solution of HA (PDA)-PCL block copolymers in the presence of DTT, leading to the formation of a O/W emulsion. Upon solvent evaporation drug-habouring HA-FPNPs were obtained with an average diameter of 200 nm. As a result of crosslinking, these FPNPs showed to be highly stable in aqueous solutions.

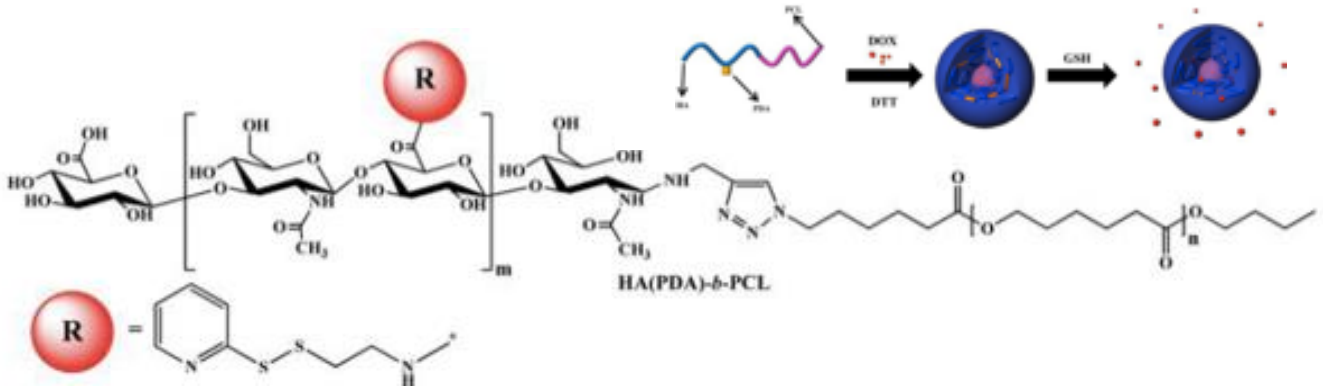

Figure 8: *Schematic illustration of the synthesized PDA-conjugated HA-b-PCL copolymer.*[113]

Drug release was facilitated in the presence of glutathione, a thiol-containing tripeptide capable of reducing disulfide bonds in the cytoplasm, mimicking the reductive intracellular environments under physiological conditions (pH 7.4). The DOX-loaded bio-reducible FPNPs greatly retarded the drug release, whereas the drug release rate was markedly enhanced in the presence of glutathione. These FPNPs showed to be highly effective tumor-targeting nanocarriers and had improved stability in the bloodstream and enhanced tumor-targeting. Although this method shows promising results, monomers need to be carefully selected, as thiols or protected thiols must be incorporated in the backbone of the block copolymer.

One major benefit of this method is that fine control over the amphiphilic block copolymers is possible, but the number or density of ligands has not been well discussed in the literature. Various polymer systems and functionality added to the block copolymer, based on this method of FPNP synthesis is referred to in Table 1. A main drawback of the block copolymer route is the fact that multiple steps are required, even though the idea is very straightforward. Targeting other sites, other ligands and ultimately different chemistries are required, which will need multiple wet-chemistry steps. Another phenomenon that was observed is that NPs coated with PEG created a “stealth” surface, that is good for prolonged circulation. However, high ligand densities can cause masking of the PEG layer, compromising the “stealth” properties *in vivo* and causing an increased PNP accumulation in the liver and spleen.[114,115] There are potentially a multitude of factors responsible for an efficient cellular uptake with low toxicity. A drawback of using a polymer, such as PLGA, that is familiar within drug delivery applications, is that difficulty is associated with synthesizing copolymers, due to the lack of functional groups on the polymer. Although the block copolymer route of synthesizing FPNPs is well documented and used, this approach presents potential exposure of the drug-loaded-NP to hydrolysis and the denaturation of ligands, depending on the polymer used.[116–118]

Table 1: *FPNPs that is utilized using the block copolymer synthesis method for drug/gene delivery.*

FPNPs	Functionality 1	Functionality 2	Drug release mechanism	Ref
PLA-PEG-A10 PSMA	Prostate-specific membrane antigen (LNCaP cells)	DEX	Ligand targeting - aptamer	77
PCL-PEG, PLGA-PEG, PLA-PEG	"Stealth" property against blood proteins	PEG	-	80
DOTA-MMA-PEG-RDG	Bind to Rvβ3 integrin and DOTA to complex with imaging 64Cu	RDG	-	68
PLGA-PEG-A10 PSMA	Avidin-Biotin interaction – Introduced avidin to biotin for recognition of biotin overexpressed on cancerous cells.	PTX	Dialysis	105
PCL-PEG-Biot, PLA-PEG-Biot and PLGA-PEG-Biot	Avidin-biotin-WGA (lectin)	Biotin	To recognize N-acetyl-d-glucosamine and N-acetylneuraminic acid, located on various cell	110
PMLABE-PEG-Biot	Streptavidin-biotin interaction – Introduced avidin to biotin for recognition of biotin overexpressed on cancerous cells or for conjugation with RDG for binding with hepatotropic peptides	DOX	Ligand targeting – peptide uptake into cells	119
PLGA-b-PEG-A10 aptamer	RNA aptamer targeting the prostate-specific mem-brane antigen (PSMA) on the surface of prostate cancer (PCa) cells	PTX	Ligand targeting - aptamer	115, 120
PLGA-PEG-NR7	NR7 peptide binding to EGF domain, enhancing cellular uptake and inhibiting growth	DOX	Ligand targeting – peptide. pH and enzyme sensitive	121
PLGA–PEG-heptapeptide	Targeting ligand to bind to EGFR	DOX	Ligand targeting – peptide	121
PLGA-PEG-anti EGFR MoAb	Targeting ligand to bind to EGFR	Gemcitabine	Ligand targeting - peptide	122
PCL-(PDA)-HA	HA receptor - CD44	DOX	Ligand targeting – glutathione, reducing disulfide bonds	113
TOS-HA and TOS-PEG-tLyP-1	HA receptor - CD44 and tumor-homing penetrating peptide tLyP-1	PTX	Ligand targeting - glycoprotein	123
MMPU-PEG	Antiepidermal growth factor receptor monoclonal antibody cetuximab	PTX	Ligand targeting – C225 antibody	124
PMLABe-b-PEG-biotin	Cyclic-RGD-biotin. Introduced via a streptavidin bridge	Biotin	Ligand targeting - peptide	125
M-PLGA-TPGS	Inhibit P-glycoprotein (P-gp) to increase permeability through cell membranes	DOX + PTX	Inside cell. Passive release. Diffusion followed by degradation	126

PAMAM-PEG-mannose and PAMAM-PEG-galactose	Transfection of cells via mannose receptor on P388D1 macrophages and asialoglyco protein receptor on HepG2 human hepatocytes	DNA	Ligand targeting – protein receptors	127
PAA-CD, PAA-AD-FA, PEG-AD	Folic acid (FA) inducing FA mediated endocytosis	DOX	Ligand targeting- cancer cells	128

Surfactant-covered nanoparticles

In this section, the functionality is introduced via a surfactant that physically adsorb onto the surface of the particle. This technique is also called Interfacial Activity Assisted Surface Functionalization (IAASF). PLGA polymer particles are the most researched particles for this approach, and the unique combination of control over the synthesis of PLGA into NPs and PLGA being physiologically compatible, makes PLGA a preferred choice. The drawback of using PLGA is that the polymer lacks chemical functional groups for further functionalization. This severely hinders the use of PLGA for traditional conjugation. The pioneering work of Fahmy (Figure 9), using surfactant-based incorporation of a target ligand via an avidin functionalized-fatty acid conjugates onto PLGA PNPs, inspired more syntheses of FPNPs in a more controlled manner.[129] The idea of his work was that the fatty acid (palmitic acid)

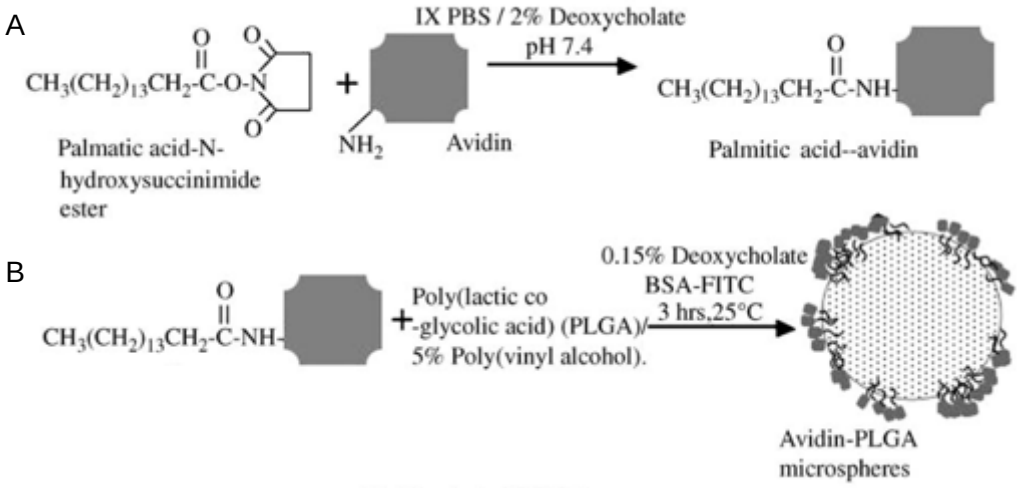

Figure 9: *Overall scheme indicating the fabrication of surfactant-covered PNPs. PLGA particles with palmitoylated avidin. (A) Conjugation of palmitic acid to avidin and (B) incorporation of avidin–palmitate to the surface of PLGA particles using a double emulsion-solvent evaporation method.*[129]

preferentially associates with the hydrophobic PLGA matrix of the microparticles (Figure 9B) rather than with the external aqueous environment, facilitating a prolonged presentation of avidin (target ligand) over several weeks. Because of his work, various studies were based on a

similar technique, using very similar chemistries, but conjugating other polymers or targeting ligands to the avidin functionality as will be shown next in this review.

Park *et al*. synthesized FPNPs and adopted a similar approach to synthesize FPNPs, similar to PLGA-palmitic acid-avidin nature, decorating the avidin-PNPs further with monoclonal antibodies that target CD4+ T lymphocytes.[116] These FPNPs showed targeted delivery of cytokine therapeutics to CD4+ cells. During the emulsification, DOX was also encapsulated. The same group varied the fatty acid lipophilicity and found that the fatty acid, linoleic acid, provided the highest density of avidin displayed on the nanoparticle surface.[130] Additionally, the higher the avidin density, the higher the ligand binding capacity and functionality. To decrease the adsorption of plasma proteins to the surface of the avidin-PNPs, biotinylated-PEG chain ends were introduced via the avidin moieties on the surface. During emulsification, DOX was also encapsulated, and spherical particles with an average diameter of 130 nm were obtained with a smooth and spherical surface. These drug encapsulated-FPNPs showed improved circulation and approximately 3% of the initial dose of PNPs was still detected in the serum 48 hours after initial administration, and enhanced the transport across mucosal barriers.

As shown in the work above, the versatility of the surfactant-covered method is the ability to easily assess surface modifications, such as the attachment of biotinylated antibodies, aptamers, or proteins for active targeting purposes, allowing for the site-specific delivery of drug-loaded PNPs to targeted cells and tissues. Even combinations of ligands can be attached in precise fashion at any point after particle manufacture and storage, allowing introduction of multiple functional groups, bettering the designed system and end application. Importantly, this methodology enables titration of targeting ligands and thereby precise control over the surface properties and coverage.

FPNPs have also been synthesized by a combination of homopolymer and an amphiphilic block copolymer instead of a surfactant at the interface of the PNP surface during processing. Patil *et al*. introduced a block copolymer (PLA-PEG) to an oil/water emulsion while PLGA PNPs were formulated (Figure 10).[39]

Initially, functional PEG-PLA block copolymers were synthesized through esterification of HO-PEG-OH with different fractions of folic acid (FA) and biotin, which serves as a site-targeting ligand. The produced FA-PEG-OH and biotin-PEG-OH, were then extended through ring-opening polymerization to produce FA-PEG-PLA or biotin-PEG-PLA block copolymers. FPNPs were then obtained via emulsification of these block copolymers in combination with PLGA and PTX producing PTX-encapsulated FA-PNPs or biotin-PNPs, of 100-150 nm, upon solvent evaporation. The PLA block of the copolymer partitioned itself into the more hydrophobic PLGA

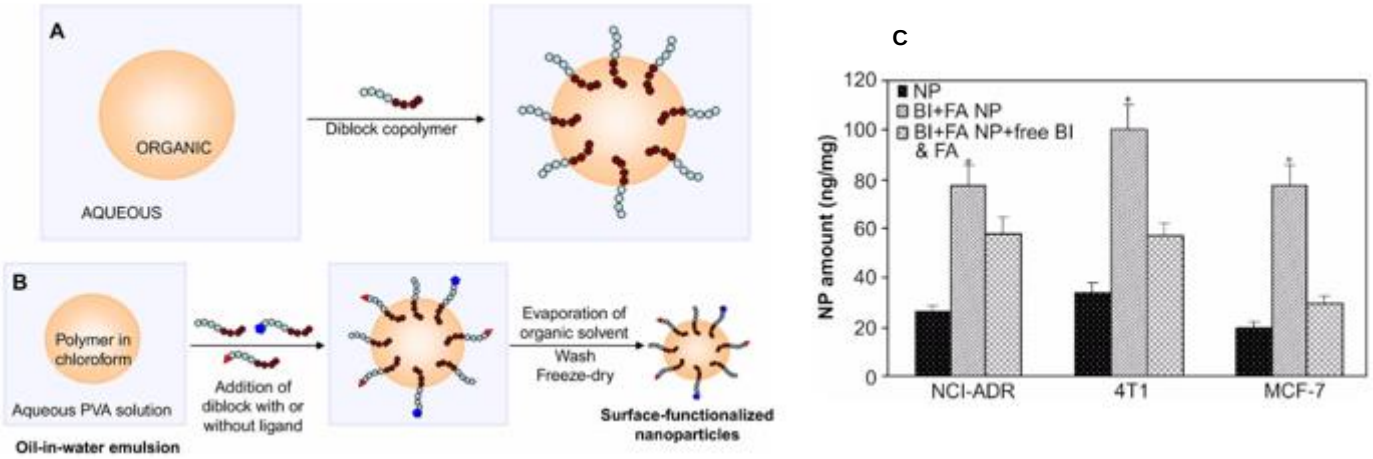

Figure 10: *(A) Amphiphilic block copolymer in an oil/water biphasic system. (B) Introduction of PLA–PEG and PLA–PEG–ligand conjugates during the emulsification fabricating FPNPs with PEG and PEG–ligand on the surface. Hydrophobic blocks (PLA) are shown as a series of brown circles while hydrophilic blocks (PEG) are shown as a series of blue circles. (C) The effect of folic acid and biotin incorporation on FPNPs accumulation in different breast cancer cells. Ligand-FPNPs are taken up extensively compared to PNPs.*[39]

polymer resulting in PNPs with PEG chains on the surface. Data from *in vitro* drug delivery experiments showed that the use of these FA-PNPs and biotin-PNP enhanced particle accumulation inside tumor cells, hence improving efficacy of PTX delivery.

Chittasupho and Fakhari formulated DOX-loaded peptide-PNPs targeting immunologically active receptors, by attaching cyclo-(1,12)-PenITDGEATDSGC (cLABL) peptide to the PNP surface. cLABL is derived from the leukocyte function associated antigen-1 (LFA-1) and has shown to inhibit homotypic and heterotypic T-cell adhesion.[131] The particles were fabricated via solvent displacement method using a combination of PLGA and carboxyl (or hydroxyl)-terminated pluronic F-127 as surfactant. Upon particle formation, and the presence of DOX, the hydrophobic block of the pluronic acid interacts with the PLGA forming the DOX-loaded core of the PNPs while the hydrophilic blocks, with functional groups, decorate the surface of the particles. Cyclo-(1,12)-PenITDGEATDSGC (cLABL) peptides were chemically conjugated, after PNP formation, via the amine functionality on the peptide, to the activated carboxyl groups on the pluronic surfactant. PNPs with an average diameter of 70-160 nm were synthesized. The DOX-loaded FPNPs showed more rapid cellular uptake by A549 lung epithelial cancer cells compared to PNPs without peptide.[132,133] Refer to Table 2 for more examples where the surfactant-covered technique is used to synthesize FPNPs.

The surfactant-covered method of synthesizing FPNPs is much easier, more general and more flexible than the block copolymer method. Therefore, because of these benefits, this strategy promises widespread utility in modifying the surface of polymer-based NPs for applications in drug delivery and tissue engineering. The benefit of the versatility also comes with a drawback in the sense that a copolymer instead of surfactant can be used, which needed to be well defined (as discussed in the block copolymer section) and might need multiple modification steps to introduce the functionality. Another major drawback of this method of producing FPNPs is that the ligand containing functionality are covalently bound to the copolymer, but the incorporation/ adsorption onto the PNPs still relies on non-covalent interaction and targeting ligands present may decrease with time due to desorption or degradation.[129]

Table 2: *FPNPs synthesized using the surfactant-covered synthesis method.*

FPNPs	Functionality 1	Functionality 2	Release mechanism	Ref
PS-PS-PEO-NS	Strain-promoted alkyn-azide cycloaddtion	DNA	-	56
PLGA-PLA-PEG-FA/Biotin	Receptor recognition on tumor cells Folate receptor	Paclitaxel	Ligand targeted – internalization and degradation of PLGA PNPs releasing drug	39
PLGA-palmitic-avidin	Avidin-biotin conjugation for further ligand functionalization	BSA	Passive release	129
PLGA-fatty acid-avidin-biot-HRP	Signal amplication to determine % avidin functionality	Cell interactions	-	116
PLGA-palmitic-avidin-biotin-PEG	Avidin-biotin conjugation. Minimizing dose-limiting cardiotoxicity	Doxorubicin	Drug released intracellularly	130
PLGA-pluronic-cLABL	Ligand for intercellular cell adhesion targeting ICAM-1	Doxorubicin	Ligand target – peptide (internalize after binding to ICAM-1)	132
PLGA-pluronic-cLABL	Ligand for intercellular cell adhesion targeting ICAM-1	-	Ligand target – peptide (internalize after binding to ICAM-1)	133
PLGA-fatty acid-avidin-biot-MoAb	Targeting of CD4+ T lymphocytes	Cytokine	Ligand targeted – antibody	134
PLGA-CS-FA	Folic acid for binding to folate receptors in prostate cancer cells	Bicalutamide	Ligand targeted	135
Chitosan-BMP-2-PEG	Promote bone healing	-	BMP-2 (glycoprotein)	136
PLGA-PEO(pluronic)-NH2	Binding of additional Boc-Phe-OH and Fmoc-Phe-OH	-	Conjugations	137

Particle surface modification

The adsorption or covalent coupling of functional material to the surface of the nanoparticles can render functional PNPs. These agents can include polymers, carbohydrates, peptides, proteins, nucleic acids, ligands and small functional molecules.[1,6,14,35] Alex *et al.* synthesized PNPs based on using poly (styrene-*alt*-maleic anhydride) (PSMA) grafted with various cationic moieties onto the polymer backbone for intracellular gene delivery. In this study, PSMA (e.g.

St:MAnh of 2:1) were initially modified with various amines containing quaternary ammonium cations (e.g. aromatic (isonicotinic acid), aliphatic (glycidyl trimethyl ammonium Cl) and cyclo aliphatic (1-(2-aminoethyl) piperazine) quaternary ammonium moieties). These compounds, respectively, have properties that include biocompatibility, DNA complexing ability and enhanced gene delivery. The modified polymers were then used to fabricate nanoparticles through nano-precipitation and sonication, producing particles of 70-120 nm.

Bio-inspired polydopamine (pD) and tannic acid (TA) have been utilized for the surface functionalization of PNPs via conjugation with various ligands, such as folate and transactivator of transcription (TAT) peptide, to only name a few, producing FPNPs.[50,59,108,138]

Abouelmagd *et al*. synthesized PLGA-pD and TA coated FPNPs via first a single emulsion solvent evaporation method, and then coating the particles with both pD and TA by incubating

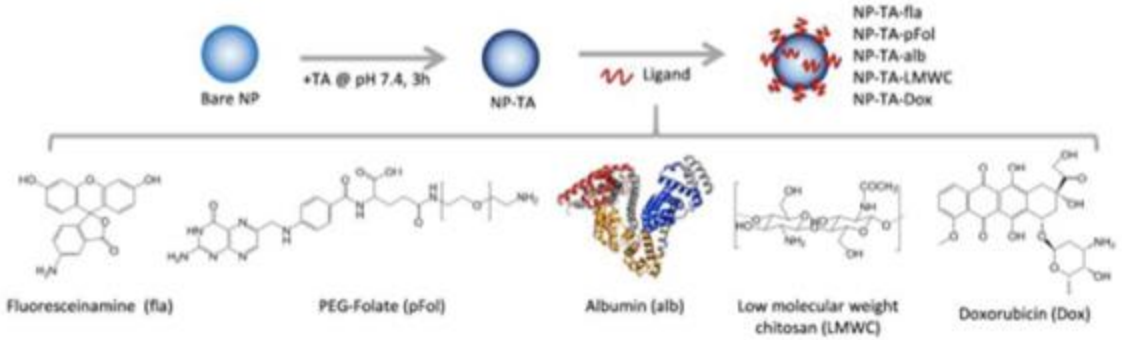

Figure 11: *Synthetic route for the synthesis of TA-decorated FPNPs and the addition of ligans.*[50]

the particles in the respective compound (Figure 11). The functionalized particles were used for cellular uptake, translocation across the endothelial cell layer, and interaction with cells having an acidic pH. The use of such functionality enhanced interaction between the PNPs and the targeted cells based on ligand-specific mechanisms.[50]

Generally, either lipid- or polymer- based nanoparticles carriers have been formulated for gene delivery applications, where they induce long circulation times and provide excellent gene complexation efficiency. However, the use of polymer-based carriers has many advantages over lipid-based carriers due to their stability and accessible chemical modification for targeted delivery as well as possible water solubility. Refer to Table 3 for more examples where surface modification of particle surfaces is utilized to synthesize FPNPs.

Table 3: *FPNPs synthesized using the direct surface modification method.*

FPNPs	Functionality 1	Functionality 2	Release mechanism	Ref
PSMA-grafted L-arginine and spermine	Intracellular gene delivery	DNA	Endosomal rupturing due to pH	139
PLGA-pD/TA	Ligand conjugation with folate, TAT peptide, chitosan and iron oxide particles	Doxorubicin and paclitaxel	Ligand targeted and pH dependent release	50,59,140

Other applications

Having different polymer architectures in mind and considering the role the FPNPs need to fill in a specific application, one can design a FPNP for different applications and fields outside of drug/gene delivery as will be shown next in this review.

Copolymers

Novel molecularly imprinted conductive polyaniline (PANI) NPs were fabricated using an amphiphilic copolymer poly(2-acrylamido-2-methyl-1-propanesulfonic acid-*co*-styrene) (P(AMPS-*co*-St)), prepared by radical copolymerization of the hydrophobic monomer styrene (St) and the hydrophilic AMPS (Figure 12).[141] Molecular imprinted PNPs were synthesized via the self-assembly of the copolymer in the presence of template molecules (paracetamol (PCM) and aniline) using water as nonsolvent. The solution was mixed for 30 minutes to allow to associate with the micelles owing to their interactions. Ammonium persulfate (APS) was added and stirred for another 24 hours over ice. Acetone was used for PNPs precipitation. Freeze drying was used to obtain molecular imprinted PANI PNPs. The PANI NPs were directly cast onto an Au electrode by microsyringe and dried in the air. Finally, the template molecules were removed from the film by extraction with a mixture of acetic acid and methanol at a ratio of 1:9 (v/v) overnight, leading to an imprinted PANI sensor with high selectivity toward paracetamol. For additional examples of FPNPs synthesized using the copolymer technique, refer to Table 4.

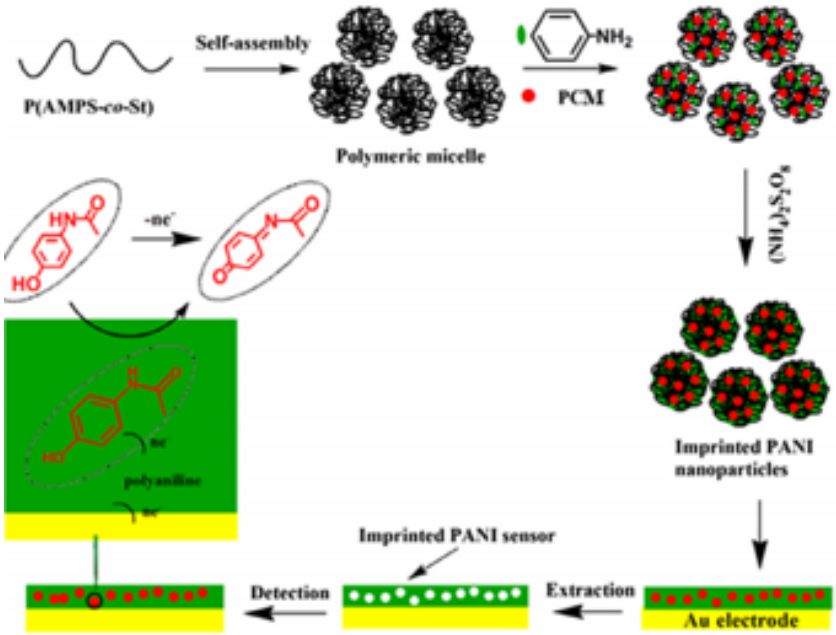

Figure 12: *Schematic illustration of the synthesis route for molecular imprinted PANI NPs and the fabrication of imprinted PANI sensor.*[141]

Table 4: *FPNPs synthesized for applications outside of drug delivery using the block copolymer method*

FPNPs	Functionality 1	Functionality 2	Reason	Ref
2-oxazolines-1°or 2° amine	Amine for further functionalization	-	-	35
MLABe-b-PEG-biotin	Encapsulated a radiotracer for radiotheraphy	Tc-SSS and Radionuclides	-	125
PAGEC-b-PPc-b-PAGEC	Negative and positive charged – clickable alkene groups	-	Functional triblock polycarbonates	142
P(AMPS-co-St)	Paracetamol imprinted	-	Detecting paracetamol	141
PAGEC-PPC-PAGEC	Alkyne		Functionalities can be “clicked” onto particle surface	142

Surfactant-covered nanoparticles

FPNPs synthesized using purified horseradish peroxidase (HRP) adsorbed on PEGylated polyurethane (PU-PEG) NPs are utilized for the determination of pharmaceutical products.[143] The NPs were prepared by mini-emulsion technique. Briefly, the monomer mixture containing diisocyanate, polyol, PEG and hydrophobic olive oil was added to the aqueous phase containing the surfactant. Nanodroplets were formed under high shear and the resulting dispersions were allowed to polymerize at 60 ºC for 4 hours to produce the polyurethane NPs having PEG on surface. Although Gref *et al.* showed that PEG decreases the adsorption of proteins to the surface, it was also shown that the core of the PNP influence the nature and the extent of

protein adsorption.[80] In this study it was shown that HRP was adsorbed via electrostatic interactions.

The influence of enzyme immobilization on the catalytic activity of HRP was studied and the FPNPs were applied for the determination of dopamine detection in pharmaceutical products. The enzymes also were shown to retain at least 50 % of their activity over more than 50 days.

Particle surface modification

Core FPNPs with highly reactive functional groups on the surface were used for further modification to allow the extraction of biomolecules from dilute solutions. In Chapter 8, we describe the synthesis of particles using a surfactant-free dispersion polymerization technique. Styrene (St), divinyl benzene (DVB) and maleic anhydride (MAnh) were copolymerized in a mixture of methyl ethyl ketone and heptane as solvents. Tunable particle sizes and morphologies could be fabricated. The MAnh-FPNPs particles already render functional groups on the surface, and for specific applications these functional and reactive groups in the form of DVB and MAnh could be used for the addition of extra functionality needed. For the extraction of biomolecules, the particles were modified with a boronic acid moiety, as well as surface grafted with a monomer having a tetraphenylborate functionality. These particles showed to successfully extract norepinephrine and octopamine from dilute solutions.

Reductively degradable crosslinked glyco-particles for protein conjugation, between the proteins on *E. coli* and glycopolymers, were synthesized by Ting *et al*. (Figure 13).[144] Glucose bearing glyco-particles were prepared via a one-step crosslinking emulsion polymerization of styrene via a glucose RAFT*stab* (reversible addition-fragmentation chain transfer colloidal stabilizer). The RAFT*stab* was produced from the monomer 2-(methacrylamido) glucopyranose (MAG) and the hydrophobic trithiocarbonate RAFT agent *S*-(methoxycarbonylphenylmethyl)-*S'*-dodecyltrithiocarbonate (MCPDT). To obtain glyco-particles, a degradable bis(2-acryloyloxyethyl)disulfide crosslinker (disulfide diacrylate, DSDA) was employed in the emulsion polymerization. Reductive degradation occurred upon the introduction of 1,4-dithiothreitol (DDT). Although the RAFT*stab* platform had to be optimized and will need to be further optimized if another polymer system is chosen, the glucose moieties were shown to still be bioactive after the reaction, tested using two classes of lectins, namely plant lectin (*Concanavalin A*, *Canavalia ensiformis*) and bacteria lectin (fimH, from *Escherichia coli*). Successful binding was demonstrated, indicating these particles can be “smart” materials in biological systems.

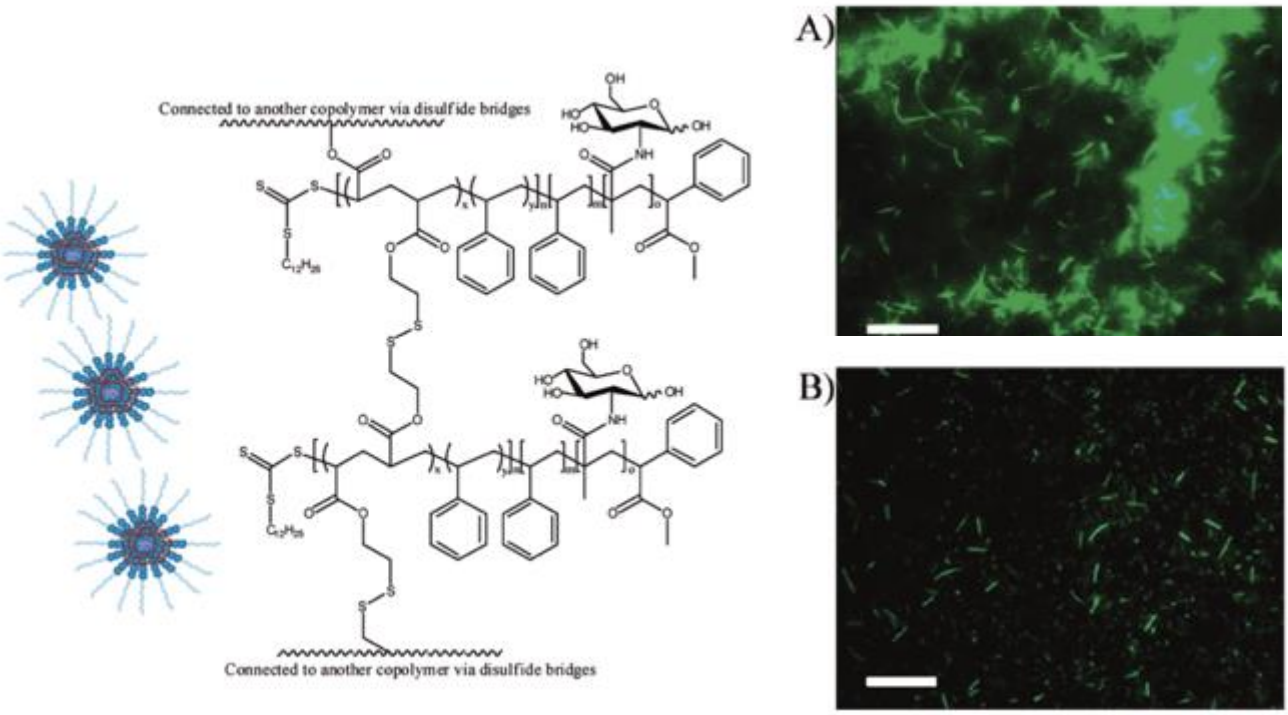

Figure 13: *Schematic glyco-particles synthesized via the disulfide bond using glucose RAFTstab in emulsion polymerization. A) Fluorescent microscopy images of GFP E. coli mixed with latex glycol-NPs without addition ligand and B) with 0.01 M ligand. Scale bar =10 µm.*

Dang *et al.* prepared PNPs, for catalytic reduction experiments, that fall under the FPNPs definition, although they did not mention the PNPs to be FPNPs.[145] FPNPs were prepared by a dispersion polymerization technique, starting with PVP added to a water/ethanol mixture and an aqueous mixture of styrene, acrylic acid and divinylbenzene. These two mixtures were mixed and polymerization was carried out at 70 °C. The obtained PNPs were redispersed and polyamidoamine (PAMAM) dendrimers were grafted onto the surface of the PNPs via an amidation of ethylenediamine (EDA) to the carboxylic groups followed by a Michael addition of methyl acrylate (MA). FPNPs, with a diameter of 450 nm and a PAMAM dendrimer shell were synthesized and used as packing particles for a catalytic column.

Other FPNPs synthesized by the direct surface modification technique are seen in Table 5.

Table 5: *FPNPs synthesized for applications outside of drug/gene delivery by direct surface modification.*

FPNPs	Functionality 1	Functionality 2	Reason	Ref
PS-Polyelectrolyte	pNiPAm		Purification of proteins	40
MAG-St-DSDA	Bind to ConA protein blocking fimH protein on *E. coli*	MAG	Passive targeting - reductive environment	144
PLA-GMA(SDS-RhB)	Rhodamine B	-	Internalization of fluorescent NPs	146
Suc-PLGA-Chol	Sucrose targeting function	-	Cellular uptake	147
PDMS-gPEA	Jeffamine L100 (polyetheramine)	PDMS-gPEA	Separation of dyes	148
PS-AA-dendrimer	PAMAM dendrimer	-	Catalytic column	145

Self-assembly of FPNPs

The utilization of FPNPs in the construction of much bigger structures for the transport or delivery of encapsulated material is a novel field that is only recently exploited.[149–151] In a recent study, which was the first of its kind, inorganic nanoparticles were functionalized and crosslinked at the interface with encapsulated material inside of the capsule.[152,149] This background motivated the study undertaken by the authors of this review to fabricate FPNPs for similar work and take advantage of PNPs, bringing to the table the polymer and forming the basis for the final structure to be designed and modified to produce already functionalized and/ or reactive PNPs. In Chapter 5, FPNPs were synthesized to render boronic acid moieties on the surface and by using inverse Pickering emulsion droplets as template, the stabilizing particles at the interface were crosslinked using a complementary group to the boronic acid in the form of a multi-diol compound, starch. In Chapter 6 these structures were further utilized for the encapsulation of viable bacteria as the capsules showed to be permeable and the capsule wall was degraded upon an introduced trigger. Although this work is only starting to gain traction, we need to look beyond FPNPs to the possibility of constructing well-defined structures using the FPNPs. As FPNPs can form the basis of larger constructs we need to consider some of the challenges that one may endure in synthesizing FPNPs.

Challenges regarding FPNPs

The selection of polymer is critical for the specific application it will be used for. Thus, the technical challenge of FPNPs is the functionalization as most PNPs have limited reactive groups, if any, on the surface. Typically, the surface modification is done by chemical reactions

involving coupling agents and purification steps. Since the reagents required in these modification reactions can introduce toxicity issues, it can limit the possible uses of the PNPs. In the case of preformed functional polymers, ligand conjugation may change the properties of the original polymer, and therefore, compromise the desired end application.

It is challenging to design systems to incorporate functionality while maintaining easy preparation and low cost. Many factors must be considered when deciding which polymer and functionalities are needed. Of course, the application is the most important aspect. Thereafter, one must consider the physico-chemistry of both the PNPs and the functional group; the PNPs compatibility towards the application; the attachment conditions (the required pH, solvent and temperature); the need for any further modifications on the polymer, and in this case what type of functional groups are needed. When attaching bioactive groups, such as peptides, the activity of these groups must be preserved post-conjugation.

The current methods for the incorporation of ligands onto the surface of the PNPs involve chemical conjugation to preformed nanoparticles, or preforming a polymer containing the functional groups and subsequently forming PNPs.[39] The drawback of functionalizing the surface of PNPs is that the typically obtained nanoparticles often lack available functional groups for modification.

Remarks

PNPs hold the possibility to provide versatile surfaces for numerous applications in different fields. Depending on the application one would need to modify the various surfaces for the desired outcome. In this review, we have seen how different polymeric nanoparticles are synthesized with the possibility to be further modified to introduce additional functionality.

The major conclusions that can be drawn from the available research on FPNPs are that mainly block copolymers either consisting of PLGA, PCL and PEG have been investigated for the synthesis of these FPNPs. The vast majority of functional groups have been added via the addition of a biotin group. The conjugation between a biotin and (strept)avidin are among the strongest known biological interactions, and biotinylation has been widely used in surface functionalization.[47] Thus, this method provides a good foundation for further investigations of FPNPs. However, still very few FPNPs exist. Well-defined polymeric nanoparticles have attracted considerable interest over the past decade due to their potential application in drug delivery and diagnostics and many other areas in material science. Most of them are used for drug delivery and are formulated using self-assembly from pre-formed polymers. The major drawback of self-assembled nanoparticles as drug carriers include stability and target efficiency.

This includes premature drug release; release of the encapsulated drugs at nonspecific locations which may cause undesirable toxicity to healthy organs; and lower therapeutic efficacy, leading to the need for higher therapeutic dosages, which in turn increases the undesirable toxicity and side effects to healthy organs. Although, there is a large scope for applications for FPNPs, the challenges of functionalization of PNPs need to be addressed for these particles to live up to their full potential.

Conclusions

The combination of nanotechnology and polymers allows for the design of extremely useful and unique materials in various applications. The first section of this review has provided information about general PNPs and the design and thought process behind FPNPs. Subsequently, this review has focused on various architectures/ FPNP designs that are followed to ultimately fabricate FPNPs. The discussed architectures include block copolymers, surfactant/block copolymer interaction with particle surfaces, and the surface modification of preformed PNPs. The FPNPs have been applied as drug/gene delivery carriers, biosensors, extraction tools for pharmaceutical molecules, dyes and proteins, cell interaction mediators, radiotracers, and particles for catalytic packing columns. Due to the main applications of FPNPs in various fields, the demand for such materials is of high importance. As has been demonstrated in this review, there has been considerable research especially in the drug/ gene delivery methods using FPNPs as carriers for small and larger molecules. Not only is the medical field taking advantage of the developments, but various other fields are able to benefit. Each individual application needs special attention, rigorous research and careful design to fabricate FPNPs specifically for that application.

References

(1) Nahar, M.; Dutta, T.; Murugesan, S.; Asthana,A.; Mishra, D.; Rajkumar, V.; Tare, M.; Saraf. S.Functional Polymeric Nanoparticles: An Efficient and Promising Tool for Active Delivery of Bioactives. *Crit. Rev. Ther. Drug Carr. Syst*. **2006**, *23* (4), 259–318.

(2) Hanemann, T.; Szavo, D. V. Polymer-Nanoparticle Composites: From Synthesis to Modern Applications. *Materials*. ***2010***, *3 (*6), 3468-3517.

(3) Nagavarma, B. V. N.; Yadav, H. K. S.; Ayaz, A.; Vasudha, L. S.; Shivakumar, H. G. Different Techniques for Preparation of Polymeric Nanoparticles - A Review. *Asian J Pharm Clin Res*. **2012**, *5* (3), 16–23.

(4) Vauthier, C.; Bouchemal, K. Methods for the Preparation and Manufacture of Polymeric Nanoparticles. *Pharm. Res*. **2009**, *26* (5), 1025–1058.

(5) Yetter, R. A.; Risha, G. A.; Son, S. F. Metal Particle Combustion and Nanotechnology. *Proc. Combust. Inst*. **2009**, *32* (2), 1819–1838.

(6) Perro, A.; Reculusa, S.; Ravaine, S.; Bourgeat-Lami, E.; Duguet, E. Design and Synthesis of Janus Micro- and Nanoparticles. J. Mater. *Chem.* **2005**, *15* (35–36), 3745–3760.

(7) Ngo, C.; van de Voorde, M. Nanotechnolgy Applications for Air and Soil. *Environ Sci Pollut. Res Int.* **2016**, *23* (14), 13754-13788.

(8) Bufon, C. C.B.; González, J. D. C.; Thurmer, D.J.; Grimm, D. Self-Assembled Ultra-Compact Energy Storage Elements Based on Hybrid Nanomembranes. *Nano Lett*. **2010**, *10* (7), 2506–2510.

(9) Zeng, K.; Baillargeat, S.; Dominique, H.; Ho-Pui, Y. Nanomaterials Enhanced Surface Plasmon Resonance for Biological and Chemical Sensing Applications. *Chem. Soc. Rev*. **2014**, *43* (10), 3426–3452.

(10) Tiwari, P. M.; Vig, K.; Dennis, V. a.; Singh, S. R. Functionalized Gold Nanoparticles and Their Biomedical Applications. *Nanomaterials*. **2011**, *1*(1), 31–63.

(11) Chomoucka, J.; Drbohlavova, J.; Huska, D.; Adam, V.; Kizek, R.; Hubalek, J. Magnetic Nanoparticles and Targeted Drug Delivering. *Pharmacol. Res*. **2010**, *62* (2), 144–149.

(12) Koichi Higuchi, M. Y. UV-Shielding Coating Composition and Coated Article. *Patent*, US20100261022 A1. **2014**.

(13) Arici, E.; Sariciftci, N.S.; Meissner, D.; Hybrid Solar Cells Based on Nanoparticles of CuInS2 in Organic Matrices. *Adv. Funct. Mater*. **2003**, *13* (2), 165–171.

(14) Rowe, M.; Su, M.; Mirin. R.Transport Properties of a Quantum Dot Based Optically Gated Field-Effect Transistor. *Conference on Lasers and Electro-Optics*. **2004**, *3387* (1997), 201307.

(15) Sperling, R; Parak, W. J. Surface Modification, Functionalization and Bioconjugation of Colloidal Inorganic Nanoparticles. *Philos. Trans. A. Math. Phys. Eng. Sci*. **2010**, *368* (1915), 1333–1383.

(16) Parak, WJ.; Gerion, D.; Pellegrino, T.; Zanchet, D.; Micheel, C.; Williams, CS.; Boudreau, R.; Le Gros, M.A.; Larabell, C.A. Biological Applications of Colloidal Nanocrystals. *Nanotechnology*. **2003**, *14*, 15–27.

(17) Han, M.; Gao, X.; Su, J. Quantum-Dot-Tagged Microbeads for Multiplexed Optical Coding of Biomolecules. *Nat. Biotechnol.* **2001**, *19*, 631–635.

(18) Bagalkot, V.; Zhang, L.; Levy-Nissenbaum, E.; Jon, S.; Kantoff, P. W.;Langer, R.;Farokhzad, O. . Quantum Dot-Aptamer Conjugates for Synchronous Cancer Imaging, Therapy, and Sensing of Drug Delivery Based on Bi-Fluorescence Resonance Energy Transfer. *Nano Lett.* **2007**, *7,* 3065−3070.

(19) Yong, K. T.; Wang, Y. C.; Roy, I.; Rui, H.; Swihart, M. T.; Law, W. C.; Kwak, S. K.; Ye, L.; Liu, J. W.; Mahajan, S. D.; Reynolds, J. L. Preparation of Quantum Dot/Drug Nanoparticle Formulations for Traceable Targeted Delivery and Therapy. *Theranostics*. **2012**, *2*, 681− 694.

(20) Rao, C. N. R.; Matte, H. S. S. R; Voggu, R.; Govindaraj, A. Recent Progress in the synthesis of inorganic nanoparticles. *Dalton Transactions.* **2012,** *42,* 5089-5120.

(21) Ladj, R.; Bitar, A.; Eissa, M.; Mugnier, Y.; Dantec, R. Le; Fessi, H.; Elaissari, A. Individual Inorganic Nanoparticles: Preparation, Functionalization and in Vitro Biomedical Diagnostic Applications. J. Mater. Chem. B. 2013, 1, 1381–1396.

(22) Liu, Z.; Liang, X. J. Nano-Carbons as Theranostics. Theranostics. 2012, 2, 235−237.

(23) Yang, S. T.; Luo,J. B.; Zhou,Q.H.; Wang, H. F. Pharmacokinetics, Metabolism and Toxicity of Carbon Nanotubes for Biomedical Purposes. Theranostics. 2012, 2, 271−282.

(24) Reich, DH.; Tanase, M.; Hultgren, A.; Bauer, LA.; Chen, CS. Biological Applications of Multifunctional Magnetic Nanowires. *J Appl Phys*. **2003**, *93*, 7275–7280.

(25) Gibson, J. D.; Khanal, B. P.; Zubarev, E. R. Paclitaxel- Functionalized Gold Nanoparticles. *J. Am. Chem. Soc*. **2007**, *129*, 1653−11661.

(26) Xiao, Y. L.; Hong, H.; Matson, V. Z.; Javadi, A.; Xu, W.; Yang, Y.A.; Zhang, Y.; Engle, J. W.; Nickles, R. J.; Cai, W. B.; Steeber, D. A.; Gong, S. Q. Gold Nanorods Conjugated with Doxorubicin

and cRGD for Combined Anticancer Drug Delivery and Pet Imaging. *Theranostics*. **2012**, *2*, 757–768.

(27) Sperling, R.; Parak, W. J. Surface Modification, Functionalization and Bioconjugation of Colloidal Inorganic Nanoparticles. *Philos. Trans. A. Math. Phys. Eng. Sci*. **2010**, *368* (1915), 1333–1383.

(28) Bhat, S.; Maitra, U. Facially Amphiphilic Thiol Capped Gold and Silver Nanoparticles. *J. Chem. Sci.* **2008**, *120* (6), 507–513.

(29) Kohler, N.; Sun, C.; Fichtenholtz, A.; Gunn, J.; Fang, C.; Zhang, M. Q. Methotrexate-Immobilized Poly(Ethylene Glycol) Magnetic Nanoparticles for MR Imaging and Drug Delivery. *Small*. **2006**, *2,* 785–792.

(30) Yu, M. K.; Park, J.; Jon, S. Targeting Strategies for Multifunctional Nanoparticles in Cancer Imaging and Therapy. *Theranostics*. **2012**, *2,* 3−44.

(31) Choi, S. J.; Oh, J. M.; Choy, J. H. Toxicological Effects of Inorganic Nanoparticles on Human Lung Cancer A549 Cells. *J. Inorg. Biochem*. **2009**, *103*, 463−471.

(32) AshaRani, P. V.; Low Kah Mun, G.; Hande, M. P.; Valiyaveettil, S. Cytotoxicity and Genotoxicity of Silver Nanoparticles in Human Cells. *ACS Nano*. **2009**, 3*,* 279−290.

(33) Lison, D.; Muller, J. L. Systemic Responses to Carbon Nanotubes (CNT) in Mice. *Toxicol. Sci*. **2008**, *101*, 179−180.

(34) Link, C.; Alexis, F.; Pridgen, E.; Molnar, L. K. Factors Affecting the Clearance and Biodistribution of polymeric nanoparticles. *Mol. Pharm*. **2015**, *5* (4), 505–515.

(35) Engelhardt, N.; Ernst, A.; Kampmann, A.-L.; Weberskirch, R. Synthesis and Characterization of Surface Functional Polymer Nanoparticles by a Bottom-Up Approach from Tailor-Made Amphiphilic Block Copolymers. *Macromol. Chem. Phys*. **2013**, *214* (24).

(36) Rao, C. N. R.; Matte, H. S. S. R; Voggu, R.; Govindaraj, A. Recent Progress in the synthesis of inorganic nanoparticles. *Dalton Transactions.* **2012,** *42,* 5089-5120.

(37) T. Niidome, M. Yamagata, Y. Okamoto, Y. Akiyama, H. Takahashi, T. Kawano, Y. Katayama and Y. Niidome, J. PEG-Modified Gold Nanorods with a Stealth Character for in Vivo Applications. *Control. Release*. **2006**, *114* (343–347).

(38) Fratoddi, I.; Venditti, I.; Cametti, C.; Palocci, C.; Chronopoulou, L.; Marino, M.; Acconcia, F.; Russo, M. V. Functional Polymeric Nanoparticles for Dexamethasone Loading and Release. *Colloids Surfaces B Biointerfaces.* **2012**.

(39) Patil, Y. B.; Toti, U. S.; Khdair, A.; Ma, L.; Panyam, J. Single-Step Surface Functionalization of Polymeric Nanoparticles for Targeted Drug Delivery. *Biomaterials.* **2009**, *30* (5), 859–866 DOI: 10.1016/j.biomaterials.2008.09.056.

(40) Welsch, N.; Lu, Y.; Dzubiella, J.; Ballauff, M. Adsorption of Proteins to Functional Polymeric Nanoparticles. Polym. (United Kingdom) **2013**.

(41) Huang, Z. W.; Laurent, V.; Chetouani, G.; Ljubimova, J. Y.; Holler, E.; Benvegnu, T.; Loyer, P.; Cammas-Marion, S. New Functional Degradable and Bio-Compatible Nanoparticles Based on Poly(malic Acid) Derivatives for Site-Specific Anti-Cancer Drug Delivery. *Int. J. Pharm*. **2012**, *423* (1), 84–92.

(42) Li, S.; Wang, K.; Zhang, Z.; Song, C.; Cheng, J.; Yang, Z.; Wen, X.; Pi, P. Preparation and Characterization of Porous Titania-Grafted Poly(styrene-Divinylbenzene)/maleic Anhydride Nanocomposite Microspheres. *Sci. China Chem*. **2010**, *53* (3), 605–611.

(43) Yang, H.; Liang, F.; Chen, Y.; Wang, Q.; Qu, X.; Yang, Z. Lotus Leaf Inspired Robust Superhydrophobic Coating from Strawberry-like Janus Particles. **2015**, *7* (4), 176

(44) Killops, K. L.; Campos, L. M.; Hawker, C. J. Robust, Efficient, and Orthogonal Synthesis of Dendrimers via Thiol-Ene “click” chemistry. *J. Am. Chem. Soc.* **2008**, *130*, 5062–5064.

(45) Dai, S.; Ravi, P.; Tam, K. C. pH-Responsive Polymers: Synthesis, Properties and Applications. *Soft Matter*. **2008**, *4* (3), 435.

(46) Salem, A. K.; Cannizzaro, S. M.; Davies, M. C.; Tendler, S. J. B.; Roberts, C. J.; Williams, P. M.; Shakesheff, K. M. Synthesis and Characterisation of a Degradable Poly (lactic Acid)-Poly(ethylene Glycol) Copolymer with Biotinylated End Groups. *Biomacromolecules*. **2001**, *2* (2), 575–580.

(47) Abd Ellah, N. H.; Abouelmagd, S. A. Surface Functionalization of Polymeric Nanoparticles for Tumor Drug Delivery: Approaches and Challenges. *Expert Opin. Drug Deliv*. **2016**, *5247*, 1–14.

(48) Nagarwal, R. C.; Kant, S.; Singh, P. N.; Maiti, P.; Pandit, J. K. Polymeric Nanoparticulate System: A Potential Approach for Ocular Drug Delivery. *J. Control. Release*. **2009**, *136* (1), 2–13.

(49) Ugelstad, J.; Berge, A.; Ellingsen, T.; Schmid, R.; Nilsen, T. N.; M??rk, P. C.; Stenstad, P.; Hornes, E.; Olsvik. Preparation and Application of New Monosized Polymer Particles. *Prog. Polym. Sci*. **1992**, *17* (1), 87–161.

(50) Abouelmagd, S. A.; Meng, F.; Kim, B.-K.; Hyun, H.; Yeo, Y. Tannic Acid-Mediated Surface Functionalization of Polymeric Nanoparticles. *ACS Biomater. Sci. Eng*. **2016**, *2* (12), 2294-2303.

(51) Ringsdorf, H. Synthetic Polymeric Drugs, In Polymeric Delivery Systems; Kostelnik, R.J., E., Ed.; *Gordon and Breach Science Publishers Inc*: New York, **1978**, 197–225.

(52) Elrika Harmzen-Pretorius, Stefan Hayward, P. S. and B. K. Preparation of Tetraphenylboron-Functionalized and Boronic Acid-Functionalized Polymeric Nanoparticles for the Extraction of Biomolecules. *Manuscr. Prep.* **2017**.

(53) Clawson, C.; Ton, L.; Aryal, S.; Fu, V.; Esener, S.; Zhang, L. Synthesis and Characterization of Lipid-Polymer Hybrid Nanoparticles with pH-Triggered Poly (Ethylene Glycol) Shedding. *Langmuir* **2011**, *27*, 10556−10561.

(54) Hu, C. M. J.; Kaushal, S.; Cao, H. S. T.; Aryal, S.; Sartor, M.; Esener, S.; Bouvet, M.; Zhang, L. Half-Antibody Functionalized Lipid- Polymer Hybrid Nanoparticles for Targeted Drug Delivery to Carcinoembryonic Antigen Presenting Pancreatic Cancer Cells. *Mol. Pharm*. **2010**, *7,* 914−920.

(55) Dobiasch, S.; Szanyi, S.; Kjaev, A.; Werner, J.; Strauss, A.; Weis, C.; Grenacher, L.; Kapilov-Buchman, K.; Israel, L.-L.; Lellouche, J.-P.; Locatelli, E.; Franchini, M. C.; Vandooren, J.; Opdenakker, G.; Felix, K. Synthesis and Functionalization of Protease-Activated Nanoparticles with Tissue Plasminogen Activator Peptides as Targeting Moiety and Diagnostic Tool for Pancreatic Cancer. J*. Nanobiotechnology*. **2016**, *14*, 81.

(56) Oh, J. S.; Wang, Y.; Pine, D. J.; Yi, G. R. High-Density PEO-B-DNA Brushes on Polymer Particles for Colloidal Superstructures. *Chem. Mater.* **2015**, *27* (24), 8337–8344.

(57) Harrisson, S.; Wooley, K. L. Shell-Crosslinked Nanostructures from Amphiphilic AB and ABA Block Copolymers of Styrene-Alt-(Maleic Anhydride) and Styrene: Polymerization, Assembly and Stabilization in One Pot. *Chem. Commun. (Camb*). **2005**, *26*, 3259–3261.

(58) Champion, J. A.; Katare, Y. K.; Mitragotri, S. Particle Shape : A New Design Parameter for Micro- and Nanoscale Drug Delivery Carriers. *J. Control. Release.* **2007**, *121*, 3–9.

(59) Gullotti, E.; Park, J.; Yeo, Y. Polydopamine-Based Surface Modification for the Development of Peritumorally Activatable Nanoparticles. *Pharm*. *Res*. ***2013***, *30* (8), 1956–1967.

(60) Liu, L.; Ren, M.; Yang, W. Preparation of Polymeric Janus Particles by Directional UV-Induced Reactions. *Langmuir 25*, 11048–11053.

(61) Matsuura, I. S. and T. Chemical Aspects of UV-Induced Crosslinking of Proteins to Nucleic Acids. Photoreactions with Lysine and Tryptophan. *Acc. Chem. Res.* **1985**, *18* (5), 134–141.

(62) Takasugi, M.; Guendouz, A.; Chassignol, M.; Decout, J. L.; Lhomme, J.; Thuong, N. T.; C.Hiline. Sequence-Specific Photo-Induced Crosslinking of the Two Strands of Double-Helical DNA by a Psoralen Covalently Linked to a Triple Helix- Forming Oligonucleotide. *Proc. Natl. Acad. Sci.* **1991**, *88*, 5602–5606.

(63) De Luzuriaga, A. R.; Perez-Baena, I.; Montes, S.; Loinaz, I.; Odriozola, I.; García, I.; Pomposo, J. A. New Route to Polymeric Nanoparticles by Click Chemistry Using Bifunctional Cross-Linkers. *Macromol. Symp.* **2010**, *296* (1), 303–310.

(64) Mahou, R.; Wandrey, C. Versatile Route to Synthesize Heterobifunctional Poly(ethylene Glycol) of Variable Functionality for Subsequent Pegylation. *Polymers (Basel).* **2012**, *4* (1), 561–589.

(65) Flores, J. D.; Shin, J.; Hoyle, C. E.; McCormick, C. L. Direct RAFT Polymerization of an Unprotected Isocyanate-Containing Monomer and Subsequent Structopendant Functionalization Using “click”-Type Reactions. *Polym. Chem.* **2010**, *1*, 213–220.

(66) Hoyle, C. E.; Bowman, C. N. Thiol-Ene Click Chemistry. *Angew. Chemie - Int. Ed.* **2010**, *49*, 1540–1573.

(67) Nair, D. P.; Podgórski, M.; Chatani, S.; Gong, T.; Xi, W.; Fenoli, C. R.; Bowman, C. N. The Thiol-Michael Addition Click Reaction: A Powerful and Widely Used Tool in Materials Chemistry. *Chem. Mater.* **2014**, *26* (1), 724–744.

(68) Shokeen, M.; Pressly, E. D.; Hagooly, A.; Zheleznyak, A.; Ramos, N.; Fiamengo, A. L.; Welch, M. J.; Hawker, C. J.; Anderson, C. J. Evaluation of Multivalent, Functional Polymeric Nanoparticles for Imaging Applications. *ACS Nano*. **2011**, *5* (2), 738–747.

(69) Elsabahy, M.; Wooley, K. L. Design of Polymeric Nanoparticles for Biomedical Delivery Applications. *Chem Soc Rev* **2013**, *41* (7), 2545–2561.

(70) Canfarotta, F.; Whitcombe, M. J.; Piletsky, S. A. Polymeric Nanoparticles for Optical Sensing. *Biotechnol. Adv.* **2013**.

(71) Huang, B.; Abraham, W. D.; Zheng, Y.; Bustamante Lopez, S. C.; Luo, S. S.; Irvine, D. J. Active Targeting of Chemotherapy to Disseminated Tumors Using Nanoparticle-Carrying T Cells. *Sci. Transl. Med.* **2015**, *7* (291).

(72) Tiwari, P. M.; Vig, K.; Dennis, V. a.; Singh, S. R. Functionalized Gold Nanoparticles and Their Biomedical Applications. *Nanomaterials*. **2011**, *1*(1), 31–63.

(73) Mout, R.; Moyano, D. F.; Rana, S.; Rotello, V. M. Surface Functionalization of Nanoparticles for Nanomedicine. *Chem. Soc. Rev*. **2012**, *41* (7), 2539.

(74) De Jong, W. H.; Borm, P. J. a. Drug Delivery and Nanoparticles:applications and Hazards. *Int. J. Nanomedicine* **2008**, *3* (2), 133–149.

(75) van Vlerken, L. E.; Amiji, M. M. Multi-Functional Polymeric Nanoparticles for Tumor-Targeted Drug Delivery. *Expert Opin. Drug Deliv.* **2006**, *3* (2), 205–216.

(76) Luk, B. T.; Zhang, L. Current Advances in Polymer-Based Nanotheranostics for Cancer Treatment and Diagnosis. *ACS Appl. Mater. Interfaces* **2014**, *6* (24), 21859–21873

(77) Farokhzad, O. C.; Jon, S.; Khademhosseini, A.; Tran, T.-N. T.; Lavan, D. A.; Langer, R. Targeting Prostate Cancer Cells Nanoparticle-Aptamer Bioconjugates: A New Approach for Nanoparticle-Aptamer Bioconjugates: A New Approach for Targeting Prostate Cancer Cells. *Cancer Res*. **2004**, *64* (64), 7668–7672.

(78) Timko, B. P.; Whitehead, K.; Gao, W. W.; Kohane, D. S.; Farokhzad, O.; Anderson, D.; Langer, R. Advances in Drug Delivery. *Annu. Rev. Mater. Res.* **2011**, *41*, 1–20.

(79) Fang, R. H.; Hu, C. M.; Chen, K. N.; Luk, B. T.; Carpenter, C. W.; Gao, W.; Li, S.; Zhang, D. E.; Lu, W.; Zhang, L. Lipid-Insertion Enables Targeting Functionalization of Erythrocyte Membrane-Cloaked Nanoparticles. *Nanoscale.* **2013**, 5*,* 8884−8888.

(80) Gref, R.; Lück, M.; Quellec, P.; Marchand, M.; Dellacherie, E.; Harnisch, S.; Blunk, T.; Müller, R. H. “Stealth” Corona-Core Nanoparticles Surface Modified by Polyethylene Glycol (PEG): Influences of the Corona (PEG Chain Length and Surface Density) and of the Core Composition on Phagocytic Uptake and Plasma Protein Adsorption. *Colloids Surfaces B Biointerfaces* **2000**, *18* (3–4), 301–313.

(81) Swami, A.; Shi, J.; Gadde, S.; Votruba, A. R. Multifunctional Nanoparticles for Drug Delivery Applications: Imaging, Targeting, and Delivery. Multifunctional Nanoparticles for Drug Delivery Applications: Imaging, Targeting, and Delivery. **2015**, 8–30.

(82) Pelicano, H.; Martin, D.S.; Xu, R.H. Glycolysis Inhibition for Anticancer Treatment. *Oncogene*.

2006, *25* (34), 4633–4646.

(83) Yatvin, M.B.; Kreutz, W.; Horwitz, B.A. pH-Sensitive Liposomes: Possible Clinical Implications. *Science*. **1980**, *210* (4475), 1253–1255.

(84) Brewer, E.; Coleman, J.; Emerging Technologies of Poly- Meric Nanoparticles in Cancer Drug Delivery. *J Nanomater*. **2011**, *2011*, 1–10.

(85) Cheng, FY.; Su, CH.; Wu, PC. Multifunctional Polymeric Nanoparticles for Combined Chemotherapeutic and near-Infrared Photothermal Cancer Therapy in Vitro and in Vivo. *Chem Commun.* **2010**, *46* (18), 3167–3169.

(86) Maeda H. The Enhanced Permeability and Retention (EPR) Effect in Tumor Vasculature: The Key Role of Tumor-Selective Macromolecular Drug Targeting. *T Adv Enzym. Regul*. **2001**, *41*, 189–207.

(87) Kaul G, A. M. Long-Circulating Poly(ethylene Glycol)-Modified Gelatin Nanoparticles for Intracellular Delivery. *Pharm. Res.* **2002**, *19* (7), 1061–1067.

(88) Byrne JD, Betancourt T, B.-P. L. Active Targeting Schemes for Nanoparticle Systems in Cancer Therapeutics. *Adv Drug Deliv Rev.* **2008**, *60* (15), 1615–1626.

(89) Brigger, I.; Dubernet, C, C. P. Nanoparticles in Cancer Therapy and Diagnosis. *Adv. Drug Del. Rev.* **2002**, *54*, 631–651.

(90) Prabhu, R. H.; Patravale, V. B.; Joshi, M. D. Polymeric Nanoparticles for Targeted Treatment in Oncology: Current Insights. *Int. J.* Nanomedicine. **2015**, *10*, 1001–1018.

(91) Carmeliet P, J. R. Angiogenesis in Cancer and Other Diseases. *Nature*. **2000**, *407* (6801), 249–257.

(92) Xiao, K.; Li, Y.; Luo, J.; Lee, J.; Xiao, W.; Gonik, A. The Effect of Surface Charge on in Vivo Biodistribution of PEG-Oligocholic Acid Based Micellar Nanoparticles. *Biomaterials*. **2011**, *32*, 3435–3446.

(93) Danhier, F.; Feron, O. To Exploit the Tumor Microenvironment: Passive and Active Tumor Targeting of Nanocarriers for Anti-Cancer Drug Delivery. *J Control Release*. **2010**, *148* (2), 135–146.

(94) Peer, D.; Karp, J. M.; Hong, S.; Farokhzad, O. C. Nanocarriers as an Emerging Platform for Cancer Therapy. *Nat. Nanotechnol*. **2007**, *2* (34), 751–760.

(95) Kirpotin, DB.; Drummond, DC.; Shao, Y. Antibody Targeting of Long-Circulating Lipidic Nanoparticles Does Not Increase Tumor Localiza- Tion but Does Increase Internalization in Animal Models. *Cancer Res.* **2006**, *66* (13), 6732–6740.

(96) Cho, K.; Wang, X.; Nie, S.; Chen, ZG. Therapeutic Nanoparticles for Drug Delivery in Cancer. *Clin Cancer Res*. **2008**, *14* (5), 1310–1316.

(97) Pastorino, F.; Brignole, C.; Di Paolo, D. Targeting Liposomal Che- Motherapy via Both Tumor Cell-Specific and Tumor Vasculature-Specific Ligands Potentiates Therapeutic Efficacy. *Cancer Res*. **2006**, *66* (20), 10073–10082.

(98) Daniels, TR.; Delgado, T.; Helguera, G. The Transferrin Receptor Part II: Targeted Delivery of Therapeutic Agents into Cancer Cells. *Clin Immunol*. **2006**, *121* (2), 159–176.

(99) Low, P.S. Folate-Targeted Therapeutic and Imaging Agents for Cancer. *Curr Opin Chem Biol*. **2009**, *13* (3), 256–262.

(100) Sudimack, J, L. R. Targeted Drug Delivery via the Folate Receptor. *Adv Drug Deliv Rev*. **2000**, *41* (2), 147–162.

(101) Nwodo, U. U.; Green, E.; Okoh, A. I. Bacterial Exopolysaccharides: Functionality and Prospects. *Int. J. Mol. Sci.* **2012**, *13* (11), 14002–14015.

(102) Desgrosellier, JS. Integrins in Cancer: Biological Impli- Cations and Therapeutic Opportunities. *Nat Rev Cancer*. **2010**, *10* (1), 9–22.

(103) Dienst, A.; Grunow, A.; Unruh, M. Specific Occlusion of Murine and Human Tumor Vasculature by

VCAM-1-Targeted Recombinant Fusion Proteins. *J Natl Cancer Inst.* 2005, *97* (10), 733–747.

(104) Osborn, L.; Hession, C.; Tizard, R. Direct Expression Cloning of Vas- Cular Cell Adhesion Molecule 1, a Cytokine Induced Endothelial Protein That Binds to Lymphocytes. *Cell*. **1989**, *59* (6), 1203–1211.

(105) Salim, M.; Minamikawa, H.; Sugimura, A.; Hashim, R. Amphiphilic Designer Nano-Carriers for Controlled Release: From Drug Delivery to Diagnostics. *Med. Chem. Commun.* **2014**, *5* (11), 1602–1618.

(106) Zambaux, M. F.; Bonneaux, F.; Gref, R.; Maincent, P.; Dellacherie, E.; Alonso, M. J. Influence of Experimental Parameters on the Characteristics of Poly (Lactic Acid) Nanoparticles Prepared by a Double Emulsion Method. *J. Control. Release.* **1998**, *50*, 31–40.

(107) Krishnamachari, Y.; Pearce, M. E.; Salem, A. K. Self-Assembly of Cell-Microparticle Hybrids. *Adv. Mater*. **2008**, *20* (5), 989–993.

(108) Kim, S. Y.; Cho, S. H.; Lee, Y. M.; Chu, L.-Y. Biotin-Conjugated Block Copolymeric Nanoparticles as Tumor-Targeted Drug Delivery Systems. *Macromol. Res*. **2007**, *15* (7), 646–655.

(109) Schmaljohann, D. Thermo- and pH-Responsive Polymers in Drug Delivery. *Adv. Drug Deliv. Rev*. **2006**, *58* (15), 1655–1670.

(110) Gref, R.; Couvreur, P.; Barratt, G.; Mysiakine, E. Surface-Engineered Nanoparticles for Multiple Ligand Coupling. *Biomaterials*. **2003**, *24* (24), 4529–4537.

(111) Yao, W.; Xu, P.; Zhao, J.; Ling, L.; Li, X.; Zhang, B.; Cheng, N.; Pang, Z. RGD Functionalized Polymeric Nanoparticles Targeting Periodontitis Epithelial Cells for the Enhanced Treatment of Periodontitis in Dogs. *J. Colloid Interface Sci*. **2015**, *458*, 14–21.

(112) Lapčík, L.; Lapčík, L.; De Smedt, S.; Demeester, J.; Chabreček, P. *Chem. Rev*. **1998**, *98*, 2663−2684.

(113) Han, HS.; Thambi, T.; Choi, KY.; Son, S.; Ko, H.; Lee, MC. Bioreducible Shell-Cross- Linked Hyaluronic Acid Nanoparticles for Tumor-Targeted Drug Delivery. *Biomacromolecules*. **2015**, *16* (2), 447–456.

(114) Sheng, Y.; Liu, C.; Yuan, Y.; Tao, X.; Yang, F.; Shan, X.; Zhou, H.; Xu, F. Long-Circulating Polymeric Nanoparticles Bearing a Combinatorial Coating of PEG and Water-Soluble Chitosan. *Biomaterials*. **2009**, *30* (12), 2340–2348.

(115) Gu, F.; Zhang, L.; Teply, B. A.; Mann, N.; Wang, A.; Radovic-Moreno, A. F.; Langer, R.; Farokhzad, O. C. Precise Engineering of Targeted Nanoparticles by Using Self-Assembled Biointegrated Block Copolymers. *Proc. Natl. Acad. Sci.* **2008**, *105* (7), 2586–2591.

(116) Park, J.; Mattessich, T.; Jay, S. M.; Agawu, A.; Saltzman, W. M.; Fahmy, T. M. Enhancement of Surface Ligand Display on PLGA Nanoparticles with Amphiphilic Ligand Conjugates. *J. Control. Release*. **2011**, *156* (1), 113–119.

(117) Beletsi, A.; Panagi, Z. Biodistribution Properties of Nanoparticles Based on Mixtures of PLGA with PLGA-PEG Diblock Copolymers. *Int. J. Pharm*. **2005**, *298*, 233–241.

(118) Kocbek, P.; Obermajer, N. Cegnar, M.; Kos, J. Targeting Cancer Cells Using PLGA Nanoparticles Surface Modified with Monoclonal Antibody. *J. Control. Release*. **2007**, *120*, 18–26.

(119) Loyer, P.; Bedhouche, W.; Huang, ZW. Degradable and Biocompatible Nanoparticles Decorated with Cyclic RGD Peptide for Efficient Drug Delivery to Hepatoma Cells in Vitro. *Int. J. Pharm.* **2013**, *454* (2), 727–737.

(120) Cheng, J.; Teply, B. A.; Sherifi, I.; Sung, J.; Luther, G.; Gu, F. X.; Levy-nissenbaum, E.; Radovic-moreno, A. F.; Langer, R.; Farokhzad, O. C. Formulation of Functionalized PLGA – PEG Nanoparticles for in Vivo Targeted Drug Delivery. *Biomaterials.* **2007**, *28* (5), 869–876.

(121) Liu, C. W.; Lin, W. J. Polymeric Nanoparticles Conjugate a Novel Heptapeptide as an Epidermal Growth Factor Receptor-Active Targeting Ligand for Doxorubicin. *Int. J. Nanomedicine.* **2012**, 4749–4767.

(122) Aggarwal, S.; Yadav, S.; Gupta, S. EGFR Targeted PLGA Nanoparticles Using Gemcitabine for Treatment of Pancreatic Cancer. *J. Biomed. Nanotechnol.* **2011**, *7* (1), 137–138.

(123) Liang, DS.; Su, H.T.; Liu, Y.J.; Wang, A.T. Tumor-Specific Penetrating Peptides- Functionalized Hyaluronic Acid-D-Alpha-Tocopheryl Succinate Based Nanoparticles for Multi-Task Delivery to Invasive Cancers. *Biomaterials*. **2015**, *71* (11–23).

(124) Ding, M.; Song, N.; He, X.; Li, J.; Zhou, L.; Tan, H.; Fu, Q.; Gu, Q.; Science, P.; Engineering, P. M.; Materials, P.; Technology, M.; Academy, C. Toward the Next-Generation Nanomedicines : Design of Multifunctional Multiblock Polyurethanes. *ACS Nano.* **2013**, *3*, 1918–1928.

(125) Chérel, M.; Huclier, S.; Lepareur, N.; Bocqué, M.; Costa L, L. E.; Leal Costa, L. E.; Blondelle, C.; Ruello, C.; Desjulets, M.; Noiret, N.; Cammas-Marion, S. Development of Biocompatible and Functional Polymeric Nanoparticles for Site-Specific Delivery of Radionuclides. *Front Med.* **2015**, 2 (63).

(126) Tao W, Zeng X, Liu T, Wang Z, Xiong Q, Ouyang C, et al. Docetaxel-Loaded Nanoparticles Based on Star-Shaped Mannitol-Core PLGA-TPGS Diblock Copolymer for Breast Cancer Therapy. *Acta Biomater.* **2013**, *9* (11), 8910–8920.

(127) Wood, K. C.; Little, S. R.; Langer, R.; Hammond, P. T. A Family of Hierarchically Self-Assembling Linear-Dendritic Hybrid Polymers for Highly Efficient Targeted Gene Delivery. *Gene Ther*. **2005**, 6862–6866.

(128) Ang, C. Y.; Tan, S. Y.; Lu, Y.; Bai, L.; Li, M.; Li, P.; Zhang, Q.; Selvan, S. T.; Zhao, Y. “Turn-On” fluorescence Probe Integrated Polymer Nanoparticles for Sensing Biological Thiol Molecules. *Sci. Rep.* **2014**, *4,* 7057.

(129) Fahmy, T. M.; Samstein, R. M.; Harness, C. C.; Saltzman, W. M. Surface Modification of Biodegradable Polyesters with Fatty Acid Conjugates for Improved Drug Targeting. *Biomaterials*. **2005**, *26* (28), 5727–5736.

(130) Park, J.; Fong, P. M.; Lu, J.; Russell, K. S.; Booth, C. J.; Saltzman, W. M.; Fahmy, T. M. PEGylated PLGA Nanoparticles for the Improved Delivery of Doxorubicin. Nanomedicine Nanotechnology, *Biol. Med.* **2009**, *5* (4), 410–418.

(131) Anderson, M. E.; Siahaan, T. J. Targeting ICAM-1/LFA-1 Interaction for Con- Trolling Autoimmunediseases: Designing Peptide and Small Molecule Inhibitors. *Peptides*. **2003**, *24*, 487–501.

(132) Chittasupho, C.; Xie, S. X.; Baoum, A.; Yakovleva, T.; Siahaan, T. J.; Berkland, C. J. ICAM-1 Targeting of Doxorubicin-Loaded PLGA Nanoparticles to Lung Epithelial Cells. *Eur. J. Pharm. Sci.* **2009**, *37* (2), 141–150.

(133) Fakhari, A.; Baoum, A.; Siahaan, T.J. Controlling Ligand Surface Density Optimizes Nanoparticle Binding to ICAM-1. *J. Pharm. Sci*. **2011**, *100* (3), 1045–1056.

(134) Park, J.; Gao, W.; Whiston, R.T.; Strom, B.; Metcalfe, S. Modulation of CD4+ T Lymphocyte Lineage Outcomes with Targeted, Nanoparticle-Mediated Cytokine Delivery. *Mol. Pharm*. **2011**, *8,* 143–152.

(135) Dhas, N. L.; Ige, P. P.; Kudarha, R. R. Design, Optimization and in-Vitro Study of Folic Acid Conjugated-Chitosan Functionalized PLGA Nanoparticle for Delivery of Bicalutamide in Prostate Cancer. *Powder Technol*. **2015**, *283*, 234–245.

(136) Xu, X.; Yang, J.; Ding, L.; Li, J. Bone Morphogenetic Protein-2-Encapsulated Grafted-Poly-Lactic Acid Polycaprolactone Nanoparticles Promote Bone Repair. *Cell Biochem. Biophys*. **2014**, *71* (1), 215–225.

(137) Gyulai, G.; Magyar, A.; Rohonczy, J.; Orosz, J.; Yamasaki, M.; Bsze, S. Preparation and Characterization of Cationic Pluronic for Surface Modification and Functionalization of Polymeric Drug Delivery Nanoparticles. *Express Polym. Lett.* **2016**, *10* (3), 216–226.

(138) Park, J.; Kadasala, N. R.; Abouelmagd, S. A.; Castanares, M. A.; Collins, D. S.; Wei, A.; Yeo, Y.

Polymer–iron Oxide Composite Nanoparticles for EPR-Independent Drug Delivery. *Biomaterials*. **2016**, *101*, 285–295.

(139) Aji Alex, M. R.; Nagpal, N.; Kulshreshtha, R.; Koul, V. Synthesis and Evaluation of Cationically Modified Poly (styrene-Alt-Maleic Anhydride) Nanocarriers for Intracellular Gene Delivery. *RSC Adv.* **2015**, *5*, 21932-21944.

(140) Abouelmagd, S.; Ku, Y. J.; Yeo, Y. Low Molecular Weight Chitosan-Coated Polymeric Nanoparticles for Sustained and Ph-Sensitive Delivery of Paclitaxel. *J. Drug Target*. **2015**, *23* (7–8), 725–735.

(141) Luo, J.; Sun, J.; Huang, J.; Liu, X. Preparation of Water-Compatible Molecular Imprinted Conductive Polyaniline Nanoparticles Using Polymeric Micelle as Nanoreactor for Enhanced Paracetamol Detection. *Chem*. *Eng*. *J*. **2016**, *283*, 1118–1126.

(142) Wang, Y.; Fan, J.; Darensbourg, D. J. Construction of Versatile and Functional Nanostructures Derived from CO2-Based Polycarbonates. *Angew*. *Chemie Int*. *Ed*. **2015**, *54*, 10206–10210.

(143) Fritzen-Garcia, M. B.; Monteiro, F. F.; Cristofolini, T.; Acuña, J. J. S.; Zanetti-Ramos, B. G.; Oliveira, I. R. W. Z.; Soldi, V.; Pasa, A. A.; Creczynski-Pasa, T. B. Characterization of Horseradish Peroxidase Immobilized on PEGylated Polyurethane Nanoparticles and Its Application for Dopamine Detection. *Sensors Actuators*, *B Chem*. **2013**, *182*, 264–272.

(144) Ting, S.; Min, E. H.; Zetterlund, P. B.; Stenzel, M. H. Controlled/Living Ab Initio Emulsion Polymerization via a Glucose Raft Stab: Degradable Crosslinked Glyco-Particles for Concanavalin A/ Fim H Conjugations to Cluster E. Coli Bacteria. *Macromolecules*. **2010**, *43* (12), 5211–5221.

(145) Dang, G.; Shi, Y.; Fu, Z.; Yang, W. Polymer Nanoparticles with Dendrimer-Ag Shell and Its Application in Catalysis. *Particuology*. **2013**, *11* (3), 346–352.

(146) Li, F.; Zhu, A.; Song, X.; Ji, L.; Wang, J. The Internalization of Fluorescence-Labeled PLA Nanoparticles by Macrophages. *Int. J. Pharm*. **2013**, *453* (2), 506–513.

(147) Crucho, C. I. C.; Barros, M. T. Formulation of Functionalized PLGA Polymeric Nanoparticles for Targeted Drug Delivery. *Polymer* (Guildf). **2015**, *68*, 41–46.

(148) Di, C.; Jiang, X.; Wang, R.; Yin, J. Multi-Responsive Polymer Nanoparticles from the Amphiphilic Poly(dimethylsiloxane) (PDMS)-Containing Poly(ether Amine) (PDMS-gPEA) and Its Potential Application for Smart Separation. *J. Mater. Chem.* **2011**, *21* (12), 4416.

(149) van Wijk, J.; van Deventer, N.; Harmzen, E.; Meuldijk, J.; Klumperman, B. Formation of Hybrid Poly (styrene-Co-Maleic Anhydride)–silica Microcapsules. *J. Mater. Chem. B.* **2014**, *2* (30), 4826.

(150) Lawrence, D. B.; Cai, T.; Hu, Z.; Marquez, M.; Dinsmore, A. D. Temperature-Responsive Semipermeable Capsules Composed of Colloidal Microgel Spheres. *Langmuir.* **2007**, *33* (*2)*, 395–398.

(151) Vilivalam, V. D.; Illum, L.; Iqbal, K. Starch Capsules: An Alternative System for Oral Drug Delivery. *Pharm. Sci. Technol.* **2000**, *3* (2), 64–69.

(152) Douglas, F. J.; Sci, M. Synthesis and Nanocharacterisation of Magnetic Nanoparticles: From Cubes and Spheres to Octapods and Wires. *Thesis.* **2012**.

(153) Chan, Y.H.; Wu, P.J. Semiconducting Polymer Nanoparticles as Fluorescent Probes for Biological Imaging and Sensing. *Part. Part. Syst. Charact.* **2014**, *32* (1), 11-28.

CHAPTER 3

Synthesis of functional polymeric nanoparticles

The results obtained from the various aspects of the synthesis of functional polymeric nanoparticles is presented in this chapter. The synthesis of functional polymeric nanoparticles is discussed, investigating the particle size and morphology as a function of various parameters that include monomer concentration, monomer seeding % and RAFT concentration.

Synthesis and characterization of poly(styrene-co-divinylbenzene-co-maleic anhydride) nanoparticles produced via a surfactant-free dispersion polymerization technique. *E. Harmzen-Pretorius and B. Klumperman. Manuscript in preparation (2017)*

Synthesis and characterization of poly (styrene-co-divinylbenzene-co-maleic anhydride) nanoparticles produced via surfactant-free dispersion polymerization

Abstract

Well-defined, functional polymeric nanoparticles (FPNPs) have a diverse range of applications in fields including electronics, catalysis, pollution control, environmental technology, pharmaceuticals and drug delivery. In this chapter, we report on the development of a one-pot synthesis method of FPNPs, fabricated through surfactant-free dispersion polymerization in a methyl ethyl ketone (MEK): heptane (Hept) mixture with 2,2'-azo-bis(isobutyronitrile) (AIBN) as initiator and butane-1-phenylethyl trithiocarbonate (BPT) as optional reversible addition−fragmentation chain-transfer (RAFT) agent. Monodispersed nanoparticles with tunable sizes and morphologies were obtained with diameters ranging from 100 nm to 1100 nm. Varying experimental parameters such as the monomer addition rate, monomer-, RAFT agent- and crosslinker concentrations, the feed ratio and solvent composition, allowed particle surface morphology and size to be adjusted. The resulting FPNPs were characterized using a field emission gun scanning electron microscope (FEG-SEM) and attenuated total reflection Fourier transform infrared spectroscopy (ATR-FTIR). Highly crosslinked FPNPs were obtained with varying sizes depending on the reaction conditions. Additionally, divinylbenzene and maleic anhydride introduce reactive and functional surface groups in the particles. The particles were found to be highly porous.

Introduction

Functional polymeric nanoparticles (FPNPs) have drawn great interest in the last few years due to their potential applications in advanced research fields such as biomedicine, optical-, information-, electronic- and environmental technologies.[3,1–3] However it is still a challenge to control the size and size distribution of FPNPs while simultaneously obtaining selective chemical compositions and reactivity. Traditionally, many efforts have been devoted to the production of FPNPs, including techniques such as emulsion polymerization, mini- and micro-emulsion polymerization, precipitation and dispersion polymerization, solvent evaporation, interfacial polymerization, spray drying and salting out.[2,4–9] However, most of these techniques need expensive equipment, or/ and consist of multistep-reactions and complex post-processing steps to include extra functionalities or reactivity in the polymeric nanoparticles (PNPs). Thus,

the development of novel techniques to synthesize FPNPs in a cost effective and simple way are in high demand.

Dispersion polymerization was selected as the FPNP synthesis technique as it is a simple, one-pot technique that allows various experimental parameters to be optimized. In dispersion polymerization, the monomer and initiator concentration is generally high, with the solvent being the major locus of polymerization. During the early stages of the polymerization, nucleation proceeds through the flocculation of soluble polymerizing species.

To better understand the driving forces for the nanoparticle (NP) formation, the basic thermodynamics of these systems must be considered. Gibbs free energy is used to explain NP formation and growth. Gibbs free energy involves entropic and enthalpic desolvation.[10–12] As heat is applied, the initiator forms free radicals, and depending on entropic and enthalpic desolvation, particle nuclei form.[13] Gibbs energy is given as $\Delta G_{mix} = \Delta H_{mix} - T\Delta S_{mix}$ and the dissolution of the polymer chains are contributed by entropy and enthalpy. ΔH_{mix} – enthalpic desolvation – is when the polymer-polymer interactions are more favourable than the polymer-solvent, causing ΔG_{mix} to become positive and polymer precipitation occurs. The second part of dissolution is the ΔS_{mix} - entropy term – that occurs due to the crosslinking reaction itself. The crosslinking causes a large decrease in free mixing of the polymer chains, leading to ΔG_{mix} becoming positive and precipitation to occur.

The precipitation of the growing polymer chains/ oligomeric species is observed once chain length/molecular weight exceeds some critical value and desolvates internally. Consequently, colloidally stable particle nuclei are formed.[10,14–16] In addition, it should be noted that oligomer formed can be considered to either nucleate, be captured by growing particles, or remain in solution. Particle growth proceeded throughout the polymerization via two processes, either particle nuclei capture monomer/ oligomer species and grow to become mature particles, or nuclei flocculate with other nuclei, also forming mature particles.[15–18] Possible heterogeneous particle formation and oligomer-capturing and -flocculation, render particle formation very complex.

We are proposing in this paper that although this mechanism is valid for particle formation, additional insight is needed with regards to particle growth as competition might exist between oligomer capturing (producing smooth particles) and the flocculation of small particle nuclei (producing popcorn-shaped particles). It can be envisaged that should nuclei be present in the reaction solution and flocculation of oligomers are preferred, the new nuclei can flocculate to produce what are called popcorn-shaped particles.[17,20, 21]

In this chapter, poly(styrene-*co*-maleic anhydride-*co*-divinylbenzene) nanoparticles (MAnh-FPNPs) with adjustable diameters and narrow size distributions were synthesized via a surfactant-free dispersion polymerization technique. This chapter reports the effects of monomer-, crosslinker- and RAFT concentration, monomer feed rate, and solvent composition on the size and morphology of these FPNPs to better understand the mechanism of particle growth. To the best of our knowledge no work has been done on copolymerizing all three monomers, synthesizing nano-sized MAnh-FPNPs via a surfactant-free dispersion polymerization method.

Materials and Methods

Materials, Potassium hydroxide pellets >85% (Merck Chemicals; Darmstadt, Germany), sodium hydroxide pellets >85% (Merck Chemicals), benzophenone 95% (Sigma; St. Louis, USA), potassium phosphate (K_3PO_4) 99% (Sigma), anhydrous carbon disulphide (CS_2) ≥99% (Sigma), 1-bromoethyl benzene 97% (Sigma) were used as received, and maleic anhydride (MAnh) 99% (Sigma Aldrich) was used after re-crystallization from chloroform. Styrene 99.5% (Fluka chemika;) was washed with KOH, distilled and stored over 4 Å molecular sieves. Divinylbenzene (DVB) >99% (Sigma Aldrich) was used after the t-butylcatechol inhibitor was removed, using a t-butylcatechol remover column, and then stored over 4 Å molecular sieves. Methyl ethyl ketone (MEK) ≥99.7% (Sigma-Aldrich) and *n*-heptane (Kimix; Cape Town, SA) were used as received. Tetrahydrofuran (Kimix), *N*,*N*-dimethylformamide (DMF) (Kimix) and methanol (Kimix) were distilled and kept over 4 Å molecular sieves. 2,2'-Azo-bis(isobutyronitrile) (AIBN) (Riedel de Haen; Morris Plains, USA) was recrystallized twice using methanol and dried under vacuum before use.

Synthesis

Butane-1-phenylethyl trithiocarbonate (BPT) RAFT agent was synthesized according to Lu et *al.*[28], by adding K_3PO_4 (1.36 g, 6.40 mmol) to THF (20 mL). After stirring, 1-butanethiol (530 mg, 5.80 mmol) was added to the mixture, which was stirred again for 10 minutes. Subsequently, carbon disulphide (1.34 g, 17.50 mmol) was added to the mixture and stirred over 1 hour after which 1-bromoethyl benzene (1.07 g, 5.80 mmol) was added. After stirring for six hours at room temperature the THF was removed under reduced pressure and the crude product was purified using flash column chromatography (100 % petroleum ether). Yield: 89 %. ^{1}H NMR (600 MHz, $CDCl_3$): δ (ppm) =0.85 (t, 3H, C**H3**CH2CH2CH2), 1.35 (m, 2H, CH3C**H2**CH2CH2-), 1.59 (m, 2H, C**H2**-S), 1.69 (d, 3H, C**H3**(CH-)), 3.27 (t, 2H, -S-C**H2**), 5.26 (q, 1H, C**H**), 7.25 (m, 5H, Ar-**H**).

FPNPs, a typical dispersion polymerization was conducted as follows: MAnh (2.04 g, 20.80 mmol) was dissolved in 15 mL of MEK in a 250 mL three neck round bottom flask. AIBN (3.00 mg, 0.02 mmol) and butane-1-phenylethyl trithiocarbonate (15.90 mg, 0.06 mmol) was added to the reaction mixture. The reaction mixture was degassed for 20 minutes. In a separate pear-shape flask 22.5 mL *n*-heptane was added with styrene (0.74 mL, 6.49 mmol) and DVB (0.98 mL, 6.90 mmol) and degassed for 20 min. Under argon gas the *n*-heptane solution with the two monomers was drawn up into a syringe and placed in a syringe pump. After the MEK solution was degassed the solution was placed in a 70 °C preheated oil bath. After 10 minutes, the *n*-heptane solution was introduced to the MAnh solution over either a 1-hour or 2-hour addition time. General MAnh-FPNPs synthesis was conducted for 2 to 24 hours, after which the particles were dried under vacuum at 80 °C for 1.5 hours. Thereafter it was left under vacuum for an

additional 16 hours to remove any unreacted monomer and residual solvent. Experiments were all conducted in triplicates.

Amount of accessible MAnh on particles was determined using a series of 100 mg particles which were dispersed in THF and sealed in a small vial. Different mole ratios of *N,N*-dimethyl-3-aminopropyl-1-amine (DMAPA) (to total MAnh in particles) was added to each vial. The reaction took place for 4 hours after which the particles were separated from the supernatant. The particles were rinsed multiple times to ensure the removal of any unbound DMAPA. The supernatant was removed and the reagent in the vial was first weighed. The weight of the excess DMAPA left in the vial was deducted from the introduced DMAPA to calculate the reacted DMAPA. Excess DMAPA that did not react with MAnh was measured and is directly related to the accessible MAnh fraction within the particles. After weighing the vial was used to prepare NMR samples (in deuterated chloroform) to confirm the presence of DMAPA.

Characterization and analysis

Electron microscopy The diameter and size distribution of the FPNPs were determined using a field emission scanning electron microscope (FEG-SEM, Zeiss, Merlin), with a Gemini column, equipped with an inlens- and scanning TEM detector. To obtain the image, the particles were dispersed and placed on a conductive material and coated with carbon to establish conductivity. The high-resolution images were taken operating the instrument at 5 kV beam energy with an iprobe/ current of 250 pA, a working distance of 3.5 – 4.1 mm and an inlens detector. The images were processed using ImageJ software, analyzing 100 measurements per image to get the average particle size and size distribution.

ATR-FTIR spectra were recorded using a Nicolet FTIR spectrometer (Nexus) from Thermo-Fischer equipped containing a Smart Golden Gate ATR accessory with a diamond/ ZnSe internal reflection crystal. The spectra were recorded from 3750 cm^{-1} to 700 cm^{-1} with a spectral resolution of 8 cm^{-1} and a sum of 64 individual scans. Samples were run in solid state and no sample preparation was necessary. Omnic software was used for data acquisition and Origin software was used for data processing.

NMR analysis were recorded on a Varian Inova 300 MHz and 400 MHz NMR spectrometer and Varian Inova 600 MHz NMR spectrometer. Characterization and integration were done using Mestrenova (version 11.0.2). Deuterated dimethyl sulfoxide (Sigma-Aldrich, 99.9 atom % DMSO-d6), deuterated acetone (Sigma-Aldrich, 99.9 atom % acetone-d6) and deuterated chloroform (Sigma-Aldrich, 99.9 atom % $CDCl_3$).

Results and discussion

ATR-FTIR characterization of poly(St-*co*-MAnh-*co*-DVB) FPNPs

The chemical nature of the polymeric nanoparticles was analyzed by ATR-FTIR analysis. The FTIR spectrum indicates that these PNPs are indeed functional (FPNPs) with reactive maleic anhydride (MAnh) and pendant vinyl groups on the FPNPs (Figure 1). These particles (unmodified) are called MAnh-FPNPs unless otherwise stated in the rest of the thesis.

The strong peaks at 1855 cm^{-1} and 1772 cm^{-1} are attributed to the symmetrical and asymmetrical carbonyl cyclo (C=O) stretch vibrations, 1087 cm^{-1} for the C-O-C stretch vibration, indicating the presence of the maleic anhydride groups. Pendant vinyl groups have a characteristic absorption band at 1629 cm^{-1} because of the divinylbenzene monomer. The bands at 947 cm^{-1} and 923 cm^{-1} are due to the =C-H out-of-plane bending vibrations from the styrenic units. The peak at 704 cm^{-1} is characteristic of the C-H out-of-plane stretching vibrations of a mono substituted aromatic ring of the styrene group. The ATR-FTIR results indicate that these nanoparticles do (as expected) consist of anhydride groups, pendant vinyl groups as well as styrenic units, and the spectrum agrees well with those reported in literature. [5,21–23]

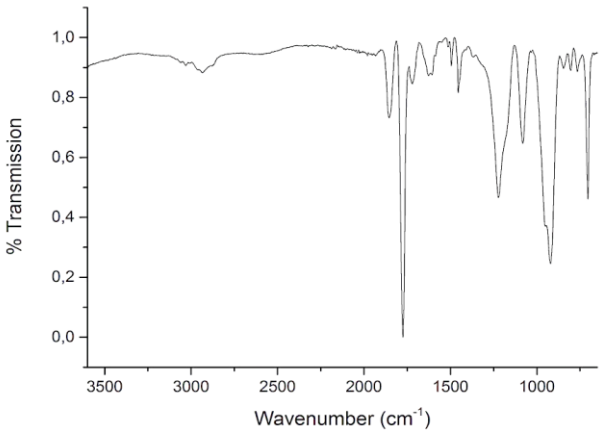

Figure 1: *ATR-FTIR spectrum of the functional polymeric nanoparticles*

Particle stabilization and growth

Particle growth proceeds by two processes: either nuclei grow by capturing monomer/oligomer species or by flocculation of various nuclei.[15,24] It is envisaged that should the process of capturing monomer/oligomer species be preferred, smooth particles can be expected compared to popcorn-shaped particles should flocculation of nuclei be preferred. The capturing of oligomers, in a system with high crosslinking (vinyl bonds) has two effects: 1) growth of the particles and 2) steric stabilization of particles. The newly captured oligomers form a solvated layer on the surface of the growing particle. This gel layer then continues to crosslink and desolvate to become another layer on the particle core. Simultaneously, new oligomers are captured, regenerating the gel layer that act as a sterically stabilized layer..[24] Naka and co-workers have shown that in the presence of a good solvent, the outer polymer layer on the surface of the particles are capable of swelling.[25] Presumably, our particles are also sterically stabilized by solvated polymer chains anchored to the surface of the particles.

Traditional dispersion polymerizations using as little as 0.3 - 0.7% crosslinker (based on total monomer weight) and a stabilizer leads to coarse particles with broad size distributions, as the stabilizer becomes buried within the particle with different degrees of crosslinking between nuclei.[13,26,27] However, we have obtained results that are not in accordance with these previous findings. We use much higher crosslinker concentrations (27 mol % based on total monomer

weight) and still obtain smooth, nano-sized particles with a narrow size distribution, indicating that the solvated layer acts as stabilizer and is present on the surface as a gel-like stabilizer (Figure 2). As will be discussed later, different surface morphologies, varying from smooth particles (Figure 2A/2B) and popcorn-shaped particles (Figure 2C/2D) can be obtained and a difference is observed in the gel-like layer. The gel-like layer seems to be more profound in the smooth particles compared to the popcorn-shaped particles. Specific experimental conditions (*vide infra*) responsible for the different conditions will be discussed, but it is more important to show at present that the gel-like layer is present, and under different experimental conditions and particle growth mechanisms (either oligomer capturing or flocculation), the gel-like layer is visually different.

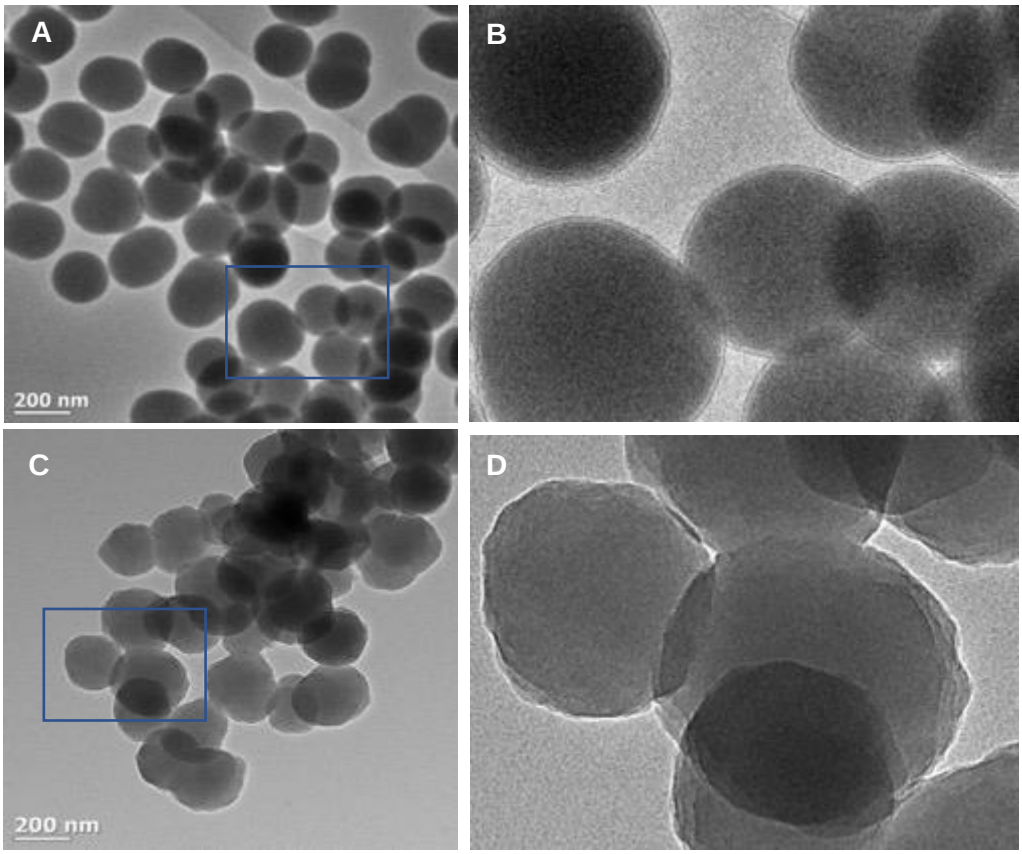

Figure 2: *STEM images of MAnh-FPNPs indicating the presence of a gel-like layer on the outside of the particle surface. A) MAnh-FPNPs having smooth morphologies and B) Zoomed in image of area in A indicated, showing a thin layer on outside of particles. C) Popcorn-shaped MAnh-FPNPs having morphologies and D) Zoomed in area of indicated area on C showing irregular surface layer.* Scale bar in images are 200 nm

Our hypothesis is that competition exists between oligomer capturing onto particle nuclei (producing smooth particles) and the flocculation of small particle nuclei (producing popcorn-shaped particles), and that under different experimental condition either will be preferred. To better understand the driving forces behind these reactions, we inaugurate the effect different experimental conditions, summarized in Table 1, have on particle size and morphology.

Table 1: *Experimental conditions tested for the synthesis of MAnh-FPNPs*

Name	MAnh (mmol)	St (mmol)	DVB (mmol)	[DVB] (wt% rel. to tot monomer)	[Monomer] (mol·L^{-1})	St/DVB seeding % (rel. to total St/DVB)	[RAFT] (mol·L^{-1})	Solvent ratio (MEK:Hept)	Morphology [a]	Particle Diameter (nm)
$FPNP_1$	5.09	1.70	1.68	28	0.91	-	-	1:4	Film	-
$FPNP_2$	5.09	1.70	1.68	28	0.91	-	-	2:3	G/P	
$FPNP_3$	5.09	1.70	1.68	28	0.91	-	-	4:1	Microgelation	-
$FPNP_4$	20.80	6.49	6.90	25	0.68	2.5	-	2:3	P	150
$FPNP_5$	20.80	6.49	6.90	25	0.68	5	-	2:3	P	430
$FPNP_6$	20.80	6.49	6.90	25	0.68	7.5	-	2:3	P/S	393
$FPNP_7$	20.80	6.49	6.90	25	0.68	10	-	2:3	P	490
$FPNP_8$	20.80	6.49	6.90	8.5	0.60	-	-	2:3	F	700
$FPNP_9$	20.80	6.49	6.90	18	0.60	-	-	2:3	S	605
$FPNP_{10}$	20.80	6.49	6.90	22	0.60	-	-	2:3	P	430
$FPNP_{11}$	20.80	6.49	6.90	30	0.60	-	-	2:3	P	210
$FPNP_{12}$	20.80	6.49	6.90	25	0.68	2.5	-	2:3	P	150
$FPNP_{13}$	20.80	6.49	6.90	25	0.68	2.5	0.67	2:3	G	270/125 [b]
$FPNP_{14}$	20.80	6.49	6.90	25	0.68	2.5	1.14	2:3	G	411/233
$FPNP_{15}$	20.80	6.49	6.90	25	0.68	2.5	3.70	2:3	S	677/282
$FPNP_{16}$	20.80	6.49	6.90	25	0.60	2.5	-	2:3	G	70
$FPNP_{17}$	20.80	6.49	6.90	25	0.60	10	-	2:3	G	170
$FPNP_{18}$	20.80	6.49	6.90	25	0.91	2.5	-	2:3	G/P	250
$FPNP_{19}$	20.80	6.49	6.90	25	0.91	10	-	2:3	P	450

a) Morphology is given a smooth (S), popcorn-shape (P), grainy (G) and fused (F). In some instances, a mixture of two morphologies were observed. b) Two distributions in particle diameter are observed.

Effect of monomer addition rate

In preliminary results, we optimized the addition rate of St/DVB to the MAnh and found that an addition time of 2 hours is optimal compared to an addition time of 1 hour. It was observed that when using a shorter addition time (1 hour), irreproducible results were obtained. This can

possibly be attributed to higher concentrations of St/DVB in the MAnh mixture causing particle growth and nucleation to occur simultaneously to different extents, depending on the monomer addition rate.

Effect of solvent composition.

In order to investigate the effect of solvent composition on the particle size and morphology, the ratio of good solvent (methyl ethyl ketone (MEK)) and poor solvent (*n*-heptane (Hept)) was varied with the total solvent volume remaining the same and having a constant final polymer concentration relative to solvent mixture). All of the polymerizations were carried out using a total monomer concentration of 0.9012 mol·L^{-1}, 28 mol % crosslinker (relative to total monomer), and identical reaction and feed times. The reaction exists as a two-phase system. The MAnh is in the MEK phase and the St/DVB in the Hept phase. The reaction solvency was adjusted by varying the ratio of the two solvents.

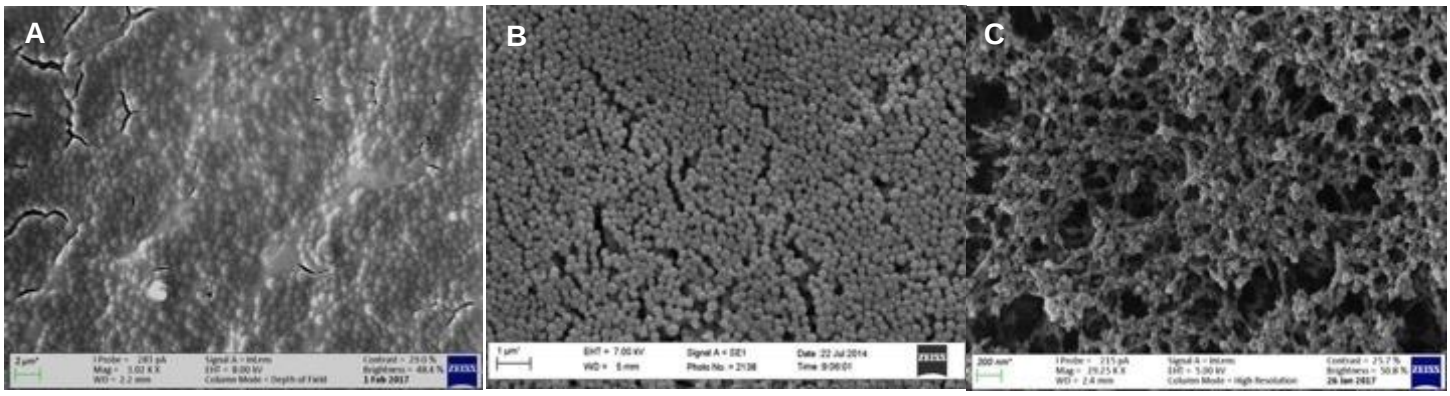

***Figure 3**: SEM images of FPNPs obtained in different solvent ratios. The following solvent compositions were experimented with: A) 1:4 MEK:HEPT ratio, B) 2:3 MEK:HEPT and C) 4:1 MEK:HEPT ratio. As the proportion of MEK increased particles were formed, and with a further increase, a micro-gel is produced (FPNP$_{1-3}$).*

Film formation was observed under the poorest solvency of 1:4 MEK: Hept in the reaction medium due to enthalpy-driven desolvation of the polymer chains/ oligomers, which occurs before particle formation occurs (Figure 3A). It was previously found that after decreasing the volume fraction of the good solvent, the swelling of the polymers decreases, and the polymer chains become shorter and will not reach the critical chain length for nucleation to occur. This leads to polymer chains desolvates in a enthalpic nature before particle nucleation can occur.[12,13,14] At a 2:3 MEK: Hept solvent ratio, spherical particles were produced, indicating that

the critical chain length necessary for particle nucleation was achieved (Figure 3B). It was further observed that by changing the MEK ratio from 2:3 to 4:1, a transition from spherical particles to micro-gelation occurred (Figure 3B to 3C). The smaller micro-gel particles appear to be connected by polymer strands (Figure 3C). This transition is likely caused by the increased swelling of the oligomers, decreasing the distance between newly formed oligomers in solution and increasing internal crosslinking between different chains. Another contribution is the solvency due to the smaller portion of Hept. This resulted in enhanced flocculation of particle nuclei, which promotes coagulation and prevents entropy-driven phase separation. Similar trends and transitions were observed while copolymerizing DVB and MAnh for the formation of micro-gels and while copolymerizing of St and DVB.[12,15]

Effect of Seeding

In this section, relative fractions of the total St /DVB mixture were added at the beginning of the reaction, a process called seeding. Seeding the reaction mixture with small percentages of the St and DVB monomers, with a corresponding fraction of heptane, was thought to promote particle nucleation and secondary nucleation reactions (polydispersed MAnh-FPNPs). This was observed when seeding the reaction with 2.5 %, 5.0 %, 7.5 % and 10 % of the total St/ DVB

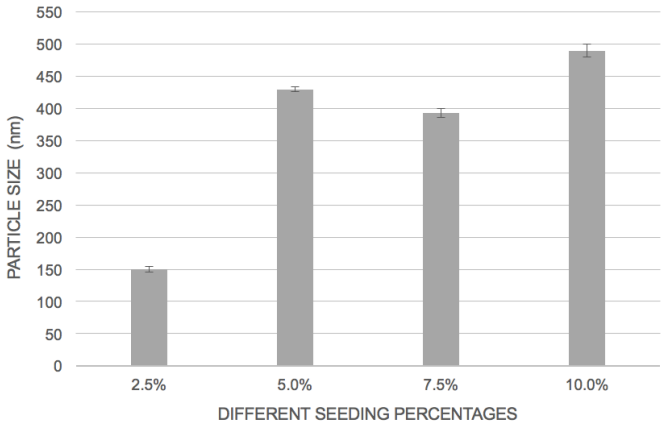

Figure 4: *Particle size as a function of seeding percentages at the start of the polymerization reaction for the synthesis of MAnh-FPNPs ($FPNP_{4-7}$).*

monomers. Adding a higher seeding % to the initial reaction medium attribute to a higher concentration of St/DVB in the MAnh solution, leading potentially to higher concentrations of oligomers in solution and more flocculation to occur between oligomers, that can result ultimately in less particle nuclei and essentially larger particles (Figure 4).[12,15] It was further

noticed that as the seeding percentage increased, the final particles size distribution also broadened.

Effect of monomer concentration

Figure 5 illustrates the effect of changing the monomer concentration using two different levels of seeding, *i.e*. 2.5 and 10 %. These seeding levels were chosen since the 2.5 % seeding experiments gave smaller particles, and the 10 % gave the biggest particles, while keeping the monomer to initiator ratios constant, MEK/hept ratio at 2:3 and only changing the total monomer concentration from 0.606 mol·L^{-1} to 0.908 mol·L^{-1}.

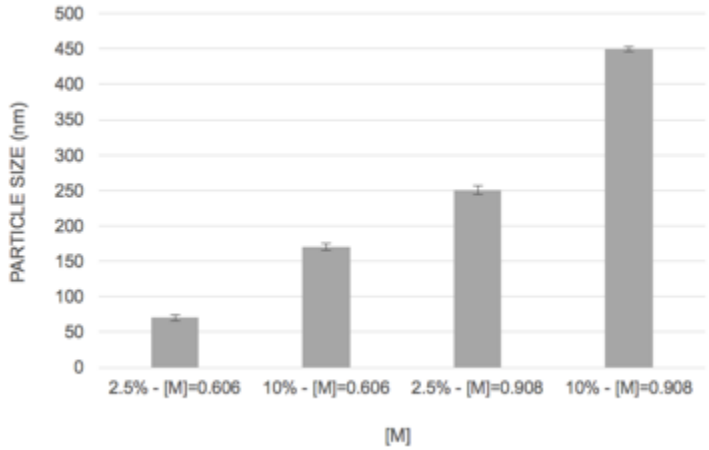

Figure 5: *Particle size as a function of the different seeding percentages at the start of the polymerization reaction for the synthesis of MAnh-FPNPs (FPNP$_{16\text{-}19}$).*

Figure 6 indicates the different morphologies obtained at different seeding percentages. At higher monomer concentration, the concentration of oligomers in solution increases, thus increasing the probability of oligomers flocculating. Ultimately, less nuclei are produced and subsequently larger polymer particles are obtained.[12,15] However, we observe that not only does the particle size increase, but the particles become popcorn-shaped.

This can be attributed to remaining monomer added to the reaction, while small amount of particle nuclei is formed. Thus, competition exist between nuclei growing (capturing of oligomers), but also the formation of new secondary nuclei (flocculation of oligomers). The already formed nuclei grow via adsorption of oligomers onto particle nuclei, however the oligomers that are not adsorbed onto the particle surface follow entropic desolvation (due to intramolecular crosslinking) causing heterogeneous nucleation (Figure 6D). This phenomenon

agrees well to what has been shown in literature.[18] Flocculation of the nuclei produces popcorn-shaped particles. This finding is in line with previous studies.[14,20,24,27]

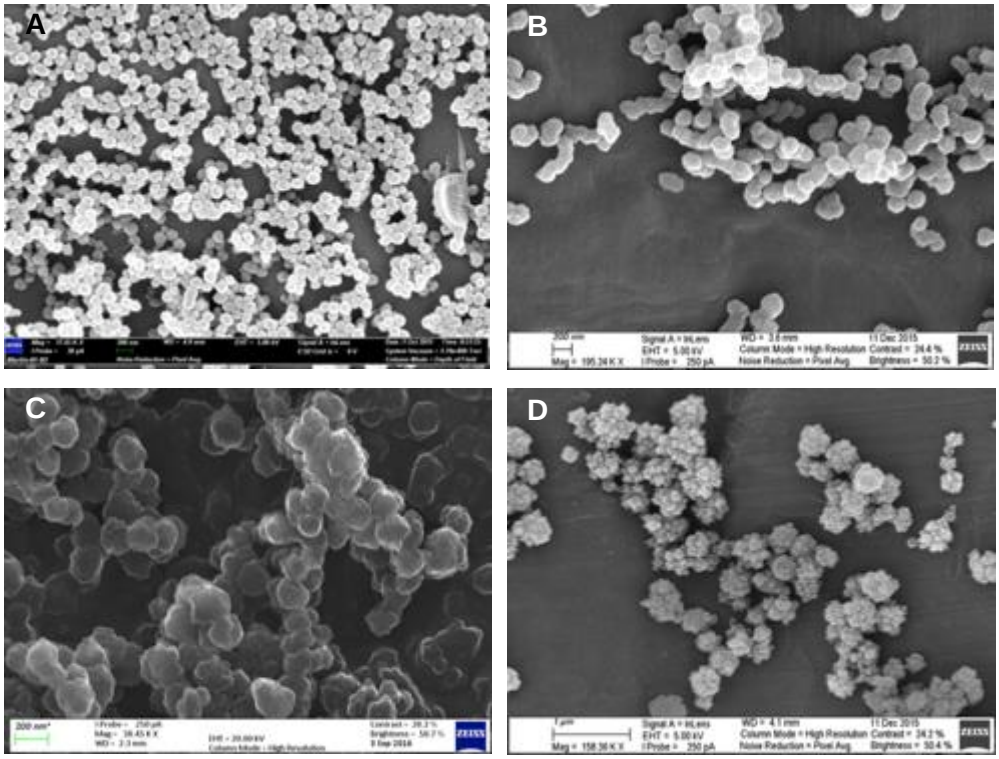

Figure 6: *Scanning electron image of MAnh-FPNPs synthesized using different experimental conditions. A) using 2.5% seeding and a monomer concentration [M] = 0.606 mol·L^{-1}. B) using 10% seeding and [M] = 0.606 mol·L^{-1}. C) 2.5% seeding and [M] of 0.908 mol·L^{-1} and D) 10% seeding and [M] = 0.908 mol·L^{-1}.*

Effect of crosslinker concentration

FPNPs prepared with different amounts of crosslinking monomer are compared. The crosslinker concentration was adjusted according to the St/DVB ratio, with the MAnh:St/DVB ratio the same, such that the mixtures contained a 2-30 mol% DVB (based on total monomer weight). The use of 2 to 8.5 mol% DVB resulted in coagulation of the dispersion and macro-gelation of particles (Figure 7A). This is attributed to the enhanced solvency of the oligomers and newly formed polymer chains because of lower crosslinker concentration.[12,24] Therefore, swelling occurs, and the distance between oligomers and polymer chains in solution decreases. Flocculation of nuclei is favoured, promoting coagulation and also causing macro-gelation to occur.[15,24,27] When 18-22 mol% DVB was used, spherical particles were obtained that possess a wide size distribution (Figure 7B). Increasing DVB concentrations to 27-30 mol% resulted in the formation of stable, well-defined FPNPs with a narrow size distribution ranging from 180-215 nm

(Figure 7C). In summary, we found that by increasing the crosslinker concentration, the particle size decreased, and concomitantly the size distribution narrowed (Figure 7D) The crosslinker is

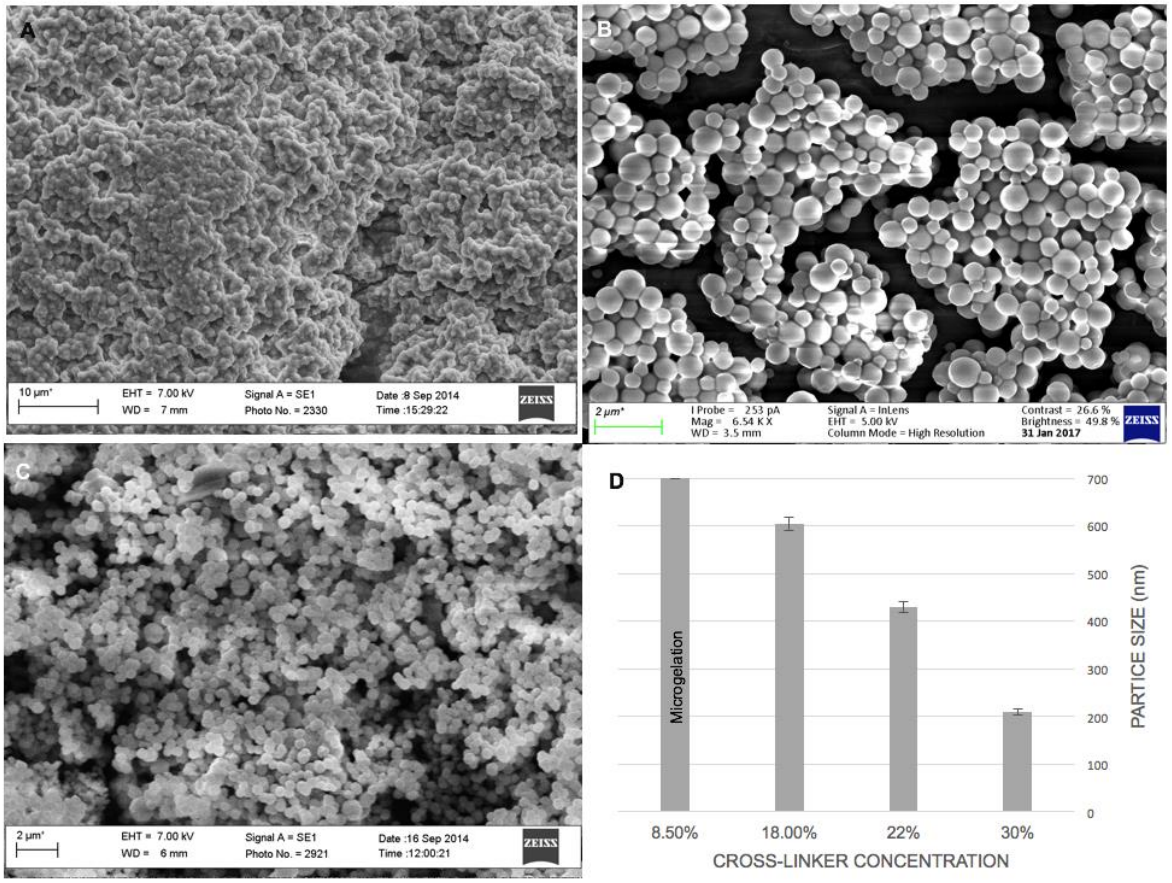

Figure 7: *Scanning electron micrographs of MAnh-FPNPs synthesized using different crosslinker concentrations. A) 8.5 mol % DVB, B) 18 mol % DVB, C) 30 mol % DVB and D) graph indicating how particle size changes with change in crosslinker concentration (FPNP$_{8\text{-}11}$).*

thus necessary for particle formation and plays an important role in particle growth and the capturing of oligomers from the solution.[13] This also indicates that the particle growth mechanism is not within the polymer particles, but rather via the desolvation of polymer chains or flocculation of oligomers onto the particles surface.

Effect of RAFT concentration

Different RAFT concentrations of 3.70 mol·L^{-1}, 1.14 mol·L^{-1}, 0.67 mol·L^{-1} and 0 mol·L^{-1} were examined while solvent composition and monomer concentration were kept the same. The RAFT agent used is shown in Figure 8.

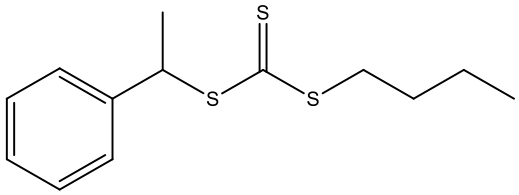

***Figure 8**: Chemical structure of the S-butane-S'-1-phenylethyl trithiocarbonate (BPT) RAFT agent used.*

Samples were taken in one-hour intervals for 4 hours and then again at 24 hours. Analysis of the particle size indicated that the particle size and bimodality decreased with decreasing RAFT concentration (Figure 8A). It was further observed that as RAFT concentration decreased, the particles became less smooth. The particles first became grainy and coarse-like, at 1.1.4 mol·L^{-1} to 0.67 mol·L^{-1} RAFT, and popcorn-shaped using no RAFT-agent (Figure 8B-E). This can possibly be attributed to the rate at which chain length increases.

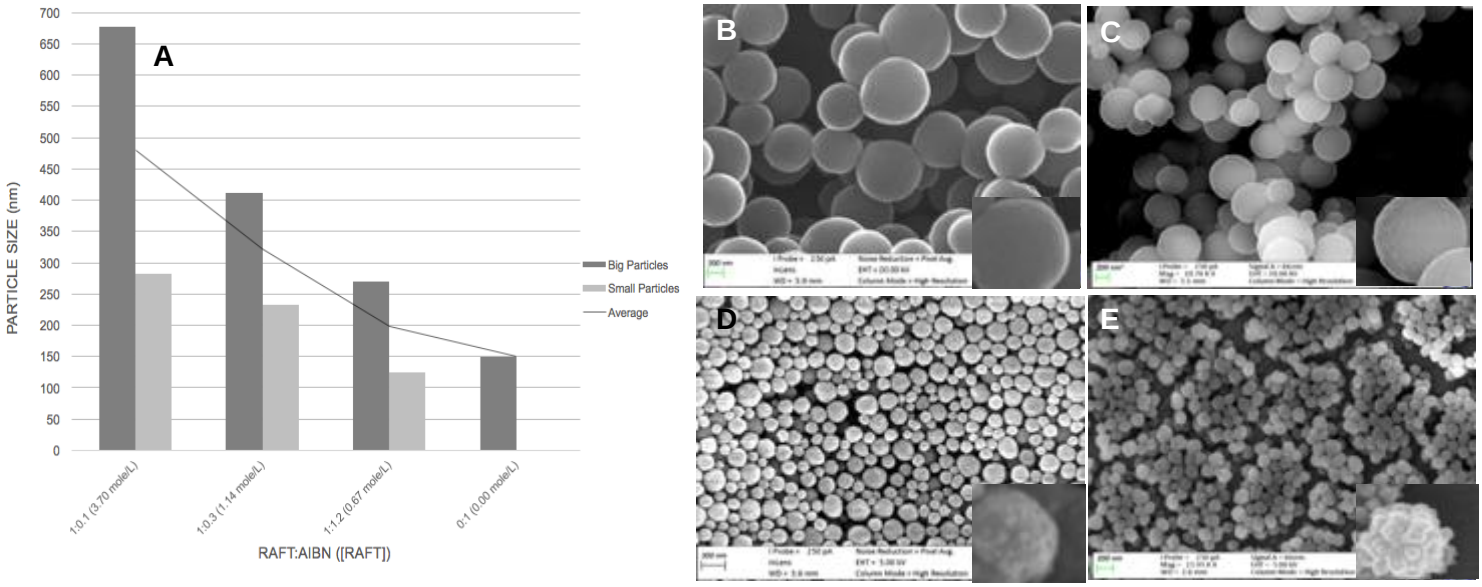

***Figure 9:** A) Particle size dependency as a functional of RAFT concentrations. SEM images illustrate the different particle morphologies, obtained at different RAFT concentrations: B) 3.70 mol·L^{-1} RAFT concentration, C) 1.14 mol·L^{-1}, D) 0.67 mol·L^{-1}and E) 0 mol·L^{-1} with an insert in each image, indicating the various morphologies and the scale bar 200 nm (FPNP$_{12\text{-}15}$).*

At high RAFT agent concentration, the polymer chains grow slowly in solution and for much longer periods short and soluble polymer chains will be in reaction mixture. Once particle nucleation occurred the particle nuclei can grow primarily via the monomer/oligomer capturing method, producing smooth particles upon monomer/polymer desolvation (Figure 8B). As the RAFT concentration decreases, the polymer chains grow to higher molecular weights and faster. Not only can oligomer capturing occur, but flocculation starts occurring among oligomers,

producing new particle nuclei. As a result, nuclei can flocculate onto initial nuclei, producing grainy particles (Figure 8D). When no RAFT is added, no control over polymerization is exerted, polymer chains grow fast and more chains are present, flocculation among oligomers and entropic desolvation produce popcorn-shaped particles (Figure 8E).

Insight into the consumption and availability of RAFT-agent during particle synthesis was gained from this work. An interesting observation was made while using RAFT-agent in that new nuclei are formed via a secondary nucleation process (Figure 9). As the RAFT concentration increased, the time after which the bimodality in size was observed increased as well. This can be attributed to the reduced rate at which polymerization occurs. Increasing the RAFT-agent concentration delays the onset of secondary nucleation. To obtain information on the particle growth mechanism, EDX was used to analyze the second-generation particles.

It was found that the second-generation particles had 0 wt% sulfur (RAFT-agent) present on the surface whereas the larger particles had 0.52 wt% S present. 0.6 wt% S is expected if one assumes that all the RAFT-agent is used in the initial polymerization reaction and is present on/in the particle. In a study by Paine *et al.* it was shown that smaller particles capture oligomers more efficiently when compared to larger particles because of their greater surface area per unit of volume.[18] In our case, the formation of second generation particles free of RAFT-agent potentially indicate and agree with previous findings that the larger particles less effectively capture new monomers/ oligomers compared to new particle nuclei formed. Due to the slow capturing of oligomers from solution, excess oligomers in solution are entropically desolvated, forming new nuclei. This confirms that newly formed oligomers would rather flocculate and crosslink instead of being captured onto larger primary particles and follow enthalpic desolvation. The particles free of RAFT agent can be explained by that the RAFT moiety is consumed and bound to the original particles and there is no mobility of RAFT agent, once the original RAFT-particles are formed and new particles are formed, by default they would not contain RAFT agent.

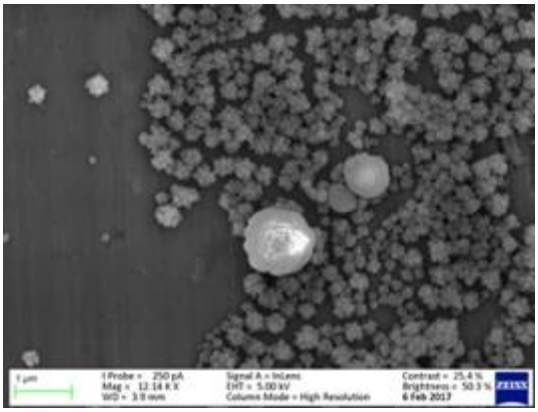

Figure 10: *SEM image of bimodality occurring in particle synthesis using 3.70 mol·L^{-1}RAFT-agent and a RAFT:AIBN ratio of 1:0.1. Larger particles are observed, with smaller particles in the background with popcorn-shaped morphologies.*

It can thus be concluded that the presence of RAFT agent and RAFT concentration influences the preferred method of particle growth, either by capturing oligomers (smooth particles) at higher RAFT concentrations compared to flocculation of oligomers (popcorn-shaped particles) at lower RAFT concentrations. These observations reinforce the proposal that these PNPs form and grow by complex mechanisms, but that the preferred method is tunable depending on the experimental conditions.

Amount of accessible MAnh

In this experiment, the amount of accessible MAnh on the particles are calculated. The smaller particles, popcorn-shaped morphology, made using no RAFT addition is used. The reason these particles are used is that in the following work, smaller particles are used. Up to 70 mol% of MAnh units were shown to be accessible (Figure 11). When a 0.7 mol ratio of DMAPA to MAnh is added, left to react and the supernatant analyzed, no DMAPA peaks are detected on NMR. Adding 0.8 mol ratio DMAPA to MAnh, small peaks, indicative of DMAPA, start appearing. This indicates that although we have highly crosslinked particles, we are able to access up to 70% of the reactive MAnh moieties, which seems to indicate that the particles made using no RAFT (popcorn-shaped) are highly porous and highly functional for post-polymerization modification reactions.

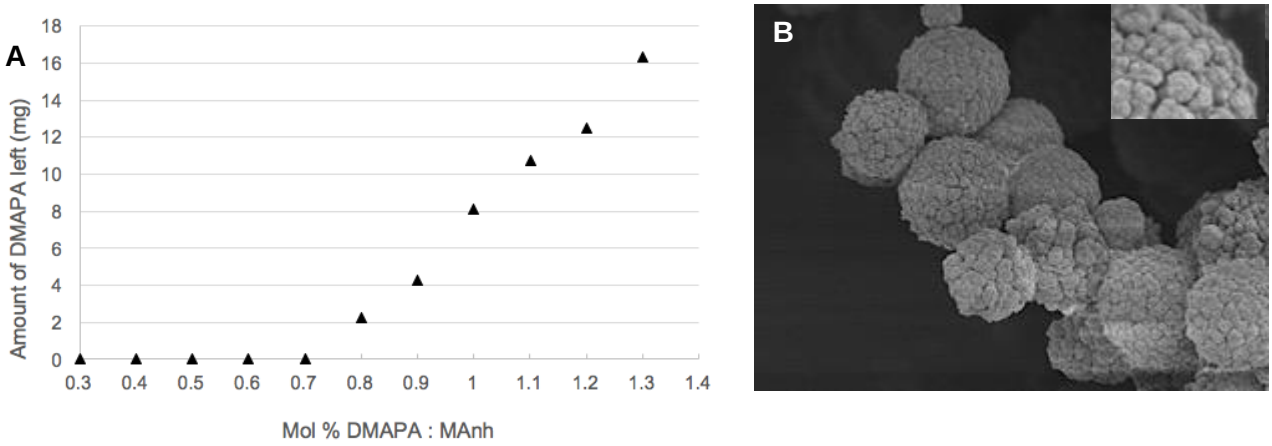

Figure 11: *A) Unreacted DMAPA as a functional of mol% DMAPA:MAnh is shown. B) SEM image of the porous MAnh-FPNPs used for the experiment.*

Conclusion

In this chapter, we have shown that we can utilize two different particle growth mechanisms, either separate on in combination to control particle size and morphology. Parameters that were

investigated in terms of their effect on particle size and morphology were monomer feed rate, crosslinker-, RAFT- and monomer concentrations.

With that we presented a facile technique for the preparation of well controlled and tunable MAnh-FPNPs, based on highly-crosslinked poly(styrene-*co*-maleic anhydride-*co*-divinylbenzene) particles. The novel and functional MAnh-FPNPs are prepared using a surfactant-free dispersion polymerization method, having surface functional groups that can be further functionalized for specific and various applications.

Fully crosslinked MAnh-FPNPs composed of varying crosslinker concentrations (18-30 mole%) and a monomer concentration of 0.606 mol·L^{-1} gave the most stable particles without any particle coagulation via the surfactant-free dispersion polymerization. This polymerization technique, compared to those in the literature, is relatively quick.

It was found that by controlling various parameters, the size and morphology of the particles can be tuned. A balance exists between particle nucleation and growth, which determines the particle size, size distribution and surface morphology.

References

(1) Murcia, M. J.; Naumann, C. A. Biofunctionalization of Fluorescent Nanoparticles. In N*anotechnologies for the Life Sciences*, 1st Ed; Kumar, CSSR, Ed.; Wiley-VCH: Weinheim, Germany, **2005**, 1, 1–40.

(2) Rao, J.P.; Geckeler, K.E. Polymer Nanoparticles: Preparation Techniques and Size-Control Parameters. *Prog. Polym. Sci.* **2011**, *36* (7), 887–913.

(3) Ugelstad, J.; Berge, A.; Ellingsen, T.; Schmid, R.; Nilsen, T. N.; Mork, P. C.; Stenstad, P.; Hornes, E.; Olsvik, O. Preparation and Application of New Monosized Polymer Particles. *Prog. Polym. Sci.* **1992**, *17* (1), 87–161.

(4) Nagavarma, B. V. N.; Yadav, H. K. S.; Ayaz, A.; Vasudha, L. S.; Shivakumar, H. G. Different Techniques for Preparation of Polymeric Nanoparticles - A Review. *Asian. J. Pharm. Clin. Res.* **2012**, *5* (3), 16–23.

(5) He, J.; Chen, D.; Fan, X.; Wang, L.; Deng, J.; Yang, W. Reactive Poly(Divinylbenzene- Co -Maleic Anhydride) Nanoparticles : Preparation and Characterization. *Chinese Chem. Lett.* **2013**, *24*, 970–974.

(6) Ganeva, D. E.; Sprong, E.; De Bruyn, H.; Warr, G. G.; Such, C. H.; Hawkett, B. S. Particle Formation in Ab Initio RAFT Mediated Emulsion Polymerization Systems. *Macromolecules* **2007**, *40* (17), 6181–6189.

(7) Link, A.; Pridgen, E.; Molnar, L. K.; Farokhzad. Factors Affecting the Clearance and Biodistribution of Polymeric Nanoparticles. *Mol. Pharm.* **2015**, *5* (4), 505–515.

(8) Engelhardt, N.; Ernst, A.; Kampmann, A.L.; Weberskirch, R. Synthesis and Characterization of Surface Functional Polymer Nanoparticles by a Bottom-Up Approach from Tailor-Made Amphiphilic Block Copolymers. *Macromol. Chem. Phys.* **2013**, *214* (24), 2783–2791.

(9) Nagarwal, R. C.; Kant, S.; Singh, P. N.; Maiti, P.; Pandit, J. K. Polymeric Nanoparticulate System: A Potential Approach for Ocular Drug Delivery. *J. Control. Release.* **2009**, *136* (1), 2–13.

(10) Lok, P. K.; Ober, C. K. Particle Size Control in Dispersion Polymerization of Polystyrene. *Can. J.*

Chem. **1985**, *63* (7), 209–216.

(11) Zetterlund, P. B.; Kagawa, Y.; Okubo, M. Controlled/Living Radical Polymerization in Dispersed Systems. *Chem. Rev.* **2008**, *108* (9), 3747–3794.

(12) Frank, R. S.; Downey, J. S.; Yu, K.; Sto, H. D. H. Poly(Divinylbenzene-Alt-Maleic Anhydride) Microgels : Intermediates to Microspheres and Macrogels in Crosslinking Copolymerization. *Macromolecules* **2002**, 35(7), 2728–2735.

(13) Downey, J. S.; Frank, R. S.; Li, W.; Stöver, H. D. H. Growth Mechanism of Poly(Divinylbenzene) Microspheres in Precipitation Polymerization. *Macromolecules* **1999**, *32*, 2838–2844.

(14) Yang, S.; Shim, S. E.; Lee, H.; Kim, G. P.; Choe, S. Size and Uniformity Variation of Poly(MMA-Co-DVB) Particles upon Precipitation Polymerization. *Macromol. Res.* **2004**, *12* (5), 519–527.

(15) Hattori, M.; Sudol, E. D.; El-aasser, M. S. Highly Crosslinked Polymer Particles by Dispersion Polymerization. *J. Appl. Polym. Sci.* **1993**, *50* (11), 2027–2034.

(16) Ober, C. K.; Lok, K. P. Formation of Large Monodisperse Copolymer Particles by Dispersion Polymerization. *Macromolecules* **1987**, *20* (2), 268–273.

(17) Paine, A. J.; Luymes, W.; McNulty, J. Dispersion Polymerization of Styrene in Polar Solvents. 6. Influence of Reaction Parameters on Particle Size and Molecular Weight in Poly(N-Vinylpyrrolidone)-Stabilized Reactions. *Macromolecules* **1990**, *23*, 3104–3109.

(18) Paine, A. J. Dispersion Polymerization of Styrene in Polar Solvents. Simple Mechanistic Model To Predict Particle Size. *Macromolecules* **1990**, *23* (12), 3109–3117.

(19) He, J.; Chen, D.; Han, K.; Huang, X.; Wang, L.; Deng, J.; Yang, W. Poly(Divinylbenzene-Alt-Maleic Anhydride) Nanoparticles as a Novel Stabilizer for Pickering Polymerization of Styrene. *J. Polym. Sci. Part A Polym. Chem.* **2014**, *52* (20), 2894–2898.

(20) Frank, R. S.; Downey, J. S.; Yu, K.; Stöver, H. D. H. Poly(Divinylbenzene-Alt-Maleic Anhydride) Microgels: Intermediates to Microspheres and Macrogels in Crosslinking Copolymerization. *Macromolecules* **2002**, *35* (7), 2728–2735.

(21) Okay, O. Porous Maleic Anhydride-Styrene-Divinylbenzene Copolymer Beads. *J. Appl. Polym. Sci.* **1987**, *34*, 307–317.

(22) Ogawa, N.; Honmyo, K.; Harada, K.; Sugii, A. Preparation of Spherical Polymer Beads of Maleic Anhydride-Styrene-Divinylbenzene and Metal Sorption of Its Derivatives. *J. Appl. Polym. Sci.* **1984**, *29*, 2851–2856.

(23) Pande, C. S.; Gupta, N. Copoly(styrene-Divinylbenzene)-G-Poly(maleic Anhydride-Styrene): Preparation Through Radiation Induced Grafting and Application in Organic Synthesis. *Polymer (Guildf).* **1997**, *66*, 847–852.

(24) Downey, J. S.; Frank, R. S.; Li, W. H.; Stöver, H. D. H. Growth Mechanism of Poly(divinylbenzene) Microspheres in Precipitation Polymerization. *Macromolecules.* **1999**, *32* (9), 2838–2844.

(25) Naka, Y.; Yamamoto, Y. Preparation of Microspheres by Radiation-induced Polymerization. II. Mechanism of Microsphere growth. *J. Polym. Sci., Part A. Polym. Chem.* **1992**, *30*, 1287–1298.

(26) Shim, S. E.; Yang, S.; Choi, H. H.; Choe, S. Fully Crosslinked Poly(Styrene-Co-Divinylbenzene) Microspheres by Precipitation Polymerization and Their Superior Thermal Properties. *J. Polym. Sci. Part A. Polym. Chem.* **2004**, *42*, 835–845.

(27) Shim, S. E.; Yang, S.; Jin, M. J.; Chang, Y. H.; Choe, S. Effect of the Polymerization Parameters on the Morphology and Spherical Particle Size of Poly(Styrene-co-Divinylbenzene) Prepared by Precipitation Polymerization. *Colloid Polym. Sci.* **2004**, *283* (1), 41–48.

(28) Lu, A.; Smart, T. P.; Epps, T. H.; Longbottom, D. A.; O'Reilly, R. K. L-proline Functionalized Polymers Prepared by RAFT Polymerization and their Assemblies as Supported Organocatalysts. *Macromolecules*. **2011**, *44* (18), 7233-7241.

CHAPTER 4

Auto-fluorescence of functional polymeric nanoparticles and cellular uptake

In this chapter the auto-fluorescent properties of the FPNPs are characterized and preliminary cellular uptake studies are conducted.

Auto-fluorescent polymeric nanoparticles: Synthesis, characterization and cellular uptake.

Abstract

In this chapter, we characterize and demonstrate the auto-fluorescence (AF) of novel highly crosslinked functional poly(styrene-*co*-maleic anhydride-*co*-divinylbenzene) polymeric nanoparticles (MAnh-FPNPs), and the uptake of these MAnh-FPNPs by human umbilical vein endothelial cells (HUVECs) and primary human monocytic cells. MAnh-FPNPs were prepared by a surfactant-free dispersion polymerization technique, in a solvent mixture of MEK and heptane with 2,2'-azo-bis(isobutyronitrile) (AIBN) as initiator and butane-1-phenylethyl trithiocarbonate (BPT) as chain transfer agent (RAFT agent). Spherical nanoparticles with smooth and popcorn-shaped morphologies were obtained containing reactive maleic anhydride moieties available for further introduction of functionality. The MAnh-FPNPs were internalized spontaneously by living cells, showing high signal-to-noise ratios using confocal fluorescence microscopy (CFM) and no significant cytotoxicity. Scanning electron microscopy (SEM) and Fourier-transform infrared spectroscopy (FTIR) studies were used to characterize the particles.

Introduction

Fluorescent materials are attractive for academic research and have many viable applications in drug delivery,[1,2] protein and chemical sensors,[3–6] DNA probing,[7] and cellular bioimaging[8]. Fluorescence stems from the absorption of light (UV) at a specific wavelength and the subsequent emittance of that light at a longer wavelength. The process is three-fold: 1) excitation of a molecule from a lower energy level to a higher energy level, 2) the conversion and vibrational relaxation of the excited state electrons to the lowest energy level, and 3) the emission of a longer wavelength photon causing the return of the molecule to the ground state. There are a few scenarios that will cause a molecule to lose fluorescence: 1) if the highly reactive excited state molecule is photo-bleached (destruction), 2) if the excited state energy is dissipated via non-radiative pathways, 3) if the molecule collides with another molecule and energy is transferred (quenched), or 4) if intersystem crossing occurs.[9,10] Traditional fluorescent molecules, having planar structures, are studied in dilute solutions, where abundant solvent molecules impede the intermolecular reactions between luminophore molecules, so no "concentration quenching" occurs.[11,12] This "concentration quenching" happens because of intermolecular interactions (π−π stacking interactions among the neighbouring molecules),

allowing excited states of the aggregates to decay via non-radiative pathways, also known as aggregation-caused quenching (ACQ). Such ACQ fluorescent materials (ACQphore) are highly emissive in solution, but non-emissive in their aggregated or condensed states.[13–20]

Traditional fluorescent materials are often quantum dots, fluorescent organic dyes, and fluorescent proteins, containing either heterocyclic or benzene groups (planar geometry). Carbon-carbon double bonds are the main building blocks, with phenyl rings (benzene or heterocyclic) forming π-aromaticity.[21] Alongside the conventional carbon-carbon double bonds, heteroatom-containing bonds such as C=O, N=O, C=N, C=S and N=N, are found to be detrimental to light emission, however they are less frequently investigated.[21,22] Fluorescence within polymers is still not completely understood, although it has been shown that a more rigid environment, prevent excitons from relaxing through non-radiative pathways, causing fluorescence.[23,24]

In 2001, Tang and co-workers discovered an opposite phenomenon to the notorious ACQ effect. Small organic and polymeric fluorescent materials, with nonplanar structures, displayed strong emissions, once aggregated; these materials are known as aggregation-induced emission (AIE) fluorescent materials (AIEgens).[25] AIEgens are non-fluorescent when molecularly dissolved in a good solvent, but highly emissive once aggregated. The conformation of the structure, once aggregated, hampers π−π stacking interactions between different AIEgens. The intrinsic mechanisms of the AIE effect is due to restriction of intramolecular rotations (RIR) (RIR is the restriction of the rotation about a single bond within a molecule) and blocking of non-radiative pathways, which results in fluorescence.

This property of AIEgens provides a new platform for fluorescent molecules and nanoaggregates.[25,26] Chromophore aggregation generally exerts one of two different effects, either ACQ or AIE. The effect that prevails is highly dependent on the chromophore structure and packing interactions in a particular system.[25] If the structure allows intramolecular rotations, the rotations consume the excited-state energy through a non-radiative relaxation channel. As a result, the fluorescence is quenched. However, if a structure is aggregated, the π−π stacking interactions are prevented and the intramolecular rotations are restricted, the non-radiative relaxation that enable the excitons to decay will be blocked, causing fluorescence. [25,27–32] It is generally accepted that the more rigid a chromophore structure is, the stronger its emission will be.[21,32]

Alongside inorganic NPs, PNPs are promising platforms for the design of multifunctional probes for imaging, diagnostics and drug-, gene- and vaccine delivery.[33,34–36] Fluorescent polymeric nanoparticles are attractive candidates to overcome some of the limitations related to inorganic NPs,[33] with PNPs exhibiting properties that allow them to be used in various applications, depending which polymer is chosen (Chapter 2). In order for FPNPs to be suitable fluorescent probes, they must have certain properties, such as high colloidal stability, uniform particle size and narrow size distribution, and no toxicity or leakage of fluorescence.[11,37]

The auto-fluorescence (AF) of materials allows the structures of interest to be illuminated, and serve as useful diagnostic indicators. Confocal fluorescence microscopy (CFM) customarily needs nanoparticles to be labelled with fluorescent probes for visualization obtained through the encapsulation of a label-bearing probe, modifying the polymer with a fluorescent probe or copolymerization using a fluorescent monomer.[36–39] Drawbacks related to these techniques include the need of multiple steps, the fact that information regarding the location of the labelling probe needs to be known, leaching of the fluorescent probe, the incorporation of fluorescent probes could lead to misinterpreted results, and changing original experimental parameters.

The benefit one would have of AF PNPs is that none of the drawbacks play a role, and the surface of the PNP is still available for further functionalization. Benefits of such a system would include a) AF particles do not need to be labelled with a fluorescent marker, b) leaching of an encapsulated dye is prevented as the AF is an inherent property of the nanoparticle and c) the surface of these particles can be tuned to interact with specific proteins or with specific epitopes in a bio-system or environment.

To the best of our knowledge, we are the first to report the AF property of highly crosslinked poly(styrene-*co*-maleic anhydride-*co*-divinylbenzene) FPNPs. Thus, we firstly wanted to characterize the AF and secondly evaluate the effect of various experimental parameters on the intensity of the AF to hopefully understand the origin of the AF within our polymer system. In addition, the MAnh-FPNPs not only showed to be AF, but the reactive maleic anhydride also contributes to extra reactivity making the particles highly functional and fluorescent FPNPs (AF FPNPs) simultaneously. These AF MAnh-FPNPs can potentially be used as fluorescent probes in various applications, such as fiducial markers or to study cellular uptake mechanisms. In addition to the characterization of the auto-fluorescent properties, we considered the uptake by cells and visualization of the AF MAnh-FPNPs within cells.

Experimental Methods

Materials, maleic anhydride (MAnh) 99% (Sigma Aldrich, St. Louis, USA) was used after recrystallization from chloroform. Styrene 99.5% (Fluka chemicals, New Jersey, USA) was purified and stored over 4 Å molecular sieves, divinylbenzene (DVB) >99% (Sigma Aldrich) was used after the t-butylcatechol inhibitor was removed using a t-butylcatechol remover column and stored over 4 Å molecular sieves. Methyl ethyl ketone (MEK) ≥99.7% (Sigma-Aldrich) and *n*-heptane (Kimix, Cape Town, SA) were both distilled and kept over 4 Å molecular sieves at room temperature (RT). Double distilled deionized water, distilled in our lab, was used throughout the work. 2,2'-azo-bis(isobutyronitrile) (AIBN) (Riedel de Haen, New Jersey, USA) was recrystallized twice using methanol and dried under vacuum before use. Ethical clearance exemption for isolation of human primary monocytes from purposely donated blood was obtained from the Subcommittee C Human Research Ethics Committee (HREC) of Stellenbosch University (Reference # X15/05/013). Monocytes were isolated from buffy coat blood, obtained from the Western Province Blood Transfusion (WPBTS), by double gradient centrifugation as stipulated by Menck, K 2014. Monocytes were cultured for a total of 6 days in advanced Roswell Park Memorial Institute (RPMI) media (Life Technologies) containing 10% human serum (Sigma-Aldrich) and 1% penicillin/streptomycin (Sigma-Aldrich) in the presence of 50 ng/mL granulocyte monocyte colony-stimulating factor (GM-CSF) (Sigma-Aldrich), before 24 h polarization to M1 type macrophages with 50 ng/mL lipopolysaccharide from *E. coli* (LPS) (Sigma-Aldrich) and 20 ng/mL interferon gamma (Sigma-Aldrich). Human Umbilical Vein Endothelial Cells (HUVECs) were cultured in Endothelial Basal Media (EBM) containing 2% FBS, 0.4% Bovine Brain Extract (BBE), 0.1% human Epidermal Growth Factor (hEGF), 0.1% ascorbic acid, 0.1% GA (30 µg/mL gentamicin and 15 µg/mL amphotericin) and 0.1% hydrocortisone, all acquired from Lonza. Mouse Embryonic Fibroblasts (MEF) and Human Embryonic Kidney Cells (HEK 293) were cultured in Dulbecco's Modified Eagle's Medium (DMEM) (Life Technologies) containing 10% Fetal Bovine Serum (FBS) and 1% penicillin/streptomycin (Sigma-Aldrich). Cell lines were kept at normal culture conditions and washed with phosphate buffered saline (PBS) (Sigma-Aldrich) before every media change. All cell cultures were used at passage number <10.

Synthesis

BPT RAFT agent was synthesized according to Lu et *al.*, with the synthesis described in Chapter 3.[56]

FPNPs. MAnh-FPNPs were synthesized according to Chapter 3 with some small changes. The RAFT-particles follows the following dispersion polymerization: maleic anhydride (MAnh) (2.04 g, 20.80 mmol) was dissolved in 15 mL of MEK in a 250 mL three neck round bottom flask. AIBN (3 mg, 0.02 mmol) and butane-1-phenylethyl trithiocarbonate (BPT) as RAFT-agent (15.9 mg, 0.06 mmol) was added to the reaction mixture. The reaction mixture was degassed for 20 minutes. In a separate pear-shape flask 22.5 mL *n*-heptane was added with styrene (0.74 mL, 6.49 mmol) and DVB (0.98 mL, 6.90 mmol) and degassed for 20 min. Under argon gas, the *n*-heptane solution with the two monomers was transferred into a syringe and placed in a syringe pump. After the MEK solution was degassed, the solution was placed in a 70 °C preheated oil bath. After 10 minutes, the *n*-heptane solution was introduced to the MAnh solution over a 2-hour addition period. The reaction was stopped after the 2 hours.

Modification of FPNPs. MAnh-FPNPs were further functionalized two-fold for the AF testing. For the first modification, the MAnh-FPNPs were hydrolyzed via the ring opening of the maleic anhydride. Hydrolysis took place in 0.5 M NaOH. After ring opening, the solution was neutralized to pH 7 to ensure protonation of the ring opened maleic acid obtaining ring opened MAnh-FPNPs. For the second modification, the maleic anhydride was modified with excess *N*, *N*-dimethyl-3-aminopropyl-1-amine (DMAPA) that attack at the MAnh via a nucleophilic substation reaction that follows a ring closure reaction obtaining DMAPA-

FPNPs modified particles. MAnh-FPNPs (100 mg, 0.299 mmol MAnh) were redispersed in DMF (10 mL). DMAPA was used in 1:1.5 excess to ensure all possible MAnh groups were reacted. DMAPA (45.86 mg, 0.448 mmol) was dissolved in DMF (2 mL), slowly added dropwise to the particle mixture, reacted and refluxed at 160 ºC for 4 hours to ensure ring closure of the maleimide rings. After the reaction, the particles were centrifuged to isolate poly(St-*co*-DMAP maleimide-*co*-DVB) PNPs (DMAPA-FPNPs) and washed with clean DMF to get rid of unreacted DMAPA. The particles were dried under vacuum to ensure all solvent was removed.

Characterization and analysis

Electron microscopy. The diameter and size distribution of the MAnh-FPNPs were determined using a field emission scanning electron microscope (FEG-SEM, Zeiss, Merlin), with a Gemini column, equipped with an inlens-, backscatter-detector coupled with EDX. To obtain the image, the particles were dispersed and placed on a conductive material and coated with carbon to establish conductivity. The high-resolution images were taken operating the instrument at 5 kV beam energy with an iprobe current of 250 pA, a working distance of 3.5 – 4.1 mm and an inlens detector. The images were processed using ImageJ software analyzing 100 measurements per image to get the average particle size and size distribution.

Confocal fluorescence microscopy (CFM) was conducted using a Carl Zeiss LSM780 Elyra S1 (Carl Zeiss, Germany) confocal microscope using the diode 405 nm CW/PS (pulsed) laser, argon multiline laser 25mW 488 nm, 514 nm and the 561 nm laser, alongside the 561 nm and 633 nm lasers. For post processing ZEN 2011 imaging software (Carl Zeiss (Germany) was used. FPNPs (after washing and complete drying) were dispersed in THF and imaged using a 100x objective. For the comparison of AF, six equally sized regions of interest (ROI) were taken in each sample. Upon irradiation at a wavelength of 405 nm for excitation, there was significant AF from the MAnh-FPNPs particles, and this wavelength was used to compare the AF from the various modified FPNPs. The AF is given as a relative mean fluorescent intensity (RMFIs) value. RMFIs are scaled units of fluorescence.[58] The images are stored as 16-bit images, varying in shades of grey. The brightness of each pixel is divided into a range from 0 to 243, with 0 being black and 243 being the brightest intensity. The RMFIs (a.u) within that range was taken and AF compared.[40]

Cytotoxicity analysis. The cytotoxicity of the MAnh-FPNPs was determined using the XTT assay, measuring the mitochondrial reductive capacity (as indirect measure of cell viability) on primary human isolated monocytes, differentiated into M1 type macrophages. Before the XTT assay, the particles were dialyzed for 3 days, changing the distilled water phase every 12 hours, to ensure that all monomers and unreacted compounds are removed. The particles were sonicated to avoid particle aggregation, centrifuged and dispersed into fresh RPMI 1640 culture media. Cells were seeded at $6x10^3$ cells/well. Cells were treated with RPMI containing particles at concentrations of 10 µg/mL and 1000 µg/mL for 1h, 2h, 4h and 24h before viability assessment by XTT assay. Experiments were done in triplicates.[41]

Cellular uptake studies. Human umbilical vein endothelial cells (HUVECs) and primary human monocytic cells were cultured under normal tissue culture conditions at the Department of Physiological Sciences, Stellenbosch University. Human monocytic cell isolates were pre-differentiated into M1 type macrophages. Monocytes were cultured in RPMI 1640 (Life Technologies) containing 10% Human Serum (Sigma Aldrich) and 100 U/mL Penicillin-Streptomycin (Sigma Aldrich). Granulocyte Macrophage Colony-Stimulating Factor (GM-CSF, Sigma Aldrich) was supplemented at 50 ng/mL throughout the 6-day differentiation period. E. coli Lipopolysaccharide (LPS, Sigma Aldrich) and Interferon-gamma (IFN-γ, Sigma Aldrich) were supplemented during the last 24h of culture at 50 ng/mL and 20 ng/mL, respectively to ensure polarization into M1 type macrophages. The cells were seeded into 8 chamber-well slides,

containing appropriate culture media and seeding densities (RPMI and $6x10^5$ cells/well, respectively), to be assessed using high magnification confocal microscopy. The intracellular localization of the particles was confirmed by CFM (LSM780 confocal microscope with ELYRA S.1 Super resolution platform, Carl Zeiss, Germany). AF FPNPs was excited by the 405 nm laser light and detected in channel 1. For further imaging of the cell membrane, cells were stained with CellMask Orange (Life Technologies), for 10 minutes prior to imaging, which was excited by 561 nm laser light and detected in channel 2. The pH specific stain, pHrodo Bioparticles (Life Technologies) was also implemented to determine intracellular localization of AF FPNPs. These particles are relatively non-fluorescent at neutral pH, but fluoresce under acidic conditions (pH<6.5) after their uptake via phagocytosis and localization in mature phagosomes/endosomes. pHrodo was supplemented into cell culture, simultaneously with AF FPNPs, at 1 mg/mL. Further image processing was performed using GIMP 2.2.13 software. To standardize visualization settings for comparative purposes, the same tone curve for the channel was used for all images. Cells that were tested (HUVECs and macrophages) do not exhibit spontaneous fluorescence in the fluorescence emission range of 405 nm – 561 nm.

Results and discussion

Particle synthesis and characterization

The MAnh-FPNPs were previously synthesized and characterized, refer to Chapter 3. Previous studies have shown that particle size is one of the important properties that affect cellular uptake, with smaller particles, in general, having a higher uptake.[42,43] Unless otherwise stated, all experiments in this work were conducted using particles, with a particle size diameter of 140-200 nm and a narrow size distribution (Figure 1).

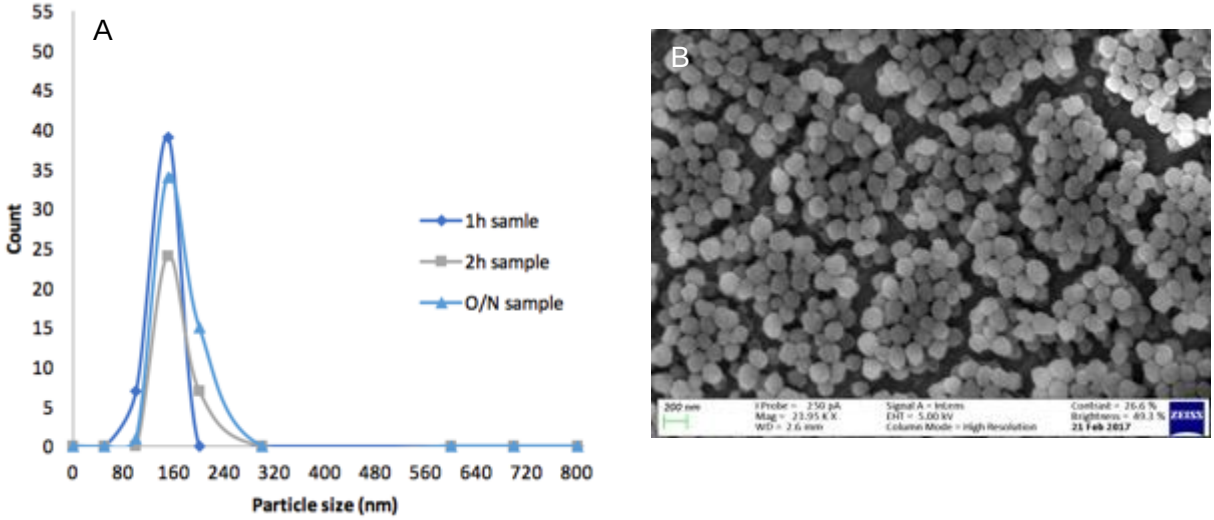

Figure 1: *A) Particle size distribution at various time intervals and B) SEM image of the MAnh-FPNPs synthesized by using surfactant-free dispersion polymerization of MAnh (20.80 mmol), St (6.49 mmol) and DVB (6.90 mmol) and AIBN (0.02 mmol) as initiator using a 2:3 MEK/Hept solvent system.*

AF of AF FPNPs

There are currently only a few reports on the AF of polymers, as most research regarding AF covers biological AF that is more commonly encountered.[21,24,44–46] The MAnh-FPNPs that were synthesized in this work were found to exhibit AF. The AF is an inherent property of the as synthesized MAnh-FPNPs. The AF of these MAnh-FPNPs was characterized using CFM in lambda scan (λ–scan) mode.[47] A lambda scan records a series of individual images covering the emission wavelength range, with each image detected at a specific emission wavelength.[48] This scan mode is used to determine AF where the spectrum is unknown. A region of interest in the x-y dimension is examined along a wavelength axis to determine how the pixel intensity and/ or colour changes due to signal level variations at different emission bands. Lasers with wavelengths of 405 nm, 458 nm, 488 nm, 514 nm, 561 nm and 633 nm were used for excitation. The obtained spectra indicated AF across the whole emission spectrum, using 405 nm, 458 nm and 488 nm (SI, Figure 1-3). For excitation with the 514 nm and 561 nm laser, AF decreases at longer wavelengths (SI, Figure 4-5) and the 633 nm laser induces very little AF (SI, Figure 6).

To determine the origin of the AF within our system, we firstly reverted to AF found in similar polymer structures in literature. It is known from literature that St and MAnh homopolymers exhibit AF.[21,45] Polystyrene is known to AF, although the orientation of the styrene units and the molecular weight governs the amount of excimer formation. Basile *et al.*[45] showed that shorter polystyrene chains have a higher probability of fluorescence being quenched and Birks *et al*. proposed that for excimers to form two aromatic side chains, need to lie parallel to each other at a distance of 3.5 Å.[49,50] MAnh homopolymer (PMAnh) emits a strong AF signal as shown by Tang *et al*.[21] PMAnh has shown to emit light due to the AIE effect, posing a rigid conformation due to bulky anhydride groups that also hinder the free rotation along the carbon-carbon single bonds, effectively: favouring the formation of carbonyl group-clusters; allowing intramolecular π-interactions; and giving rise to the AF as a result of UV excitation.[21,51] The same group developed AF copolymers lacking conventional fluorescent units. Tang *et al*. observed that the copolymerization of MAnh and vinyl acetate (VAc) in an alternating fashion results in a copolymer (poly(MAnh-*alt*-VAc or PMV)) that also exhibits strong light emissions and AIE effects attributed due to the intermolecular interactions between carbonyl groups within a polymer chain, allowing carbonyl groups to cluster and restrict the intramolecular rotation (RIR).[21] However, upon hydrolysis of the MAnh, the carbonyl groups can rotate freely, which leads to non-radiative relaxation and a decrease in AF. This indicated that a relatively rigid environment is indeed needed for the carbonyl groups to interact, RIR and light to be emitted.

Interesting poly(St-*alt*-MAnh) (SMA) (M_w = 58,000 g/mol and ring closed) dissolved in THF does not show AF (Figure 2A). The lack of AF of SMA in THF solution is potentially due to the clustering of MAnh that in influenced or the phenyl rings associate close enough to cause non-radiative dissipation of the excited state by comparison to the PMV system. Now, it is reasonable to expect that the MAnh-FPNPs, with a molecular structure similar to SMA, having an additional crosslinker that causes highly crosslinking densities, little mobility and the rotational motions to be restricted will can the MAnh-FPNPs to become fluorescent.[21,16,52] It is also envisaged that within our highly crosslinked FPNP system, once the MAnh group is hydrolyzed, AF will still occur as rotation is still prevented due to the crosslinks still being present. This hypothesis is tested by the modification of the MAnh group as well as by varying the concentration of DVB crosslinker added.

Modification of MAnh moiety

Confirmation of the MAnh moiety not being responsible for AF in our system, but rather being

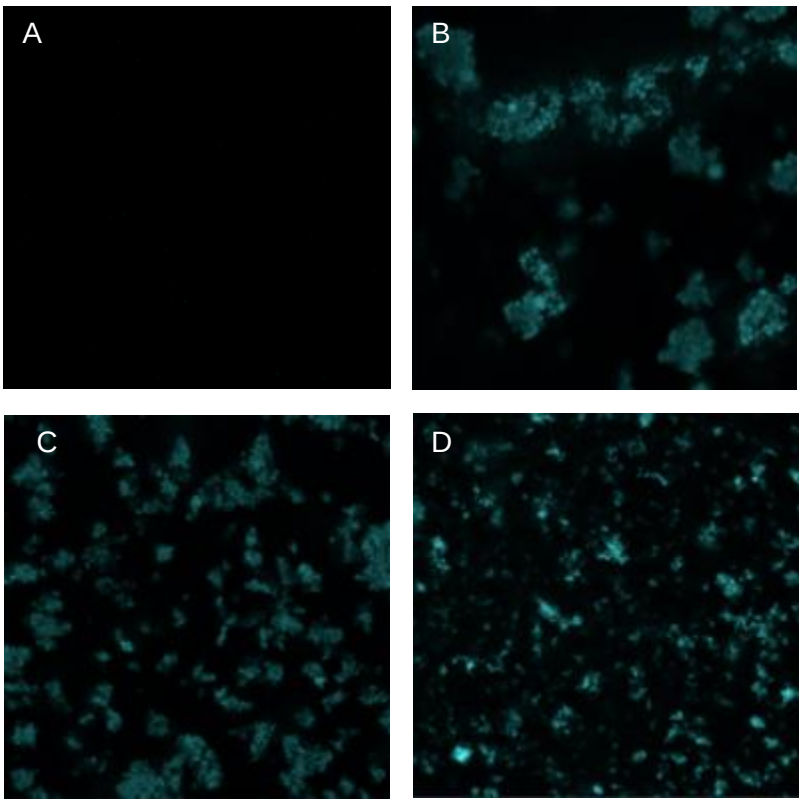

Figure 2: *CFM image indicating AF at 405 nm excitation of A) SMA, B) MAnh-FPNPs, C) hydrolyzed (ring opened MAnh-FPNPs) and D) DMAPA-FPNPs.*

due to the crosslinking nature (RIR), the AF MAnh-FPNPs (Figure 2B) were fully hydrolyzed and in a parallel experiment the MAnh-FPNPs were modified via a nucleophilic substitution reaction of DMAPA at the MAnh group on the particles. Both the hydrolyzed and DMAPA-modified particles still show AF (Figure 2C-D). The modification of the MAnh did not significantly alter the brightness of the AF, potentially indicating that the MAnh ring structure did not contribute to the AF of the MAnh-FPNPs, but rather the crosslinking nature (RIR effect) of the MAnh-FPNPs and that the AF is an inherent property of the MAnh-FPNPs regardless of further modification in the form of hydrolysis or amidation.

Effect of varying crosslinker concentration

The more rigid a structure and RIR within a polymer chains will lead to stronger emissions.[21,51] Crosslinking prevents chains from close packing (non-planar), RIR and makes the whole structure more rigid,[53,54] all in favour of emission induced by UV irradiation. Our system showed the same phenomena, as the fluorescence intensity markedly increases upon increasing the concentration of crosslinker (Figure 3); this effect is presumably due to the increased crosslink density, which decreases the internal rotation ability of the polymers, thus blocking the nonradiative relaxation channel. This causes MAnh-FPNPs to become emissive, following the same phenomena as aggregation induced emission (AIE).[18,25,53,54] At a lower crosslinking nature the low AF intensity can potentially be attributed to the lower crosslinking nature within the particles allowing swelling to occur and hence increasing the mobility of the chains that leads to the quenching of fluorescence.

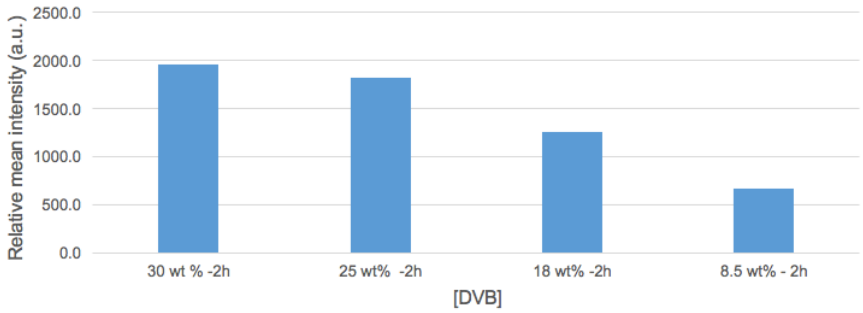

Figure 3: *AF as a function of varying crosslinker concentrations: 30 wt%, 25 wt%, 18 wt% and 8.5 wt% relative to total monomer concentration.*

By testing this hypothesis, we have shown that the hydrolysis of the MAnh group does not cause a decrease in AF, indicating that the rigidness is still intact and that contribute to the AF

nature of the MAnh-FPNPs. To fully understand the mechanism of AF within the MAnh-FPNPs, a much more in-depth analysis will be needed, but we have shown here that the introduction of DVB as crosslinker plays a pivotal role in the AF property.

Particle formation and morphology effects on AF property

Although the effect of morphology on AF are not yet understood, an interesting phenomenon is observed, *i.e*. the morphology of the particles affects the intensity of AF. We investigated parameters, such as RAFT-agent- and monomer concentration that influence particle morphology (Chapter 3), and the effect on AF. It was observed that the longer the reaction time, the more particles became unstable and coagulated (Figure 4B-D).

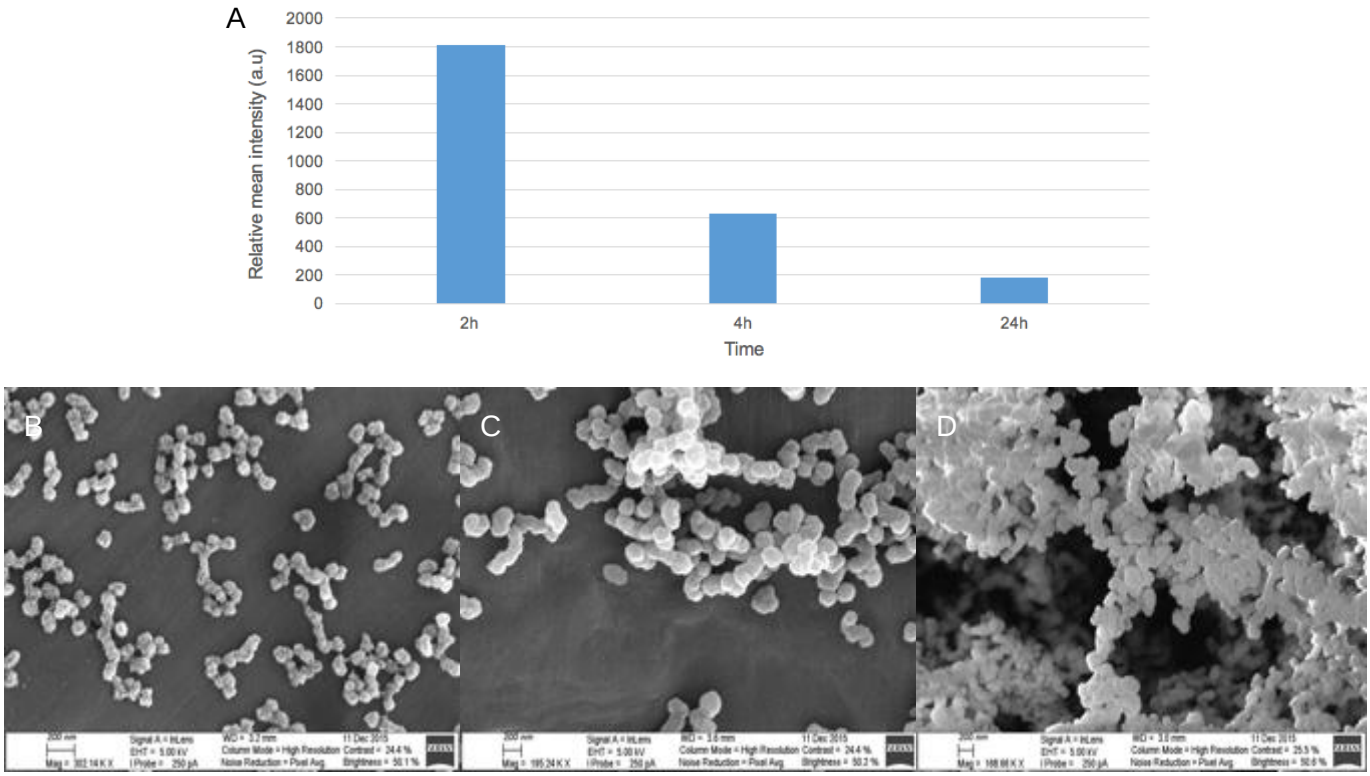

Figure 4: *AF as a function of time, at time intervals 2 hours, 4 hours and 24 hours. Particle samples taken at hourly intervals (e.g. 2h, 4h and 24 hours). SEM images at B) 2 hour, C) 4 hours and D) 24 hour time intervals.*

Although the nature of the polymer is virtually identical, one would expect little effect on the AF intensity, but we observed that there is almost no AF in coagulated MAnh-FPNPs compared to significant AF in well-defined MAnh-FPNPs (Figure 4A).

Another change in morphology was observed when the particles were synthesized using RAFT-agent. MAnh-FPNPs synthesized in the absence of RAFT-agent led to popcorn-shaped particles being obtained, and significant AF was observed (Figure 5B). In the presence of RAFT-agent, almost no AF is observed. Increasing the RAFT-agent concentration to 0.67 mol·L^{-1}, grainy particles are observed (Figure 5C), and to 3.70 mol·L^{-1}, smooth particles are observed (Figure 5D) with a drastic decrease in AF intensity (Figure 5A).

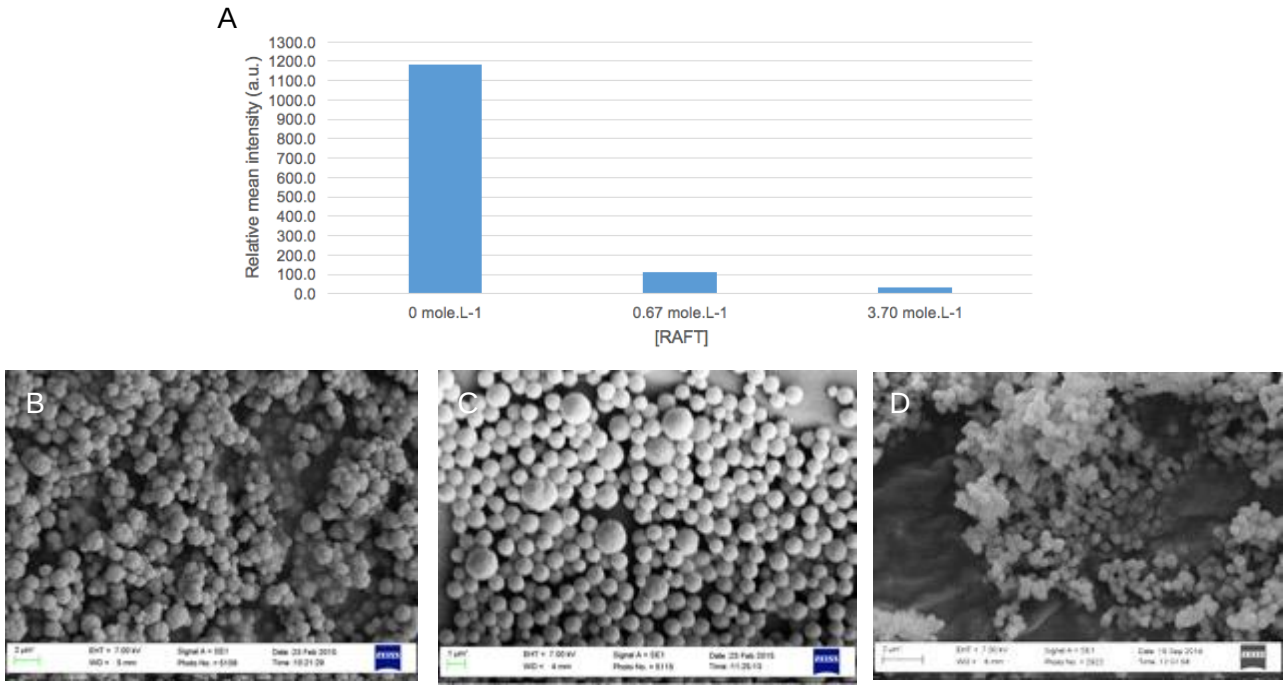

Figure 5: *AF is shown as a function of RAFT-agent concentration. SEM images at B) 0 mole.L^{-1} RAFT (popcorn-shaped, 2μm scale bar), B) 0.67 mole.L^{-1} RAFT (grainy, 1 μm scale bar) and C) 3.70 mole.L^{-1} RAFT (smooth, 1 μm scale bar).*

It must be noted that the introduction of RAFT agent not only changed morphology, but can also add to a chemical change in the system, that can influence the AF. We did however expect that the RAFT agent will not influence the AF property as the presence of RAFT agent should not interfere with crosslink density or the crosslinking nature (RIR of chains) to a large effect, but the results showed otherwise. The decrease of AF in the presence of RAFT-agent can potentially

be attributed to the process in which the chains grow in the presence of RAFT that changes in comparison to an experiment without RAFT-agent. For much longer time periods, there will be soluble and shorter polymer chains/oligomers in the reaction mixture that eventually lead to nucleation and particle growth, via monomer capturing (Chapter 3). Alongside the slower growth of polymer chains, the chains potentially have longer times to adopt a conformation of lower energy or packing that could influence the AF of the final particles.

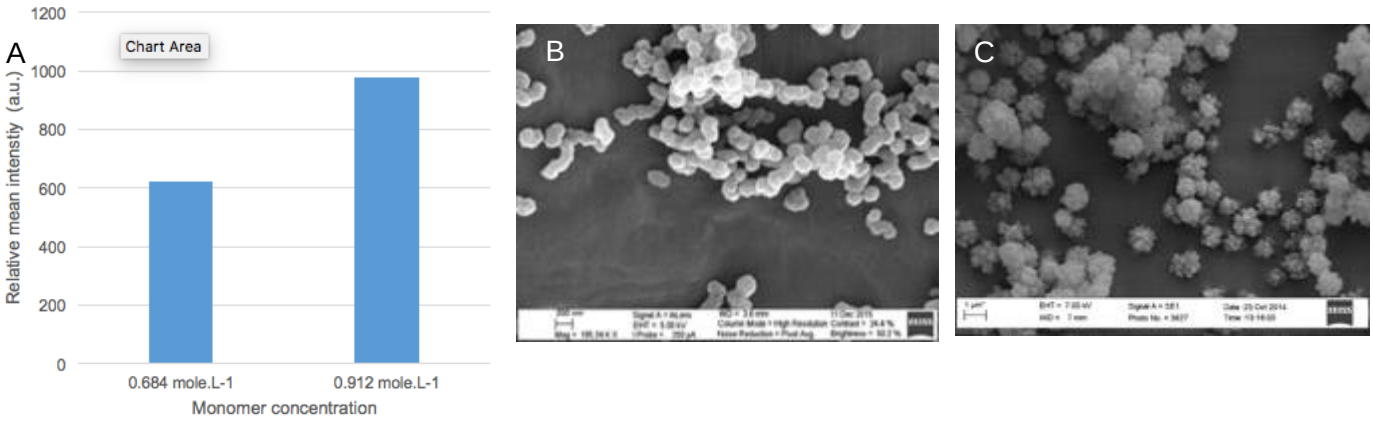

Figure 6: *AF shown as a function of monomer concentration. SEM images at B) 0.684 mol·L^{-1} monomer and C) 0.912 mol·L^{-1} monomer. The images also show the particle morphology changes from grainy to popcorn shaped.*

Particle morphology changed drastically with a change in monomer concentration. Two monomer concentrations were chosen; a higher monomer concentration (0.912 mol·L^{-1} monomer) that produced popcorn shaped particles (Figure 6B), that showed a significantly higher intensity AF compared to smooth particles synthesized using lower monomer concentrations (0.684 mol·L^{-1} monomer) (Figure 6C). The AF was shown to potentially stem from the role DVB plays in crosslinking that prevents chains of close packing (non-planar), RIR and making the whole structure more rigid, which corresponds well with literature.[53,54] Although it cannot be fully concluded yet, the AF also seems to be influenced by the nature of the polymer that is dependent on the experimental parameters while synthesizing the MAnh-FPNPs.

Cytotoxicity of MAnh-FPNPs

The feasibility was assessed of the use of AF MAnh-FPNPs as fluorescent probes or markers in biological contexts. The potential cytotoxicity of MAnh-FPNPs was tested against primary

human isolated monocytes, differentiated into M1 type macrophages. The XTT assay is an advanced version of MTT, whereby the mitochondrial activity is assessed, which is a sign of metabolic activity and therefor cell viability.

The relative cell viability (%), relative to control wells containing cell culture medium without nanoparticles, is expressed mathematically as follows and are a routine XTT assay[55] :

$$relative\ cell\ viability\ (\%) = \frac{Test492nm(cells/particles) - Control492nm(no\ cells/particles)}{Control492nm(no\ cells/particles) - Control\ 492nm(no\ cells/particles)}$$

Equation 1: *Equation to calculate the relative cell viability as a function of the control values.*

From these results, the introduction of AF MAnh-FPNPs at low concentrations (10 μg/mL) resulted in reduced mitochondrial activity over short time periods (1h, 2h, 4h) (Figure 7A). Whereas mitochondrial activity was significantly rescued (109%) during extended treatment with AF MAnh-FPNPs (24h) at the same concentration, compared to 1h ($p<0.01$), 2h ($p<0.05$) and 4h treatments ($p<0.01$).

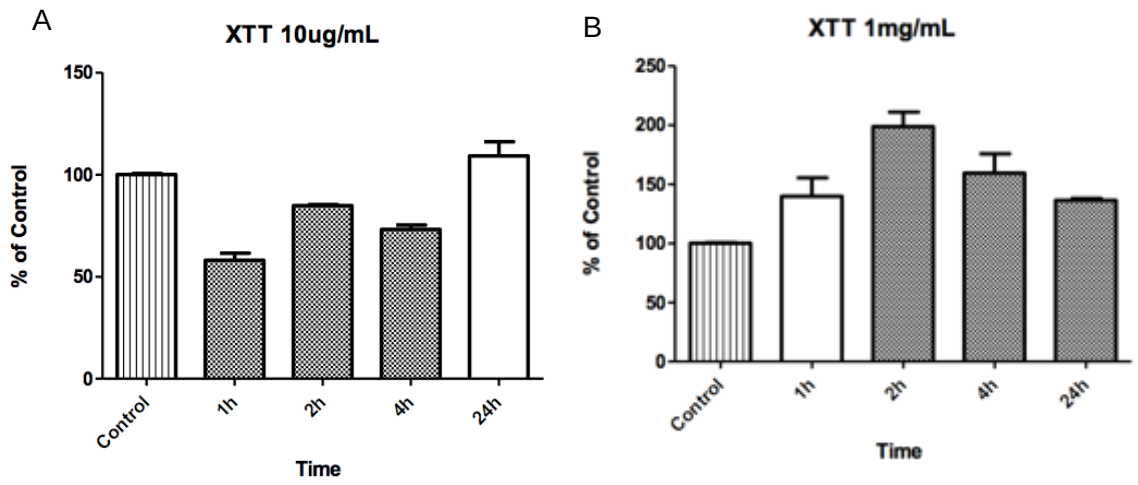

Figure 7*: Results of the XTT assay, showing the cytotoxic results for the Control, 10 μg/mL and 1 mg/mL experiments. Patterned bars showed a significant change compared to control ($p<0.05$). Bars with no pattern had no significant change when compared to control.*

A similar but inverse trend is observed under more concentrated conditions (1 mg/mL). Mitochondrial activity is significantly upregulated during short treatment periods when compared to control (2h $p<0.01$ and 4h $p<0.05$). Notwithstanding significant upregulation at 24h treatment compared to control ($p<0.0001$), a significant reduction is still observed when compared to the

earlier 2h ($p<0.01$) time point and this downward trend is also observed at 4h treatment, however nonsignificant compared to 24h (Figure 7B). Therefore, these novel, highly reactive AF MAnh-FPNPs are suitable for fluorescence microscopy studies to observe the uptake and localization of the functionalized particles. These assays where also done on mouse embryonic fibroblasts (MEFs) (SI Figure 7-8).

Cellular uptake of AF MAnh-FPNPs

Finally, to explore the applicability of these novel AF MAnh-FPNPs for fluorescent imaging as viable fiducial markers or probes, we incubated the AF MAnh-FPNPs with living cells and visualized the uptake of these particles using CFM. No extra fluorescent dyes had to be added to image the particle itself, as the particles exhibit auto-fluorescence. The AF MAnh-FPNPs can be used to study the intercellular distribution, co-localization and time it takes to internalize the particles.

MAnh-FPNPs interaction with monocyte cell (macrophages)

The uptake of AF MAnh-FPNPs was rapid, and already after 1 minute of incubation, the AF MAnh-FPNPs can be observed “lined up” on the cell membrane as bright blue spots (Figure 8A). For imaging of the cell membrane, cells were stained with CellMask Orange (Life Technologies). After 3 minutes, the particles appear clearly inside the cell as blue/green spots (Figure 8B). The particles that were seen on the cell membrane (Figure 8A) are now inside the cell (Figure 8B) alongside a slight intensity/colour change. After 6 minutes, the particles are fully

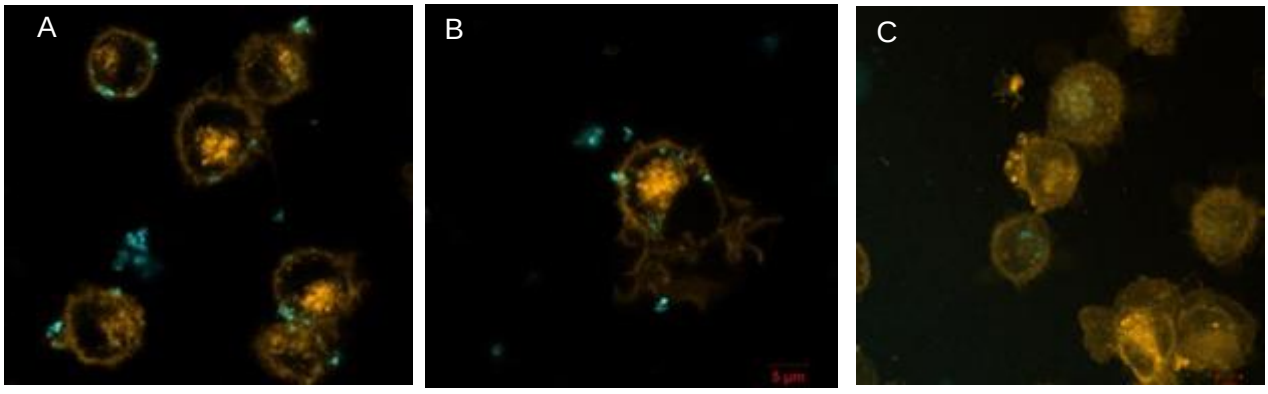

Figure 8: *AF FPNPs uptake by primary human macrophages. Image A) is taken after 1 min incubation, B) after 3 min and C) is a maximum intensity projection done on multiple stacks taken through the cell after 20 minutes of incubation.*

inside the cytosol particles (Figure 8C). This method clearly illustrates the location of particles inside host cells, as we focused on a certain plane, we observe the particles inside the cell in that specific plane.

After 20 minutes of incubation, all the nanoparticles were internalized, with no apparent detrimental effect on the host cells. Figure 8C is a composite image compiled from a series of 2D focus stacking images made by focusing up and down through the cells to acquire images at different planes though the cell, to provide a more comprehensive image of each cell, as can be evidenced for example by the relatively complete representation of the cell membrane, which can be seen as the 2D projection of the 3D structure instead of the usual ring-shape which is obtained in a single plane focus-image.[48]

MAnh-FPNPs interaction with HUVECs

Similar to the results in the macrophages, the uptake of AF MAnh-FPNPs by HUVECs was also rapid. The AF MAnh-FPNPs can be observed residing on the cell membrane (Figure 9A) as bright blue spots. After 3 minutes the particles are clearly observed within the cells as blue/ green spots (Figure 9B). The colour and intensity change is also apparent. After 20 minutes of incubation, the nanoparticles were internalized, again with no apparent negative effects on the host cells. Figure 9C is again a representative image of a HUVEC cell visualized by stacked images.

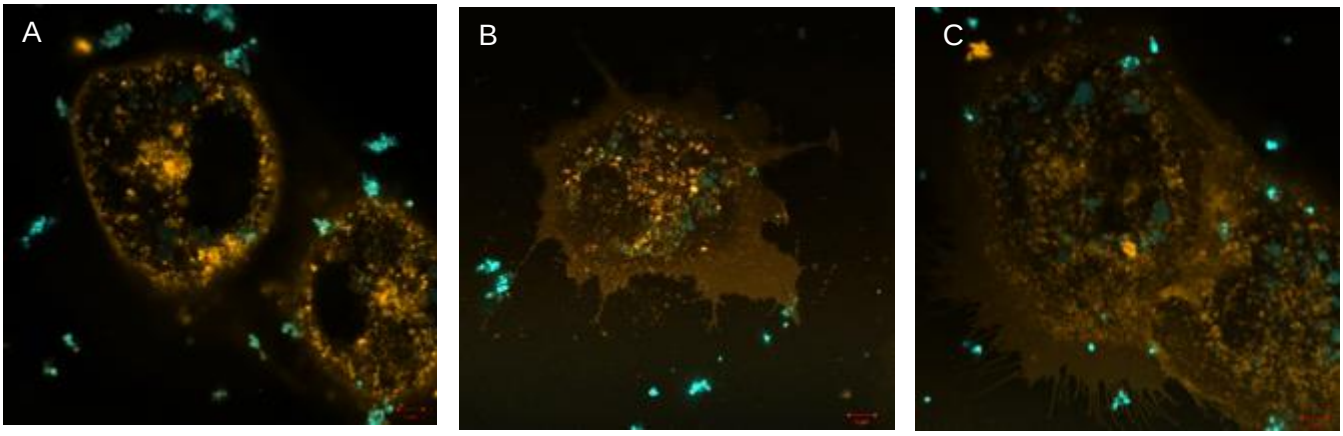

Figure 9: AF FPNPs uptake by HUVECs. Image A) are taken after 1 min incubation, B) 3 min and C) is a maximum intensity projection done on multiple stacks taken through the cell.

Current study design was not sufficient to conclusively confirm the mode of uptake; potential routes of uptake such as pinocytosis mediated by phosphoinositide 3-kinase (PI3K) and granulocyte-macrophage colony-stimulating factor (GM-CSF), as previously demonstrated[57] in a somewhat different context, would need confirmation by immunocytochemical assessments. As preliminary investigation into uptake route, the potential of particles to provoke a phagocytic response (in that the cells recognize the particles as foreign objects to break down or remove from the body) in professional phagocytes (primary human macrophages) was assessed by using pHrodo bioparticles to monitor the phagosomal acidification indicative of phagocyte maturation, which is normally seen after phagocytic engulfment of particles. pHrodo bioparticle (incorporated into standard particles) is relatively non-fluorescent at neutral pH, with exponential increased fluorescence in acidic environments (pH<6.5).

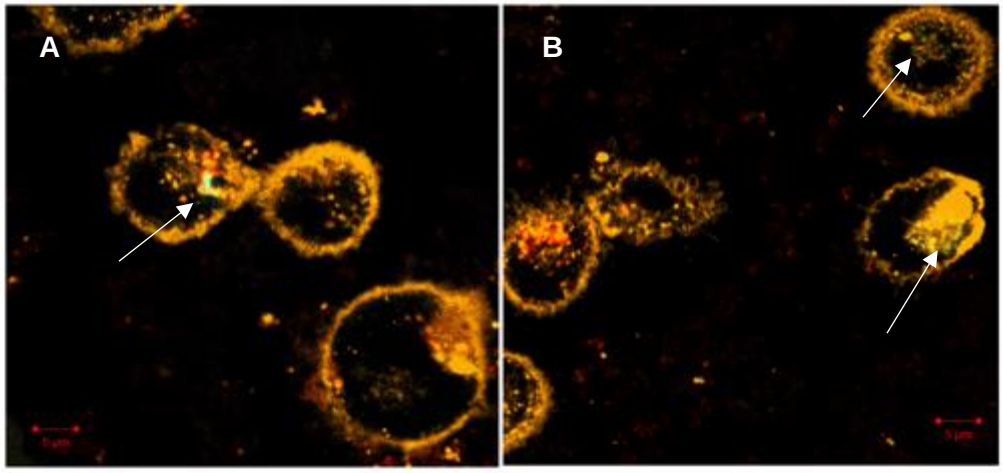

Figure 10: *AF FPNPs uptake by primary human macrophages in the presence of pHrodo particles. Co-localization of both the particles and dye would indicate a phagocytic engulfment. In both images co-localization is not observed.*

The co-localization of pHrodo (selected as red) and particles (blue) would thus indicate a phagocytic response of the cells to the particles. The fact that pHrodo dye and particles did not co-localize (Figure 10A-B) shows evidence counter to the idea of the particles eliciting a phagocytic response. Other uptake routes remain to be investigated.

Conclusions

We have characterized novel MAnh-FPNPs that show AF, which stems from the highly crosslinked nature of the particles, making the particles more rigid and inhibiting intramolecular rotation, both characteristics that allow fluorescence. Although it cannot be fully concluded yet,

the AF also seems to be influenced by the nature of the polymer that is dependent on the experimental parameters while synthesizing the MAnh-FPNPs.

As the fluorescent property is incorporated within the polymer backbone, no addition of a fluorescent marker is needed. Additional benefits of these novel AF MAnh-FPNPs are that they show a high level of colloidal stability, possess uniform particle size and narrow size distributions with no leakage of fluorescence.

Remarkably, despite the use of low particle concentrations, the signal obtained from the internalized particles was strong enough to obtain great signal-to-noise ratios, also suggesting the AF does not bleach or contaminate the surroundings. Moreover, these AF MAnh-FPNPs, in 10 µg/mL and 1000 µg/mL concentrations, showed no signs of cytotoxicity. It was shown that these MAnh-FPNPs are internalized within 2 minutes and do not provoke a phagocytic response in professional phagocytes (primary macrophages). This is indicative of the absence of an antigenic response toward the particles by macrophages, which is an indication for biocompatibility.

The AF MAnh-FPNPs could serve as useful probes in cell studies or fiducial markers for correlative microscopy, studying FPNP uptake, retention and distribution as the MAnh-FPNPs did not provoke a phagocytic response, and the particle size and morphology can be tuned. The particles can readily and easily be modified at the MAnh moiety, and hold the potential to introduce multiple functionalities on the surface.

References

(1) Zhang, W.; Xu, L.; Qin, J.; Yang, C. New Water-Soluble Cationic Poly(p-phenylenevinylene) Derivative: The Interaction with DNA and Selective Fluorescence Enhancement Induced by ssDNA. *Macromol. Rapid Commun.* **2013**, *34*, 442–446.

(2) Li, D.; Yu, J.; Xu, R. Mesoporous Silica Functionalized with an AIE Luminogen for Drug Delivery. *Chem. Commun.* **2011**, *47*, 11077–11079.

(3) Song, Z.; Hong, Y.;Kwok, R. T. K.;Lam, J. W. Y.; Liu. B.; Zhong, B. A Dual-Mode Fluorescence “turn-On” Biosensor Based on an Aggregation-Induced Emission Luminogen. *J. Mater. Chem. B.* **2014**, *2*, 1717–1723.

(4) Prodi, L.; Bolletta, F.; Montalti. M.; Zaccheroni, N. Luminescent Chemosensors for Transition Metal Ions. *Coord. Chem. Rev.* **2000**, *205*, 59–83.

(5) Wang, B.; Wasielewski, M. R. Design and Synthesis of Metal Ion-Recognition-Induced Conjugated Polymers: An Approach to Metal Ion Sensory Materials. *J. Am. Chem. Soc.* **1997**, *19*, 12–21.

(6) Keppler, A.; Pick, H.; Arrivoli, C. Labeling of Fusion Proteins with Synthetic Fluorophores in Live Cells. *Proc. Natl. Acad. Sci.* **2004**, *101*, 9955–9959.

(7) Dore, K.; Dubus, S.; Ho, H.; Levesque, I.; Bruntte, M.; Corbeil, G.; Boissinot, M.; Boivin, G.; Bergeron, M. G.; Boudreau D.; Leclerc, M. Fluorescent Polymeric Transducer for the Rapid,

Simple, and Specific Detection of Nucleic Acids at the Zeptomole Level. *J. Am. Chem. Soc.* **2004**, *126*, 4240–4244.

(8) Li, C. L.; Miao, X. D.; Wang, X. H.; Yu, J. H. Y. Fluorescent Polymeric Transducer for the Rapid, Simple, and Specific Detection of Nucleic Acids at the Zeptomole Level. *Chem. Commun.* **2013**, *49*, 9549–9551.

(9) Michael, W.D.; Herman, B.; Centonze Frohlich, V. E.; Lakowicz, J. R.; Murphy, D. B. Basic Concepts in Fluorescence. *Retrieved from https://micro.magnet.fsu.edu/primer/techniques/fluorescence/*.

(10) Dobrucki, J. Photobleaching. In *Handbook Of Biological Confocal Microscopy*. 3rd Ed. Pawley, J. B Ed. **2006**, 690–702.

(11) Wolfbeis, O. S. An Overview of Nanoparticles Commonly Used in Fluorescent Bioimaging. *Chem. Soc. Rev.* **2015**, *44*, 4743–4768.

(12) Ruedas-Rama, M. J.; Walters, J. D.; Orte, A.; Hall, E. H. Fluorescent Nanoparticles for Intracellular Sensing: A Review. *Anal. Chim. Acta.* **2012**, *751*, 1–23.

(13) Wu, J. H; Liou, G. S. High-Efficiency Fluorescent Polyimides Based on Locally Excited Triarylamine-Containing Dianhydride Moieties. *Polym. Chem.* **2015**, *6*, 5225– 5232.

(14) Jiang, B. P.; Guo, D. S.; Liu, Y. C. Photomodulated Fluorescence of Supramolecular Assemblies of Sulfonatocalixarenes and Tetraphenylethene. *ACS Nano.* **2014**, *8*, 1609–1618.

(15) Liu, L.; Wu, B.; Yu, P. Sub-20 Nm Nontoxic Aggregation-Induced Emission Micellar Fluorescent Light-up Probe for Highly Specific and Sensitive Mitochondrial Imaging of Hydrogen Sulfide. *Polym. Chem.,* **2015**, *6*, 5185–5189.

(16) Huang, S. H.; Chiang, Y. W.; Hong, J. L. Luminescent Polymers and Blends with Hydrogen Bond Interactions. *Polym. Chem.* **2015**, *6*, 497–508.

(17) Munkholm, C.; Parkinson, D. R.; Walt, D. R. Intramolecular Fluorescence Self-Quenching of Fluoresceinamine. *J. Am. Chem. Soc.* **1990**, *112*, 2608–2612.

(18) Dong, W.; Fei, T. Aggregation Induced Emission and Amplified Explosive Detection of Tetraphenylethylene-Substituted Polycarbazoles. *Polym. Chem.* **2014**, *5*, 4048– 4053.

(19) Belletete, M.; Bouchard, J.; Leclerc, M.; Durocher, G. Photophysics and Solvent-Induced Aggregation of 2, 7-Carbazole-Based Conjugated Polymers. *Macromolecules.* **2005**, *38*, 880–887.

(20) Jakubiak, R.; Collison, C. J.; Wan, W. C.; Rothberg, L. J. Aggregation Quenching of Luminescence in Electroluminescent Conjugated Polymers. *J. Phys. Chem. A.* **1999**, *103*, 2394–2401.

(21) Zhao, E.; Lam, J. W. Y.; Meng, L.; Hong, Y.; Deng, H.; Bai, G.; Huang, X.; Hao, J.; Tang, B. Z. Poly[(maleic Anhydride)- Alt -(Vinyl Acetate)]: A Pure Oxygenic Nonconjugated Macromolecule with Strong Light Emission and Solvatochromic Effect. *Macromolecules*. **2014**, *48* (1). 64-71.

(22) Wang, R.; Xin-yuan, Z.; Yuan, W. Aggregation-Induced Emission of Non-Conjugated Poly(Amido Amine)s: Discovering, Luminescent Mechanism Understanding and Bioapplication. *Chinese J. Polym. Sci.* **2015**, *33* (5), 680–987.

(23) Wang, D.; Imae, T.; Miki, M. Fluorescence Emission from Dendrimers and Its pH Dependence. *J. Colloid Interface Sci.* **2004**, *306*, 222-227.

(24) Wang, D.; Imae, T.; Miki, M. Fluorescence Emission from PAMAM and PPI Dendrimers. *J. Colloid Interface Sci.* **2007**, *306*, 222–227.

(25) Wang, H.; Zhao, E.; Lam, J. W. Y.; Tang, B. Z. AIE Luminogens: Emission Brightened by Aggregation. *Mater. Today.* **2015**, *18* (7), 365–377.

(26) Ding, D.; Li, K.; Liu, B.; Tang, B. Z. Bioprobes Based on AIE Fluorogens. *Acc. Chem. Res.* **2013**, *46* (11), 2441–2453.

(27) Huang, T.; Wang, Z.; Qin, A.; Sun, J.; Tang, B. Z. Luminescent Polymers Containing Unconventional Chromophores. Chin. J. Polym. Sci. **2015**, *33* (5), 680-687.

(28) Li, S.; Wang, Q.; Qian, Y.; Wang, S.; Li, Y.; Yang, l. G. Understanding the Pressure-Induced Emission Enhancement for Triple Fluorescent Compound with Excited-State Intramolecular Proton Transfer. *J. Phys. Chem. A.* **2007**, *111* (46), 11793-11800.

(29) Chen, J.; Law, C. C. W.; Lam, J. W. Y.;Dong, Y.; Lo, S. M. F.; Williams, I. D.; Zhu, D.; Tang, B. Z. Synthesis, Light Emission, Nanoaggregation, and Restricted Intramolecular Rotation of 1,1-Substituted 2,3,4,5-Tetraphenylsiloles. *Chem. Mater.* **2003**, *15*, 1535-1546.

(30) Fan, X.; Sun, J.; Wang, F.; Chu, Z.; Wang, P.; Dong, Y.; Hu, R.; Tang, B. Z. Photoluminescence and Electroluminescence of Hexaphenylsilole Are Enhanced by Pressurization in the Solid State. *Chem. Commun.* **2008**, *26*, 2989-2991.

(31) Peng, Q.; Yi, Y.; Shuai, Z.; Shao, J. Toward Quantitative Prediction of Molecular Fluorescence Quantum Efficiency: Role of Duschinsky Rotation. *J. Am. Chem. Soc.* **2007**, *129*, 9333-9339.

(32) Hong, Y.; Lam, J. W. Y.; Tang, B. Z. Aggregation-Induced Emission: Phenomenon, Mechanism and Applications. *Chem. Commun.* **2009**, 29, 4332-4353.

(33) Reisch, A.; Didier, P.; Richert, L.; Oncul, S.; Arntz, Y.; Mély, Y.; Klymchenko, A. S. Collective Fluorescence Switching of Counterion-Assembled Dyes in Polymer Nanoparticles. *Nat. Commun.* **2014**, *5* , 1-9.

(34) Patil, Y. B.; Toti, U. S.; Khdair, A.; Ma, L.; Panyam, J. Single-Step Surface Functionalization of Polymeric Nanoparticles for Targeted Drug Delivery. *Biomaterials* **2009**, *30* (5), 859–866.

(35) Saha, B.; Evers, T. H. How Antibody Surface Coverage on Nanoparticles Determines the Activity and Kinetics of Antigen Capturing for Biosensing. *Anal. Chem.* **2014**, *86* (16), 8158–8166.

(36) Panyam, J.; Sahoo, S. K.; Prabha, S.; Bargar, T.; Labhasetwar, V. Fluorescence and Electron Microscopy Probes for Cellular and Tissue Uptake of poly(D,L-Lactide-Co-Glycolide) Nanoparticles. *Int. J. Pharm.* **2003**, *262* (1–2), 1–11.

(37) Cao, Y. C, Jin, R.; Nam, J. M.; Thaxton, C.S, Raman Dye-Labeled Nanoparticle Probes for Proteins. *JACS.* **2003**, *125*, 14676–14677.

(38) Vauthier, C.; Bouchemal, K. Methods for the Preparation and Manufacture of Polymeric Nanoparticles. *Pharm. Res.* **2009**, *26* (5), 1025–1058.

(39) Huang, Z. W.; Laurent, V.; Chetouani, G.; Ljubimova, J. Y.; Holler, E.; Benvegnu, T.; Loyer, P.; Cammas-Marion, S. New Functional Degradable and Bio-Compatible Nanoparticles Based on Poly(malic Acid) Derivatives for Site-Specific Anti-Cancer Drug Delivery. *Int. J. Pharm.* **2012**, *423* (1), 84–92.

(40) Lu, B.; Zheng, S.; Quach, Q.; Tai, Y. A Study of the Autofluorescence of Parylene Materials for M TAS Applications. **2010**, 1826–1834.

(41) K, Präbst,; H, Engelhardt,; H, Hübner,;S, R. Basic Colorimetric Proliferation Assays: MTT, WST, and Resazurin. *Cell Viability Assays.* **2013**, *1601*, 1–17.

(42) Davda, J.; Labhasetwar, V. Characterization of Nanoparticle Uptake by Endothelial Cells. *Int. J. Pharm.* **2002**, *233* (1–2), 51–59.

(43) Urban, M.; Musyanovych, A.; Landfester, K. Fluorescent Superparamagnetic Polylactide Nanoparticles by Combination of Miniemulsion and Emulsion/solvent Evaporation Techniques. *Macromol. Chem. Phys.* **2009**, *210* (11), 961–970.

(44) Piruska, A.; Nikcevic, I.; Lee, H.; Ahn, C.; Heineman, W. R.; Limbach, A.; Seliskar, C. J. The Autofluorescence of Plastic Materials and Chips Measured under Laser Irradiation. **2005**, 1348–1354.

(45) Basile, L. J. Effect of Styrene Monomer on the Fluorescence Properties of Polystyrene. *J. Chem. Phys.* **1962**, *36*, 2204–2210.

(46) García-plazaola, J. I.; Fernández-marín, B.; Duke, S. O.; Hernández, A.; López-arbeloa, F.; María, J. Autofluorescence : Biological Functions and Technical Applications. *Plant Sci.* **2015**, *236*, 136–145.

(47) Introduction to spectral imaging and linear unmixing, *Retrieved from: http://zeiss-campus.magnet.fsu.edu/articles/spectralimaging/introduction.html*

(48) LSM 710, Operation Manual. Zeiss. **2010**, 0–138.

(49) Wang, Y.-C.; Morawetz, H. Excimer Fluorescence of Polymers with Aromatic Substituents, 1. Dependence of Excimer Formation on Polymer Structure. *Die Makromol. Chemie.* **1975**, *1*, 283–295.

(50) Birks, J. B. Excimers. *Progr. React. Kinet.* **1970**, *5*, 181-272.

(51) Kim, W. C.; Lee, D. C. Synthesis of Poly(Maleic Anhydride) and Its Conformation in DMF. *Polym. Eng. Sci*. **1995**, *35* (20), 1600–1604.

(52) Y. Ruff and J. M. Lehn. Glycodynamers: Fluorescent Dynamic Analogues of Polysaccharides. *Angew. Chem. Int. Ed.* **2008**, *47*, 3556-3650.

(53) a) Bhushan, B. Molecularly Thick Films for Lubrication. In *Handbook of Nanotechnology,* 2nd Ed; Brushan, Ed.; Springer Science & Business Media, **2006**, 1322-1339. b) RCS (**2015**) Changing the Properties of Polymers and Plastics. Retrieved from *http://www.rsc.org /Resources/inspirational/resources/3.1.5.*

(54) Boundy, R. H.; Boyer, R. F. Styrene: Its Polymers, Co-Polymers, and Derivatives. In *Styrene: Its Polymers, Co-Polymers, and Derivatives,* 2nd Ed; Reinhold Publishing&COG. **1952**, 1304-1310.

(55) XTT Cell Proliferation Assay Kit by Cellular Enzymes I, Manual. **1988**, 2-6.

(56) Lu, A.; Smart, T. P.; Epps, T. H.; Longbottom, D. A.; O'Reilly, R. K. L-proline Functionalized Polymers Prepared by RAFT Polymerization and their Assemblies as Supported Organocatalysts. *Macromolecules*. **2011**, *44* (18), 7233-7241.

(57) Weissleder, R.; Nahrendorf, M.; Pittet, M. J. Imaging macrophages with nanoparticles. *Nat. Mater.* **2014**, *13,* 125-138.

(58) Waller, B. H.; Olon, D. G.; Currie, D. H.; Guss, A.M.; Lynd, L.R. Exchange of type II dockerin-containing subunits of the Clostridium termocellum cellulosome as revealed by SNAP-tags. *FEMS. Microbiol. Lett.* **2012**, *338* (2013), 46-53.

CHAPTER 5

Poly(styrene-co-maleic anhydride-co-divinylbenzene) nanoparticles at the interface of a Pickering emulsion droplets as template for permeable microcapsules formation

In this chapter Inverse Pickering emulsions were used as template for permeable hybrid polymer-based microcapsule formation.

Poly(styrene-co-maleic anhydride-co-divinylbenzene) nanoparticles stabilizing Pickering emulsion droplets at the interface as template for permeable microcapsules formation. *E Harmzen and B Klumperman. Manuscript in preparation (2017)*

Poly(styrene-co-maleic anhydride-co-divinylbenzene) nanoparticles at the interface of a Pickering emulsion droplets as template for permeable microcapsules formation

Abstract

In this study, we report the synthesis of hybrid starch/poly(styrene-*co*-divinylbenzene-*co*-maleic anhydride) microcapsules (MCs) by crosslinking the stabilizing particles at the interface of an inverse Pickering emulsion droplet. Initially, poly(styrene-*co*-divinylbenzene-*co*-maleic anhydride) nanoparticles with sizes ranging from 200-400 nm were prepared via radical dispersion polymerization. The obtained nanoparticles were then modified with 3-aminophenylboronic acid through a nucleophilic substitution on the MAnh residues. The resulting functional polymeric nanoparticles (MAnh-FPNPs) were subsequently used to fabricate 50 µm microcapsules via inverse Pickering emulsion using water-soluble starch, with multiple 1,2-hydroxyl groups to crosslink the capsules via borate ester formation. The successful crosslinking is shown by scanning electron microscopy (SEM), light microscopy (LM) and confocal fluorescence microscopy (CFM) analysis.

Introduction

The synthesis of microcapsules has gained widespread interest over the past decade due to their potential application in many fields including bio-medicine, the food industry and the oil industry.[1,2] Encapsulation is defined as the process of entrapping or enclosing a core material (e.g. liquid, solid, living mammalian cells or bacteria etc.) inside a hollow cavity within a solid shell that serves as a protective physical barrier. Encapsulation processes offer great advantages in applications that require controlled release or immobilization of the core materials, such as in drug delivery systems, stabilization of food ingredients and the construction of inorganic protocells, functioning as confined reaction compartments for in situ gene expression.[2–5] Traditionally, microcapsules (MCs) have been fabricated through polymerization at the interface between two immiscible solvents to produce the protective shell. However, this technique is associated with a number of disadvantages, such that the introduced components can increase or decrease the interfacial tension. The interfacial tension will affect the three-phase contact angle (θ) and a temperature change can cause big phase changes that will ultimately influence the stability of the emulsion.[6–9]

The components for the interfacial polymerization thus need to be carefully selected, not only for the change in the θ it can cause, but the components can cause possible side reactions, such as leaving behind unwanted material encapsulated, reactivity differences causing difficulty in controlling capsule dimensions and compatibility issues.[2,10] A relatively new approach utilizes the pioneering work of Pickering[11] and Ramsden[12] on Pickering emulsions, and additionally crosslinks the stabilizing particles at the interface.[13] This introduces a new and powerful approach to fabricate MCs, as illustrated in Figure 1.

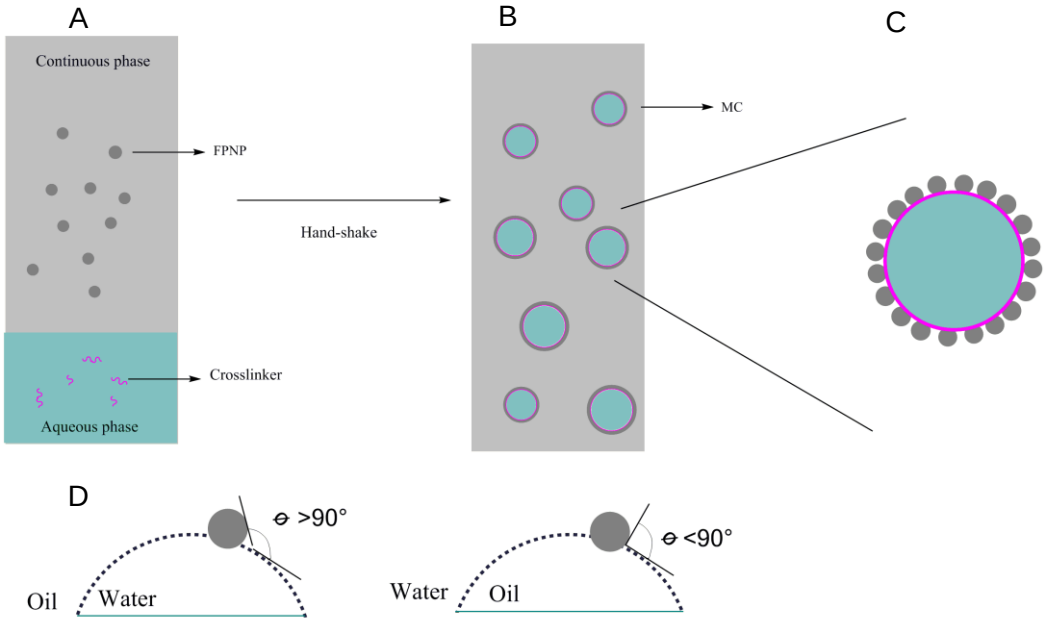

Figure 1: *General illustration of the steps necessary for microcapsule formation. A) FPNPs dispersed in a continuous phase and the crosslinker in the aqueous phase. B) Pickering emulsion is made using hand shaking as energy and C) individual MC made by using an appropriate crosslinker that allows the crosslinking of multiple FPNPs at the interface. D) The contact angle the particles make at the interface will stabilize a different emulsion. If the contact angle is < 90 º, an inverse Pickering emulsion will be preferred (o/w emulsion), if the contact angle is > 90 º, a Pickering emulsion will be preferred (w/o emulsion).*

Colloidal particles form the basis of a Pickering emulsion, and various parameters need to be optimized, such as the decrease of interfacial energy, the wettability of the particles by both phases (also θ), the particle concentration, and volume of dispersed phase. A strong indicator and important parameter of Pickering emulsion stability is the θ the particles make with the two immiscible liquids. If the contact angle is < 90 º, an inverse Pickering emulsion will be preferred (w/o emulsion) and if the contact angle is > 90 º, a Pickering emulsion will be preferred (o/w emulsion) (Figure 1D). The closer the θ to 90 º and the smaller the particles, the higher the

energy of detachment from the interface, resulting in Pickering emulsions with high stability.[14,15] In Pickering emulsions, the radius of the emulsion droplet depends on the volume of dispersed phase, the total number of particles present and the area occupied by one particle. In equation 1, that dependency of the emulsion droplet on the parameters is shown.[16]

$$r_{\mathrm{D}} = \frac{3V_{\mathrm{D}}}{N_{\mathrm{A}} 2Ap}$$

Equation 1: *Equation to calculate the different parameters of a Pickering emulsion for MC formation*

Where: $\mathrm{r_D}$ is the radius of the Pickering droplet (m), $\mathrm{V_D}$ is the total volume of the dispersed phase (m^3), $\mathrm{N_A}$ is the number of particles attached to the droplet interface when the particles are hexagonally packed, and A_p is the area occupied by an individual particle which can be described as $\mathrm{A_p} = 2\sqrt{3}\mathrm{R}^2$ (m^2), where R is the radius of the particles (m).

Pickering emulsions are becoming more apparent as suitable templates for MC formation because of their extreme stability compared to their traditional surfactant stabilized counterparts, and the various benefits when compared to traditional ways of synthesizing MCs. The use of solid particles as shell material offers additional advantages when a permeable shell is required as the crosslinking of the stabilizing particles at the interface allows interstitial spaces among the crosslinked particles to contribute to the permeability of the capsules.[17] This is particularly important when bioactive compounds or viable cells are encapsulated to allow passive diffusion of entrapped substrates or nutrients with low molecular weight through the semipermeable membrane.[4] In such applications the shell should not interfere with the core material but protect it from the environmental conditions and/or processes, and be semi-permeable.[3] Although a couple of examples of MCs mentioned above have been reported, mostly inorganic silica nanoparticles are utilized to produce MCs. [6,4,10,13,18,19]

Currently, inverse Pickering emulsions as templates for MCs offer many advantages and interesting applications. The main advantage of using inverse Pickering emulsions as MC synthesis template, is that sensitive and delicate materials that are water soluble can be encapsulated. Additionally, contamination of the core can be prevented during synthesis as the shell can be synthesized using benign components to the encapsulated material, allowing more control over the crosslinking parameter beforehand. Structures of this nature can possibly be found useful in applications such as drug carriers for sensitive materials, encapsulation of sensitive material or loci for catalytic reactions.[1,17,20]

Herein, we describe a simple and effective method to fabricate hybrid MCs based on starch/MAnh-FPNPs via templating inverse Pickering emulsions. Initially, MAnh-FPNPs based on poly(styrene-*co*-maleic anhydride-co-divinylbenzene) were synthesized, as seen in Figure 1A, via a dispersion radical terpolymerization of maleic anhydride (MAnh), styrene (St), and divinylbenzene (DVB).[21] The introduction of the highly reactive maleic anhydride moieties allows for a wide scope of additional modification as MAnh can react with various different functionalities, most notably with primary amines, and several functionalities of choice can be introduced via this chemistry.[13,22,23] Additionally, upon ring opening of the maleic anhydride, the MAnh becomes more hydrophilic, favoring the aqueous phase while the styrene favors the continuous phase. For stable Pickering emulsions, the affinity for both phases or the ability of the particles being wetted by both phases are needed for the particles to adsorb at the interface, thus making these MAnh-FPNPs suitable stabilizing moieties for a Pickering emulsion.[24] The reactive MAnh-FPNPs were further modified using a boronic acid (BA) obtaining BA-FPNPs that

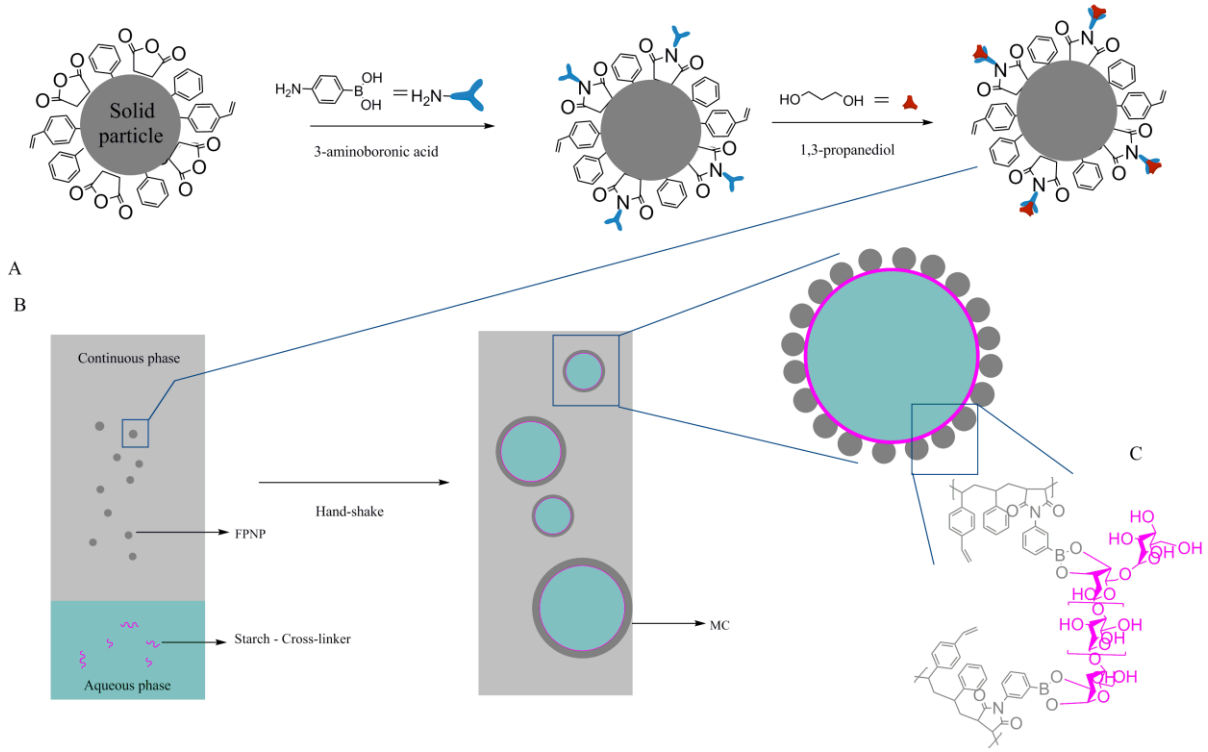

Figure 2: *Schematic overview of the synthesis route to produce hybrid starch-FPNPs MCs. In the top illustration, the modification of PNPs with 3-aminophenylboronic acid is shown, producing BA-FPNPs. The BA-FPNPs are further modified using 1,3-propanediol to obtain BE-FPNPs. In the Pickering emulsion, the BE-FPNPs stabilize the aqueous phase and the purple band indicates the crosslinking that crosslink multiple BE-FPNPs at the interface producing novel MCs.*

uphold the possibility of being crosslinked if a multifunctional polymer is added that has complementary groups to those on the BA-FPNPs (Figure 2A).

In this study, starch was used as a polymeric crosslinker that facilitates the crosslinking due to its multiple diol functionalities. Thus, by stabilizing inverse Pickering emulsions (Figure 2B), and by crosslinking the stabilizing particles at the interface, MCs that are stable and permeable can be produced (Figure 2C).

Materials and Methods

Materials. Maleic anhydride (MAnh, Sigma Aldrich, 99%) was recrystallized from chloroform. Styrene (St, Fluka, 99.5%) was purified by distillation and stored over 4 Å molecular sieves at 4 °C, divinylbenzene (DVB, Sigma Aldrich, >99%) was used after inhibitor, t-butylcatechol, was removed by passing through an alumina column and stored over 4 Å molecular sieves also at 4 °C. Methyl ethyl ketone (MEK, Sigma Aldrich, >99.7%). *n*-Heptane (Kimix, anhydrous), toluene (Sigma Aldrich, anhydrous 99.5%), and tetrahydrofuran (THF) were distilled before use and stored over molecular sieves and double distilled deionized water (ddH_2O, our lab), starch (Fluka, starch from potatoes) and 3-aminophenylboronic acid monohydrate (BA, Sigma Aldrich, >99.9%) and 1,3 propanediol (which was kindly donated by the W.A.L van Otterlo group) was used as received. 2,2'-Azo-bis(isobutyronitrile) (AIBN, Riedel de Haen) was recrystallized twice from methanol and dried under vacuum and stored at 4 °C.

Synthesis

MAnh-FPNPs. PNPs were synthesized as described in Chapter 3.

Modification of the MAnh-FPNPs to obtain BE-FPNPs. Poly(St-*co*-DVB-*co*-MAnh) FPNPs (100 mg, 0.30 mmol MAnh) were redispersed in DMF (10 mL). Various BA amounts 20%, 50% and 100% (mol% relative to MAnh) were used to fabricate the respective 20BA-, 50BA- and 100BA-FPNPs. In a typical experiment, to modify 20% MAnh, a solution of BA (16.47 mg, 0.120 mmol) in DMF (5 mL), was added dropwise to MAnh-FPNPs (200 mg MAnh-FPNPs, 0.60 mmol MAnh) dispersed in DMF. The reaction mixture was then refluxed to ensure ring closure of the maleimide rings. Thereafter, the mixture was allowed to cool to RT and the BA-FPNPs were washed with DMF twice, to ensure all unreacted reagents were removed and centrifuged to isolate BA-FPNPs. The particles were then dried under vacuum.
For a typical synthesis of BE-FPNPs a 1:1 ratio of BA-PNPs to 1,3-propanediol was used to ensure boronate formation on the surface of the particles, producing BE-FPNPs. To 100 mg 20BA-PNPs (0.026 mmol BA-functionality) in 5 mL THF was added 1,3-propanediol (1.94 mg, 0.026 mmol) in 2 mL dropwise. The mixture was allowed to react for 12 hours at 25 ºC, following two washing steps to ensure all unreacted reagents were removed, isolated by centrifugation and drying.

Preparation of hybrid MCs. In a typical experiment, 5.4 mg starch was dissolved in water (0.1 mL) and the BE-FPNPs (10 mg) were dispersed into the toluene phase (8 mL) using a sonicator to ensure all particles were well dispersed within the continuous phase. The two phases were mixed and hand-shaken to ensure all particles formed part of the Pickering emulsion droplets.

Rhodamine functionalization of starch. In an additional experiment, the starch was labelled with a red fluorescent dye, Rhodamine B, via the OH functionality on the starch using a DCC coupling reaction. Rhodamine B (14.78 mg, 0.03 mmol, 1 mol% relative to OH functionality on starch) was added to 5 mL THF in a three neck round bottom and subsequently cooled to 0 ºC and degassed using argon. A catalytic amount of DMAP (0.38 mg, 3 µmol) was added to the mixture and allowed to stir for 10 minutes at 0 ºC, after which starch was added. DCC (6.37 mg, 0.03 mmol) was added dropwise under inert conditions. The reaction temperature was gradually increased to room temperature and the reaction was allowed to proceed for 12 hours.[25]

Characterization and analysis

Equipment. The PNPs were dispersed in the continuous phase using a sonicator. Pickering emulsions were formed by using a shear force created by a IKA Ultra-Turrax T25 Digital Homogenizer at 12000 rpm for 20 seconds, or using hand shaking.

Electron microscopy measurements were performed on a Zeiss Merlin FEG-SEM unit working at a working distance of 3-4 mm, voltage of 5 kV, Iprobe of 250 pA and the inlens detector for high resolution imaging.

CFM imaging was done using a Carl Zeiss LSM780 (Carl Zeiss, Germany) confocal microscope using the diode 405 nm CW/PS (pulsed) laser and the 655 nm laser to excite the auto-fluorescent particles and the rhodamine-labelled starch respectively. The objectives that were used include the EC "Plan apochromat"20x/0.8 M27, LD "Plan-Nuofluar" 40x/0.6 Corr M27 and LCI "Plan-Apochromat"63x/1.4 Oil DIC M27. For post processing ZEN 2011 imaging software (Carl Zeiss, Germany) was used.

Light microscopy was conducted on a Zeiss Axio Scope.A1 Polarized Light Microscope. The microscope is fitted with various objectives, N-Achroplan pol 20x0.45, EC plan-Neofluar Pol 40x/0.9, EC Epoplan pol 50x/0.7, EC Epoplan-neopluar Pol 50x/0.8 and Epoplan-neofluar Pol 50x/1.0

Results and discussion

Synthesis of MAnh-FPNPs

Previously synthesized monodispersed functional poly(styrene-*co*-maleic anhydride-*co*-divinylbenzene) nanoparticles (the FPNP) (Chapter 3) with tunable sizes ranging from 200-300 nm, were utilized for further modification (Figure 3). Modification via a nucleophilic substitution on the reactive MAnh residues, using 3-aminophenylboronic acid monohydrate was done to introduce 3-aminophenylboronic acid (BA) functional groups and produce BA-functional nanoparticles (BA-FPNPs). The BA moieties serve as reactive functional groups towards diols

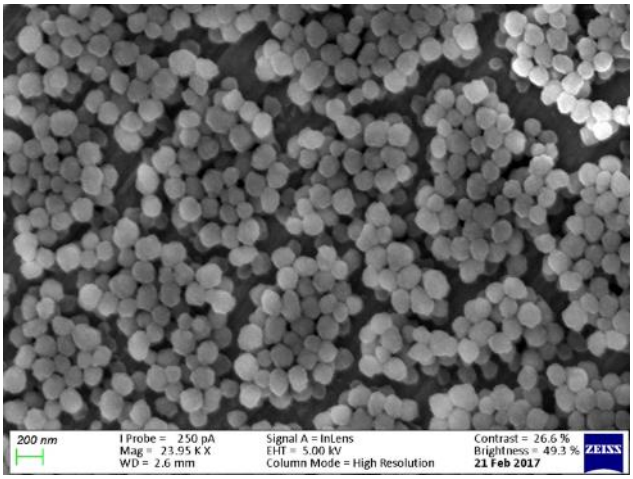

Figure 3: *Represented SEM image of the FPNPs used in the study. The particles had an average size of 200 nm and a narrow size distribution. Scale bar is 200 nm.*

that can be used to crosslink the nanoparticles at the oil-water interface.

The synthesis of the MAnh-FPNPs consisted of a surfactant-free dispersion polymerization in a methyl ethyl ketone (MEK): heptane (Hept) mixture with 2,2'-azo-bis(isobutyronitrile) (AIBN) as initiator. The styrene and DVB monomers were introduced to the reaction mixture and allowed seeding in the MAnh mixture to occur. Particle size and size distribution were controlled by varying the seeding % of the styrenic monomers, monomer addition rate as well as the crosslinker concentrations within the polymerization setup. An important reason to choose for small diameter particles is that the smaller the particle diameter, the higher the energy of detachment from the interface, hence better stability of the Pickering emulsion droplets and less coalescence between droplets.[7,26,27] Monodispersed particles are a prerequisite, because the diameter and surface area in conjunction with a certain volume of dispersed phase is the basis for calculating the number of particles necessary to close-pack and cover the entire interface of a pre-decided droplet size. Another prerequisite for stabilizing Pickering emulsions is the contact angle between the particles and the two phases. A contact angle close to ninety degrees leads to a high energy of detachment of the particles from the interface, which results in an emulsion droplet with high stability.[7,28,29] The synthesized FPNPs stabilized both oil-in-water and water-in-oil Pickering emulsion droplets, indicating that the 3-phase contact angle of the particle with the two phases is close to 90°. The amphiphilic nature of the particles, caused by the ring-opened MAnh and the hydrophobic segment of the styrene, contribute to this contact angle. Furthermore, the high reactivity of the MAnh makes it an attractive template for MC formation.

Formation of inverse Pickering emulsions

Inverse Pickering emulsions, *i.e*. water-in-oil emulsions, were produced under various experimental conditions. In our previous work,[1,10,13] emulsification was achieved using a homogenizer (*i.e*. high shear emulsification techniques, that can deliver enough energy to disperse particles homogeneously at the interface and to promote droplets homogeneous in size). However, applications such as encapsulation of delicate matter such as living cells are incompatible with the use of such techniques since the high shear will affect the viability of the cells. Therefore, in this study the droplets were formed through hand-shaking for 20 seconds. As a result, the production of droplets of a homogeneous size as well as droplets of a specific size proved to be challenging. An average droplet diameter of 60 µm, unless indicated otherwise, was targeted according to the calculation that was introduced in the introduction.

For the preparation of Pickering emulsions utilizing various experimental conditions, hand-shaking vs homogenization, changing the diameter of the stabilizing particles from 200 – 1300 nm and particle concentrations from 0.5 wt% to 20 wt% relative to the dispersed phase were investigated. After the formation of Pickering emulsions using hand-shaking and homogenization, the particle layer at the interface is compared. In the case that hand-shaking is used as emulsification technique, debris is observed at the interface of the droplet (Figure 4A), compared to almost no debris in Figure 4B using homogenization. The debris is attributed to insufficient energy introduced to the Pickering emulsion during hand-shaking for emulsification, causing residual nanoparticles in the continuous phase to aggregate at the interface, whereas

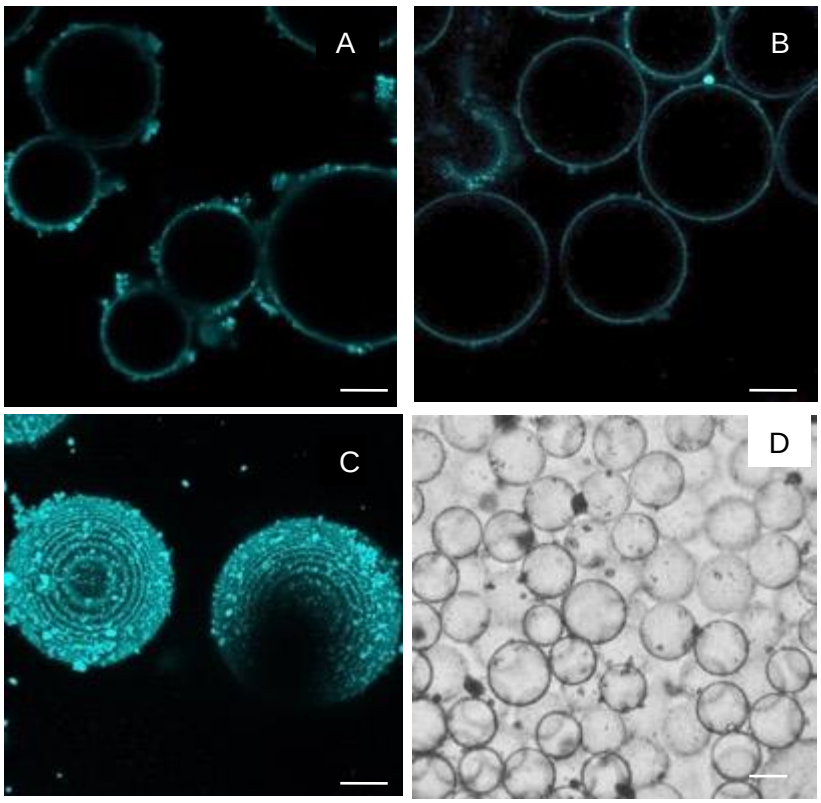

Figure 4: *Pickering emulsions produced via A) handshaking and B) homogenizing. The two different methods were both successful in transferring enough particles to the droplet interface. A) Image indicates visible aggregated FPNPs at the interface responsible for the debris. B) Image indicates Pickering emulsion droplets with less debris at the interface. C) Is a 3D reconstructed image of hand-shaken Pickering droplets. D) LM image D of inverse Pickering emulsions produced. Scale bar on the CFM images are 20 µm and on the LM image 100 µm. Pickering emulsions were produced using 200 nm FPNPs, particle concentration of 10 wt% relative to 0.1 mL dispersed phase and 8 mL continuous phase*.

high shear homogenization would ensure most of the particles at the monolayer in a closed-packed formation. Refer to Figure 4C showing a 3D reconstruction of images taken through the hand-shaken droplets, showing the debris quite clearly. The rings in the image are attributed to artefacts of the Z-stacking technique. Figure 4D shows a LM image of the hand-shaking-produced Pickering emulsion droplets. The reason we used hand-shaking in the following sections is that for applications like the encapsulation of live cells, the encapsulated cells will not survive homogenization (or high shear).

Additionally, it was observed that the stability of Pickering emulsions was greatly affected by the size and concentration of MAnh-FPNPs. Stable Pickering emulsions, *i.e*. several months, were obtained using MAnh-FPNPs of 200 nm diameter and a particle concentration of 10 wt% (relative to dispersed phase) as seen in Figure 4D. The MAnh-FPNPs with 200 nm particle diameter gave the most stable Pickering emulsion droplets, and the various parameters tested are shown in Table 1.

***Table** 1: Overview of the different Pickering emulsions produced with varying parameters.*

Particle size (nm)	Particle [c]	Dispersed phase	Continuous phase	Emulsion	Stable
200	0.5 wt%	Water	Toluene	No	No
200	1.0 wt%	Water	Toluene	Yes	No
200	2.2 wt%	Water	Toluene	Yes	No
200	5.0 wt%	Water	Toluene	Yes	1/2
200	10 wt%	Water	Toluene	Yes	Yes
200	10 wt%	Water	Ethyl acetate	Yes	Yes
200	10 wt%	Water	Cyclohexane	Yes	No

It was seen that the particle size and particle concentration play an important role in the stability of the inverse Pickering emulsions, which is in agreement with literature.[30–32] It was also observed (images not shown) that stable Pickering emulsions could be obtained, which further strengthens the idea that these MAnh-FPNPs have a θ close to 90 º resulting in Pickering and inverse Pickering emulsions with high stability.[14,15]

The continuous phase was replaced to assess the stability of the Pickering emulsion droplets. As no crosslinking of individual particles at the interface had occurred yet, the droplets will fall apart if there is water on the outside and on the inside. It was indeed shown that by direct transfer of the droplets from the emulsion phase into pure water, replacing the continuous phase

of a w/o Pickering emulsion by water leads to complete destabilization of the structure. By crosslinking the particles at the interface (i.e. introduction of a shell to prevent droplet coalescence) stable MCs can fabricated.

Microcapsule synthesis

A water-soluble starch, with 1,2-dihydroxy functionalities, was used as a stabilizer to crosslink BA-FPNPs on the droplet interface, via boronate-ester bond formation. The stability of the MCs as a function of BA concentration was investigated by decorating the FPNP with different fractions of BA, *viz*. 20%, 50% and 100%, relative to the amount of accessible MAnh on the particle, to produce respectively 20BA-, 50BA- and 100BA-FPNPs. The reaction between the MAnh residues and BA producing BA-FPNPs can been seen in Scheme 1.

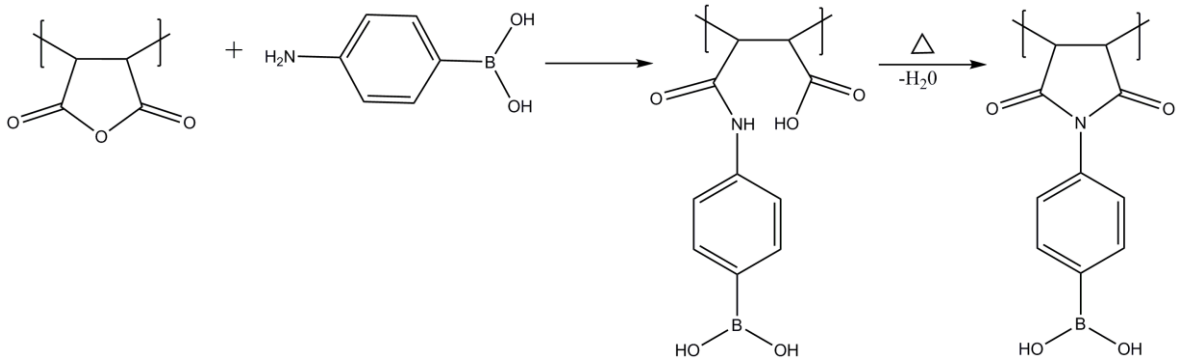

Scheme 1: *Chemical modification of the MAnh groups via a nucleophilic substitution reaction via the introduction of the primary amine on BA, followed by a ring closure reaction, obtaining BA-FPNPs.*

When BA-FPNPs were used for the synthesis of starch crosslinked MCs, the droplets were destabilized before MCs could be formed. This instability was tentatively attributed to the reaction between boronic acid and the 1,2-diol of starch being very quick.[33–35] In literature, the ionization of boronic acid in the presence of a diol is well documented.[33–35] Boronic acid is able to interact with a base through a pair of electrons, like a hydroxide, via a transesterification reactions to form a boronate ester.[34,36] Polyols with multiple 1,2-diol pairs have been shown to have a higher equilibrium constant compared to single diol compounds.[34] The affinity of boronates for diols in most carbohydrates is in the order: 1,2-diol > 1,3-diol, making the boron-1,2-diol interaction preferred and more stable.[36]

Following the literature, it was hypothesized that reacting the BA moieties on the surface of the particles with 1,3-propanediol, the resulting BE-FPNPs will be more stable once the starch is

introduced and the destabilization of the droplets will be prevented. Consequently, the BA-FPNPs were further modified using 1,3-propandiol to produce boronate ester decorated FPNPs (BE-FPNPs) (Scheme 2). The exchange of the starch's 1,2-diol, with the 1,3-diol on the surface of the particles, is more preferred and slower than just introducing the starch to the BA moieties, thus slowing the crosslinking of multiple particles at the interface once the starch was added.

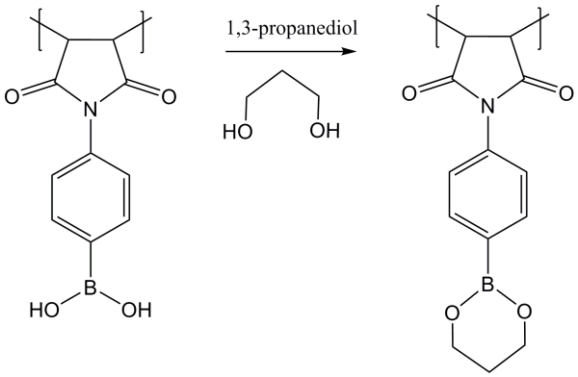

Scheme 2: *Chemical illustration of the end capping/protection of the boronic acid (BA) group using 1,3-propanediol forming a boronate ester bond*

Figure 5 shows the ATR-FTIR spectra of FPNP, BA-FPNPs and BE-FPNPs. The MAnh-FPNPs before any modification had the characteristic MAnh carbonyl bands at 1772 cm^{-1} and 1854 cm^{-1}. After surface modification and dialysis to ensure all excess or unbound modification agents are removed (refer to Figure 5B and 5C), the appearance of a new strong band at 1720 cm^{-1} and 1645 cm^{-1} is due to successful introduction of BA and formation of the imide group.[37] Intensity also increases from 20-BA (refer to Figure 5B) to 100-BA FPNPs (refer to Figure 5C). Additionally the newly introduced B-OH band at 1388 cm^{-1} and 1226 cm^{-1} is confirmation of successful modification.[35] After further modification of the BA moieties with 1,3-propanediol to BE-FPNPs, the disappearance of the B-OH peaks at 1388 cm^{-1} and 1226 cm^{-1} and the appearance of boronate-ester (B-O-C) bands at 1178 cm^{-1} and 919 cm^{-1}, suggests a successful modification process.[36,38]

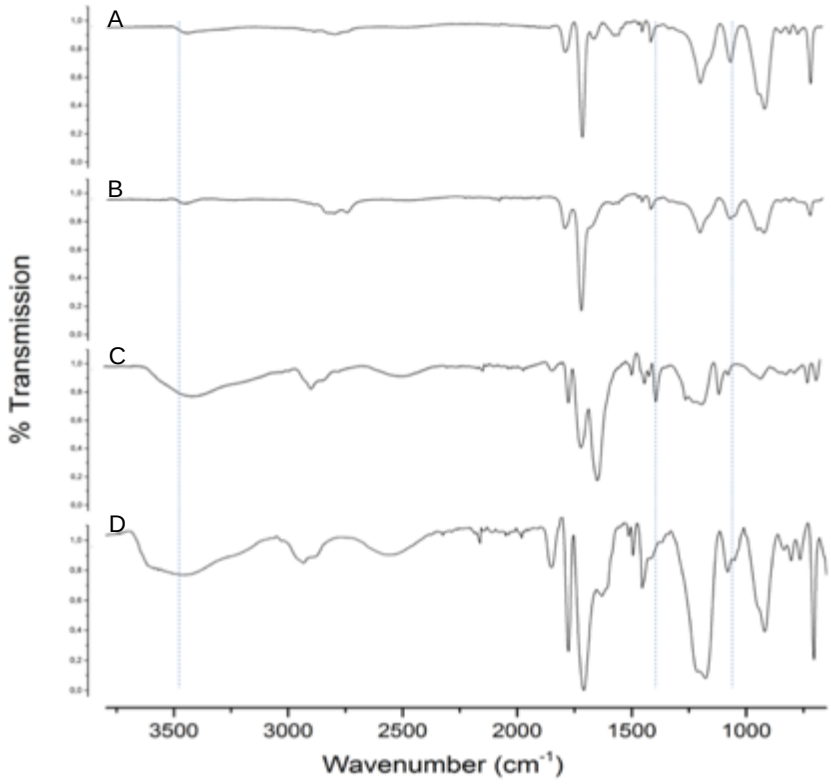

Figure 5: *ATR-FTIR spectra of the A) FPNPs, B) 20-BA-FPNPs, C) 100-BA FPNPs and D) BE-FPNPs*

The MCs are produced, with encapsulated starch inside the droplets, allowing crosslinking between one multi-diol containing starch-chain and multiple BE-FPNPs particles that are in close proximity, which results in shell formation at the interface (Scheme 3). Crosslinking of the particles at the water-oil interface occurs via the starch displacing the 1,3-diol on the BE-FPNPs

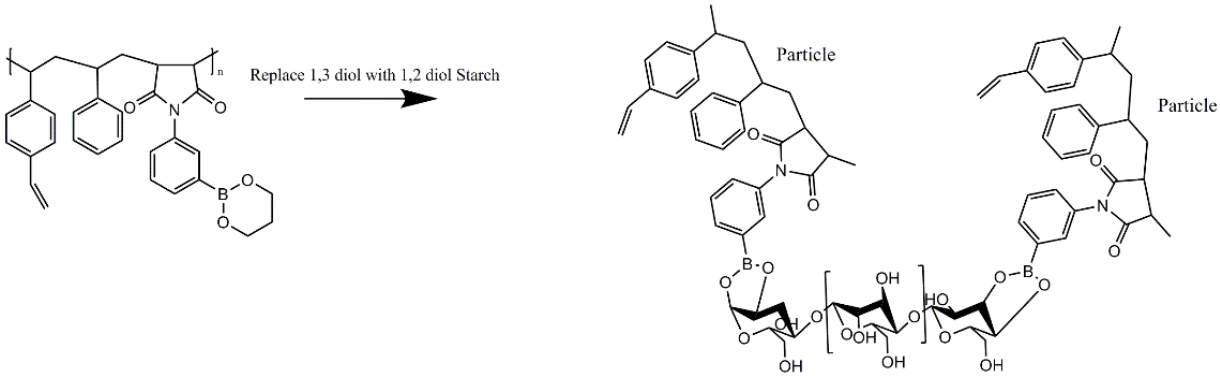

Scheme 3: *Illustration showing the crosslinking of multiple FPNPs with one multi-diol starch chain via the displacement of the 1, 3-propanediol on the BE-FPNPs surface with the 1,2-diols on the starch chain. The displacement of a 1,3-diol with a 1,2-diol to a boronic acid is preferred.* [33–35,36]

surface as polyols with multiple 1,2-diol pairs have been shown to have a higher equilibrium constant compared to single diol compounds.[34] Not only does multiple diols get preferred but the affinity of boronates for diols in most carbohydrates is in the order: 1,2-diol > 1,3-diol, making the boron-1,2-diol interaction preferred and more stable[36], resulting in hybrid starch-FPNPs MCs (starch-MCs).

The fabrication of stable starch-MCs requires sufficient amounts of starch to effectively crosslink multiple BE-FPNPs at the interface. Insufficient amounts of starch will not crosslink enough particles to stabilize the particles at the interface for stable MC formation. To fabricate MCs, MAnh-FPNPs with different BE-content as well as various starch concentrations were used (Table 2). Table 2 indicates the conditions where stable MCs are produced that could be redispersed/ transferred into a THF/aqueous phase mixture.

Table 2: *Summary of the parameters tested for MC formation. MCs stability was tested as a function of BE functionalization and starch concentration.*

			BE-FPNPs*			
Starch (wt%)	Vol.Dispers phase (mL)	Vol. Cont phase (mL)	0BE-particles	20BE-particles	50BE-particles	100BE-particles
1	0.1	8.0	-	-	-	-
2.8	0.1	8.0	-	-	y	y
5.4	0.1	8.0	-	y	y	y
10	0.1	8.0	-	y	y	y
20	0.1	8.0	-	y	-	-

** y indicates successful MC production and - indicates unsuccessful MC production.*

Stable starch-MCs were successfully obtained using 5.4 - 10 wt% starch (relative to dispersed phase) as indicated by SEM and LM images (refer to Figure 6). Figure 6A shows a LM image of the produced MCs with intact spherical capsules. MCs are not attached to each other, which is expected as the capsule-forming reaction occurred within each droplet from the inside out. LM as a technique to visualize the MCs is non-destructive, as no vacuum is needed. However, due to the nature of the SEM analysis, which is performed at high vacuum, deformed spherical shape (*i.e*. deflated) MCs are expected. Should insufficient crosslinking occur and the MCs do not form, MCs would collapse under the high vacuum of the SEM technique, resulting in no structure and mostly individual particles. Should sufficient crosslinking of individual particles

occur and MCs produced, deflated MCs will be seen under the high vacuum of the SEM technique. Indeed, SEM images in Figures 6B-6D show a number of deflated individual MCs with retained shell structures, suggesting the successful formation of stable MCs using 5.4 -10 wt% starch. MC formation was unsuccessful using only 1 wt% starch, indicative of insufficient starch for the crosslinking to stabilize particles at the interface. It was also observed that in the case of 20 wt% starch, no MCs were produced. This observation at 20 wt% starch can possibly be attributed to the addition of excess crosslinker, leading to one BE-functional group reacting with one crosslinker chain, which will also lead to unsuccessful crosslinking. At the high starch concentrations, possible solubility problems may arise due to an increased local viscosity within each droplet leading to early precipitation of starch.

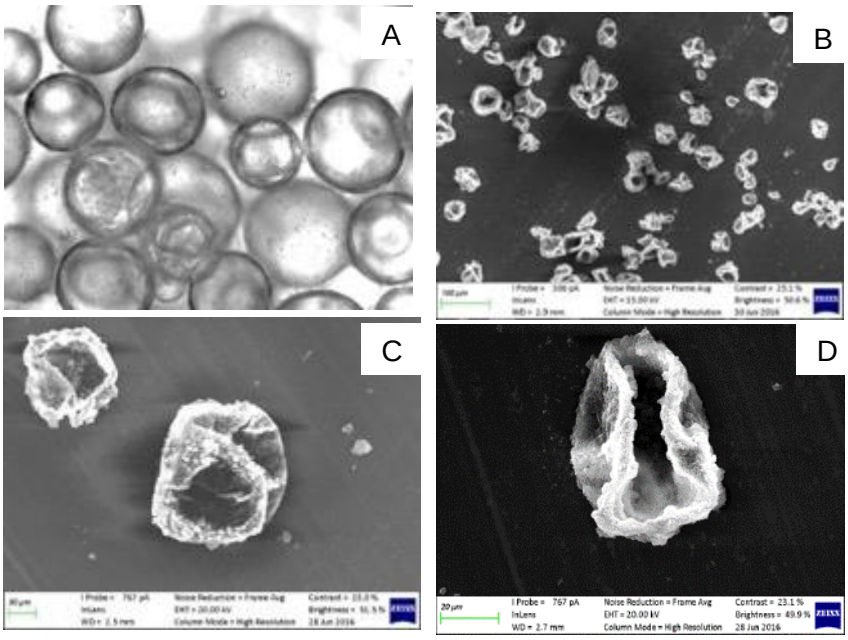

Figure 6: *A) LM image of MCs produced, scale bar in the LM image is 40 µm. B-C) SEM images of MCs showing deflated MCs, due to the high vacuum, but structures still intact, scale bar is 100 µm and 30 µm respectively. D) SEM image of a capsule after redispersion into THF showing an intact capsule, scale bar is 20 µm.*

Confocal Fluorescence Microscopy (CFM) was also used to visualize and confirm the starch layer as well as the successful synthesis of MCs. The starch used in this experiment, was first tagged with Rhodamine B through EDC coupling. Using 100-BE FPNPs and 1 wt% starch, one can see the disjointed starch layer, indicated by the arrows (Figure 7A). This indicates insufficient crosslinking of particles at the interface, and the unsuccessful capsule formation is

confirmed. Capsules made using 10 wt% starch, show a more continuous layer of starch at the interface (Figure 7B), which is an indication that successful capsule formation occurred in good correlation to the redispersion results indicated in Table 2.

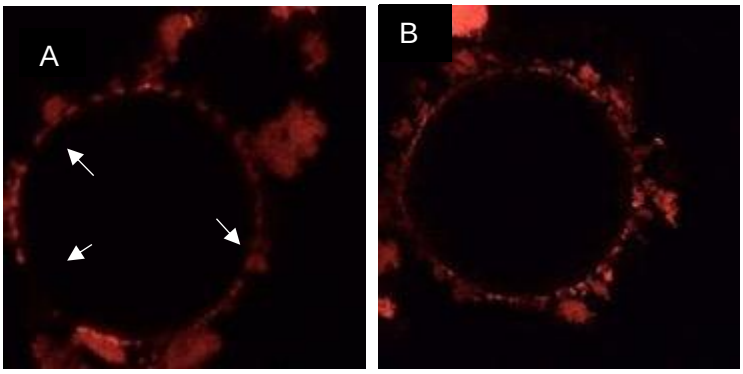

Figure 7: *Images showing only the starch layer at two different starch concentrations using 100-BE FPNPs. A) MCs produced using 1 wt% starch and B) MCs produced using 10 wt% starch. Scale bar is 20 µm.*

Permeability is particularly important when encapsulating live cells to allow the exchange of small molecules, such as nutrients and excreted products, across the barrier or shell. For the preparation of MCs dispersed in one phase, both continuous and dispersed phase were gradually replaced by 100% THF to assess the permeability of the MCs. Hence, MCs deflate as water molecules leave the MC. Figure 8A shows a LM image of hybrid starch-MCs that were redispersed into 100% THF. Interestingly, the MCs shows to be permeable and able to re-inflated upon addition of original solvent, the deflated MC start re-inflating, seen Figure 8B-E that was taken as a function of solvent added. The re-inflation is indicated by the arrow until solvent composition inside and outside the MCs equilibrate, which indicates the permeability of these MCs.

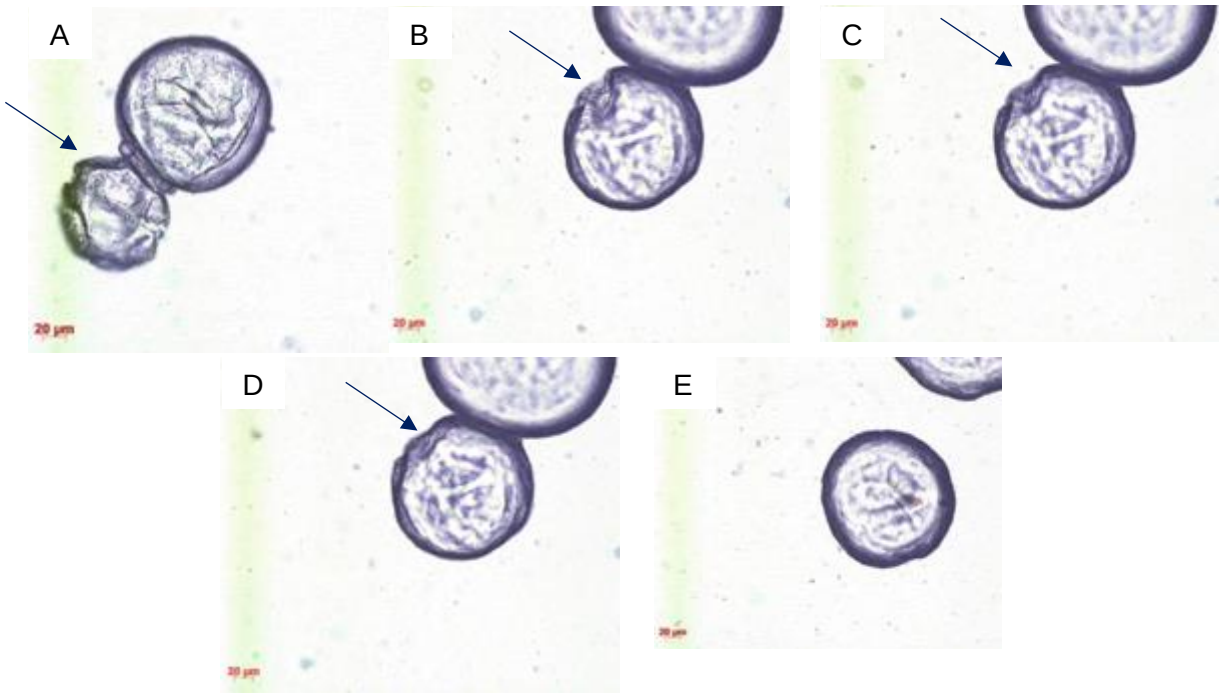

Figure 8: *A) LM image of hybrid starch-MCs that were redispersed into 100% THF B-E) Images of re-inflating MCs as equilibrium is reached to almost 100% original size. Indicated scale bar is 20 µm.*

Interestingly, as shown in Figure 9A, the BE-FPNPs auto-fluoresce at an excitation wavelength of 405 nm. Figure 9B shows the fluorescent dye labelled-starch, excited using 655 nm wavelength, with Figure 9C an overlay of the two colours. This suggests that the starch is in contact with the BE-FPNPs within the MCs, confirming the formation of stable MCs. This further indicates that almost all the polymer is in close proximity of the BE-FPNPs around the water droplets. The capsules showed successful crosslinking of the BE-FPNPs at the interface that led to stable and permeable capsules that adds value and scope to FPNPs, making these particles and template promising candidates for various applications such as the encapsulation of live organisms, due to the ease of decorating them with a wide variety of functional groups.

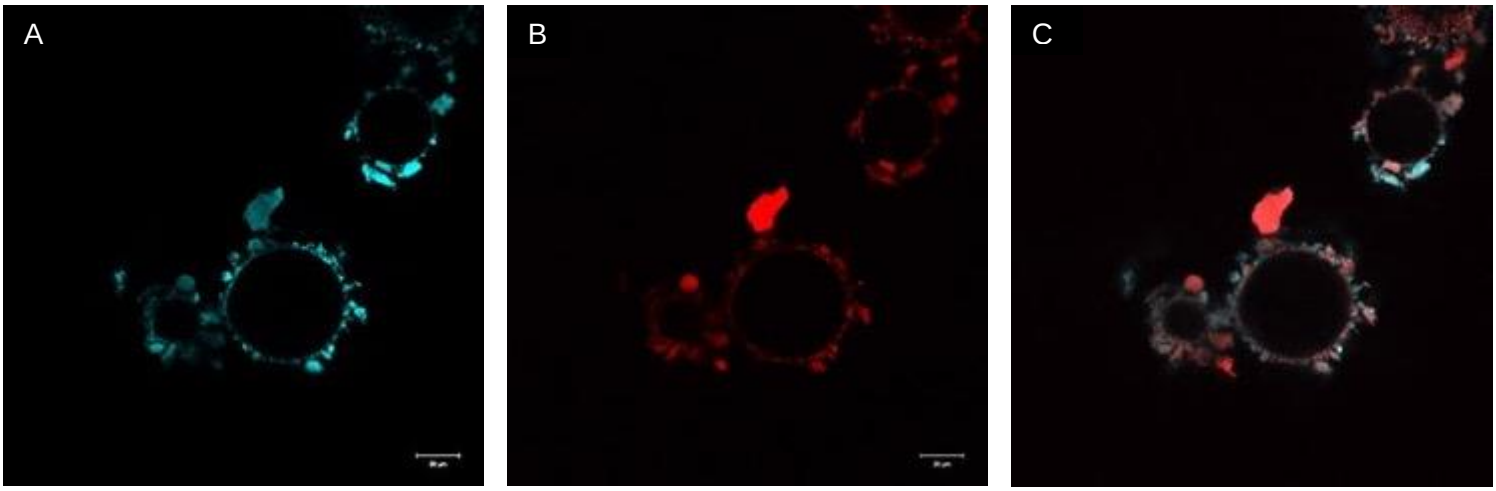

Figure 9: *Images A-C) are of capsules that were formed using 10 mg starch. A) auto-fluorescent BE-FPNPs, B) the fluorescently labelled starch and C) an overlay of both layers. The scale bar in the images is 20 µm.*

Conclusions

In conclusion, we have successfully prepared hybrid starch-poly(styrene-*co*-divinylbenzene-*co*-maleic anhydride) MCs using inverse Pickering emulsion droplets as template, comprising of the self-organization of FPNPs at the interface of the droplets and the crosslinking thereof using a multifunctional polymer. The PNPs were successfully decorated with BA and further modified with a 1,3-diol to obtain BE-FPNPs. The reaction of the multiple functional starch with complementary groups on the individual particles resulted in the MCs forming from the inside of the emulsion droplets.

The diameter of these hybrid hollow spheres can be tailored in the range of 10-300 µm by the variation of the total relative amount of aqueous phase added and the particle concentration. Such hybrid MCs may find applications as drug carriers or encapsulation vessels.

This type of MC can be further used in the field of encapsulation of sensitive live micro-organisms. Considering the versatility and the straightforward synthesis method, the procedure might be applicable to the encapsulation of delicate materials, live cells or live organisms.

References

(1) van Wijk, J.; Heunis, T.; Harmzen, E.; Dicks, L. M. T.; Meuldijk, J.; Klumperman, B. Compartmentalization of Bacteria in Microcapsules. *Chem. Commun. (Camb).* **2014**, *50*, 15427-15430.

(2) Wang, J. X.; Wang, Z. H.; Chen, J. F.; Yun, J. Direct Encapsulation of Water-Soluble Drug into

Silica Microcapsules for Sustained Release Applications. *Mater. Res. Bull.* **2008**, *43* (12), 3374–3381.

(3) Nedovic, V.; Kalusevic, A.; Manojlovic, V.; Levic, S.; Bugarski, B. An Overview of Encapsulation Technologies for Food Applications. *Procedia Food Sci.* **2011**, *1*, 1806–1815.

(4) Li, M.; Harbron, R. L. R.; Weaver, J. V. M. J.; Binks, B. B. P.; Mann, S. Electrostatically Gated Membrane Permeability in Inorganic Protocells. *Nat. Chem.* **2013**, *5*, 529–536.

(5) Li, M., Green, D. C., Anderson, J. L. R., Binks, B. P. & Mann, S. In Vitro Gene Expression and Enzyme Catalysis in Bio-Inorganic Protocells. *Chem. Sci.* **2011**, *2*, 1739–1745.

(6) Wang, B.; Wang, M.; Zhang, H.; Sobal, N. S.; Tong, W.; Gao, C.; Wang, Y.; Giersig, M.; Wang, D.; Möhwald, H. Stepwise Interfacial Self-Assembly of Nanoparticles via Specific DNA Pairing. *Phys. Chem. Chem. Phys.* **2007**, *9* (48), 6313–6318.

(7) Vignati, E.; Piazza, R.; Lockhart, T. P. Pickering Emulsions: Interfacial Tension, Colloidal Layer Morphology, and Trapped-Particle Motion. *Langmuir.* **2003**, *19* (17), 6650–6656.

(8) Li, J.; Hitchcock, A. P.; Stöver, H. D. H. Pickering Emulsion Templated Interfacial Atom Transfer Radical Polymerization for Microencapsulation. *Langmuir.* **2010**, *26* (23), 17926–17935.

(9) Abbott, S. Emulsions. In *Practical Surfactant Science: Principles and Practice,* 1st Ed; *Creative Commons BY-ND: UK,* **2016**, 13-247.

(10) van Wijk, J.; Salari, J. W. O.; Zaquen, N.; Meuldijk, J.; Klumperman, B. Poly(methyl Methacrylate)–silica Microcapsules Synthesized by Templating Pickering Emulsion Droplets. *J. Mater. Chem. B* **2013**, *1* (18), 2394-2406.

(11) Spencer, P.; Pickering, U. Emulsions. *J. Chem. Soc. Trans.* **1907**, *91*, 2001–2021.

(12) Ramsden, W.; Separation of Solids in the Surface-Layers of Solutions and "Suspensions" (Observations on Surface-Membranes, Bubbles, Emulsions, and Mechanical Coagulation).-Preliminary Account. *Proc. R. Soc. Lond.* **1903**, *72*, 156-164.

(13) van Wijk, J.; van Deventer, N.; Harmzen, E.; Meuldijk, J.; Klumperman, B. Formation of Hybrid Poly(styrene-Co-Maleic Anhydride)–silica Microcapsules. *J. Mater. Chem. B.* **2014**, *2* (30), 4826-4835.

(14) Kaptay, G. On the Equation of the Maximum Capillary Pressure Induced by Solid Particles to Stabilize Emulsions and Foams and on the Emulsion Stability Diagrams. *Colloid. Surface. Physicochem. Eng. Asp.* **2006**, *282*, 387–401.

(15) Yan, N.; Gray, M. R.; Masliyah, J. H. On Water-in-Oil Emulsions Stabilized by Fine Solids. *Colloid. Surface. Physicochem. Eng. Asp.* **2001**, *193*, 97–107.

(16) Salari, J. W. O.; Jemwa, G. T.; Wyss, H. M.; Klumperman, B. Reconstruction of the 3D Structure of Colloidosomes from a Single SEM Image. *Soft Matter.* **2011**, *7* (5), 2033-2041.

(17) Chen, T.; Colver, P. J.; Bon, S. a. F. Organic–Inorganic Hybrid Hollow Spheres Prepared from TiO2-Stabilized Pickering Emulsion Polymerization. *Adv. Mater.* **2007**, *19* (17), 2286–2289.

(18) Dinsmore, D.; Hsu, M. F.; Nikolaides, M. G.; Marquez, M.; Bausch, a R.; Weitz, D. a. Colloidosomes: Selectively Permeable Capsules Composed of Colloidal Particles. *Science* **2002**, *298* (5595), 1006–1009.

(19) Li, M.; Green, D. C.; Anderson, J. L. R.; Binks, B. P.; Mann, S. In Vitro Gene Expression and Enzyme Catalysis in Bio-Inorganic Protocells. *Chem. Sci.* **2011**, 2, 1739–1745.

(20) van Wijk, J. **2014**. *Production of Microcapsules by Templating Pickering Emulsion Droplets : Mechanism and Practical Applications*. Doctoral thesis. Eindhoven University of Technology.

(21) Harmzen-Pretorius, E.; Klumperman, B. Synthesis and Characterization of Novel Multifunctional Poly(Styrene-Co-Divinylbenzene-Co-Maleic Anhydride) Nanoparticles Produced via a Surfactant-Free Dispersion Polymerization Technique. *Manuscript in Preparation.* ***2017****.*

(22) Lin, J.J.; Hsu, Y.C. Temperature and pH-Responsive Properties of Poly(styrene-Co-Maleic Anhydride)-Grafting Poly(oxypropylene)-Amines. *J. Colloid Interface Sci.* **2009**, *336* (1), 82–89.

(23) Henry, S. M.; El-sayed, M. E. H.; Pirie, C. M.; Hoffman, A. S.; Stayton, P. S. pH-Responsive Poly(styrene-co-Maleic Anhydride) Alkylamide Copolymers for Intracellular Drug Delivery. *Biomacromolecules.* **2006**, *7*, 2407–2414.

(24) Destribats, M.; Gineste, S.; Laurichesse, E.; Tanner, H.; Leal-Calderon, F.; Héroguez, V. Pickering Emulsions: What Are the Main Parameters Determining the Emulsion Type and Interfacial Properties? *Langmuir.* **2014**, *30* (31), 9313–9326.

(25) Tsakos, M.; Schaffert, E. S.; Clement, L. L.; Villadsen, N. L.; Poulsen, T. B. Ester Coupling Reactions – an Enduring Challenge in the Chemical Synthesis of Bioactive Natural Products. *Nat.*

Prod. Rep. **2015**, 605–632.
(26) Kaewsaneha, C.; Tangboriboonrat, P.; Polpanich, D. Colloids and Surfaces A : Physicochemical and Engineering Aspects Preparation of Janus Colloidal Particles via Pickering Emulsion : An Overview. *Colloids Surfaces A Physicochem. Eng. Asp.* **2013**, *439*, 35–42.
(27) Melle, S.; Lask, M.; Fuller, G. G. Pickering Emulsions with Controllable Stability. *Langmuir.* **2005**, *21* (6), 2158–2162.
(28) Aveyard, R. Can Janus Particles Give Thermodynamically Stable Pickering Emulsions? *Soft Matter.* **2012**, *8* (19), 5233-5240.
(29) Chevalier, Y.; Bolzinger, M. A. Emulsions Stabilized with Solid Nanoparticles: Pickering Emulsions. *Colloids Surfaces A Physicochem. Eng. Asp.* **2013**, *439*, 23–34.
(30) Sacanna, S.; Kegel, W.; Philipse, A. Thermodynamically Stable Pickering Emulsions. *Phys. Rev. Lett.* **2007**, *98* (15), 1-4.
(31) Binks, B. P.; Clint, J. H. Solid Wettability from Surface Energy Components: Relevance to Pickering Emulsions. *Langmuir.* **2002**, *18* (4), 1270–1273.
(32) de Folter, J. W. J.; van Ruijven, M. W. M.; Velikov, K. P. Oil-in-Water Pickering Emulsions Stabilized by Colloidal Particles from the Water-Insoluble Protein Zein. *Soft Matter.* **2012**, *8* (25), 6807–6815.
(33) Furikado, Y.; Nagahata, T.; Okamoto, T.; Sugaya, T.; Iwatsuki, S.; Inamo, M.; Takagi, H. D.; Odani, A.; Ishihara, K. Universal Reaction Mechanism of Boronic Acids with Diols in Aqueous Solution: Kinetics and the Basic Concept of a Conditional Formation Constant. *Chem.* **2014**, *20* (41), 13194-13202.
(34) Marinaro, W. A.; Prankerd, R.; Kinnari, K.; Stella, V. J. Interaction of Model Aryl- and Alkyl-Boronic Acids and 1,2-Diols in Aqueous Solution. *J. Pharm. Sci.* **2015**, *104* (4), 1399-1408.
(35) Cegłowski, M.; Gierczyk, B.; Schroeder, G. Poly(methyl Vinyl Ether-Alt-Maleic Anhydride) Functionalized with 3-Aminophenylboronic Acid: A New Boronic Acid Polymer for Sensing Diols in Neutral Water. *J. Appl. Polym. Sci.* **2014**, *131* (18), 9358–9364.
(36) Pappin, B.; Kiefel, M. J.; Houston, T. A. Boron-Carbohydrate Interactions. In *Carbohydrates - Comprehensive Studies on Glycobiology and Glycotechnology*. 1st Ed, Chuan-Fa Chang, InTech. **2012**, 37-54.
(37) Kong, J.; Yu, S. Fourier transform infrared spectroscopic analysis of protein secondary structures. *Acta Biochim. Biophys. Sin.* **2007**, *39* (8), 549–559.
(38) Hageman, J. H.; Kuehn, G. D. Boronic Acid Matrices for the Affinity Purification of Glycoproteins and Enzymes.*Methods Mol Biol.* **1992**, 11, 45-71.
(39) Binks, B. P.; Clint, J. H. Solid Wettability from Surface Energy Components: Relevance to Pickering Emulsions. *Langmuir.* **2002**, *18* (4), 1270–1273.

CHAPTER 6

Triggered degradation of permeable hybrid polymer-FPNP capsules and encapsulation of micro-organisms

A simple, effective and benign method for the fabrication of hybrid permeable starch-FPNP based-MCs and the encapsulation of *E. coli*. along with the triggered degradation of the capsule wall is investigated.

Triggered degradation of hybrid starch-poly(styrene-co-divinylbenzene)-co-maleic anhydride) nanoparticle-based capsules using encapsulated micro-organisms. *E Harmzen-Pretorius, R. Cripwell, E. van Zyl and B. Klumperman. Manuscript in preparation (2017)*

Triggered degradation of hybrid starch-poly(styrene-co-divinylbenzene-co-maleic anhydride) nanoparticle-based capsules using encapsulated micro-organisms

Abstract

The triggered degradation of hybrid starch-poly(styrene-*co*-maleic anhydride-*co*-divinylbenzene) nanoparticle-based microcapsules (MCs) was tracked after encapsulation of genetically modified *Escherichia coli* cells expressing recombinant amylase. The AmyA α-amylase was under the control of the inducible GAL10 promotor. This allowed for the triggered release of the enzyme upon exposure to a galactose trigger. The permeable MCs were produced by simultaneous templating of inverse Pickering emulsions and interfacial crosslinking of the stabilizing nanoparticles at the emulsion droplet interface. Starch was added to a bacteria suspension in growth media, and introduced as the aqueous phase in the Pickering emulsion that was created via hand-shaking. The crosslinking reaction to produce capsules took place concurrently with the emulsification process. Amylases cleave internal bonds in starch molecules, which results in the degradation of starch serving to crosslink multiple boronate ester-FPNPs at the interface.

Introduction

The encapsulation of viable microbial cells within microcapsules (MCs) has gained increasing interest over the past decade.[1–3] Encapsulation is the process where a substance (the core) is surrounded, covered and/or protected by a physical barrier (the shell). Specifically, in applications where bioactive materials or viable cells are encapsulated, the barrier should not interfere with the encapsulated material, but protect it from environmental conditions and/or processes, and simultaneously be permeable.[2,4–9] The barrier or capsule should be permeable to small molecules and even macromolecules, but impermeable to larger encapsulated materials, like mammalian cells or bacteria. Furthermore, the capsule should be benign towards encapsulated microorganisms or cells.[6] During the synthesis of the capsules, the viability of the encapsulated material is the most challenging, as microorganisms and mammalian cells are sensitive towards small fluctuations in environmental conditions that include: temperature, pH and the introduction of toxic chemicals during the capsule-formation process.[7,10,11]

Currently, various techniques exist to synthesize microcapsules (MCs), however for the preparation of MCs using inverse Pickering emulsions as templates (Figure 1) has seldom been reported[2,12,13] but offers high colloidal stability and tunable droplet sizes. Additionally, the

interstitial spaces along the interface allow for permeable capsules to be synthesized[14–16]. The main challenge arises in that chemistries used for capsule formation should allow a benign environment for the encapsulated material, as shown by only a few exceptions that bacteria can survive harsh environments.[17]

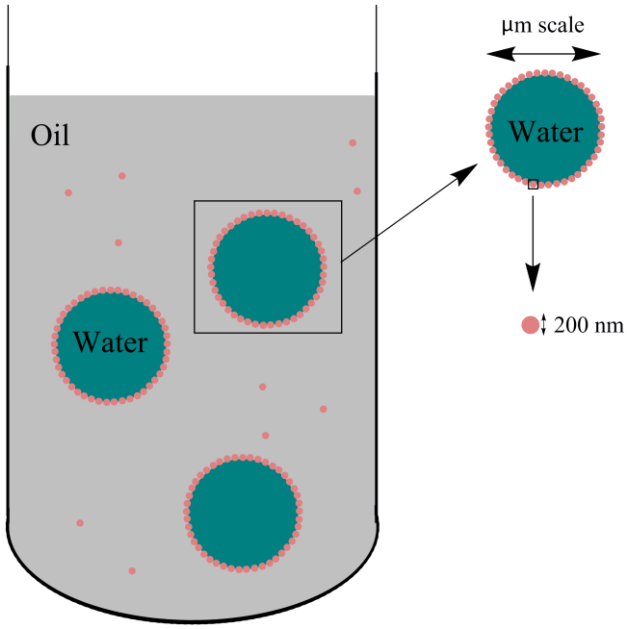

Figure 1: *Schematic illustration of general inverse Pickering emulsion (w/o) emulsion stabilized by colloidal particles.*

Microcapsules composed of nanometer-sized colloidal building blocks can potentially be applied in fields such as carriers for sensitive materials[1,18], loci for catalytic reactions[19] and encapsulation of food products to name only a few.[20,21,22]

Using functional polymeric nanoparticles (FPNPs) that have an affinity for both the continuous phase and the aqueous phase, inverse Pickering emulsions can be stabilized, and by crosslinking the particles at the interface, MCs that are stable and permeable can be produced (Chapter 5).[23] The method for MC formation and simultaneous encapsulation of live micro-organisms needs to have certain characteristics. Firstly, the barrier should be permeable for small molecules, but impermeable for the encapsulated micro-organisms. Secondly, the formation of the MC shell should not interfere with the viability of the encapsulated micro-organisms.

Hybrid permeable starch-FPNP based-MCs synthesized in Chapter 5 were used for the encapsulation of *E. coli. E. coli* is commonly used as a model system for the expression of specific proteins. One of the obvious advantages is that this modified *E. coli* allows for the secretion of AmyA without additional expression vectors needed. AmyA is required for the anticipated triggered degradation of the capsule wall. These MCs are synthesized and produced, as shown in Figure2, by crosslinking the particles (indicated by the purple band) from an inverse Pickering emulsion stabilized by BE-FPNPs. The MAnh-FPNPs were synthesized previously, and contain highly reactive maleic anhydride moieties that can react with various

other functionalities (Chapters 3 and 5). In this work, the MAnh moieties are used to introduce pendant boronic acid (BA) moieties on the particle surface, as described in Chapter 5. Starch was used as the polymeric crosslinker that facilitates the crosslinking of multiple individual FPNPs at the inverse Pickering emulsion droplet interface, through multiple diol functionalities on the starch interacting with the BA moieties on the BA-FPNPs. Beneficial characteristics of starch as a crosslinker are its biodegradability and the benign properties it has towards live cells. For the encapsulation of viable micro-organisms, the ability for the MCs to be permeable and stable is a prerequist, since the viability is dependant on the introduction of nutrients that are used by the micro-organisms for their metabolic processes. It is thus envisaged that the formation of permeable capsules and the encapsulation/ entrapment of live bacteria that could, upon a trigger, degrade the capsule wall, could be simultaneously achieved through this encapsulation procedure. The triggered release of the encapsualted material is a novel feature of the MCs that we hope to achieve. The general fabrication of MCs is presented in Chapter 5, Figure 2.

To the authors' knowledge, this is the first time that work is reported on the development of permeable MC formation benign to the encapsulate bacteria, with the addition of triggered degradation of the MC wall leading to the possible release of the encapsulated bacteria. The encapsulation and viability of the bacteria within the MCs was determined using confocal fluorescence microscopy (CFM). To demonstrate the scope of FPNP-stabilized MCs having potential triggered release of the encapsulated material, live bacteria were encapsulated, that upon a trigger can degrade the starch-FPNPs MC wall.

Experimental Methods

Materials. Maleic anhydride (MAnh, Sigma Aldrich, 99%) was re-crystallized from chloroform. Styrene (St, Fluka, 99.5%) was purified by distillation and stored over 4 Å molecular sieves at 4 °C, divinylbenzene (DVB, Sigma Aldrich, >99%) was used after inhibitor, t-butylcatechol, was removed by passing through an alumina column and stored over 4 Å molecular sieves also at 4 °C. Methyl ethyl ketone (MEK, Sigma Aldrich, >99.7%), *n*-heptane (Kimix, anhydrous), toluene (Sigma Aldrich, anhydrous 99.5%), tetrahydrofuran (THF) were distilled before use and stored over molecular sieves. Double distilled deionized water (ddH2O, our lab), starch (Fluka, starch from potatoes), 3-aminophenylboronic acid monohydrate (BA, Sigma Aldrich, >99.9%) and 1,3 propanediol (kindly donated by the W.A.L van Otterlo group) was used as received. 2, 2'-Azo-bis(isobutyronitrile) (AIBN, Riedel de Haen) was recrystallized twice from methanol and dried under vacuum, and stored at 4 °C.

DNA manipulations and transformations. The polymerase chain reaction (PCR) was performed using a Perkin Elmer Gene Amp® PCR System 2400 and TaKaRa Ex Taq™ (Takara Bio Inc, Japan), as per the manufacturer's recommendations. The GAL10 promoter was amplified using primers listed in Table 1

(Inqaba Biotec, Pretoria, South Africa) designed for yeast mediated ligation (YML) and visualized on a 0.80% agarose gel. DNA was eluted from agarose gels with the Zymoclean™ Gel Recovery Kit (Zymo Research, California, USA).

***Table 1**. Primers used for PCR amplification of the GAL10 promoter*

Primer name	Sequence (5' - 3')
GAL10_YML-AmyA-L	ATGATTACGAATTAATTCGAGCTCGGTACCGCTAGGGCCCGATCAAAA ATCATCG
GALl10_YML-AmyA-R	ATACTTGAAGTCGACACTCTCATGAATTCGTACTTAATTAAGAATTTTC AAAAATTCT

The yBBH1-AmyA_Gal10 episomal plasmid was constructed using YML with *S. cerevisiae* Y294 as host.[31] *S. cerevisiae* Y294[AmyA_Gal10] transformants were selected according to Cripwell *et al*.,[32] the yBBH1-AmyA_Gal10 vector was retrieved and transformed into *E. coli* DH5α. Plasmid DNA was isolated using the High Pure Plasmid Isolation kit (Roche, Mannheim, Germany). Standard protocols were followed for all DNA manipulations and *E. coli* transformations.[33] Unless stated otherwise, all chemicals for *E. coli* transformation were of analytical grade and were obtained from Merck (Darmstadt, Germany). The *E. coli* transformants were cultivated at 37 °C in Terrific Broth (12 $g \cdot L^{-1}$ tryptone, 24 $g \cdot L^{-1}$ yeast extract, 4 $mL \cdot L^{-1}$ glycerol, 0.1 M potassium phosphate buffer) containing 100 $\mu g \cdot mL^{-1}$ ampicillin for selective pressure.[33]

Amylase gene and GenBank accession number. The amyA gene originated from *Aspergillus tubingensis* (Accession number JF809672).

Strains and plasmids. The genotypes of the bacterial strains, as well as the plasmids used in this study are summarized in Table 2.

***Table 2**. Strains and plasmids used in this study*

Strains and plasmids	Genotype	Reference/Source
Strains		
E. coli DH5α	supE44 ΔlacU169 (ϕ80lacZΔM15) hsdR17 recA1 endA1 gyrA96 thi-1 relA1	[34]
E. coli DH5α[AmyA_GAL10]	bla $GAL10_P$-amyA-$ENO1_T$	This study
S. cerevisiae Y294	α leu2-3,112 ura3-52 his3 trp1-289	ATCC 201160
S. cerevisiae Y294[AmyA_Gal10]	URA3 $GAL10_P$-amyA-$ENO1_T$	This study
Plasmids		
pUC19-GAL10X	URA3-$GAL10_p$-XYN2-$PGK1_T$-G418-URA3	Microbiology Dept.Stellenbosch
yBBH1-AmyA	bla URA3 $ENO1_P$-amyA-$ENO1_T$	[35]
yBBH1-AmyA_GAL10	bla URA3 $GAL10_P$-amyA-$ENO1_T$	This study

Synthesis

MAnh-FPNPs. PNPs were synthesized as reported in Chapter 3.

Modification of the MAnh-FPNPs to obtain 100BE-FPNPs, Rhodamine B labelling of starch and preparation of hybrid MCs. The modification of the MAnh-FPNPs and the labelling of the starch

necessary for capsule formation is similar to the procedures described in Chapter 5 for producing the MCs.

Encapsulation of bacteria and degradation of MC wall. The same general procedure was followed as in Chapter 5 for MC formation was followed for the production of MCs . Instead of using water as dispersed phase, TB broth containing viable bacteria was used. In a typical experiment, 5.4 mg starch was dissolved in the bacteria suspension in TB broth (0.1 mL). BE-FPNPs (10 mg) were dispersed in the toluene layer using a sonicator to ensure all particles were well dispersed. Once the starch was dissolved the two phases were mixed and hand-shaken to produce MCs hosting viable bacteria. For the degradation studies, galactose was added to the TB broth right before encapsulation to allow bacteria to produce amylase.

Characterization and analysis

Electron microscopy measurements were performed on a Zeiss Merlin FEGSEM unit working at a working distance of 3-4 mm, voltage of 5 kV, Iprobe of 250 pA and the inlens detector for high resolution imaging.

Confocal fluorescent microscopy (CFM) imaging was done using a Carl Zeiss LSM780 (Carl Zeiss, Germany) confocal microscope using the diode 405 nm CW/PS (pulsed) laser, argon multiline laser 25mW at 488 nm and the 561 nm laser to excite the auto-fluorescent particles, DAPI and the rhodamine-labelled starch respectively. The objectives that were used includes the EC “Plan-Apochromat”20x/0.8 M27, LD “Plan-Nuofluar” 40x/0.6 Corr M27 and LCI “Plan-Apochromat”63x/1.4 Oil DIC M27. For post processing ZEN 2011 imaging software (Carl Zeiss (Germany) was used**.** To compare the fluorescence of the Rhodamine-B starch degradation, the fluorescence was measured using standard setup parameters. All intensities were measured using the same settings and the fluorescence is given as a relative mean fluorescent intensity (RMFIs) value. RMFIs are scaled units of fluorescence.[58] The images are stored as 16-bit images, varying in shades of grey. The brightness of each pixel is divided into a range from 0 to 243, with 0 being black and 243 being the brightest intensity. The RMFIs (a.u) within that range was taken and AF compared.[40]

Light microscopy was conducted on a Zeiss Axio Scope.A1 Polarized Light Microscope. Microscope is fitted with various objectives, N-Achroplan pol 20x0.45, EC plan-Neofluar Pol 40x/0.9, EC Epoplan pol 50x/0.7, EC Epoplan-neopluar Pol 50x/0.8 and Epoplan-neofluar Pol 50x/1.0.

Results and Discussion

Synthesis of MAnh-FPNPs

Previously reported MAnh-FPNPs, with tunable size, morphology and surface chemistries, were used as the basis for MC formation using an inverse Pickering emulsion as a template (refer to Chapter 3 and Chapter 5). The particles are synthesized via a surfactant-free dispersion polymerization of styrene (St), divinylbenzene (DVB) and maleic anhydride (MAnh) in a butanone-*n*-heptane mixture in the presence of a radical initiator.

Subsequently, the MAnh-FPNPs were decorated with 3-aminophenylboronic acid monohydrate (BA) via the reactive MAnh group introducing functional groups, to obtain BA-modified FPNPs

(BA-FPNPs). This was achieved using a nucleophilic substitution reaction at the MAnh group, including the ring opening reaction of the MAnh moiety, and a nucleophilic addition of the amine, followed by a ring closure reaction producing a five-membered imide ring. Further modification of the BA functionality, using a 1,3-propanediol, was performed to obtain the corresponding boronate ester decorated FPNPs (BE-FPNPs) (Refer to Chapter 5).

Formation of inverse Pickering emulsions

Ultimately, for MC fabrication (Chapter 5), the individual particles at a Pickering emulsion droplet interface had to be crosslinked. Stable inverse Pickering emulsions were produced, although polydisperse droplets and clumps at the interface were observed (Figure 2A/2B), the emulsions showed to be stable, and macroscopic phase separation was not observed for several months.

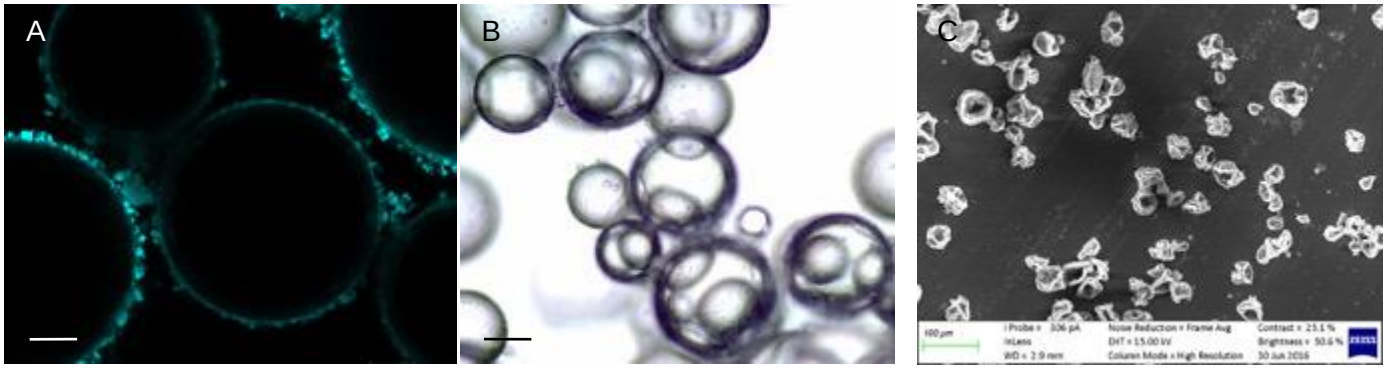

Figure 2: *A) CFM image of a stable inverse Pickering emulsion produced via hand shaking, scale bar is 10 µm. B) LM image of capsules that were formed after the introduction of starch, scale bar is 30 µm and C) SEM image of capsules after redispersion experiment, scale bar 100 µm.*

The clumps on the interface can be attributed to the amount of energy required to produce a monolayer of particles at the interface. The process requires enough energy and time to transfer all the particles to the interface. Emulsification obtained by hand-shaking did not allow the amount of energy added to the emulsion to be sufficient, resulting in an emulsion with a broader polydispersity in droplets size and aggregates of particles at the interface. Despite this, the encapsulation of viable bacteria does not allow the use of high shear.

Microcapsule synthesis and encapsulation

Starch, being a hydrophilic biopolymer, was added to the aqueous phase before emulsification, and the reaction between a boronic acid and 1,2-diol is well documented in literature.[26–29] The further modification of the BA-FPNPs to BE-FPNPs was done as the reactivity between BA-

FPNPs and 1,2-diol (starch) resulted in destabilization of the Pickering emulsion droplets before MCs could be produced. It was shown in previous chapter that the presence of BE-FPNPs instead of BA-FPNPs slows down the reaction between the 1,2-diol-starch and BE-FPNPs sufficiently for MC formation to occur (Chapter 5). A transesterification reaction between a 1,2-diol and the BE-FPNPs proceeded at the Pickering emulsion droplet interface by the replacement of the 1,3-diol with the 1,2-diol, with this reaction being preferred, and resulted in crosslinking of the individual particles from the inside of the droplet, sufficient to produce the MCs. Using LM that is a non-destructive imaging technique, the produced MCs could be visualized (Figure 2B). The capsules needed to be dried before SEM analysis, and the analysis itself took place under high vacuum. Consequently, collapsed/deflated capsules were expected as a result of evaporation of the aqueous phase from within the capsules (Figure 2C). These results are indicative of successful MC formation. For a more in-depth report on the MC formation, please refer to previous chapter.

MCs with encapsulated bacteria were produced by the addition of *E. coli*, that was transfected and cloned to be able to produce amylase upon exposure to a galactose trigger, suspended in Terrific Broth (TB broth) as the aqueous phase, combined with various concentrations of starch to ensure that the crosslinking occurred at the interface. It was found that 5.4-10 wt% starch, relative to growth medium also gave permeable and the most stable MCs, similar to Chapter 5. The aqueous phase was added to the particle dispersion in toluene (as the continuous phase) and hand-shaking took place for 30 seconds. As discussed in Chapter 5, the addition of starch did not influence the stability of the inverse Pickering emulsion. However, the starch proved to crosslink sufficient individual particles for MC formation. Confocal fluorescence microscopy

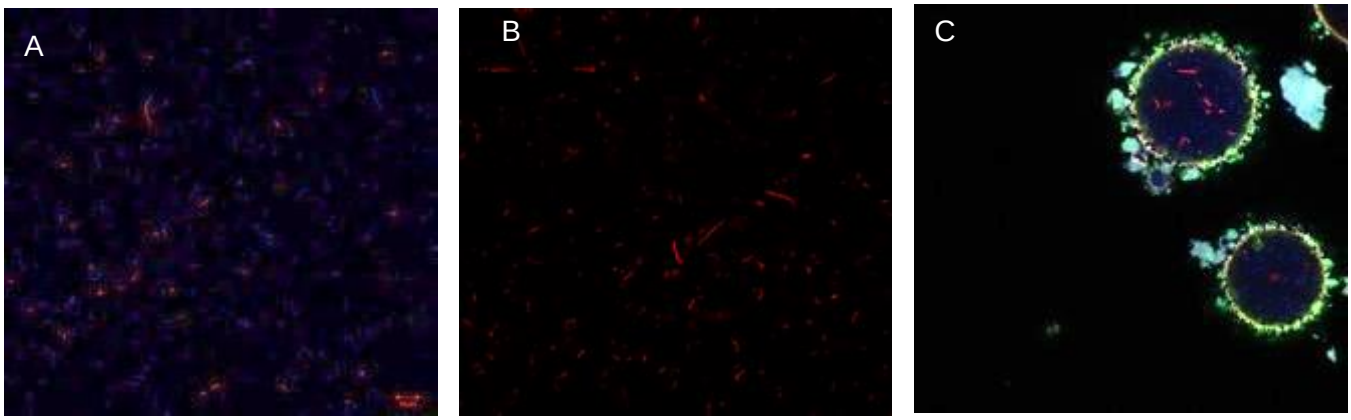

Figure 3: *A) Positive control of viable bacteria stained with DAPI, B) Negative control of dead bacteria stained with PI and C) MCs with encapsulated bacteria. Scale bar is 50 µm*

(CFM) was used to image the newly formed MCs, hosting encapsulated bacteria (Figure 3). The MAnh-FPNPs were previously shown to be benign to cells (Chapter 4) and to evaluate the viability of the encapsulated bacteria, techniques based on fluorescent staining were utilized. Viable cells were stained with 4',6-diamidino-2-phenylindole (DAPI, blue), and propidium iodide (PI, red) that only penetrates a cell once the cell membrane is compromised, which is indicative of non-viable cells. Positive and negative controls of *E. coli* were imaged and are shown in Figure 3A and Figure 3B respectively with the MC hosting the encapsulated bacteria in Figure 3C. Positive control experiments were done by dispersing the bacterial cells in the growth medium and imaged after the addition of DAPI and PI, and for the negative control, ethanol was added to the cells to ensure cell death. The MAnh-FPNPs were previously shown to be auto-fluorescent (Chapter 4) and were excited using the 405 nm laser (green), that overlapped with the absorption spectrum of DAPI to a small degree, that is excited using the 488 nm laser (blue). PI was excited using 633 nm laser (red). *E. coli* was dispersed in TB medium and encapsulated within the MCs, and it was apparent that at least 90% of the bacteria remained viable within the MCs (Figure 3C).

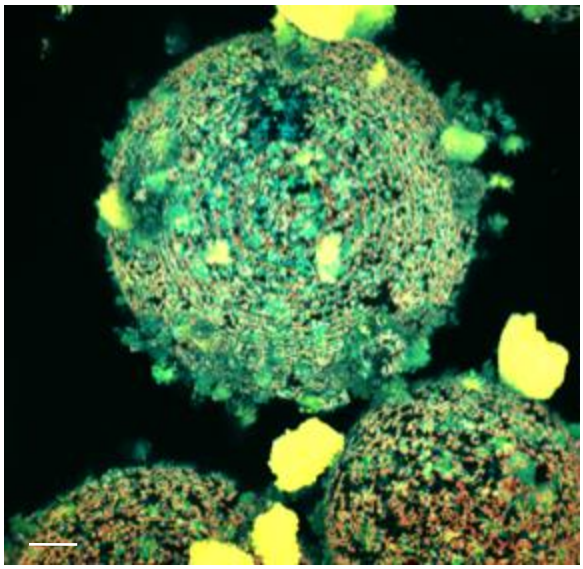

Figure 4: *Maximum projected image of the individual stacks taken through a MC. The particles at the interface are visible (green and yellow) with the red starch layer indicative of the crosslinking that took place at the interface. The viable bacteria are also visible within the MC. Scale bar is 10 µm.*

Finally, to visualize the starch MC wall and the degradation of it upon a trigger, starch was fluorescently labelled with Rhodamine-B.

Figure 4 is a composite image compiled from a series of 2D focus stacking images, using CFM, made by focusing up and down through the MCs to acquire images at different planes, to provide a more comprehensive image of the MCs.[30] The stacks were reconstructed and projected into a 2D image of the 3D structure of individual MCs with encapsulated bacteria (Figure 4). The image shows the MC wall stays intact throughout the MC synthesis, with the starch layer clearly visible inside the capsule (red) with visible pores on the interface with all of the bacteria residing inside the MC (nuclei of the bacteria visible as blue within the MC).

Triggered degradation of MC wall

In experiments tracking degradation of the MC wall, galactose was added to the aqueous phase straight before encapsulation. Experiments were conducted in triplicate and MCs were formed with and without the introduction of galactose to compare the degradation of the starch layer using the relative intensity of fluorescence indicative of the Rhodamine-B (starch). The same fluorescent dyes as in the previous section were added before the emulsification step, and the same lasers used for excitation, with the addition of the 561 nm laser for the excitation of Rhodamine B. The encapsulation procedure, in the presence of starch within the aqueous phase, resulted in the simultaneous encapsulation of live bacteria and the crosslinking of individual particles at the interface, visible as a red layer at the particle interface (Figure 5A/5C). Previously, stable and permeable MCs were obtained using 5.4 wt% and 10 wt% starch, relative to the dispersed phase using 100BA-FPNPs. For that reason and for comparison purposes, two different MCs with encapsulated bacteria were fabricated; first, using 5.4 wt% starch and secondly, using 10 wt% starch to establish whether a difference in the degradation of starch at the MCs interface can be observed.

After the MCs were produced, with and without galactose as trigger, the viability of the bacteria was not affected, and individual dyes were recognized (Figure 5A/5C). From the CFM images that were taken 1 hour after MC formation (Figure 5B/5D), it could be seen that the viability did not change as a function of starch concentration, as the starch concentration increases from Figure 5A (5.4 wt%) to Figure 5C (10 wt%). Comparing Figure 5A and Figure 5C, it was observed that the intensity of fluorescence at the interface, indicative of starch (red), appears higher for the higher concentration starch (Figure 5C). Figure 5B and Figure 5D are images showing MCs with the addition of galactose, as a trigger for the recombinant *E. coli* to start producing amylase. The produced amylase degrades the starch that crosslinks individual BE-FPNPs, forming the MC wall. A decrease in starch fluorescence was observed (Figure 5A compared to Figure 5B, and similarly Figure 5C compared to Figure 5D). To confirm this observation, post-processing of the images was conducted. The relative mean fluorescence intensity (RMFI) was taken at six areas of interest of equal size, on the MC wall.

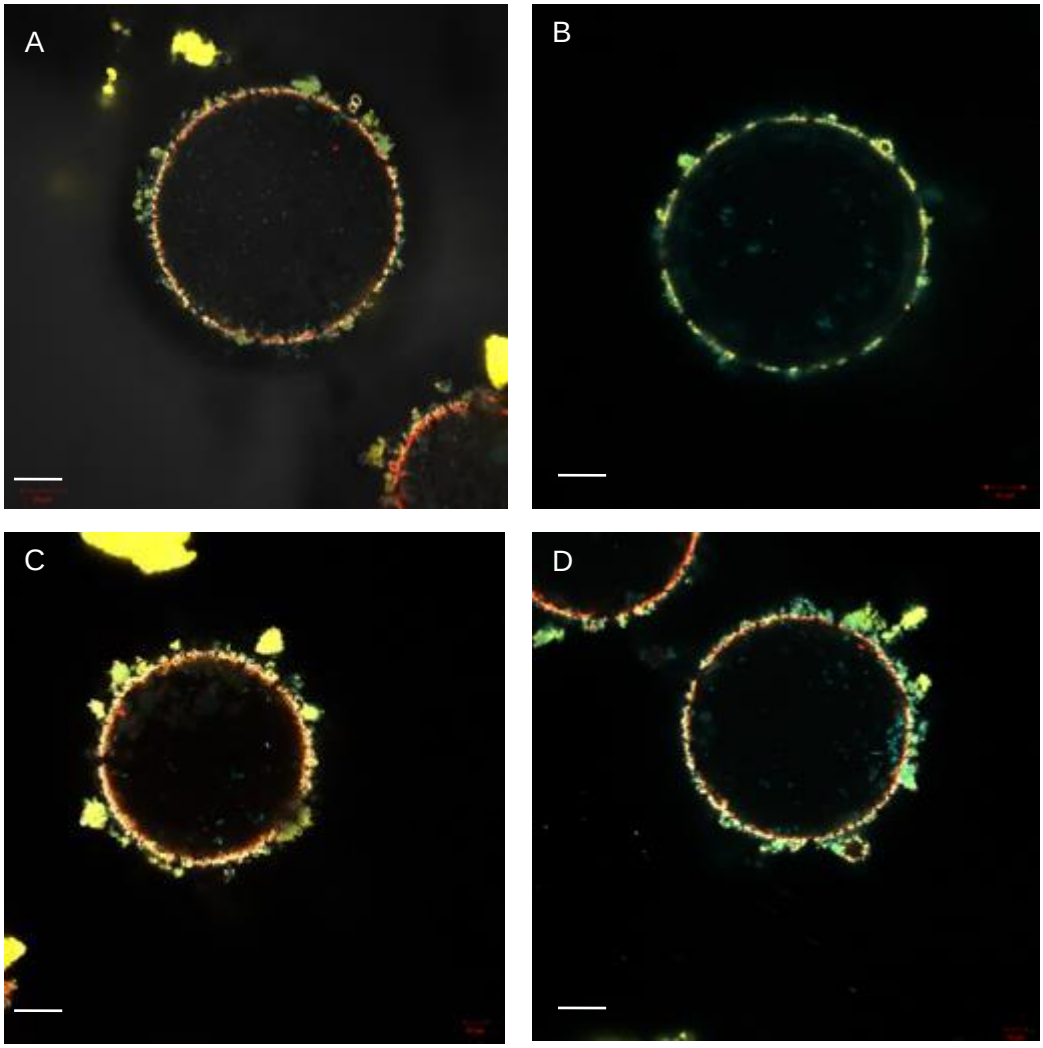

Figure 5: *Images of MCs with encapsulated bacteria. A) MC produced using 5.4 wt% starch. B) MC produced using 5.4 wt% starch and galactose as trigger to allow production of amylase. C) MCs produced using 10 wt% starch and D) MCs produced using 10wt% starch galactose as trigger for amylase production.*

The intensity of fluorescence vs the frequency for each sample were compared as an average of the six areas. The results are shown in Figure 6. Column A represents the MCs produced using 10 wt% starch, also indicating the highest RFI. Ccolumn B represents the MCs after the trigger is activated (after 1 hour) and is lower in RFI compared to the initial 10 wt% starch-MCs. The same trend was observed for the MC produced using 5.4 wt% starch, represented by Column C, and Column D the 5.4 wt % starch-MCs after the trigger is activated.

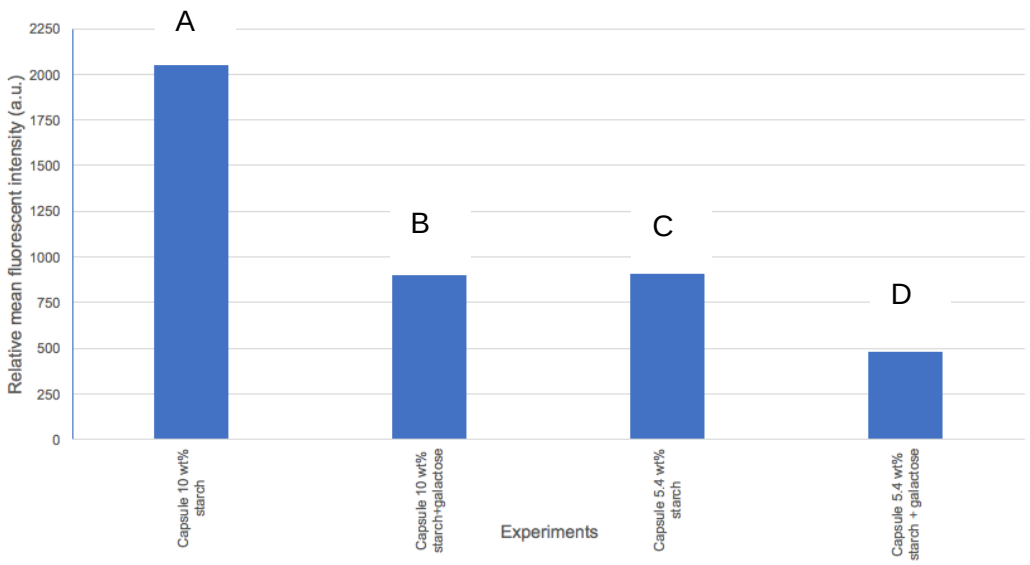

Figure 6: *Relative fluorescent intensity of the fluorescent-labelled MC wall as a function of starch concentration and introduced galactose. The column A represents the MC produced using 10 wt% starch, also indicating the highest RFI. Column B represents the MC after the trigger is activated and a lower RFI is observed. The same trend was observed for the MC produced using 5.4 wt% starch represented by column C, and MCs after the trigger is activated are represented by column D..*

The graph confirms a decrease in RFI of starch in both experiments, with the 5.4 wt% starch-MC having the least amount of fluorescence related to the rhodamine labelled starch after 1 hour. Although some fluorescence is left, this work shows that the approach could be promising for the triggered release of encapsulated bacteria.

The above results suggest that the stabilization of BE-FPNPs, through the interfacial crosslinking of the individual particles at the Pickering emulsion droplet interface, led to a porous MC providing a benign environment to live bacteria. To develop the scope of such a system as potential drug carrier or micro-compartments for biochemical reactions, the triggered degradation of the MC wall was shown. In this case, the *E. coli* was constructed to express recombinant *AmyA* under the control of a galactose inducible promoter so that amylase production could be prompted upon exposure to the trigger. In a system without the addition of galactose, the intensity of fluorescent dye from the starch did not decrease. The opposite was true after the addition of galactose and concomitant amylase release. Amylase degraded the starch that crosslinks the individual particles at the interface. Intensity studies of the fluorescence signal of the rhodamine-labelled starch were conducted. It was shown that the introduction of galactose made the starch layer less visible and the intensity of the starch layer decreasing as time proceeded (after 1 hour of MC formation and introduction of galactose)

confirmed the degradation of the starch. These results indicate that the MCs can potentially be used as a triggered release system.

Conclusion

Pickering emulsion droplets served as successful templates for the assembly and crosslinking of particles at the interface, producing novel hybrid MCs. This contribution also reported the successful encapsulation of *E. coli* and showed that these bacteria could be kept viable during and after the emulsification and MC formation. MC formation was accomplished by the interfacial crosslinking of boronate ester-decorated PNPs using starch. The environment inside the MCs is benign to the bacteria, and the MCs can be degraded using a trigger.

As a proof-of-principle for triggered release applications, live bacteria which are able to release an enzyme that can degrade the starch MC crosslinker were encapsulated, and once a trigger is introduced the MC wall degraded.

This work serves as a proof-of-principle for the targeted release of amylolytic enzymes by encapsulated bacterial cells that degrade the starch MC wall upon induction of a trigger.

References

(1) van Wijk, J.; Heunis, T.; Harmzen, E.; Dicks, L. M. T.; Meuldijk, J.; Klumperman, B. Compartmentalization of Bacteria in Microcapsules. *Chem. Commun.* **2014**, *50*, 15427-15430

(2) Dinsmore, D.; Hsu, M. F.; Nikolaides, M. G.; Marquez, M.; Bausch, a R.; Weitz, D. a. Colloidosomes: Selectively Permeable Capsules Composed of Colloidal Particles. *Science.* **2002**, *298* (5595), 1006–1009.

(3) Wang, J. X.; Wang, Z. H.; Chen, J. F.; Yun, J. Direct Encapsulation of Water-Soluble Drug into Silica Microcapsules for Sustained Release Applications. *Mater. Res. Bull.* **2008**, *43* (12), 3374–3381.

(4) Rozynek, Z.; Mikkelsen, A.; Dommersnes, P.; Fossum, J. O. Electroformation of Janus and Patchy Capsules. *Nat. Commun.* **2014**, *5* (3945), 1-6.

(5) Lawrence, D. B.; Cai, T.; Hu, Z.; Marquez, M.; Dinsmore, A. D. Temperature-Responsive Semipermeable Capsules Composed of Colloidal Microgel Spheres. *Langmuir.* **2007**, *23* (2), 395–398.

(6) Nedovic, V.; Kalusevic, A.; Manojlovic, V.; Levic, S.; Bugarski, B. An Overview of Encapsulation Technologies for Food Applications. *Procedia Food Sci.* **2011**, *1*, 1806–1815.

(7) Vidhyalakshmi, R.; Bhakyaraj, R.; Subhasree, R. S. Encapsulation " The Future of Probiotics " -A Review. *Biol. Res.* **2009**, *3* (3–4), 96–103.

(8) Keating, C. D. Inorganic Protocells: Gated Access to Microreactors. *Nat. Chem.* **2013**, *5*, 449.451.

(9) Bu, Z.; Callaway, D. J. E. Proteins Move! Protein Dynamics and Long-Range Allostery in Cell Signaling. *Adv. Protein Chem. Struct. Biol.* **2011**, *83*, 163–221.

(10) Krasaekoopt, W.; Bhandari, B.; Deeth, H. Evaluation of Encapsulation Techniques of Probiotics for Yoghurt. *Int. Dairy J.* **2003**, *13* (1), 3–13.

(11) Keen, P. H. R.; Slater, N. K. H.; Routh, A. F. Encapsulation of Lactic Acid Bacteria in Colloidosomes. *Langmuir.* **2012**, *28* (46), 16007–16014.

(12) van Wijk, J.; Salari, J. W. O.; Zaquen, N.; Meuldijk, J.; Klumperman, B. Poly(methyl Methacrylate)–silica Microcapsules Synthesized by Templating Pickering Emulsion Droplets. *J. Mater. Chem. B* **2013**, *1* (18), 2394-2406.

(13) van Wijk, J.; van Deventer, N.; Harmzen, E.; Meuldijk, J.; Klumperman, B. Formation of Hybrid Poly(styrene-Co-Maleic Anhydride)–silica Microcapsules. *J. Mater. Chem. B.* **2014**, *2* (30), 4826-4835.

(14) Ramsden, W. Separation of Solids in the Surface-Layers of Solutions and "Suspensions" (Observations on Surface-Membranes, Bubbles, Emulsions, and Mechanical Coagulation).-Preliminary Account. *Proc. R. Soc. Lond.* **1903**, *72* (477-486), 156-164.

(15) Pickering, S. U. Pickering: Emulsions. *J. Chem. Soc.* **1907**, *91*, 2001–2021.

(16) Salari, J. W. O.; Jemwa, G. T.; Wyss, H. M.; Klumperman, B. Reconstruction of the 3D Structure of Colloidosomes from a Single SEM Image. *Soft Matter.* **2011**, *7* (5), 2033-2041.

(17) Sardessai, Y.; Bhosle, S. Tolerance of Bacteria to Organic Solvents. *Res. Microbiol.* **2002**, *153*, 263–268.

(18) Cui, J.; Wang, Y.; Postma, A.; Hao, J.; Hosta-Rigau, L.; Caruso, F. Monodisperse Polymer Capsules: Tailoring Size, Shell Thickness, and Hydrophobic Cargo Loading via Emulsion Templating. *Adv. Funct. Mater.* **2010**, *20* (10), 1625–1631.

(19) Shchukin, D. G.; Ustinovich, E.; Sukhorukov, G. B. Photocatalytic Microreactors Based on TiO2-Modified Polyelectrolyte Multilayer Capsules. *Photochem. Photobiol. Sci.* **2003**, *2*, 975-977.

(20) Vilivalam, V. D.; Illum, L.; Iqbal, K. Starch Capsules: An Alternative System for Oral Drug Delivery. *Pharm. Sci. Technol.* **2000**, *3* (2), 64–69.

(21) Chen, T.; Colver, P. J.; Bon, S. a. F. Organic–Inorganic Hybrid Hollow Spheres Prepared from TiO2-Stabilized Pickering Emulsion Polymerization. *Adv. Mater.* **2007**, *19* (17), 2286–2289.

(22) van Wijk, J. **2014**. *Production of Microcapsules by Templating Pickering Emulsion Droplets : Mechanism and Practical Applications*. Doctoral thesis. Eindhoven University of Technology.

(23) Van Wijk, J.; Van Deventer, N.; Harmzen, E.; Meuldijk, J.; Klumperman, B. Formation of Hybrid Poly(styrene-Co-Maleic Anhydride)-Silica Microcapsules. *J. Mater. Chem. B.* **2014**, *2* (30), 4826-4835.

(24) Harmzen-Pretorius, E.; Klumperman, B. Stabilization of Poly(Styrene-Co-Divinyl Benzene-Co-Maleic Anhydride) Nanoparticles at Interface of Pickering Emulsion Droplet as Template for Permeable Microcapsule Formation. *Manuscript in Preparation*. **2017**.

(25) Binks, B. P.; Clint, J. H. Solid Wettability from Surface Energy Components: Relevance to Pickering Emulsions. *Langmuir.* **2002**, *18* (4), 1270–1273.

(26) Furikado, Y.; Nagahata, T.; Okamoto, T.; Sugaya, T.; Iwatsuki, S.; Inamo, M.; Takagi, H. D.; Odani, A.; Ishihara, K. Universal Reaction Mechanism of Boronic Acids with Diols in Aqueous Solution: Kinetics and the Basic Concept of a Conditional Formation Constant. *Chemistry.* **2014**, *20* (41), 13194-13202.

(27) Marinaro, W. A.; Prankerd, R.; Kinnari, K.; Stella, V. J. Interaction of Model Aryl- and Alkyl-Boronic Acids and 1,2-Diols in Aqueous Solution. *J. Pharm. Sci.* **2015**. *104* (4), 1399-1408.

(28) Cegłowski, M.; Gierczyk, B.; Schroeder, G. Poly(methyl Vinyl Ether-Alt-Maleic Anhydride) Functionalized with 3-Aminophenylboronic Acid: A New Boronic Acid Polymer for Sensing Diols in Neutral Water. *J. Appl. Polym. Sci.* **2014**, *131* (18), 9358–9364.

(29) Pappin, B.; Kiefel, M. J.; Houston, T. A. Boron-Carbohydrate Interactions. In *Carbohydrates - Comprehensive Studies on Glycobiology and Glycotechnology*. 1st Ed, Chuan-Fa Chang, InTech. **2012**, 37-54.

(30) LSM 710. *Operating Manual*. Zeiss. **2010**, 0–138.

(31) Cho, K.; Yoo, Y.; Kang, H. δ-Integration of Endo/exoglucanase and β-Glucosidase Genes into the Yeast Chromosomes for Direct Conversion of Cellulose to Ethanol. *Enzym. Microb Technol.* **1999**,

25, 23–30.

(32) Cripwell, R.A., Rose, S.H., van Zyl, Van Zyl, W. H. Expression and Comparison of Codon Optimised Aspergillus Tubingensis Amylase Variants in Saccharomyces Cerevisiae. *FEMS Yeast Res.* **2017**, *17* (4), 1-27.

(33) Bean, K.; Black, C. F.; Govan, N.; Reynolds, P.; Sambrook, M. R. Preparation of Aqueous Core/silica Shell Microcapsules. *J. Colloid Interface Sci.* **2012**, *366* (1), 16–22.

(34) Sambrook, J.; Fritsch, E. F. *Molecular Cloning: A Laboratory Manual*. Cold Spring Harbor:New York, Ed.; Cold Spring Harbor Laboratory Press, **1989**.

(35) Viktor, M. J.; Rose, S. H.; Zyl, W. H. Van; Viljoen-bloom, M. Raw Starch Conversion by Saccharomyces Cerevisiae Expressing Aspergillus Tubingensis Amylases. *Biotechnol Biofuels.* **2013**, *6* (1), 167.

(36) Tsakos, M.; Schaffert, E. S.; Clement, L. L.; Villadsen, N. L.; Poulsen, T. B. Ester Coupling Reactions – an Enduring Challenge in the Chemical Synthesis of Bioactive Natural Products. *Nat. Prod. Rep.* **2015**, 605–632.

CHAPTER 7

One-pot synthesis of Janus particles via a Pickering emulsion droplet template utilizing the rotation of particles at the interface

Functional polymer-based Janus particles are synthesized with utilizing the rotational movement of a particle at a droplet interface.

Synthesis of Janus nanoparticles synthesized by templating inverse Pickering emulsion droplets in a one-pot fashion through utilizing the rotation of the particles at the interface. *E. Harmzen, R. Dreyer and B. Klumperman. Manuscript in preparation (2017)*

Synthesis of Janus nanoparticles synthesized by templating inverse Pickering emulsion droplets in a one-pot fashion through utilizing the rotation of the particles at the interface

Abstract

In this chapter, we report the facile one-pot synthesis of functional polymeric Janus nanoparticles (JNPs) by partially reacting the stabilizing particles, at the interphase, of an inverse Pickering emulsion droplet. The approach utilizes the reaction between gold ions in the dispersed phase and functionalized poly(styrene-*co*-maleic anhydride-*co*-divinylbenzene) nanoparticles that stabilize the Pickering emulsion droplets. Finally, correlative imaging allowed visualization of the partially decorated particles. JNPs were successfully characterized by field emission electron microscopy (FEG-SEM) using inlens-, backscatter- and STEM detector. This forms a starting point for the synthesis of JNPs with varying fractions of surface coverage, in an easy, one-pot fashion, with different hemispheres, leading to promising nanomaterials with specific properties, which could be exploited through different chemical functionalities.

Introduction

One of the more intriguing and challenging aspects of current material science is the synthesis of anisotropic particles with novel morphologies, as theoretical work has shown that such particles could be useful in various potential applications.[1–5] Previous work showed that particles in the nanometer scale display unique properties that are not always observed in the bulk material, and these properties can be tuned and adjusted in order to obtain a material with desired properties.[6] In general, functional polymeric nanoparticles (FPNPs) which have reactive groups on their surface, can be further modified through complementary reactions.[7,8] However, the control over the functional groups and degree of functionalization are challenging. To our knowledge, there have only been few reports on this topic.[7,9–11] A specific approach to anisotropic particles is the preparation of particles with differently functionalized hemispheres, also known as Janus nanoparticles (JNPs).[12] In 1988 and 1991, Casagrande and De Gennes, respectively, were the first to mention and describe JNPs.[13,14] Beyond the use as elementary building blocks for supramolecular assembly, JNPs have numerous promising applications within material science and biomedical fields, including highly specific biosensors, etc.[2,4,15,16]

The most basic JNP is a sphere consisting of two distinct hemispheres, *i.e*. hemispheres that are physically or chemically different from each other.[17,18]

Combining specific physical and chemical properties of nanoparticles in different hemispheres can afford opportunities to create revolutionary material combinations, such as modulated optical (bio) sensors, display technologies or electronic paper applications.[19,41,42.43] In the last decade the term JNPs has emerged as a new division of structures, and the synthesis and applications of these structures have been and continue to be studied broadly.[17,18,19] In literature, it is seen that the most profound challenges remain the ability to modify one hemisphere without altering the surface of the other, as well as producing nanometer-sized JNPs.[3,6]

Pickering discovered that fine, solid particles could be used to stabilize an emulsion droplet (Figure 1B). Particles are partially wetted by an organic phase and partially wetted by an aqueous phase. The combination of the affinity of the particles for both these phases, the three phase contact angle, and the energy of detachment, allows effective stabilization of oil or water droplets of submicron diameter for periods exceeding several years.[1,13,14]

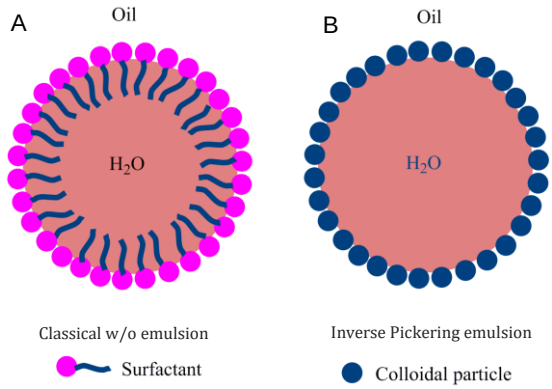

Figure 1: *Illustration of A) a classical inverse emulsion stabilized by surfactants and B) an inverse Pickering emulsion stabilized by colloidal particles. Structures are not drawn to scale*.

In Pickering emulsions, solid particles diffuse to an interfacial region and remain there in a stable mechanical equilibrium.[22] The rotation and dynamics of these particles at the interface of the two different phases have not yet received widespread attention.[23,24] Closed interfaces, such as those of dispersed droplets, would be promising tools for the synthesis of JNPs, due to the fact that the working area is a substantially greater interfacial area than a planar interface. [6,25] The hypothesis in literature is that the particles rotate at an interface, and in order to make JNPs, research groups have always taken the approach of immobilizing the particles at the interface before doing the different chemistries on the two hemispheres.[3,15,25–27] There are various

methods of producing JNPs. Some of these methods include partial masking, template-directed self-assembly of particles, phase separation, and controlled surface nucleation reactions.[2,4,8,10–12] These techniques are tedious and require multiple steps. Whereas previous work until now has always prevented the rotation of the particles, we have found a way to utilize the rotation of the particles, which entails the fast reaction of gold ions being reduced relative to the time scale of the rotational movement of the particles. This was utilized to control the fraction of the surface that is covered by the gold NPs, thus making JNPs with varying surface coverage.

The current study details the combination of already reactive FPNPs, at an inverse Pickering emulsion droplet interface, and explains how a complementary chemical reaction proved to be a powerful method to produce JNPs. The basis for this work is formed by inverse Pickering emulsion droplets as template for JNP synthesis, having a complementary chemical compound with affinity towards the reactive FPNP surface placed only in the aqueous phase. The reaction between the FPNP surface exposed to the aqueous phase, and the complementary introduced group in the aqueous phase, can only take place from within that phase, producing JNPs. Our hypothesis is that by the selective reaction of a compound from one phase and the rotation of the particles at the interface, we can control the fraction of surface being covered.

The hypothesis will be tested by firstly synthesizing FPNPs with reactivity towards a complementary compound in the aqueous phase of the Pickering emulsion droplet. The reactivity introduced to the surface of the particles will be a pendant tertiary amine and the complimentary compound in the aqueous phase will be gold ions, know to be able to interact with each other. Secondly, the two phases that make up the Pickering emulsion are used to produce JNPs along the interface.[29] Finally, it is essential that the particles that stabilize the Pickering emulsion should be easy to synthesize and modify, and must have tunable hydrophobicity in order to be suitable stabilizers.[29–31] The use of Pickering emulsion droplets as templates leads to each particle at the interface being exposed on one side to the

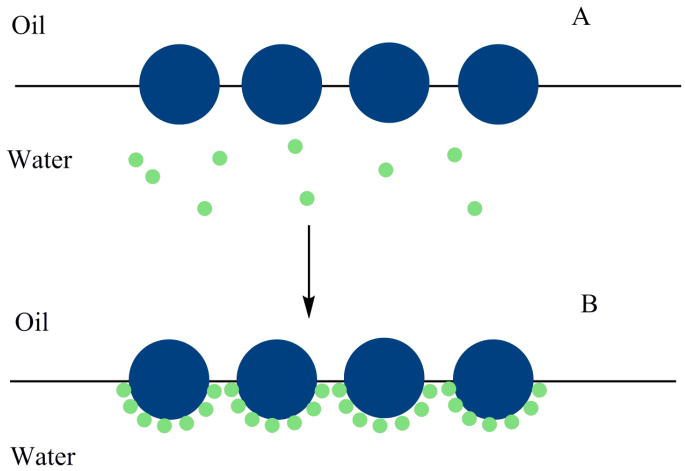

Figure 2: *Illustration of interaction at interface of Pickering emulsion interface*

dispersed aqueous phase, and on the other side to the continuous (oil) phase (Figure 2A). Therefore, these particles are no longer exposed to identical phases, and thus, it is possible to introduce different functionalities through the separate phases (Figure 2B).

MAnh-FPNPs are synthesized via a surfactant-free dispersion polymerization (Chapter 3). Additional reactivity can be introduced to the surface of the nanoparticles via a post-polymerization functionalization step. Here we introduce 3-(*N*,*N*-dimethylamino)propyl-1-amine (DMAPA) to the MAnh moiety, followed by a ring closure reaction to obtain DMAP-maleimide moieties on the DMAPA-FPNPs (Figure 3A). These modified DMAPA-FPNPs are used for the formation of inverse Pickering emulsions. The surface of the DMAPA-FPNPs, at the interface, can be decorated due to the stabilization of the droplet of the inverse Pickering emulsion and complementary reactions, between the Au^{3+} ions in solution and the exposed modified particle surface at the interface, allowing strong specific interactions between the tertiary amine moiety and Au ions (Figure 3B).

The reaction between gold(III) (Au^{3+}) ions and tertiary amines in acid solution is well documented in literature.[32–34] The amine can also act as a reducing agent. Transfer of electrons from the amine to the Au-ion causes the reduction of $HAuCl_4$, resulting in the formation of metallic Au. The resulting metallic-Au can then undergo nucleation and form Au NPs.[34] Tertiary amines are thus extremely good ligands or scavengers for $[AuCl_4]^-$ ions from acidic solutions. The surface exposed to the aqueous phase allows for the DMAPA to extract Au^{3+} ions from solution, and reduce Au-ions to Au-NPs, covering the DMAPA-FPNPs surface exposed to the aqueous phase with Au, producing JNPs. Thus, producing JNPs with adsorbed gold NPs onto the exposed PNP surface (Figure 3C).

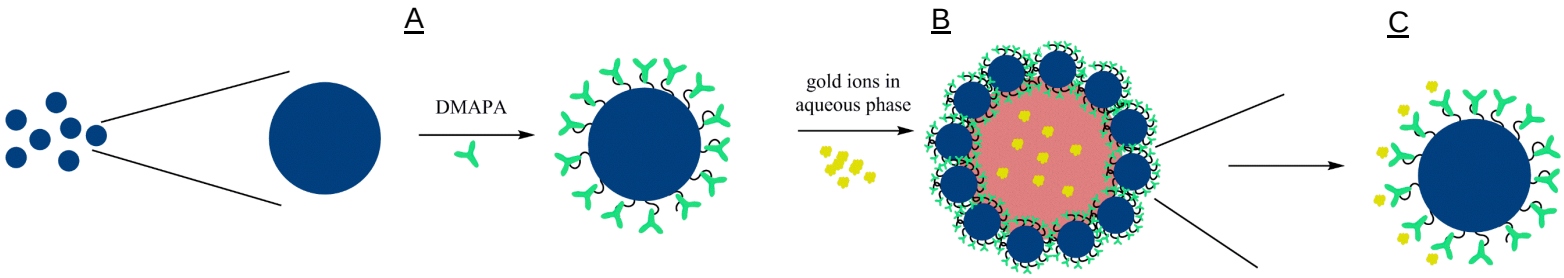

Figure 3: *Schematic overview of the synthesis route to produce functional JNPs. Blue indicates the MAnh- FPNPs. A) Indicating DMAPA-FPNPs, utilized to B) produce an inverse Pickering emulsion. The yellow is the 2M gold(iii) ions added to the dispersed phase and finally, JNPs produced, poly(St-co-DMAP Maleimide-co DVB)-Au JNPs.*

Previous research produced JNPs using “liquid-liquid” interfaces, whereby on phase was solidified, followed by reacting the exposed area. However, taking the solidification in context, this method is no longer a liquid-liquid interfacial reaction.[2,3] To the authors’ knowledge, there are only two articles that have used droplets, without the use of solidification steps, in order to successfully produce JNPs while still trying to restrict rotation.[21,35]

Experimental Methods

Materials. Maleic anhydride (MAnh, Sigma Aldrich, 99%) was used after recrystallization from chloroform. Styrene (St, Fluka, 99.5%) was purified and stored over 4 Å molecular sieves, divinylbenzene (DVB, Sigma Aldrich, >99%) was used after inhibitor, t-butylcatechol, was removed and stored over 4 Å molecular sieves. Methyl ethyl ketone (MEK, Sigma Aldrich, >99.7%). *n*-Heptane (Kimix, anhydrous), cyclohexane (CH, Sigma Aldrich, anhydrous 99.5%), double deionized water (ddH_2O, our lab) and hydrogen chloride (HCl, Sigma Aldrich, 32%) were used as received. 2,2’-Azo-bis(isobutyronitrile) (AIBN, Riedel de Haen) was recrystallized twice using methanol and dried under vacuum before use. 3-(*N*,*N*-Dimethylamino)-1-propylamine (DMAPA, Sigma Aldrich, 99%) and gold(iii)chloride ($AuCl_3$, Sigma Aldrich, >99.99%) were used as received.

Synthesis

MAnh-FPNPs. Particles were synthesized by a method similar to Chapter with some small modifications. Maleic anhydride (2.04 g, 20.80 mmol) was dissolved in MEK (20 mL) in a 250 mL three neck round bottom flask and AIBN (6.8 mg, 4.26×10^{-2} mmol) was added to the reaction mixture. The MEK mixture was degassed for 30 minutes and in a separate flask, *n*-heptane (30 mL) was added with styrene (0.74 mL, 6.49 mmol) and DVB (0.98 mL, 6.90 mmol, 30 %) and degassed for 30 min. After the MEK-MAnh solution was degassed, the solution was placed in a 70 ºC preheated oil bath for 30 min. Under inert conditions the *n*-heptane-St-DVB solution was fed into the MEK mixture over 2 hours. The final dispersion medium was a MEK-*n*-heptane mixture (40:60) and the reaction was stopped after 4 hours.

Further modification of the PNPs. DMAPA modification of MAnh-FPNPs was done similarly to Chapter 4.

Janus particle formation. An inverse Pickering emulsion was formulated using 20 mg DMAPA -FPNPs dispersed in cyclohexane (8 mL). The mixture was sonicated for 2 minutes to ensure all particles were well dispersed within the continuous phase. 1 mL water (containing an Au concentration of 2M in HCl) was added to the particle-containing continuous phase (2 wt % particles) and vigorously hand-shaken for 30 seconds to ensure all particles migrated to the interface of the water droplets.

Characterization and analyses

Electron microscopy. The size and morphology of the particles were characterized by scanning electron microscopy (SEM) using a Zeiss MERLIN field emission gun scanning electron microscope, using an inlens, high resolution detector, a STEM detector that is for transmission electron microscopy and a backscatter detector that can detect chemical phase differences. Diameter measurements were done on ImageJ version 2.0.0. For MAnh-FPNPs particles, prior to high resolution imaging using the inlens detector, a thin layer of carbon was evaporated onto a stub containing particles, to render conductivity, avoiding surface charging caused by the electron beam. Prior to transmission imaging, dispersions were

diluted and dropped onto a carbon-coated 200 mesh copper grid and dried at ambient temperature. Backscatter images were acquired on the carbon coated grids without any coating to prevent any influence from the carbon coating.

Light microscopy was conducted on a Zeiss Axio Scope.A1 Polarized Light Microscope. The microscope is fitted with various objectives, N-Achroplan pol 20x0.45, EC plan-Neofluar Pol 40x/0.9, EC Epoplan pol 50x/0.7, EC Epoplan-neopluar Pol 50x/0.8 and Epoplan-neofluar Pol 50x/1.0

ATR-FTIR spectra were recorded using a Nicolet FTIR spectrometer (Nexus) from Thermo-Fischer equipped containing a Smart Golden Gate ATR accessory with a diamond/ ZnSe internal reflection crystal. The spectra were recorded from 3750 cm^{-1} to 700 cm^{-1} with a spectral resolution of 8 cm^{-1} and a sum of 64 individual scans. Samples were run in solid state and no sample preparation was necessary. Omnic software was used for data acquisition and Origin software was used for data processing.

Results and Discussion

There are two main limitations of the proposed method: firstly, it is important to synthesize monodispersed particles as the diameter of the particles is necessary to calculate the different particle concentrations in the inverse Pickering emulsion; and secondly, the particle layer at the interface needs to be as close as possible to a monolayer. Optimization of the inverse Pickering emulsions is, thus, of utmost importance.

Synthesis and modification of MAnh-FPNPs

Primarily, poly(St-*co*-DVB-*co*-MAnh) nanoparticles were synthesized according to Chapter 3. Additional functionality on the surface of the particles was introduced via the reaction with excess DMAPA, whereby the primary amine reacts with the reactive anhydride group via a

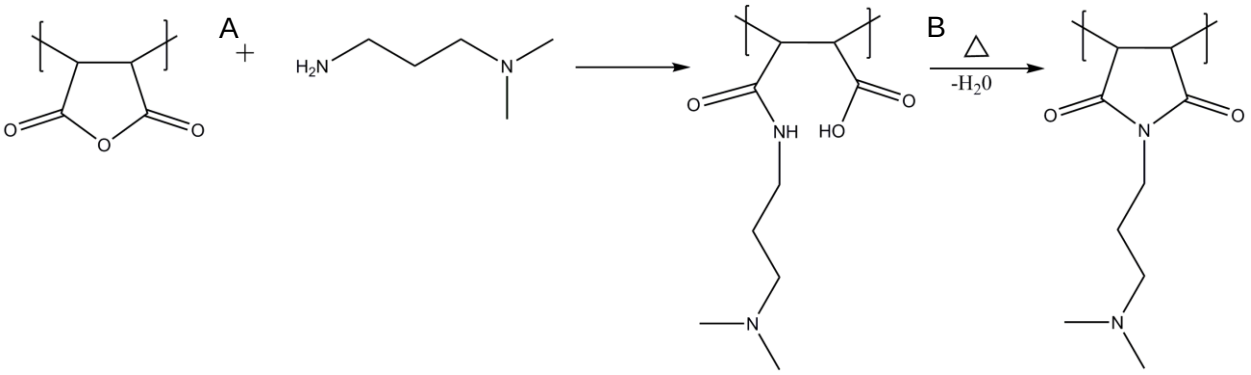

Scheme 1: *Illustration of the reaction of DMAPA onto the FPNPs followed by a ring closure reaction*

nucleophilic substitution reaction (Figure 4A).[32,33,36] After ring closure poly(St-*co*-DMAP maleimide-*co*-DVB) PNPs (DMAPA-FPNPs) having pendant tertiary amines available on the surface of the nanoparticles were obtained (Scheme 1B). The final nitrogen content was

determined to be 6.31% (calc. 7.29%) by EDX measurements, which relates well to calculated amounts should almost all MAnh be modified with DMAPA. The size of these particles was characterized by scanning electron microscopy (SEM), obtaining highly monodispersed MAnh-FPNPs with diameters of approximately 600 nm and a narrow particle size distribution.

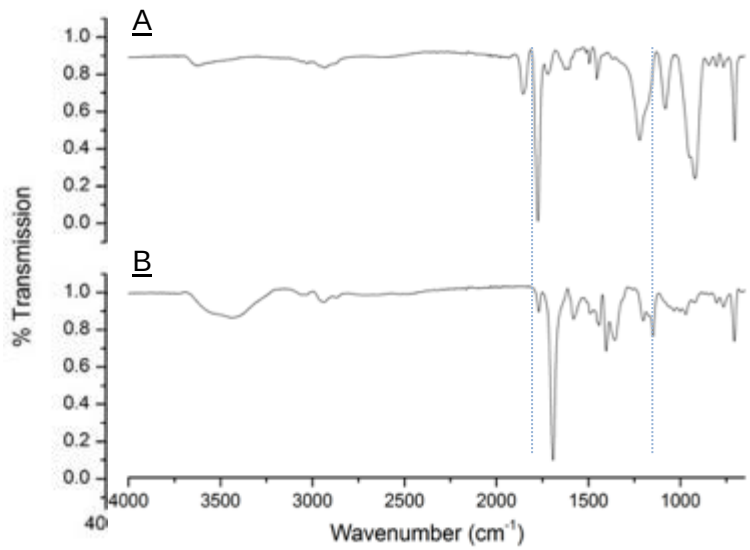

Figure 4: *ATR-FTIR spectra of A) MAnh-FPNPs and B) decorated DMAPA-FPNPs.*

ATR-FTIR analysis was conducted to confirm the introduction of DMAPA to the surface of the particles. Successful imidization of the MAnh residues was present on the particles. This is easily verified due to the disappearance of the C-O band at 1772 cm^{-1} and the appearance of a strong band at 1691 cm^{-1}, characteristic of a cyclic imide bond. Further confirmation of the ring closure is the absence of a N-H bending band, indicative of the presence of a secondary amine, at 1550 cm^{-1}.[37–39] The presence of a tertiary amine peak at 1151 cm^{-1} is confirmation of successful functionalization of the PNP surface with DMAPA onto the particle surface (Figure 4)

These particles are of interest for several reasons, firstly, they are relatively easily synthesized and their average size is easily controlled (Chapter 3). Secondly, their surface composition can be tailor-made by introducing multiple functionalities to the already-reactive surface groups. An example of this was shown above, whereby tertiary amine functionalities were introduced onto the particle surface using DMAPA.

Interfacial self-assembly of MAnh-FPNPs at water/oil droplet interface

Pickering emulsion droplets are necessary as a template for JNP formation. A calculation is made, based on Equation [40], to determine the volume of dispersed phase necessary, and to produce a stable inverse Pickering emulsion consisting of droplets with a size of 60 µm.

$$V_{\mathrm{D}} = \frac{\mathrm{r}_{\mathrm{D}}\, N_{\mathrm{A}} 2\sqrt{3}R^2}{3}$$

Equation 1: *Equation to calculate the different parameters of a Pickering emulsion*

where, N_{A} is the number of particles, based on the mass of particles used, attached to the interface of the droplet, having the particles hexagonally closed packed, R is the radius of the particles, $A_{\mathrm{p}} = 2\sqrt{3}R^2$ is the area occupied by a particle, V_{D} is the total volume of the dispersed phase and r_{D} is the radius of the Pickering droplet set as a constant.

It is known that a liquid-liquid interface particles will adsorb if their surface energy lies between those of the two layers, thus lowering the total free energy.[40] The possible amphiphilic nature of our MAnh-FPNPs, stemming from the ability of maleic anhydride to ring open and become hydrophilic, and the hydrophobic nature of the styrene, means that MAnh-FPNPs can adsorb both on oil-in-water and on water-in-oil droplets. Various parameters were optimized to obtain the ideal conditions for stable Pickering emulsion droplets with a monolayer of particles at the interface (Table 1). These parameters include particle size, particle concentration and different continuous phases. In Table 1, only the results for cyclohexane as the continuous phase are shown, although ethyl acetate and toluene were tested, as that gave the most promising Pickering emulsions for these specific FPNPs.

After each Pickering emulsion preparation, the droplets were viewed using light microscopy and confocal microscopy to visualize the droplet uniformity as well as the particles on the interface. It was observed that both 200 nm and 600 nm sized particles, at a particle concentration of 2 wt% (relative to dispersed phase), yielded the most stable and well-defined inverse Pickering emulsions.

Table 1: *Parameters tested to optimize stable inverse Pickering emulsions.*

Size (nm)	Concentration	Dispersed phase	Continuous phase	[A] Stable	[B] Duration stable
200-300	0.5 wt%	4 mL	8 mL	Y	W
	1 wt%	2 mL	8 mL	Y	W
	2 wt%	1 mL	8 mL	Y	W
	3 wt%	0.67 mL	8 mL	Y	W
500-600	0.5 wt%	4 mL	8 mL	Y	W
	1 wt%	2 mL	8 mL	Y	W
	2 wt%	1 mL	8 mL	Y	W
	3 wt%	0.67 mL	8 mL	Y	W
800	0.5 wt%	4 mL	8 mL	Y	M
	1 wt%	2 mL	8 mL	Y	M
	2 wt%	1 mL	8 mL	Y	M
	3 wt%	0.67 mL	8 mL	Y	M
1300	0.5 wt%	4 mL	8 mL	N	-
	1 wt%	2 mL	8 mL	N	-
	2 wt%	1 mL	8 mL	Y	M
	3 wt%	0.67 mL	8 mL	Y	M

Additional information 1: [A] The stability is divided into Y= yes and N= no. [B] The duration is divided into M= minutes, D= days and W= weeks.

An examination of the Pickering emulsions showed, 1) the Pickering emulsions did not phase separate, even several weeks after emulsification, 2) all particles adsorbed at the interface and not in the aqueous phase, showed as particles (blue fluorescence) at the interface of the droplets (Figure 5A-B), and 3) a monolayer of closely packed particles is observed at the interface (Figure 5C). This behavior allows for nearly all particles to be accessible for further modification, such as the reactions described below.

Well-defined Pickering emulsion droplets were synthesized, although some particle aggregation is seen in the fluorescence images. It is possible that more well-defined particle layers could be produced if a high shear homogenizer was used. This would ensure that sufficient energy is supplied, and therefore controlling that all particles sit at the interface as a monolayer. However, the metal on the homogenizer would reduce the gold ions in the dispersed phase. For that reason, the Pickering emulsions were produced through manual shaking obtaining Pickering emulsions sufficiently well-defined for the desired applications. All following work was also based on using 600 nm particles, to be able to visualize the product easier.

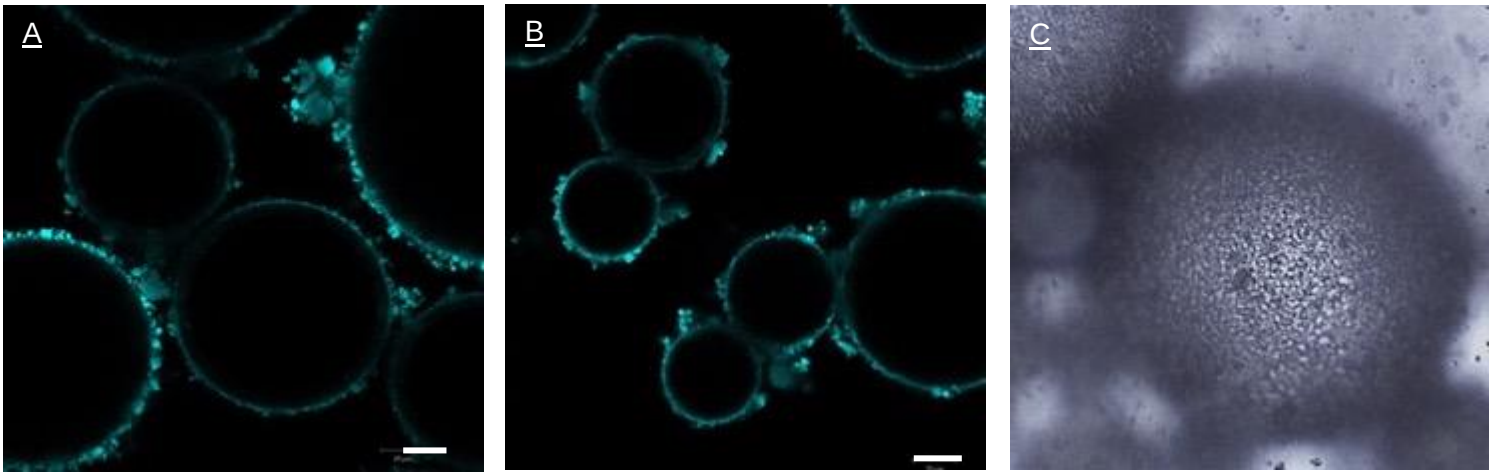

Figure 5: *A-B) Confocal microscopy images of an inverse Pickering emulsions. The Pickering emulsions were produced by the addition of 1 mL distilled water to 20 mg DMAPA-FPNPs (dp = 600 nm) dispersed in 8 mL of cyclohexane. Emulsification was obtained by handshaking. Scale bar is 20 µm. C) Light microscopy image of same emulsion indicating sufficient close packing of the particles in a hexagonal manner at the interface.*

Stepwise modification of various surface percentages utilizing particle rotation

Finally, from the preliminary parameters tested for the formation of inverse Pickering emulsions, JNPs syntheses were based on using 2 wt% particles (relative to dispersed phase). Inverse Pickering emulsions were produced using 20 mg DMAPA-FPNPs dispersed in 8 mL cyclohexane as continuous phase, and various volumes of a 2 M Au^{3+} HCl in aqueous phase (Table 2).

Table 6: *Table of different reaction parameters optimized to synthesize JNPs..*

Sample nr	Particle mass mg	MAnh-DMAPA mmol	Molar ratio DMAPA:Au	Au mmol	Au mass (mg) added (total of 1 mL 2M HCl)
A	20	0.0448	1: 1	0.0448	17.636
B	20	0.0448	1:0.75	0.0336	13.227
C	20	0.0448	1:0.5	0.0224	8.818
D	20	0.0448	1:0.25	0.0112	4.409
E	20	0.0448	1: 01	0.0045	1.764

Following the addition of the Au^{3+}-containing aqueous phase, emulsification was achieved by vigorous, manual shaking of the mixture for 20 seconds. After Pickering emulsion formation, small amounts of the droplets were dispersed into THF solution to break the droplets into

individual particles. These particle solutions were dried onto prepared SEM stubs and viewed under the FEG-SEM microscope whereby the resolution allowed for individual particles to be visualized utilizing the STEM detector. The inlens detector and backscatter detector (BSD) were used to correlate morphologies and chemical phase differences. The STEM detector allows the visualization of synthesized JNPs, due to the difference in contrast between the organic polymeric phase and the attached gold NPs. Since the particles are made up of organic matter and the gold has a substantially heavier atomic mass, a contrast can be observed,[29] whereby, the higher electron density of gold, *i.e*. the gold phase, appears darker in STEM, and the DMAPA-FPNPs appear lighter. The inlens detector allows for the visualization of high-resolution morphology and particle surfaces, while the BSD detects chemical phase differences because of atomic mass differences.

Figure 6 depicts JNPs that were synthesized using various concentrations of gold ions in the

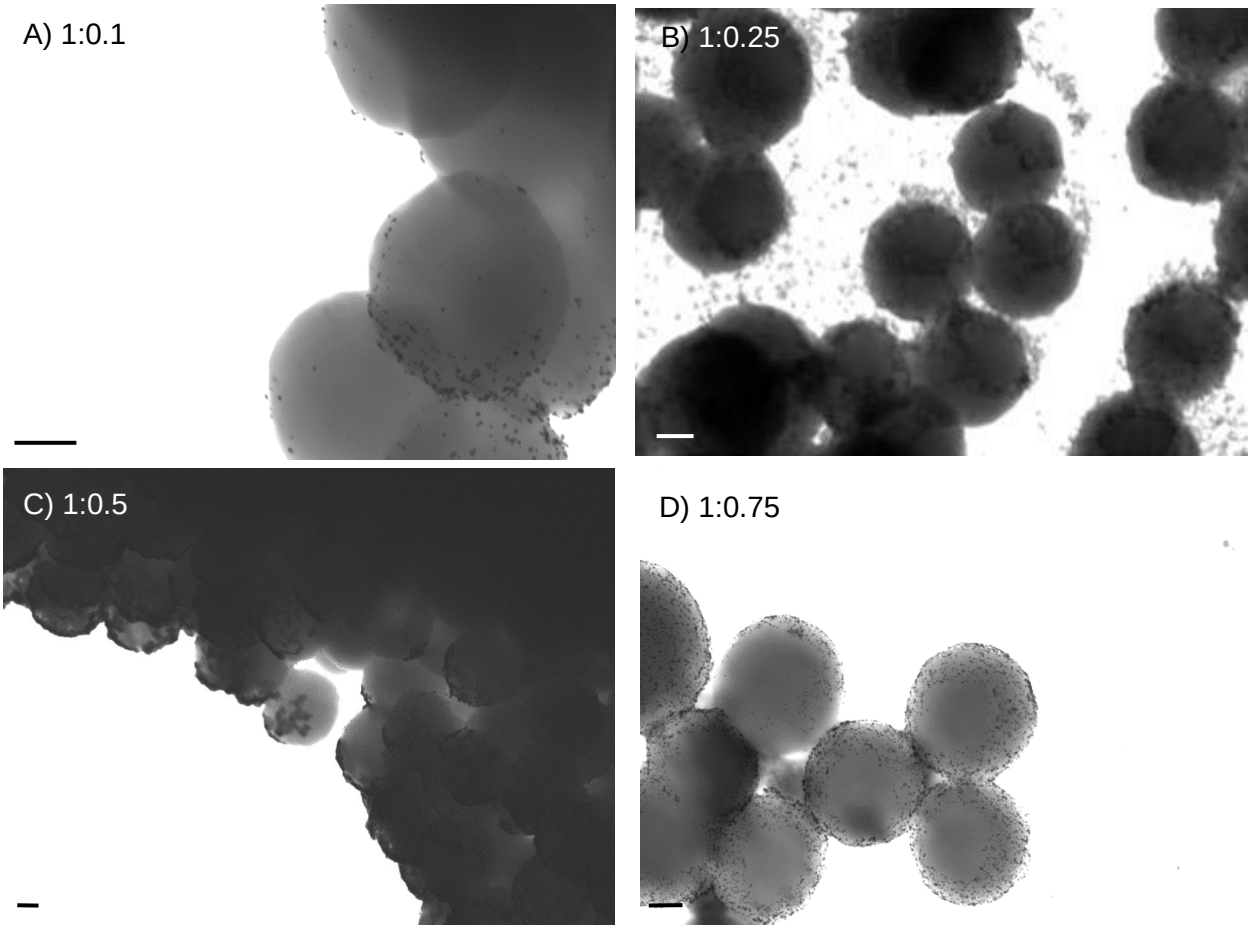

Figure 6: *STEM images of JNPs synthesized using various amounts of Au-ions in the dispersed phase. A) 1:0.1 DMAPA/Au^{3+},B) 1:0.25 DMAPA/Au^{3+}, C) 1.0.5 DMAPA/Au^{3+} and D) 1:075 DMAPA/Au^{3+} The scale bars in the images are 200 nm.*

dispersed phase. An increase in the concentration of Au^{3+}-ions in the aqueous phase, leads to an increase in Au-modified surface area. This is illustrated by JNPs prepared from a molar ratio of 1:0.25 DMAPA/Au^{3+} resulting in JNPs with approximately 25% surface coverage of gold (Figure 6B) compared to JNPs prepared by 1:0.75 DMPAPA/ Au^{3+} that resulted in approximately 75% surface covered (Figure 6D). This was further confirmed using SEM to visualize 1:0.5 DMAPA/Au^{3+} resulting in JNPs with approximately 50% surface coverage (Figure 7).

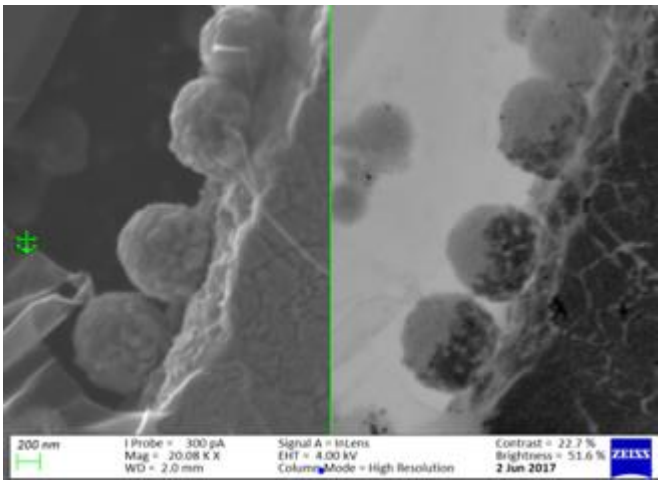

Figure 7: *Correlated image visualizing JNPs made using a DMAPA/Au3+-ion ratio of 1:0.5 using simultaneously the inlens detector (left) coupled with a BSD (right). Scale in the image is 200 nm.*

This can possibly be explained by the rotational movement of the particles at the interface. DMAPA moieties that are accessible on the surface of the DMAPA-FPNPs come into contact with the Au^{3+}-ions in the aqueous solution, and react with the Au^{3+}-ions. To the authors knowledge the rotation of the particles at a droplet interface has never been experimentally shown.[3,27] With this work, showing that JNPs with varying fractions of surface coverage can be produced, it not only shows that these particles rotate at the interface, but that we can use this property to synthesize tunable Janus particles.

If the rate at which the particles rotated was extremely fast, the particle surface would be homogenously covered by gold NPs, and that is not what we observed. We hypothesize that the particles rotate or rather tumble slower than the speed at which the gold ions are reduced. The fact that at a 1:1 mole ratio we synthesized FPNPs that are completely covered by gold NPs, indicates that the particles do rotate completely; even when they are partially covered with gold they continue to tumble until all the gold is reacted from within the aqueous phase. Based on this, our results are in line with our hypothesis, that through the utilization of the selective reaction from only one phase and the rotation of particles, we could control the fraction of covered surface area.

If only a small amount of Au^{3+}-ions are added to the dispersed phase, all the available Au^{3+}-ions in the solution react with the accessible DMAPA. Then, as the particles rotate, there are no Au^{3+}-ions left in solution to decorate the rest of the particle surface. When there is a higher concentration of Au^{3+}-ions, there are not enough available DMAPA molecules to react with all of

the Au^{3+}-ions, leaving unreacted Au^{3+}-ions in the dispersed phase. Subsequently, as the particles rotate and expose more DMAPA to the Au^{3+}-ions, they are able to react, and the surface area decorated with gold increases. When a 1:1 molar ratio of the Au^{3+}-ions in solution to DMAPA on the particles, the entire particle gets covered by gold (image is not show). This suggests that the percentage of particle surface area decorated is directly proportional to the concentration of Au^{3+}-ions added to the disperse phase. This process results in controlled synthesis of poly(St-*co*-DMAPA maleimide-*co*-DVB)-Au JNPs.

Conclusion

To our knowledge, this is the first time that the rotation of the particles at the interface of a Pickering emulsion was used to synthesize JNPs with a controlled fraction of the surface of the NP being covered.

We showed a facile synthesis method of the synthesis of functional JNPs. The JNPs were successfully synthesized by templating inverse Pickering emulsion droplets. The utilization of these DMAPA-FPNPs and complementary Au^{3+}-ions resulted in the facile synthesis of functional poly(St-*co*-DMAPA maleimide-*co*-DVB)-Au JNPs. The JNPs were successfully visualized using various detectors on a FEG-SEM system, and correlative imaging was done for the first time on JNPs, confirming the morphology of the JNPs.

The ratio of Au^{3+}-ions to DMAPA directly influenced the percentage of the nanoparticle surface that was decorated. When a 1:1 molar ratio exists of the gold ions in solution to DMAPA on the particles, the entire particle was covered by gold. Conversely, when a 0.75:1 molar ratio was used, approximately ¾ of the particle surface was covered by Au, leaving roughly ¼ of the surface unaffected. The inverse affect was observed when using 0.25:1 ratios. When using a 0.5:1 ratio it was observed that 50% of the particle surface was decorated. It was noted that the gold coating occurred in localized areas, leaving distinct patches of unreacted and reacted areas on the particle surface.

Thus, it was confirmed that simple and inexpensive Pickering emulsions could be used as an elegant approach for the formation of JNPs using crosslinked DMAPA-FPNPs. Various chemistries can be introduced via the two different phases leading to promising nanomaterials with specific properties. We, therefore, can develop new organic-inorganic nanomaterials with spatial and chemical anisotropy. Indeed, each hemisphere of the JNPs can potentially be specifically functionalized, leading to systems that could be highly useful in biological or optical applications.

References

(1) Chevalier, Y.; Bolzinger, M. A. Emulsions Stabilized with Solid Nanoparticles: Pickering Emulsions. *Colloids Surfaces A Physicochem. Eng. Asp.* **2013**, *439*, 23–34.

(2) Berger, S.; Synytska, A.; Ionov, L.; Eichhorn, K.; Stamm, M. Stimuli-Responsive Bicomponent Polymer Janus Particles by " Grafting from "/" Grafting to " Approaches. *Macromolecules.* **2008**, *41* (24), 9669–9676.

(3) Hong, L.; Jiang, S.; Granick, S. Simple Method to Produce Janus Colloidal Particles in Large Quantity. *Lingmuir.* **2006**, *22* (23), 9495–9499.

(4) Kaewsaneha, C.; Tangboriboonrat, P.; Polpanich, D.; Eissa, M.; Elaissari, A. Preparation of Janus Colloidal Particles via Pickering Emulsion: An Overview. *Colloids Surfaces A Physicochem. Eng. Asp.* **2013**, *439*, 35–42.

(5) Jiang, S.; Chen, Q.; Tripathy, M.; Luijten, E.; Schweizer, K. S.; Granick, S. Janus Particle Synthesis and Assembly. *Adv. Mater.* **2010**, *22* (10), 1060–1071.

(6) Perro, A.; Reculusa, S.; Ravaine, S.; Bourgeat-Lami, E.; Duguet, E. Design and Synthesis of Janus Micro- and Nanoparticles. *J. Mater. Chem.* **2005**, *15* (35–36), 3745–3760.

(7) Engelhardt, N.; Ernst, A.; Kampmann, A.-L.; Weberskirch, R. Synthesis and Characterization of Surface Functional Polymer Nanoparticles by a Bottom-Up Approach from Tailor-Made Amphiphilic Block Copolymers. *Macromol. Chem. Phys.* **2013**, *214* (24), 2783–2791.

(8) Ballauff, M.; Lu, Y. "Smart" Nanoparticles: Preparation, Characterization and Applications. *Polymer (Guildf).* **2007**, *48* (7), 1815–1823.

(9) He, J.; Chen, D.; Fan, X.; Wang, L.; Deng, J.; Yang, W. Reactive Poly(Divinyl Benzene- Co - Maleic Anhydride) Nanoparticles : Preparation and Characterization. *Chinese Chem. Lett.* **2013**, *24*, 970–974.

(10) Lu, J.; Shi, M.; Shoichet, S. M. Click Chemistry Functionalized Polymeric Nanoparticles Target Corneal Epithelial Cells through RGD-Cell Surface Receptors. *Bioconjug. Chem.* **2009**, *20* (1), 87–94.

(11) Nahar, M.; Dutta, T.; Murugesan, S.; Asthana,A.; Mishra, D.; Rajkumar, V.; Tare, M.; Saraf. S.Functional Polymeric Nanoparticles: An Efficient and Promising Tool for Active Delivery of Bioactives. Crit. Rev. Ther. Drug Carr. Syst. **2006**, 23 (4), 259–318.

(12) Rozynek, Z.; Mikkelsen, A.; Dommersnes, P.; Fossum, J. O. Electroformation of Janus and Patchy Capsules. *Nat. Commun.* **2014**, *5* (May), 3945.

(13) de Gennes, P. G. Soft Matter (Nobel Lecture). *Angew. Chemie* **1992**, *31* (7), 842–845.

(14) Casagrande, C.; Fabre, P.; Raphaël, E.; Veyssié, M. "Janus Beads": Realization and Behaviour at Water/Oil Interfaces. *Europhys. Lett.* **1989**, *9* (3), 251–255.

(15) Pardhy, N. P.; Budhlall, B. M. Pickering Emulsion as a Template to Synthesize Janus Colloids with Anisotropy in the Surface Potential. *Langmuir.* **2010**, *26* (16), 13130–13141.

(16) Suzuki, D.; Tsuji, S.; Kawaguchi, H. Janus Microgels Prepared by Surfactant-Free Pickering Emulsion-Based Modification and Their Self-Assembly. *J. Am. Chem. Soc.* **2007**, *129* (26), 8088–8089.

(17) Wurm, F.; Kilbinger, A. F. M. Polymeric Janus Particles. *Angew. Chem. Int. Ed. Engl.* **2009**, *48* (45), 8412–8421.

(18) Walther, A.; Müller, A. H. E. Janus Particles. *Soft Matter.* **2008**, *4* (4), 663.

(19) Glaser, N.; Adams, D. J.; Bo, A.; Krausch, G. Janus Particles at Liquid - Liquid Interfaces. *Lingmuir.* **2006**, *22* (12), 5227–5229.

(20) Laredj-bourezg, F.; Chevalier, Y.; Boyron, O.; Bolzinger, M. Emulsions Stabilized with Solid Nanoparticles: Pickering Emulsions. *Colloids Surfaces A Physicochem. Eng. Asp.* **2012**, *413*, 252–259.

(21) Liu, B.; Wei, W.; Qu, X.; Yang, Z. Janus Colloids Formed by Biphasic Grafting at a Pickering Emulsion Interface. *Angew. Chemie.* **2008**, *120* (21), 4037–4039.

(22) Melle, S.; Lask, M.; Fuller, G. G. Pickering Emulsions with Controllable Stability. *Langmuir.* **2005**, *21* (6), 2158–2162.

(23) Stancik, E. J.; Gavranovic, G. T.; Widenbrant, M. J. O.; Laschitsch, A. T.; Vermant, J.; Fuller, G. G. Structure and Dynamics of Particle Monolayers at a Liquid–liquid Interface Subjected to Shear Flow. *Faraday Discuss.* **2003**, *123*, 145–156.

(24) Stancik, E. J.; Widenbrant, M. J. O.; Laschitsch, A. T.; Vermant, J.; Fuller, G. G. Structure and Dynamics of Particle Monolayers at a Liquid - Liquid Interface Subjected to Extensional Flow. *Langmuir.* **2002**, *18* (8), 4372–4375.

(25) Lin, Y.; Bo, A.; Skaff, H.; Cookson, D.; Dinsmore, A. D.; Emrick, T.; Russell, T. P. Nanoparticle Assembly at Fluid Interfaces : Structure and Dynamics. *Langmuir.* **2005**, *21* (1), 191–194.

(26) Wang, B.; Wang, M.; Zhang, H.; Sobal, N. S.; Tong, W.; Gao, C.; Wang, Y.; Giersig, M.; Wang, D.; Möhwald, H. Stepwise Interfacial Self-Assembly of Nanoparticles via Specific DNA Pairing. *Phys. Chem. Chem. Phys.* **2007**, *9* (48), 6313–6318.

(27) Li, D.; He, Y.; Wang, S. On the Rotation of the Janus CuO/CuS Colloids Formed at a Pickering Emulsion Interface. *J. Phys. Chem. C.* **2009**, *113* (30), 12927–12929.

(28) Cayre, O.; Paunov, V. N.; Velev, O. D. Fabrication of Asymmetrically Coated Colloid Particles by Microcontact Printing Techniques. *J. Mater. Chem.* **2003**, *13* (10), 2445-2450.

(29) Petit, L.; Sellier, E.; Duguet, E.; Ravaine, S.; Mingotaud, C.; Schweitzer, A. A.; Schweitzer, A. A. Dissymmetric Silica Nanospheres: A First Step to Difunctionalized Nanomaterials. *J. Mater. Chem.* **2000**, 10, 253–254.

(30) Norris, D.; Sinko, P. Effect of Size, Surface Charge, and Hydrophobicity on the Translocation of Polystyrene Microspheres through Gastrointestinal Mucin. *J. Appl. Polym. Sci.* **1997**, 1481–1492.

(31) Jiang, J.; Zhu, Y.; Cui, Z.; Binks, B. P. Switchable Pickering Emulsions Stabilized by Silica Nanoparticles Hydrophobized In Situ with a Switchable Surfactant. *Angew. Chemie.* **2013**, *125* (47), 12599–12602.

(32) Martineza, S.; Sastreb, A. M.; Alguacil, F. J. Solvent Extraction of Gold Ž III / by the Chloride Salt of the Tertiary Amine Hostarex A327. Estimation of the Interaction Coefficient between $AuCl^{-4}$ and H^{+}. *Hydrometallurgy.* **1999**, *52* (1), 63-70.

(33) Alguacil, F. J.; Caravaca, C. Study of Gold(III)HCl Amine Alamine 304 Extraction Equilibrium System. *Hydrometallurgy.* **1993**, *34* (2), 91–98.

(34) Newman, J. D. S.; Blanchard, G. J. Formation of Gold Nanoparticles Using Amine Reducing Agents. *Langmuir.* **2006**, *22* (26), 5882–5887.

(35) Pan, Y.; Gao, J.; Zhang, B.; Zhang, X.; Xu, B. Colloidosome-Based Synthesis of a Multifunctional Nanostructure of Silver and Hollow Iron Oxide Nanoparticles. *Langmuir.* **2010**, *26* (6), 4184–4187.

(36) Lakay, E. (**2013**) *Novel Ion-Exchange Materials Derived from Poly(Styrene- Co -Maleimide) and a Study of the Extraction and Recovery of Gold (III) Chloride from Acidic Solution*s. Doctoral thesis. Stellenbosch University.

(37) Kiekens, P.; De Vrieze, S.; Van Camp, T.; Decostere, B.; Audenaert, W.; Westbroek, P. (**2008)** Electrospinning Based Nanofibrous Structures for Water Filtration. Biella-Italy. In: *Proceedings of the 8th Autex conference*.

(38) Teo, W.E.; Gopal, R.; Ramaseshan, R.; Fujihara, K.; Ramakrishna, S. Electrospun Nanofibers: Solving Global Issues. *Polymer.* **2007**, *48*, 3400–3405.

(39) Uyar, T.; Besenbacher, F. Electrospinning of uniform polystyrene fibers: The effect of solvent conductivity. *Polymer.* **2008**, *49* (24), 5336–5342.

(40) Aveyard, R.; Binks, B. P.; Clint, J. H. Emulsions Stabilised Solely by Colloidal Particles. *Adv. Colloid Interface Sci.* **2003**, *100-102*, 503–546.

(41) Yu, H.; Chen, M.; Rice, P.M.; Wang, S.X.; White. R.L.; Sun, S. Dumbbell-like Bifunctional Au−Fe_3O_4 Nanoparticles. *Nano Lett.* **2005**, *5* (2), 379-382.

(42) Crowley, P.B.; Rabe, K.S.; Worrall, J. A. R.; Canters, G. W.; Ubbink, M. The Ternary Complex of Cytochrome *f* and Cytochrome *c*: Identification of a Second Binding Site and Competition for Plastocyanin Binding. *Chem. Bio. Chem.* **2002**, *3*(6), 526-533.

(43) Sheridon, N. K. (**1998**) "Eggcrate" Substrate for a Twisting Ball Display. *Patent 4*.

CHAPTER 8

Extraction of biomolecules from dilute solutions

The last section explains the decoration of the particle surface for biomolecule extraction.

Preparation of tetraphenylborate-functionalized polymeric nanoparticles via a grafting from approach for the extraction of biomolecules**.** *E. Harmzen-Pretorius, S. Howard, B. Klumperman and P. Swart. Manuscript in preparation (2017)*

Preparation of tetraphenylborate-functionalized and boronic acid-functionalized polymeric nanoparticles for the extraction of norepinephrine and octopamine

Abstract

Surface modified- and polymer-grafted functional polymeric nanoparticles were synthesized and utilized for the extraction of norepinephrine and octopamine from dilute solutions. The surface modification was achieved by a nucleophilic substitution reaction. The grafting of a functional monomer onto functional polymeric nanoparticles (MAnh-FPNPs) was done with reversible addition-fragmentation chain transfer (RAFT) polymerization and conventional free radical polymerization. The core MAnh-FPNPs were synthesized by a surfactant-free dispersion polymerization. The successful addition of functional groups to the surface of the MAnh-FPNPs was confirmed by ATR-FTIR and the particles characterized using SEM. Boron-derivative-FPNPs showed good preliminary results with regards to the extraction of biomolecules.

Introduction

The extraction of biomolecules is a critical method used in molecular biology.[1] Catecholic compounds such as norepinephrine and its homologue, octopamine, are important small molecules in biological systems, and the detection thereof is of high importance.[2,3] These molecules are biomarkers used to detect diseases such as Parkinson′s, Alzheimer′s, and pheochromocytoma, to only name a few.[5,62-64] Due to the small amounts of catecholic compounds present in biological samples and their relative instability, their extraction presents a major challenge.[2] In recent years, extraction of catecholic compounds has been the subject of many studies employing several different approaches. These include chromatography, solid phase extraction (SPE) and molecular imprinted matrixes or complexation in aqueous solution, with compounds such as sodium tetraphenylborate (Na-TPB) (Figure 1A) or boronic acids (Figure 1B), followed by solvent extraction procedures, to name only a few.[4–10] However, the detection and extraction of these compounds are generally associated with major difficulty that results in high costs, lengthy procedures and inefficient isolation.[11–14] There is no doubt that SPE has become the method of choice for extraction.[15] Recently, more efficient approaches are the subject of ongoing research.

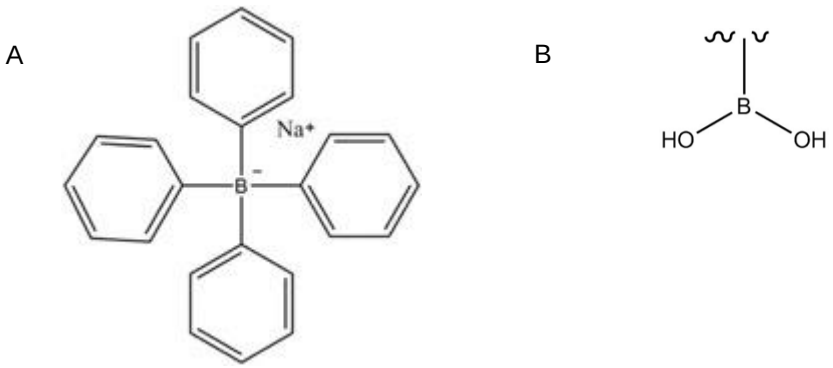

Figure 1: *A) Chemical structure of sodium tetraphenylborate ($NaBPh_4$) and B) Generic form of a boronic acid (BA) molecule*

Various particles of different size (*e.g* nano- and micrometer) and nature have been investigated as functional materials. These materials include organic materials such as polymeric particles, or inorganic materials such as metal oxides.[16–19] Among all functional polymer-based particles of nanometer size, FPNPs have received significant attention because of ease of synthesis, their tunable nature, and the wide range of functionalities that can be introduced.[20–23] FPNPs can be prepared via various methods, including micelle formation using functionalized block copolymers followed by solvent extraction,[24,25] introduction of a functionality via a non-covalent bond to the surface of the particles,[26,27] and the covalent attachment[28,29] and the grafting of functional monomers to the surface of the partices[30] (Chapter 2).

The grafting of a functional polymer on the particle surface for the preparation of "hairy-like" FPNPs represents an existing approach as each graft offers a multi-functional arm. This is particularly important in extraction applications, as it would increase the extraction efficiency of the particles.[31,32] The polymeric grafts can be introduced through a direct polymerization using vinyl functionalized-PNPs. In this case, the functional particle acts as a monomeric unit which adds to a growing polymeric radical. A drawback of this method is possible crosslinking. Alternatively, the polymeric arms can be slowly grown from the FPNPs through living radical polymerization. The advantage of using living polymerization is that the growing chains are of a specific length, and slower polymer growth occurs, hence minimizing crosslinking. Extensive research has been done on living radical polymerizations – where RAFT mediated polymerization has been used extensively to synthesize polymers of a wide-range of

functionalities.[33,34] RAFT has also been used to create complex macromolecular architectures, having defined end groups to additionally control and design advanced "hairy-like" FPNPs.[35–39]

In the present study, novel MAnh-FPNPs based on poly(styrene-*co*-maleic anhydride-*co*-divinylbenzene) are synthesized via a surfactant-free dispersion polymerization (Chapter 3). The particles having available reactive groups (MAnh, vinyl bonds or RAFT end group) on the surface are subject to further modification for biomolecule extraction. The general synthesis of the two approaches are shown in Figure 2.

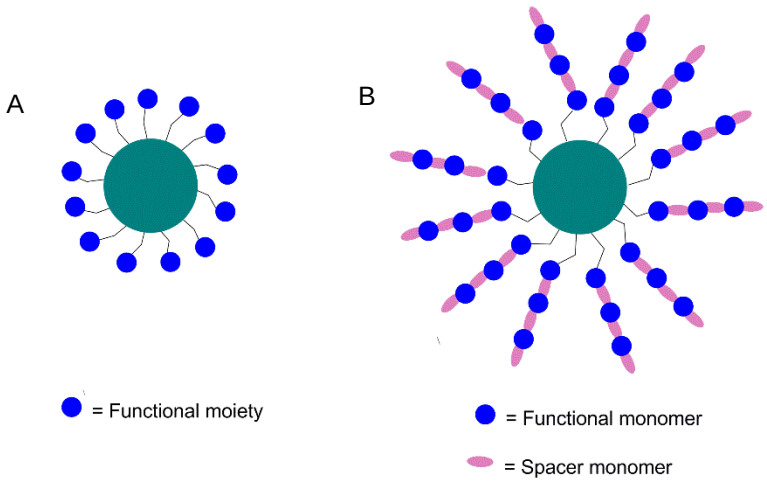

Figure 2: *Two generic approaches for surface modification are shown. A) The surface modification of a single functional moiety per complementary group on PNP. B) Graft-polymerization from a FPNP surface, introducing multiple functional moieties per initiation site.*

Firstly, the direct modification of the MAnh groups on the surface particles is utilized to introduce a boronic acid functionality (the boronic acid is represent as a blue dot, Figure 2A). Lewis acids such as boronic acid and its derivatives have been used in the extraction or isolation of catecholic molecules.[7] The unique feature of boronic acid-based materials is their ability to undergo a reversible reaction (*e.g.* complexing) with alcohols and diols to form boronate ester bonds.[40–42] The reaction affinity of boronic acid (*e.g.* ionization) with diol and alcohols follows the order 1,2-diol > 1,3-diol > alcohol, making the boron-1,2-diol interaction preferred and most stable.[41,43–45]

Secondly the polymerizable groups (*e.g.* vinyl) or groups capable of controlling radical polymerization (*e.g.* dithioester) are utilized to fabricate hairy-like particles through copolymerization of MAnh and a specific tetraphenylborate derivative (TPBD) with

polymerizable bonds. TPB has been extensively studied and used for the extraction of choline esters and catechols. [6,12,13,46,47]

FPNPs can thus be designed to be used for extraction purposes from directly modifying particle surfaces, or the incorporation of functional polymers onto the surface of particles. We envisage that solid particles with selective functional groups can be used for biomolecule extraction, specifically norepinephrine and octopamine. The biggest benefit of using nanoparticles is the increased surface area available for extraction. Two different functional groups such as a tertraphenylborate derivate and boronic acid derivative are fixed onto the surface of nanoparticles as a form of SPE method.

Materials and Methods

Materials. Potassium hydroxide pellets (>85%, Merck Chemicals; Darmstadt, Germany), sodium hydroxide pellets (>85%, Merck Chemicals), benzophenone (95%, Sigma Aldrich; St. Louis, USA), potassium phosphate (K_3PO_4) (99%, Sigma Aldrich), anhydrous carbon disulphide (CS_2) (≥99%, Sigma Aldrich), 1-bromoethyl benzene (97%, Sigma-Aldrich), 3-aminophenylboronic acid monohydrate (BA, >99.9%, Sigma Aldrich), sodium hydride (NaH) (60% dispersed in mineral oil, Sigma Aldrich), 2-(2-(vinyloxy) ethoxy)-ethanol (98%, Sigma Aldrich), 1-bromo-4-(bromomethyl)benzene (98%, Sigma Aldrich), *n*-butyllithium (2.5 M solution in hexane, Sigma Aldrich), triphenylborane (0.25 M solution in THF, Sigma Aldrich), maleic anhydride (MAnh) (99% ,Sigma Aldrich) was used after recrystallization from chloroform. Styrene (99.5%, Fluka chemika) was washed with KOH, distilled and stored over 4 Å molecular sieves in a fridge at 4 °C, divinylbenzene (DVB) (>99%, Sigma Aldrich) was used after the t-butylcatechol inhibitor was removed using a t-butylcatechol inhibitor removal column and stored over 4 Å molecular sieves at 4 °C. Anhydrous methyl ethyl ketone (MEK) (≥99.7%, Sigma-Aldrich) and *n*-heptane (Kimix; Cape Town, SA) was used as received. Tetrahydrofuran (Kimix), *N*,*N*-dimethylformamide (DMF) (Kimix), ethyl acetate (Kimix), pentane (Kimix) and methanol (Kimix) were distilled and kept over 4 Å molecular sieves at room temperature. 2, 2'-azo-bis (isobutyronitrile) (AIBN) (Riedel de Haen; Morris Plains, USA) was recrystallized twice using methanol and dried under vacuum before use. BPT was synthesized, according to Skey *et al*.[52], and stored in a fridge at 4 °C.

Synthesis

BPT RAFT agent[52] was synthesized by adding potassium phosphate, K_3PO_4 (1.36 g, 6.4 mmol) to THF (20 mL). To the stirred mixture, 1-butanethiol (530 mg, 5.8 mmol) was added and stirred for 10 minutes. Subsequently, carbon disulphide (1.34 g, 17.5 mmol) was added to the mixture and stirred over 1 hour, after which 1-bromoethyl benzene (1.07 g, 5.8 mmol) was added. After 6 hours of stirring at room temperature, the THF was removed under reduced pressure, and the crude product was purified using flash column chromatography (100% petroleum ether). Yield: 89%. ^{1}H NMR (600 MHz, $CDCl_3$): δ (ppm) =0.85 (t, 3H, C**H3**CH2CH2CH2), 1.35 (m, 2H, CH3C**H2**CH2CH2-), 1.59 (m, 2H, C**H2**-S), 1.69 (d, 3H, C**H3**(CH-)), 3.27 (t, 2H, -S-C**H2**), 5.26 (q, 1H, C**H**), 7.25 (m, 5H, Ar-**H**).

FPNPs. Particles were synthesized by a method similar to Chapter 3 with some small modifications. Maleic anhydride (2.04 g, 20.80 mmol) was dissolved in MEK (20 mL) in a 250 mL three neck round bottom flask and AIBN (6.8 mg, 4.14×10^{-2} mmol) and BPT RAFT agent (10 mg, 0.18 mmol) was added to

the reaction mixture. The MEK mixture was degassed for 30 minutes and in a separate flask, *n*-heptane (30 mL) was added with styrene (0.74 mL, 6.485 mmol) and DVB (0.98 mL, 6.901 mmol) and degassed for 30 min. After the MEK-MAnh solution was degassed, the solution was placed in a 70 ºC preheated oil bath for 30 min with 2.5 % of the St/DVB mixture in the MEK mixture (this reaction was done by first seeding a % and then feeding the rest in, refer to Chapter 3). Under inert conditions the *n*-heptane-St-DVB solution was fed into the MEK mixture over 2 hours. The final dispersion medium was a MEK-*n*-heptane mixture (20:30), and the reaction was stopped after a total of 4 hours obtaining BPT-MAnh-FPNPs

The synthesis of the extraction ligand precursor, 1-bromo-4-((2-(2-(vinyloxy) ethoxy) ethoxy) methyl) benzene (BM100)[50] NaH (1.44 g, 60% in mineral oil) were dispersed in THF (20 mL, anhydrous) was added to 2-(2-(vinyloxy) ethoxy)-ethanol (4.05 g, 0.031mol) at 0 °C via a dropping funnel. The mixture was stirred for 3 h before added to a solution of 1-bromo-4-(bromomethyl)benzene (7.42 g, 0.030 mol) in THF (20 mL, anhydrous). To complete the reaction the mixture was reacted overnight. The solvent was evaporated, and the residue was purified by column chromatography on SiO_2 with hexane/ethyl acetate (4:1) to obtain BM100 as a light yellow liquid (8 g, 89%). NMR analysis was conducted on the compound and successful synthesis was concluded. ^{1}H NMR (in d-acetone), δ(ppm) 7.52 (d, 2H, o-C_6H_4),7.36 (d, 2H, m-C_6H_4), 6.51(m, 1H, CH=), 4.549 (s, 2H, $CH_2C_6H_4$),4.19(d, cis H of = CH_2), 3.96 (d, trans H of = CH_2), 3.8−3.6 (m, 8H,OCH_2CH_2O); 13CNMR (in d6-acetone), δ(ppm) 152.4 (CH=), 138, 131,129.7, 120.1 (c-Br), 86 (=CH_2), 72.1, 70.8, 70, 69.8, 67.9. Representative ^{1}H, and ^{13}C NMR spectra are shown in SI, Figure 7-8.

Lithium triphenyl (4-((2-(2-vinyloxy) ethoxy) ethoxy) methyl)-phenyl) borate (TBVE)[50] BM100 (500 mg, 1.61 mmol) in THF (5 mL, anhydrous) was cooled to -78 °C using ice/acetone. A 0.70 mL (1.76 mmol) portion of BuLi (2.5 M in hexane) was added dropwise over 30 min. The mixture was stirred at -78 °C for another hour before the solution of triphenylborane (6.64 mL, 1.61 mmol) in THF (3 mL, anhydrous) was added. The reaction mixture was allowed to warm up to room temperature while stirring overnight to complete the reaction. The solvent was evaporated and pentane (20 mL x 3, anhydrous) was used for washing the yellow residue. The pentane solution was removed by syringe, and the yellow residue was further dried in a vacuum oven at 50 °C for 24 h to yield TBVE as an ivory-white powder (953 mg, 94.4%). The synthetic schemes of the synthesis of the tetraphenylborate salt derivative are shown in SI, scheme 1-2. Successfully synthesis and characterization was done using NMR analysis. ^{1}H NMR (in d_6-acetone), δ(ppm) 7.35 (m, 8H, o-C_4H_4 and o-C6H5), 7.05 (d, 2H, m-C_4H_4), 6.93 (m, 6H, m-C_6H_5), 6.82 (t, 3H, p-$_{C6H5)}$, 6.51(m, 1H, CH=), 4.43 (s, 2H, $CH_2C_6H_4$), 4.22(d, cis H of = CH_2), 3.96 (d, trans H of = CH_2), 3.8−3.6 (m,8H, OCH_2CH_2O); ^{13}C NMR (in d_6-acetone), δ(ppm) 165 (m, C−B), 152.4 (CH=), 136, 132, 126, 120.1, 86.4 (CH_2=), 74.3, 70.8, 70, 69.7, 67.8. Representative ^{1}H, and ^{13}C NMR spectra are shown in SI Figure 9-10.

Graft polymerization from surface of the BPT-MAnh-FPNPs. Pre-synthesized RAFT-particles (100 mg, 0.06 mmol RAFT) are dispersed into 1,4-dioxane (20 mL) with maleic anhydride (98.2 mg, 1.00 mmol), and TBVE (470.7 mg, 1.00 mmol). RAFT agent (29 mg, 0.11 mmol) and AIBN (2.2 mg, 0.01 mmol) was added to the polymerizations to ensure control over the grafted chains. The reaction mixture is then deoxygenated by argon bubbling for 30 minutes. The reaction flask is placed in a preheated oil bath at 70 °C. The reaction takes place for 48 hours. After polymerization, the particles are separated from free polymer via centrifugation, supernatant is removed and fresh solvent added. These washing steps are repeated three times to ensure all unreacted and ungrafted chains are removed. The free polymer chains were analyzed via SEC to get an indication of the molecular weight of the grafted chains on the surface of the particles. Free radical graft polymerization was done without the use of RAFT agent.

Direct surface modification of the MAnh-FPNPs to obtain BA-FPNPs. MAnh-FPNPs (100 mg, 0.30 mmol MAnh) were redispersed in DMF (10 mL). In a typical experiment, to modify all acessible MAnh, a solution, with excess BA (69.50 mg, 0.45 mmol) in DMF (5 mL), was added dropwise to MAnh-FPNPs dispersed in DMF. The reaction was left to proceed at room temperature for 30 minutes. The reaction mixture was then gradually heated and refluxed for 4 hours to ensure ring closure towards the maleimide rings. Thereafter, the mixture was allowed to cool to RT and the BA-FPNPs were washed with DMF twice, to ensure all unreacted reagents were removed and centrifuged to isolate BA-FPNPs. The particles were then dried under vacuum.

Extraction of Norepinephrine. 0.25 mM Norepinephrine (51.4 µg/mL) prepared in deionized water (pH 5.5). All the washing, immobilization and final collection steps were performed in centrifugal filters containing a 0.45 µm filter membrane. Prior to loading 1 mL of the 0.25 mM norepinephrine solution, the particles were weighed and rinsed three times using 1 mL deionized water. The water was removed using centrifugation. Following addition of 1 mL 0.25 mM norepinephrine solution, the particles were shaken at 1500 RPM using a IKA VibraMax benchtop shaker for 30 min. After 30 min the liquid phase was collected by centrifugation and analyzed directly using HPLC-UV at 210 nm.

Characterization and analysis

E**lectron microscopy** was used to visualize the size and morphology of the particles using a Zeiss MERLIN field emission gun scanning electron microscope using an inlens, high resolution detector and a STEM detector that is used for transmission electron microscopy images. Diameter measurements were done on ImageJ version 2.0.0. Prior to high resolution imaging, particles are placed on an aluminum stub and coated with a thin layer of carbon to render conductivity, avoiding surface charging caused by the electron beam. Prior to transmission imaging, dispersions were diluted and dropped onto a carbon-coated 200 mesh copper grid and dried at ambient temperature.

ATR-FTIR spectra were recorded using a Nicolet FTIR spectrometer (Nexus) from Thermo-Fischer equipped with a Smart Golden Gate ATR accessory with a diamond/ZnSe internal reflection crystal. The spectra were recorded from 4000 cm^{-1} to 650 cm^{-1} with a spectral resolution of 8 cm^{-1} and a sum of 64 individual scans. Samples were run in solid state and no sample preparation was necessary. Omnic software was used for data acquisition, and Origin software was used for data processing.

Size exclusion chromatography (SEC) was done to obtain molar mass and dispersity (*Đ*). SEC analysis was carried out on a THF solvent system. The SEC instrument consists of a Waters 95 isocratic HPLC pump, a Waters 717 plus auto-sampler, Waters 600E system controller (run by Breeze Version 3.30 SPA) and a Waters in-line Degasser AF. A Waters 2414 differential refractometer was used at 30 ºC in series with a Waters 2487 dual wavelength absorbance UV/Vis detector operating at variable wavelengths. THF (HPLC grade and stabilized with 0.125% BHT) was used as eluent at flow rates of 1 $mL \cdot min^{-1}$. The column oven was kept at 30 °C and the injection volume to 100 µL. Two PLgel (Polymer Laboratories) 5 µm Mixed-C (300 x 7.5 mm) columns and a pre-column (PLgel 5 µm Guard, 50 x 7.5 mm) were used. Calibration was done using narrow polystyrene standards ranging from 580 to $2x10^6$ $g \cdot mol^{-1}$. All molecular weights were reported as polystyrene equivalents. Data acquisition was done using Millennium software, version 4. Samples were prepared by dissolving samples in BHT stabilized THF (2 mg/mL). Sample solutions were filtered via syringe through 0.45 µm nylon filters before being subjected to analysis.

Results and Discussion

Surface grafting from FPNPs surface

Polymer chains, consisting of TBVE and MAnh copolymerized, are surface grafted onto the surface of the BPT-MAnh-FPNPs on two ways. The first method entails that the chains are grafted onto the surface of the particles using the pendant vinyl groups, that has not be used in the polymerization of the particles to attach new functionalities and a grafting-through technique to introduce the functionalities. The second method involving the chains to be grafted onto the surface using the RAFT-end groups and a grafting-from technique.[32] The BPT-MAnh-FPNPs, having residual vinyl bonds located on the surface, permit further growth by radical capturing via conventional free radical (FR) grafting through approach.[32,53,54] As the functional monomer (TBVE) and MAnh are copolymerized, the pendant vinyl groups on the particle surface will be incorporated in the growing poly(TBVE-*co*-MAnh) chains. This results in free radical poly(TBVE-*co*-MAnh) grafted FPNPs (poly FR-(TBVE-co-MAnh)-g-FPNPs) via the grafting-through technique (Scheme 1).

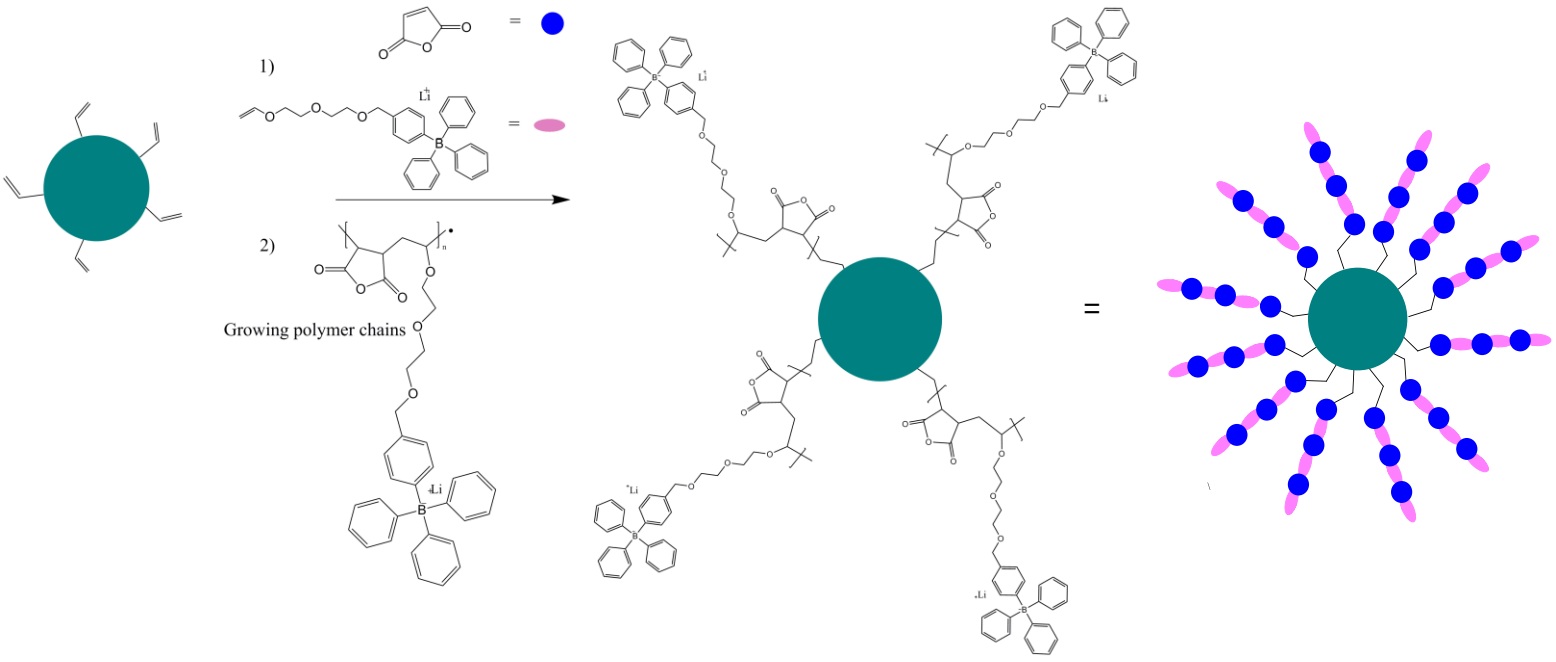

Scheme 1: *Synthesis of modified particles using the TBVE and MAnh via FR polymerization on the surface of the particles, obtaining FR-poly(TBVE-co-MAnh)-g-FPNPs.*

RAFT-core particles will be used for the living RAFT-grafting from/ through polymerization approach.[17] A sacrificial amount of BPT RAFT-agent was added to ensure all polymer chains grafted from the MAnh-FPNPs surface and formed in solution are polymerized in a controlled fashion (Scheme 2) This results in RAFT mediated poly(TBVE-*co*-MAnh) grafted FPNPs (RAFT-poly(TBVE-co-MAnh)-g-FPNPs). Both approaches are aimed to yield nanoparticles with highly crosslinked cores and an outer layer consisting of covalently attached functional polymer chains. The resulting hairy particles were characterized in terms of particle size increase and surface functional groups.

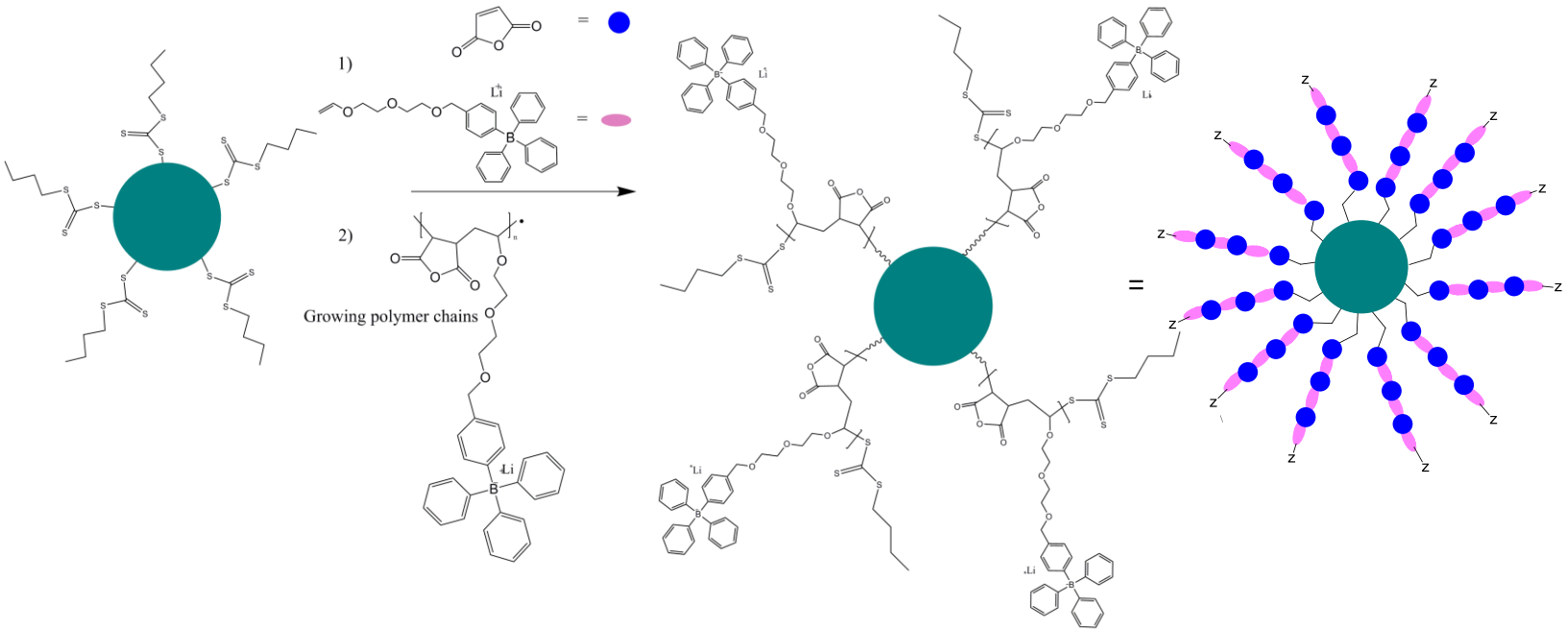

Scheme 2: *Synthesis of modified particles using the TBVE and MAnh via RAFT polymerization on the surface of the particles, obtaining RAFT-poly(TBVE-co-MAnh)-g-FPNPs, with z defined as the RAFT end group.*

The FPNPs had a particle size of 785 nm (Figure 3A). SEM images of the FR-grafted FPNPs (Figure 3B) and the RAFT-grafted FPNPs (Figure 3C) are shown. Particle size measurements were carried out on the core-FPNPs and the grafted-FPNPs. After 48 hours the particles size of the RAFT-grafted and FR-grafted increased to 905 nm and 998 nm, respectively.

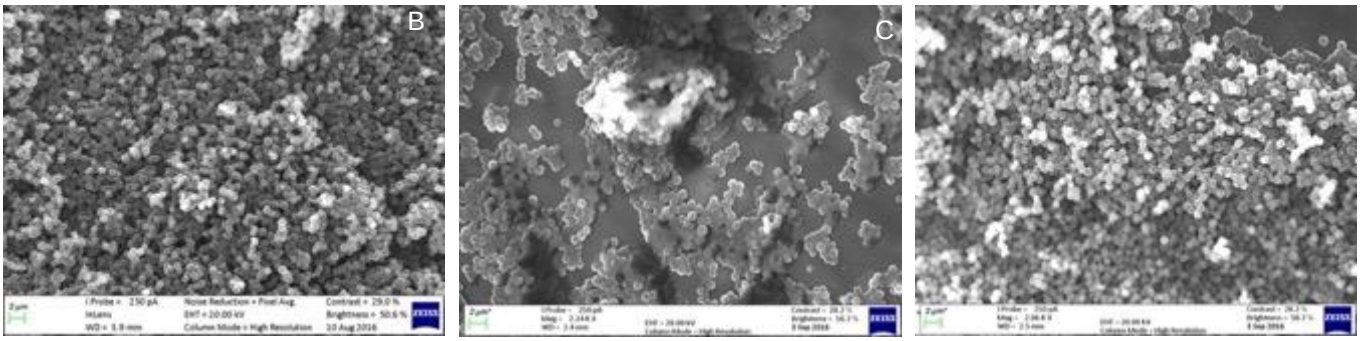

Figure 3: *SEM images of A) FPNPs, B) FR-poly(TBVE-co-MAnh)-g-FPNPs and C) RAFT-poly(TBVE-co-MAnh)-g-FPNPs.*

The molecular weight and dispersity of the grafted polymer chains could not be determined, as grafted chains are covalently bound to the surface of the highly-crosslinked FPNPs. A rough estimate of the increase of particle size can be related to the molecular weight of the grafted polymer chains, that can be established using the unbound residual polymer chains within the supernatant.[55,56] FR-grafted experiments obtained a number-average molecular weight (M_n) of 11 395 g·mol^{-1} ($Đ$ = 1.74) and the RAFT-grafted experiments obtained a number-average molecular weight (M_n) of 9 195 g·mol^{-1} ($Đ$ = 1.28). The dispersity of the RAFT-polymerization gave a strong indication that the RAFT-agent BPT controls the molecular weight of polymer. This method of relating the particle size increase and molecular weight of the grafted polymer is not very precise as the grafting onto the particle surface is more complex. Crosslinking can occur due to the dangling vinyl bonds (DVB) that has not participated and grafting onto the particles can occur.

A further confirmation of the grafting was observed in the ATR-FTIR analysis. After surface grafting onto the FPNPs (Figure 5C), the presence of the newly introduced C-O-C, on the TBVE monomer, appear at 870 cm^{-1}- 923 cm^{-1} and 1073 cm^{-1}- 1115 cm^{-1}.[57] The bands at 2820 cm^{-1} – 2998 cm^{-1} are due to the sp^2 aliphatic C-H bending vibrations of the polymer chain.[58,59] The characteristic carbonyl bands at 1774 cm^{-1} and 1857 cm^{-1} are indicative of the MAnh present on the particle surface. The para-disubstituted aromatic rings appear at 707 cm^{-1}. These results relate well to previous research, and confirm the successful grafting-through of the TBVE and MAnh monomers onto the surface of the FPNPs.[57,58,60]

Surface modification of MAnh-FPNPs

The MAnh-FPNPs comprise of accessible and reactive MAnh moieties that can be further modified by various reactions. The particles were surface modified using 3-aminophenylboronic

acid, in excess, to ensure all accessible MAnh units are modified (refer to Figure 4). The successful surface modification is confirmed with ATR-FTIR analysis.

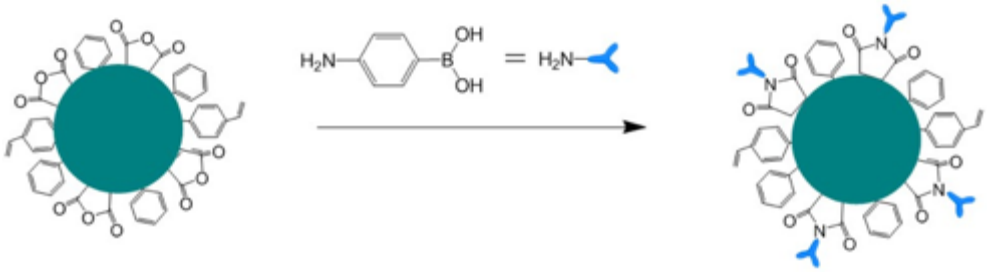

Figure 4: *Surface modification of FPNPs using BA via the reactive MAnh to obtain BA-FPNPs.*

The MAnh-FPNPs before modification (Figure 5A), had the characteristic MAnh carbonyl bands at 1772 cm^{-1} and 1854 cm^{-1}. After surface modification (Figure 5B) the appearance of a new strong band at 1720 cm^{-1} and 1645 cm^{-1} is due to successful formation of the imide group.[61] Confirmation of ring closure is established by the absence of the N-H bending band at 1550 cm^{-}

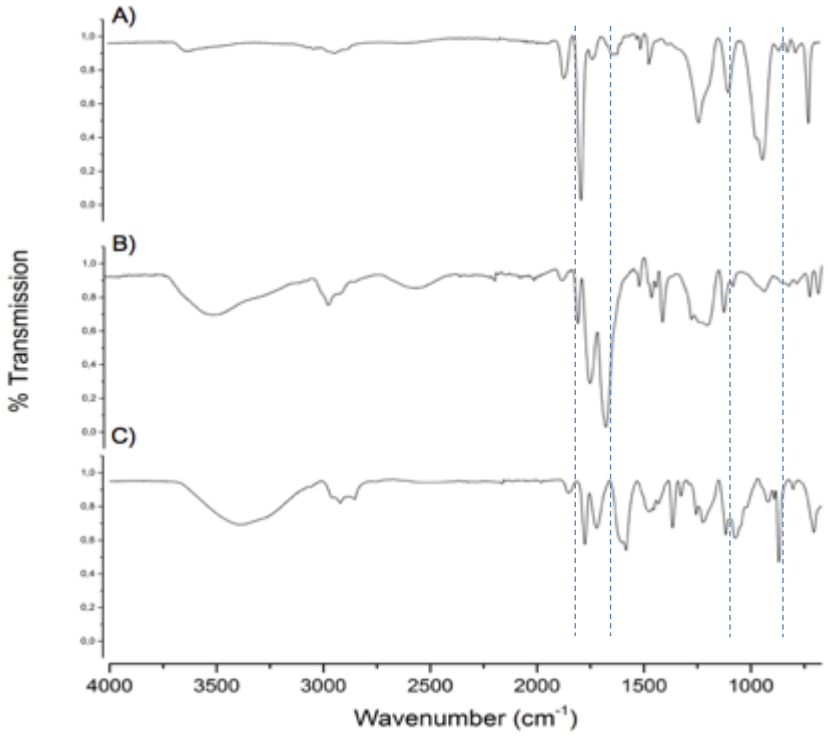

Figure 5: *ATR-FTIR spectra of A) FPNPs, B) BA-FPNPs and C) (TBVE-co-MAnh)-g-FPNPs.*

[1].[60] The broad, sharp bands at 3467 cm^{-1}, 1388 cm^{-1} and 1226 cm^{-1} are assigned to the stretching and bending of the OH groups, after surface modification of BA, due to diol functionality on the BA.[44] The meta-disubstituted aromatic ring appear at 708 cm^{-1} and 809 cm^{-1}.

Extraction of biomolecules using BA-FPNPs and (TBVE-co-MAnh)-g-FPNPs

Preliminary extraction experiments were carried out, as the purpose of this study was to functionalize FPNP surfaces with moieties able to extract the biomolecule, norepinephrine. The first set of experiments were done to establish the extraction potential of the various FPNPs. BA-FPNPs and FR-(TBVE-co-MAnh)-g-FPNPs extract more norepinephrine than the RAFT-(TBVE-co-MAnh)-g-FPNPs (Figure 6). The difference in extraction between the RAFT- and FR-graft FPNPs can possibly be explained by the amount of polymer grafted onto the core-FPNPs. The FR-(TBVE-co-MAnh)-g-FPNPs showed a greater increase in particle size and higher molecular weight, which can relate to more polymer grafted onto the particle surface, furthermore relating to more functionality available for extraction. The % recovery of norepinephrine could not be established due to analyte degrading in the HPLC column.

A second set of experiments was carried out using FR-(TBVE-co-MAnh)-g-FPNPs and BA-FPNPs, and a compound closely related to norepinephrine, octopamine, to establish the recovery of the extractant from the particles. The extraction of the compound is shown in Figure 7. The binding capacity is given in concentration analyte extracted per mass particles. It was observed that BA-FPNPs had a lower binding capacity ($^{m}/_{m}$), 4.15 µM/mg particles, compared to FR-grafted BM200 FPNPs' binding capacity of 5.01 µM/mg particles. This can possibly be attributed to the effective amount of functionality on the different FPNPs. The BA-FPNPs could

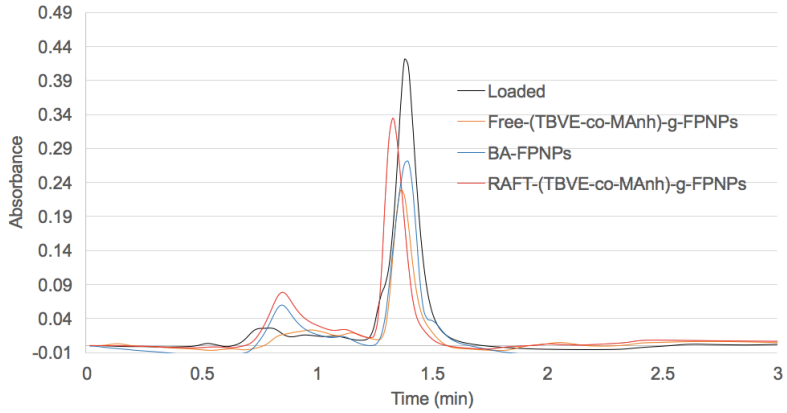

Figure 6: *HPLC chromatogram showing the decrease in concentration of norepinephrine as a result of immobilization onto the FPNPs.*

only have one BA-functionality per MAnh group, whereas the FR-grafted FPNPs had more repeat units of TBVE, effectively increasing the amount of extraction capacity. It was interesting to note that the BA-FPNPs percentage recovery of analyte, using 0.1 M HCl to wash off the analyte from the particles, was 92%, which was much higher than the FR-(TBVE-co-MAnh)-g-FPNPs recovery of 57%, however the recovery of the analytes can still be optimized.

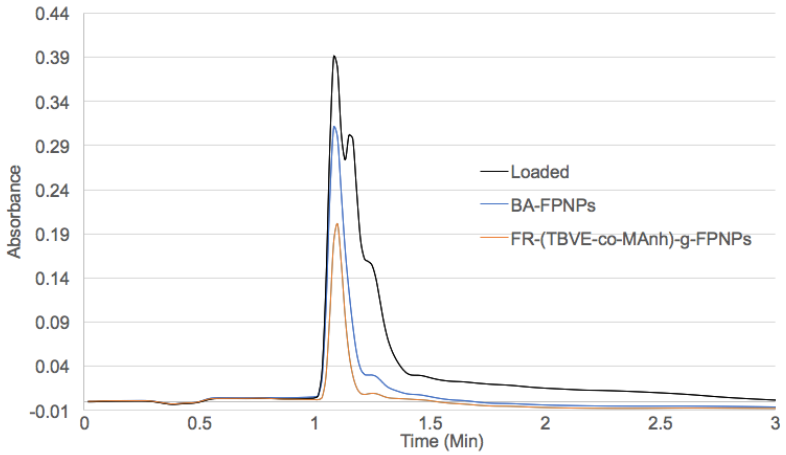

Figure 7: *HPLC chromatogram showing the decrease in concentration of norepinephrine as a result of immobilization onto the FPNPs.*

Conclusion

We report the successful surface modification of poly(STY-*co*-DVB-*co*-MAnh) FPNPs and the synthesis of "hairy-like" functional polymer nanoparticles through integrating nanoparticle synthesis and free radical- and living radical polymerizations, for the extraction of norepinephrine and octopamine from dilute solutions. We successfully extracted both norepinephrine and octopamine analyte from dilute solutions.

References

(1) Wink, M. *In An Introduction to Molecular Biotechnology: Molecular Fundamentals, Methods and Application in Modern Biotechnology*. 2nd Ed, Micheal Wink, Wiley-Blackwell. **2006**.

(2) Chen, L.; Zhu, X.; Shen, J.; Zhang, W. Selective solid-phase extraction of catecholamines from plasma using nanofibers doped with crown ether and their quantitation by HPLC with electrochemical detection. *Anal Bioanal Chem.* **2016**. *408,* 4987-4994.

(3) Biotage. *Extraction of Epinephrine, Norepinephrine and Dopamine from Human Plasma Using EVOLUTE*. Retrieved from https://theanalyticalscientist.com/10515-app-note-biotage-supplied.pdf. **2015**.

(4) Hansson, L.; Boronic Acid-Silica: A New Tool for the Purification of Catechilic Compounds on-Line with Reverse-Phase High-Performance Liquid Chromatography. *J. Chromatogr.* **1983**, *265*, 37–44.

(5) Baker, G. B.; Coutts, R. T.; Legatt, D. F. A Procedure for Extraction and Separation of

Phenethylamine, Tyramine and Octopamine. **1980**, *8* (5), 622-623.

(6) Da Prada, M.; Zürcher, G. Simultaneous Radioenzymatic Determination of Plasma and Tissue Adrenaline, Noradrenaline and Dopamine within the Femtomole Range. *Life Sci.* **1976**, *19* (8), 1161–1174.

(7) Pizer, R.; Babcock, L. Mechanism of the Complexation of Boron Acids with Catechol and Substituted Catechols. *Inorg. Chem* **1977**, *16* (7), 1677–1681.

(8) Tarley, C. R. T.; Kubota, L. T. Molecularly-Imprinted Solid Phase Extraction of Catechol from Aqueous Effluents for Its Selective Determination by Differential Pulse Voltammetry. *Anal. Chim. Acta.* **2005**, *548* (1–2), 11–19.

(9) Padhye, V. V.; York,C.; Burkiewicz, A.; Nucleic Acid Purification on Silica Gel and Glass Mixtures, *Patent. US5658545A.* **1997**.

(10) Nalewajko, E.; Wiszowata, A.; Kojło, A. Determination of Catecholamines by Flow-Injection Analysis and High-Performance Liquid Chromatography with Chemiluminescence Detection. *J Pharm Biomed Anal* **2007**, *43* (5), 1673–1681.

(11) De Jong, W. H.; Borm, P. J. a. Drug Delivery and Nanoparticles:applications and Hazards. *Int. J. Nanomedicine* **2008**, *3* (2), 133–149.

(12) Fonnum, F. Isolation of Choline Esters from Aqueous Solutions by Extraction with Sodium Tetraphenylboron in Organic Solvents. *Biochem.* **1969**, *113* (2), 291–298.

(13) Stanaszek, P. M.; Snell, J. F.; O'Neill, J. J. Isolation, Extraction, and Measurement of Acetylcholine from Lactobacillus Plantarum. *Appl. Environ. Microbiol.* **1977**, *34* (2), 237–239.

(14) Louros, C. L. S.; Cláudio, A. F. M.; Neves, C. M. S. S.; Freire, M. G.; Marrucho, I. M.; Pauly, J.; Coutinho, J. a P. Extraction of Biomolecules Using Phosphonium-Based Ionic Liquids + K 3PO 4 Aqueous Biphasic Systems. *Int. J. Mol. Sci.* **2010**, *11*, 1777–1791.

(15) Pichon, V. Solid-Phase Extraction for Multiresidue Analysis of Organic Contaminants in Water. *J. Chromatogr. A.* **2000**, *885* (1–2), 195–215.

(16) Welsch, N.; Lu, Y.; Dzubiella, J.; Ballauff, M. Adsorption of Proteins to Functional Polymeric Nanoparticles. *Polym.* **2013**. *54 (12), 2835-2849.*

(17) Sperling, R.; Parak, W. J. Surface Modification, Functionalization and Bioconjugation of Colloidal Inorganic Nanoparticles. *Philos. Trans. A. Math. Phys. Eng. Sci.* **2010**, *368* (1915), 1333–1383.

(18) Gao, D.; Zhang, Z.; Wu, M.; Xie, C.; Guan, G.; Wang, D. A Surface Functional Monomer-Directing Strategy for Highly Dense Imprinting of TNT at Surface of Silica Nanoparticles. *J. Am. Chem. Soc.* **2007**, *129* (25), 7859–7866.

(19) Desai, R. P.; Bhati, A.; Chaniyilparampu, R. N.; Pathak, H. S.; Upadhyay, R. V. Method for Extraction of Biomolecules by Magnetic Particles, *Patent, WO2015040633 A1.***2015**.

(20) Nahar, M.; Dutta, T.; Murugesan, S.; Asthana, A.; Mishra, D.; Rajkumar, V.; Tare, M.; Saraf, S.; Functional Polymeric Nanoparticles: An Efficient and Promising Tool for Active Delivery of Bioactives. *Crit. Rev. Ther. Drug Carr. Syst.* **2006**, 23 (4), 259–318.

(21) Chérel, M.; Huclier, S.; Lepareur, N.; Bocqué, M.; Costa L, L. E.; Leal Costa, L. E.; Blondelle, C.; Ruello, C.; Desjulets, M.; Noiret, N.; Cammas-Marion, S. Development of Biocompatible and Functional Polymeric Nanoparticles for Site-Specific Delivery of Radionuclides. *Front. Med.* **2015**, *2* (63), 1-9.

(22) Shokeen, M.; Pressly, E. D.; Hagooly, A.; Zheleznyak, A.; Ramos, N.; Fiamengo, A. L.; Welch, M. J.; Hawker, C. J.; Anderson, C. J. Evaluation of Multivalent, Functional Polymeric Nanoparticles for Imaging Applications. *ACS Nano.* **2011**, *5* (2), 738–747.

(23) Fratoddi, I.; Venditti, I.; Cametti, C.; Palocci, C.; Chronopoulou, L.; Marino, M.; Acconcia, F.; Russo, M. V. Functional Polymeric Nanoparticles for Dexamethasone Loading and Release. *Colloids Surfaces B Biointerfaces.* **2012**, *93* (1), 59-66.

(24) Gref, R.; Couvreur, P.; Barratt, G.; Mysiakine, E. Surface-Engineered Nanoparticles for Multiple

Ligand Coupling. *Biomaterials.* **2003**, *24* (24), 4529–4537.

(25) Yao, W.; Xu, P.; Zhao, J.; Ling, L.; Li, X.; Zhang, B.; Cheng, N.; Pang, Z. RGD Functionalized Polymeric Nanoparticles Targeting Periodontitis Epithelial Cells for the Enhanced Treatment of Periodontitis in Dogs. *J. Colloid Interface Sci.* **2015**, *458*, 14–21.

(26) Patil, Y. B.; Toti, U. S.; Khdair, A.; Ma, L.; Panyam, J. Single-Step Surface Functionalization of Polymeric Nanoparticles for Targeted Drug Delivery. *Biomaterials* **2009**, *30* (5), 859–866.

(27) Fahmy, T. M.; Samstein, R. M.; Harness, C. C.; Saltzman, W. M. Surface Modification of Biodegradable Polyesters with Fatty Acid Conjugates for Improved Drug Targeting. *Biomaterials.* **2005**, *26* (28), 5727–5736.

(28) Rowe, M.A.; Su, M.; Mirin, R. Transport Properties of a Quantum Dot Based Optically Gated Field-Effect Transistor. In: *Conf. on Lasers and Electro-Optics (CLEO).* **2002**.

(29) Engelhardt, N.; Ernst, A.; Kampmann, A.-L.; Weberskirch, R. Synthesis and Characterization of Surface Functional Polymer Nanoparticles by a Bottom-Up Approach from Tailor-Made Amphiphilic Block Copolymers. *Macromol. Chem. Phys.* **2013**, *214* (24), 2783–2791.

(30) Lin, J.J.; Hsu, Y.C. Temperature and pH-Responsive Properties of Poly(styrene-Co-Maleic Anhydride)-Grafting Poly(oxypropylene)-Amines. *J. Colloid Interface Sci.* **2009**, *336* (1), 82–89.

(31) Joso, R.; Stenzel, M. H.; Davis, T. P.; Barner-Kowollik, C.; Barner, L. Grafting of N -Butyl Acrylate and N , N ’-Dimethyl Acrylamide from Poly(divinylbenzene) Microspheres by RAFT Polymerization. *Aust. J. Chem.* **2005**, *58* (6), 468-471.

(32) Barner, L.; Li, C.; Hao, X.; Stenzel, M. H.; Barner-Kowollik, C.; Davis, T. P. Synthesis of Core-Shell Poly(divinylbenzene) Microspheres via Reversible Addition Fragmentation Chain Transfer Graft Polymerization of Styrene. *J. Polym. Sci. Part A Polym. Chem.* **2004**, *42* (20), 5067–5076.

(33) Chiefari, J.; Chong, Y. K. B.; Ercole, F.; Krstina, J.; Jeffery, J.; Le, T. P. T.; Mayadunne, R. T. A.; Meijs, G. F.; Moad, C. L.; Moad, G.; Rizzardo, E.; Thang, S. H.; South, C. Living Free-Radical Polymerization by Reversible Addition - Fragmentation Chain Transfer : The RAFT Process. *Macromolecules.* **1998**, *31*, 5559–5562.

(34) Flores, J. D.; Shin, J.; Hoyle, C. E.; McCormick, C. L. Direct RAFT Polymerization of an Unprotected Isocyanate-Containing Monomer and Subsequent Structopendant Functionalization Using “click”-Type Reactions. *Polym. Chem.* **2010**, *1*, 213–220.

(35) Rizzardo, E.; Chiefari, J; Mayadunne, R. T. A.; Moad, G.; Thang, S. H. Matyjaszewski, K. Controlled/Living Radcal Polymerization: Progress in ATRP, NMP, and RAFT. *Polym. Int*. **2002**, *51* (370), 370-400.

(36) Stenzel-Rosenbaum, M.; Davis, T. P.; Chen, V.; Fane, A. G. Star-polymer synthesis via radical reversible addition-fragmentation chain transfer polymerization. *J. Polym. Sci.: Part A: Polym. Chem*. **2001**, *39*, 2777–2783.

(37) Jesberger, M.; Barner, L.; Stenzel, M. H.; Malmstro M, E.; Davis, T. P.; Barner-Kowollik, C. Hyperbranched polymers as scaffolds for multifunctional reversible addition–fragmentation chain-transfer agents: A route to polystyrene-*core*-polyesters and polystyrene-*block*-poly(butyl acrylate)-*core*-polyesters. *J Polym Sci. Part A. Polym Chem.* **2003**, *41* (23), 3847-3861.

(38) Barner, L.; Barner-Kowollik, C.; Davis, T. P.; Stenzel, M. H. RAFTing down under: Tales of missing radicals, fancy architectures, and mysterious holes. *J. Polym. Sci. Part A. Polym. Chem.* **2003**, *41* (3), 365-375.

(39) Chevigny, C.; Dalmas, F.; Di Cola, E.; Gigmes, D.; Bertin, D.; Boué, F.; Jestin, J. Polymer-Grafted-Nanoparticles Nanocomposites: Dispersion, Grafted Chain Conformation, and Rheological Behavior. *Macromolecules.* **2011**, *44* (1), 122–133.

(40) Kidwell, R. L.; Murphy, M.; Darling, S. D. Phenols: 6-Methoxy-2-Naphthol. *Org. Synth.* **1969**, *5*, 918.

(41) Marinaro, W. A.; Prankerd, R.; Kinnari, K.; Stella, V. J. Interaction of Model Aryl- and Alkyl-Boronic

Acids and 1,2-Diols in Aqueous Solution. *J. Pharm. Sci.* **2015**, *104* (4), 1399-1408.

(42) Hageman, J. H.; Kuehn, G. D. Boronic Acid Matrices for the Affinity Purification of Glycoproteins and Enzymes. *Methods Mol Biol.* **1992**, *11,* 45-71.

(43) Furikado, Y.; Nagahata, T.; Okamoto, T.; Sugaya, T.; Iwatsuki, S.; Inamo, M.; Takagi, H. D.; Odani, A.; Ishihara, K. Universal Reaction Mechanism of Boronic Acids with Diols in Aqueous Solution: Kinetics and the Basic Concept of a Conditional Formation Constant. *Chem.* **2014**, *20* (41), 13194-13202

(44) Cegłowski, M.; Gierczyk, B.; Schroeder, G. Poly(methyl Vinyl Ether-Alt-Maleic Anhydride) Functionalized with 3-Aminophenylboronic Acid: A New Boronic Acid Polymer for Sensing Diols in Neutral Water. *J. Appl. Polym. Sci.* **2014**, *131* (18), 9358–9364.

(45) Pappin, B.; Kiefel, M. J.; Houston, T. A. Boron-Carbohydrate Interactions. In *Carbohydrates - Comprehensive Studies on Glycobiology and Glycotechnology*. 1st Ed, Chuan-Fa Chang, InTech. **2012**, 37-54.

(46) Fonnum, F. Isolation of Choline Esters from Aqueous Solutions by Extraction with Sodium Tetraphenylboron in Organic Solvents. *Biochem. J.* **1969**, *113* (2), 291–298.

(47) Barnes, M. J. (**1990**) Decomposition of Sodium Tetraphenylborate. Aiken: Westinghouse Savannah River C47ompany. Retrieved from: https://www.osti.gov/

(48) Broeke, J. (**2003**) Arylborate Anions; Versatile Counterions in Homogeneous Catalysis with Potential for Use in Novel Reaction media. *Doctoral Thesis, Universiteit Utrecht*.

(49) Wittig, G.; Keicher, G. Reaction of alkal metals and their hydrides with triphenylaluminum. *Naturwissenschaften.* **1947**, *34*, 216-219.

(50) Liang, S.; Choi, U. H.; Liu, W.; Reilly, M. O.; Karen, I. Synthesis and Lithium Ion Conduction of Single-Ion Conductors Containing Novel Weak- Binding Borates. *Chem. Mater.* **2012**, *24* (12), 2316-2323.

(51) Chevigny, C.; Gigmes, D.; Bertin, D.; Jestin, J.; Boué, F. Polystyrene Grafting from Silica Nanoparticles via Nitroxide-Mediated- Polymerization (NMP): Synthesis and SANS Analysis with Contrast Variation Method. *Soft Mater.* **2009**, *5, 3741-3753.*

(52) J. Skey and R. K. O'Reilly. Facile One Pot Synthesis of a Range of Reversible Addition Fragmentation Chain Transfer (RAFT) Agents. *Chem. Commun.* **2008**, *35*, 4183–4185.

(53) Harmzen-Pretorius, E.; Klumperman, B. Synthesis and Characterization of Novel Multifunctional Poly(Styrene-Co-Divinyl Benzene-Co-Maleic Anhydride) Nanoparticles Produced via a Surfactant-Free Dispersion Polymerization Technique. *Manuscript in preparation.* **2017.**

(54) Downey, J. S.; Frank, R. S.; Li, W. H.; Stöver, H. D. H. Growth Mechanism of Poly(divinylbenzene) Microspheres in Precipitation Polymerization. *Macromolecules* **1999**, *32* (9), 2838–2844.

(55) Zheng, G.; Sto, H. D. H. Grafting of Polystyrene from Narrow Disperse Polymer Particles by Surface-Initiated Atom Transfer Radical Polymerization. *Macromolecules.* **2002**, *35,* 6828–6834.

(56) Barner, L.; Li, C.; Hao, X.; Stenzel, M. H.; Barner-Kowollik, C.; Davis, T. P. Synthesis of Core-Shell Poly(divinylbenzene) Microspheres via Reversible Addition Fragmentation Chain Transfer Graft Polymerization of Styrene. *J. Polym. Sci. Part A Polym. Chem.* **2004**, *42* (20), 5067–5076.

(57) Sadat, F.; Mirakabad, T.; Akbarzadeh, A.; Milani, M.; Zarghami, N. A Comparison between the Cytotoxic Effects of Pure Curcumin and Curcumin-Loaded PLGA- PEG Nanoparticles on the MCF-7 Human Breast. *Artif Cells Nanomed Biotechnol.* **2016**, *8*, 3-8.

(58) Stoilova, O.; Ignatova, M.; Manolova, N.; Godjevargova, T.; Mita, D. G.; Rashkov, I. Functionalized electrospun mats from styrene–maleic anhydride copolymers for immobilization of acetylcholinesterase. *Eur. Polym. J.* **2010**, *46* (10), 1966–1974.

(59) Chen, G.; Zhang, Y.; Zhou, X.; Xu, J. Synthesis of styrene-maleic anhydride copolymer esters and their surface enriched properties when blended with polyethylene. *Appl. Surf. Sci.* **2006**, *253* (3), 1107–1110.

(60) Jeong, J.H.; Byoun, Y.S.; Ko, S.B.; Lee, Y.S. Chemical Modification of Poly(styrene-alt-maleic anhydride) with Antimicrobial 4-Aminobenzoic Acid and 4-Hydroxybenzoic Acid. *J. Ind. Eng. Chem.* **2001**, *7* (5), 310–315.

(61) Kong, J.; Yu, S. Fourier transform infrared spectroscopic analysis of protein secondary structures. *Acta Biochim. Biophys. Sin.* **2007**, *39* (8), 549–559.

(62) D'Andrea, G.;Nordera, G.; Pizzolato, G.; Bolner, A.; Colavito,; D.; Flaibani, R.; Leon, A. Trace amine metabolism in Parkinson's disease: Low circulating levels of octopamine in early disease stages. *Neurosci. Lett.* **2010.** *469* (3), 348-351.

(63) Chalermpalanupap, T.; Kinkead, B.; Hu, T. W.; Kummer, M. P.; Hammerschmidt, T.; Heneka, M. T.; Weinshenker, D.; Levey, A. I. Targeting norepinephrine in mild cognitive impairment and Alzheimer's disease. *Alzheimer's Res. Ther.* **2013**. *5* (21), 1-9.

(64) Eisenhofer, G.; Tischler, A. S.; de Krijger, R. R. Diagnostic Tests and Biomarkers for Pheochromocytoma and Extra-adrenal Paraganglioma: From Routine Laboratory Methods to Disease Stratification. *Endocr. Pathol.* **2012**. *23* (1), 4-14.

CHAPTER 9

Conclusions and Future Recommendations

General conclusions

The primary focus of this thesis is the synthesis of functional polymeric nanoparticles (FPNPs). It was demonstrated that FPNPs could be synthesized using a surfactant-free dispersion polymerization technique to obtain NPs with tunable sizes (nanometer up to micrometer scale) and morphologies (smooth to popcorn-shaped). The FPNPs were proven to be highly versatile and reactive compounds, making them interesting components for a plethora of applications. What follows is a summary of the most important findings gathered during this study, as well as an outlook presented for future work.

In Chapter 3, an in-depth study on the surfactant-free dispersion polymerization technique for the fabrication of the FPNPs was conducted. Various experimental conditions were tested, including monomer, RAFT and crosslinker concentrations, as well as the monomer feed rate and reaction time. The results indicated that particles with tunable sizes and morphologies could be synthesized in a reproducible manner, retaining functionality (maleic anhydride and vinylic bonds) on the surface of the FPNPs. In a supplementary experiment, it was shown that 70% of the MAnh groups are accessible for further modification reactions, indicating high porosity within the particles.

The FPNPs displayed auto-fluorescent properties, which are discussed in Chapter 4. The auto-fluorescence was attributed to the crosslinking nature (divinylbenzene content) and morphology of the particles. In addition, these particles showed no cytotoxicity towards cells, and due to their auto-fluorescent nature, could be incubated with cells to track cellular interactions. It was found that the particles were very quickly taken up into the cells, which did not occur via a phagocytosis pathway. This makes the particles interesting tools for fluorescent markers, with high functionality available for further modification and introduction of targeting ligands or drugs.

Chapter 5 includes the first application for which these FPNPs were used for. Inverse Pickering emulsion droplets were successfully made by boronate ester (BE)-decorated particles, which stabilized the Pickering emulsion. The particles were successfully decorated with varying amounts of boronic acid (BA) and were further modified with 1,3-propanediol to obtain BE-FPNPs. The presence of boronate ester functionalities and multiple diols on the biopolymer (starch) from within the aqueous layer, allowed for the crosslinking of multiple particles at the interface, successfully producing hybrid permeable microcapsules (MCs).

The triggered degradation of the hybrid MC wall was studied in Chapter 6. Bacteria, which were constructed/ transfected to produce and release amylase under an inducible GAL10 promoter, were encapsulated and shown to degrade the capsule wall upon the introduction of the galactose trigger.

In another application, the FPNPs were decorated with a tertiary amine functionality to synthesize Janus particles using Pickering emulsion droplets as templates, as discussed in Chapter 7. This was achieved by the introduction of gold ions in the aqueous phase which are known in literature to have a great affinity towards tertiary amines. At the interface, the particles rotate and the surface that is exposed to the aqueous phase has the possibility of reducing the gold ions to metallic gold nanoparticles. This technique that utilized the rotation of the particles at the interface, was shown to be a powerful method of producing Janus particles with tunable surface coverage. Correlative imaging on these novel Janus particles was also done for the first time to confirm the synthesis of Janus particles using Pickering emulsion droplets as templates.

The last application that these multi-FPNPs were utilized for is discussed in Chapter 8. It was shown that the decorating of the particle surface with specific functional groups, either in a direct surface modification reaction or grafting polymeric chains from the particle surface, can be beneficial for the extraction of biomolecules from dilute solutions. The surface of PNPs were successfully decorated with hairy-like polymers by introducing tetraphenylborate to the surface of the PNPs, well known in literature to complex with biomolecules. Additionally, the surfaces were decorated with BA, which is well known to complex with a compound having OH groups. These methods proved that these FPNPs can be used as solid phase extraction materials for the extraction of biomolecules.

The overall results demonstrate that these reactive FPNPs are truly multifunctional in nature and can be utilized in various applications, have tunable sizes and morphologies, and are highly resistant to harsh environments. These are important characteristics in demand by many applications.

Recommendations

For complex functional particle formation, different parameters can still be experimented with to fully understand the formation of these multi-monomer, functional particles. Therefore, it is suggested that the addition time of the crosslinker be varied alongside various other monomers in the polymerization being optimized to provide a more detailed picture of how these parameters influence the particle size and morphology. It is clearly observed from the first part

of this study that the introduction of three monomers and high reactive MAnh influence the polymerization of particles, and for future studies, the introduction of different monomers would make the fabrication of various materials with different functionalities possible. This opens the door to unlimited possibilities of FPNPs. Modifying the particles with targeting ligands and drugs will be a fruitful avenue to explore.

Interesting auto-fluorescence was observed, although the mechanism for the AF could not yet be proved, this work opens up the possibility to investigate the AF within polymer systems. Preliminary investigation was done on the influence of the MAnh structure (rotation) and DVB concentration observing the effect on the AF. However more in-depth experiments will be needed (varying the monomer concentration, RAFT concentration, residual vinyl bonds and crosslinker concentration) to conclude the origin of AF and what is responsible for the AF.

Another recommendation is the optimization of the capsule wall degradation. Various parameters can be optimized. Firstly, future studies could characterize the starch to be able to exactly determine the necessary addition concentration of starch and the ratio between 1,2-diols and BE-functionality. Secondly, it would be important to optimize the constructed/ transfected *E. coli*. The *E. coli* was transfected to release amylase via a galactose trigger. It is unknown still what amount of galactose is needed to stimulate amylase release, and how much amylase is needed to degrade the capsule wall. For that, it would be necessary to first determine the activity of the amylase producing *E. coli* under different concentrations of galactose. It would also be necessary to determine the time it takes to degrade different amounts of starch used in the capsule forming steps. With that information, it will be possible to calculate the exact concentration of *E. coli* needed, with introduced concentration of galactose, to degrade capsules in specific times.

Research Output

(Manuscripts in progress that will be submitted soon)

Functional and reactive polymeric nanoparticles – A Review. E. Harmzen-Pretorius and B. Klumperman

Synthesis and characterization of novel multifunctional poly(styrene-co-divinylbenzene-co-maleic anhydride) nanoparticles produced via a surfactant-free dispersion polymerization technique. E. Harmzen-Pretorius and B. Klumperman.

Auto-fluorescent polymeric nanoparticles: Synthesis, characterization and cellular uptake. E. Harmzen-Pretorius, J. Visser, C. Smith and B. Klumperman.

Stabilization of poly(styrene-co-divinylbenzene-co-maleic anhydride) nanoparticles at interface of Pickering emulsion droplet as template for permeable microcapsule formation. E. Harmzen and B. Klumperman.

Triggered degradation of hybrid starch-poly(styrene-co-divinylbenzene)-co-maleic anhydride) nanoparticle-based colloidosomes/capsules using encapsulated micro-organisms. E. Harmzen-Pretorius, R. Cripwell, E. van Zyl and B. Klumperman.

Synthesis of Janus nanoparticles synthesized by templating inverse Pickering emulsion droplets in a one-pot fashion through utilizing the rotation of the particles at the interface. E. Harmzen, R. Dreyer and B. Klumperman.

Preparation of tetraphenylborate-functionalized and boronic acid-functionalized polymeric nanoparticles for the extraction of biomolecules. E. Harmzen-Pretorius, S. Howard, R. Pfukwa, B. Klumperman and P. Swart.

Conference attendance

13th Annual IUPAC/Unesco conference on macromolecules and materials. Synthesis of poly(styrene-co-maleic anhydride-co-divinylbenzene) nanoparticles, *Oral presentation, September **2015**, PE, South Africa.*

Warwick 2016 “The polymer Conference”. Self-assembly of poly(styrene-co-maleic anhydride-co-divinylbenzene) nanoparticles for capsule formation, *Oral presentation, June **2016**, Coventry, UK.*

Warwick 2016 “The polymer Conference”. Self-assembly of poly(styrene-co-maleic anhydride-co-divinylbenzene) nanoparticles for capsule formation, *Poster presentation, June **2016**, Coventry, UK.*

Supplementary Information

Lambda scans using lasers 405 nm, 458 nm, 514 nm, 561 nm and 633 nm.

Excited with 405 nm

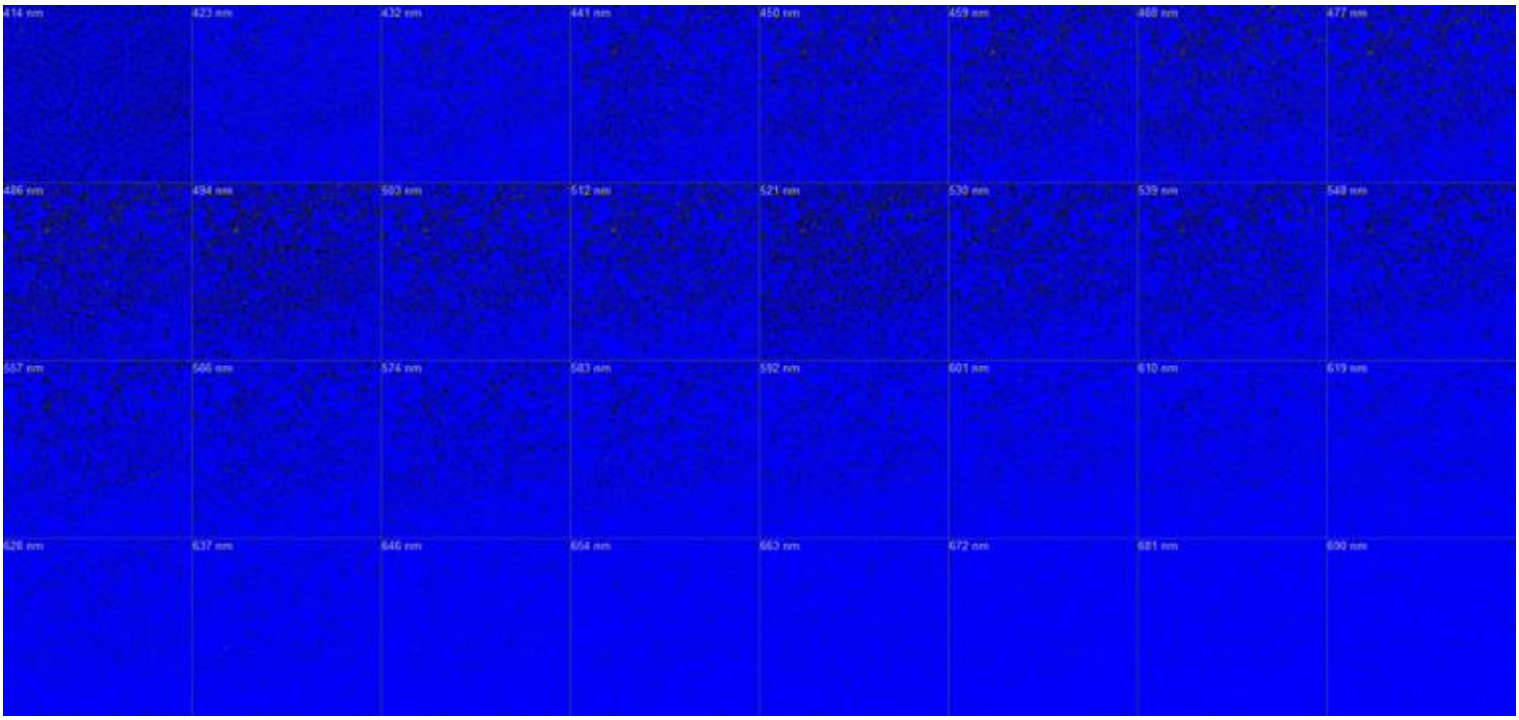

Figure 1: *AF detected using 405 nm laser in increments of 9 nm wavelengths.*

Excited with 458 nm

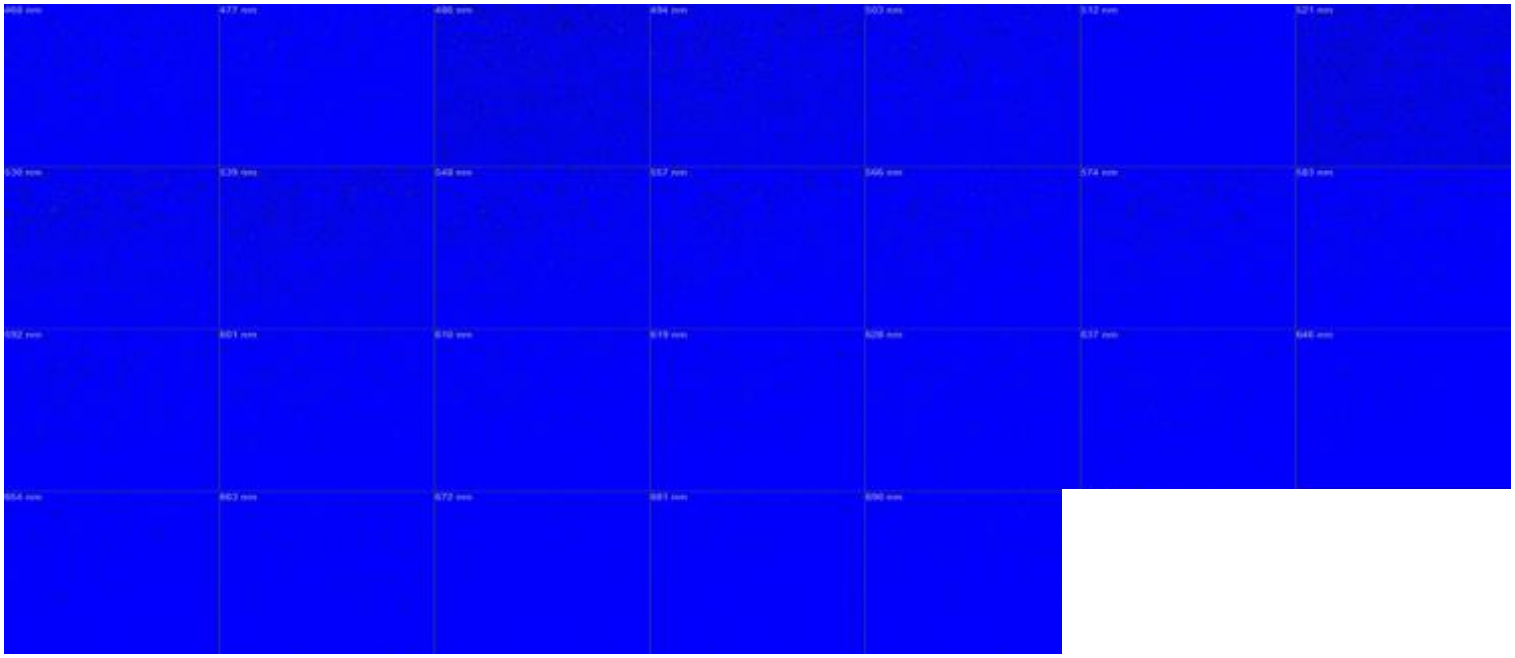

Figure 2: *AF detected using 458 nm laser in increments of 9 nm wavelengths.*

Excited with 488 nm

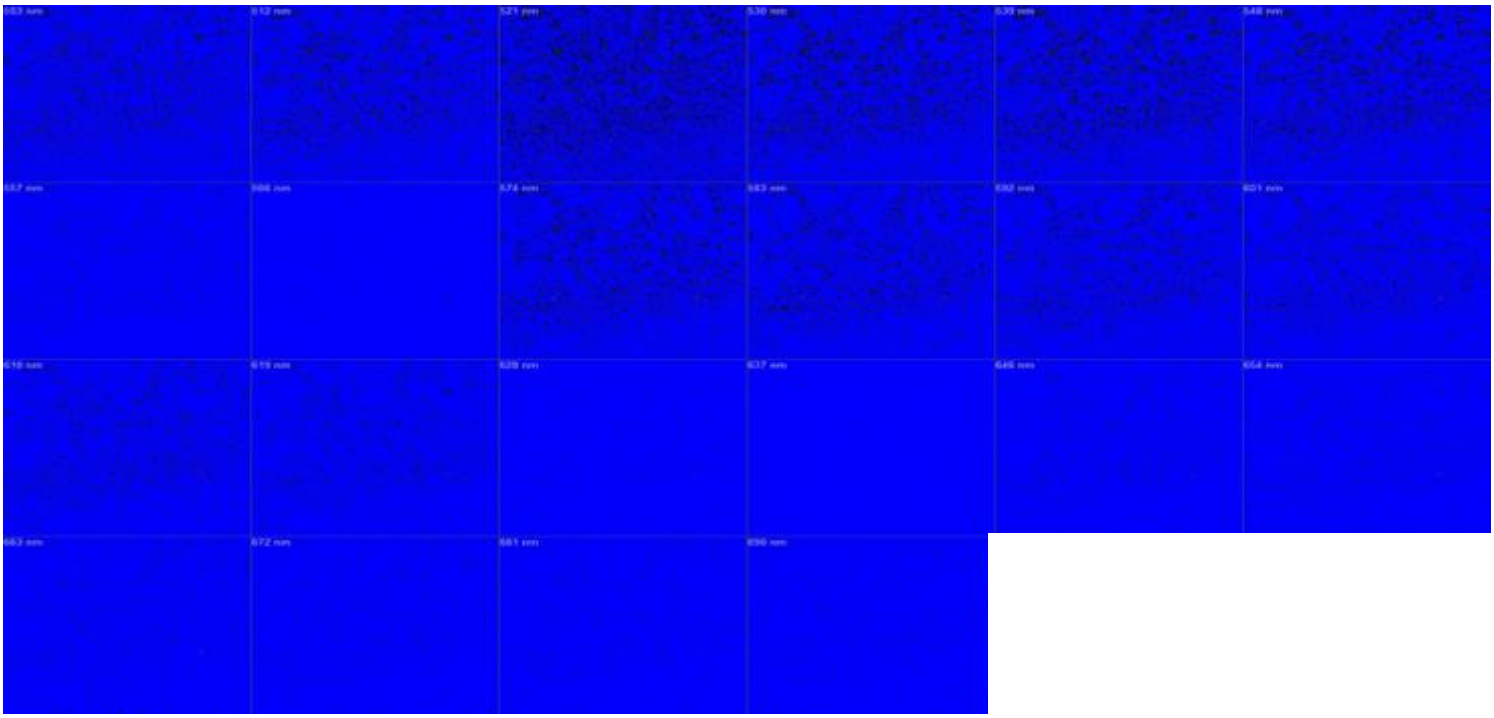

Figure 3: *AF detected using 488 nm laser in increments of 9 nm wavelengths.*

Excited with 514 nm

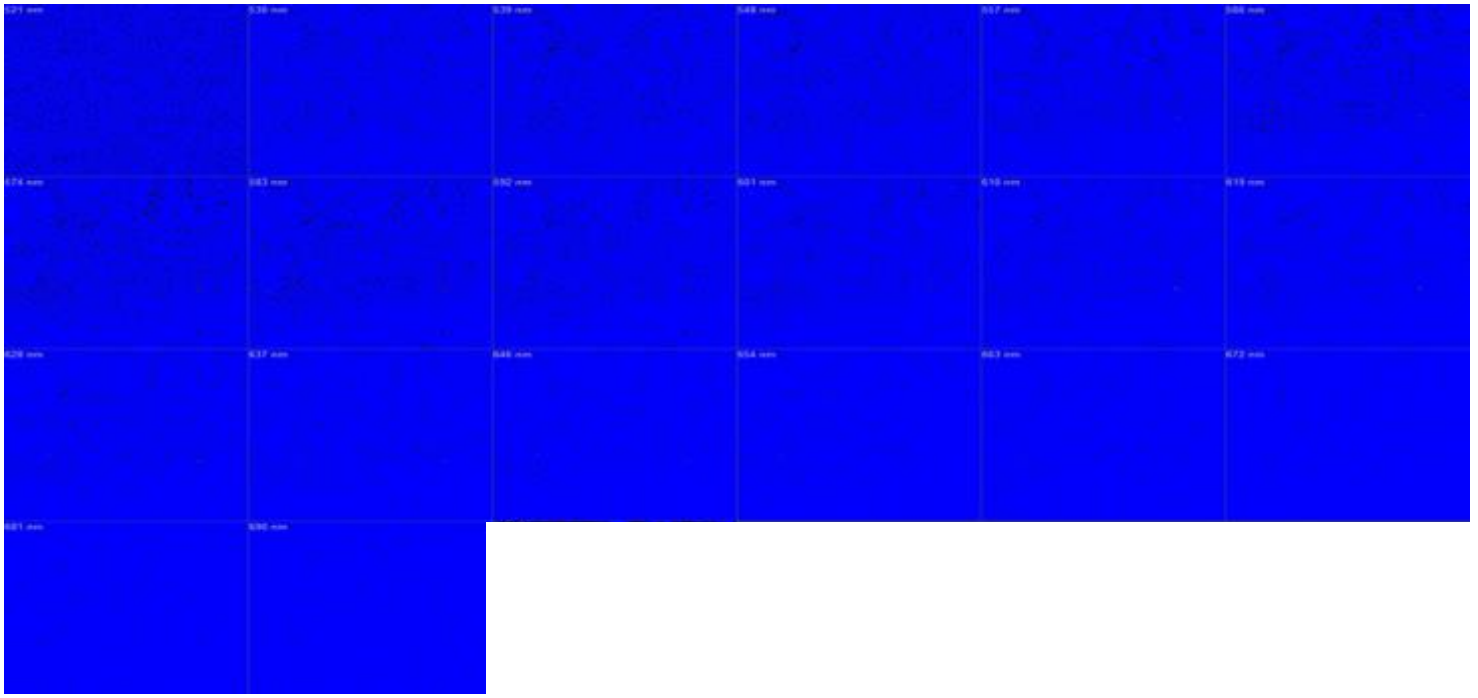

Figure 4: *AF detected using 514 nm laser in increments of 9 nm wavelengths.*

Excited with 561 nm

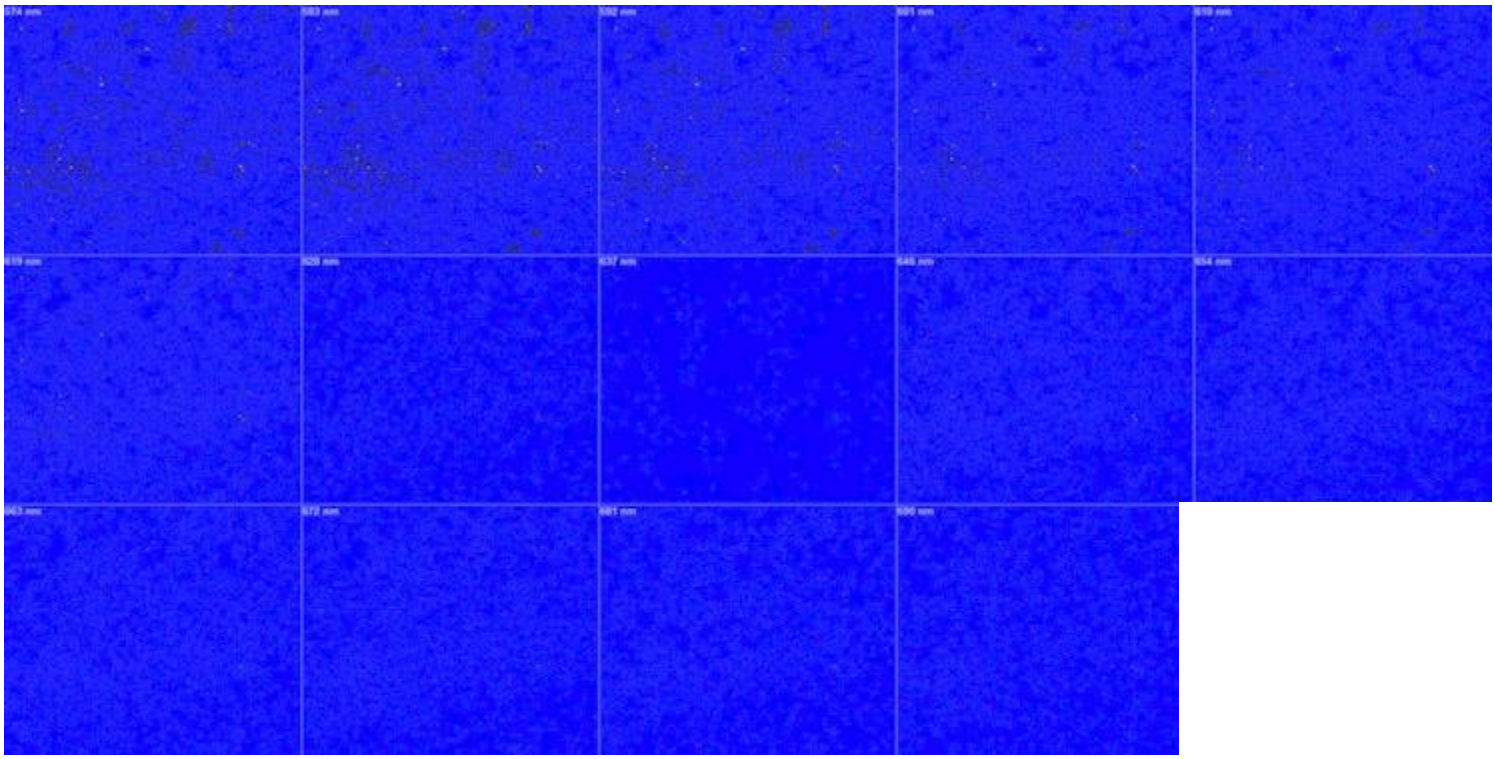

Figure 5: *AF detected using 561 nm laser in increments of 9 nm wavelengths.*

Excited with 633 nm

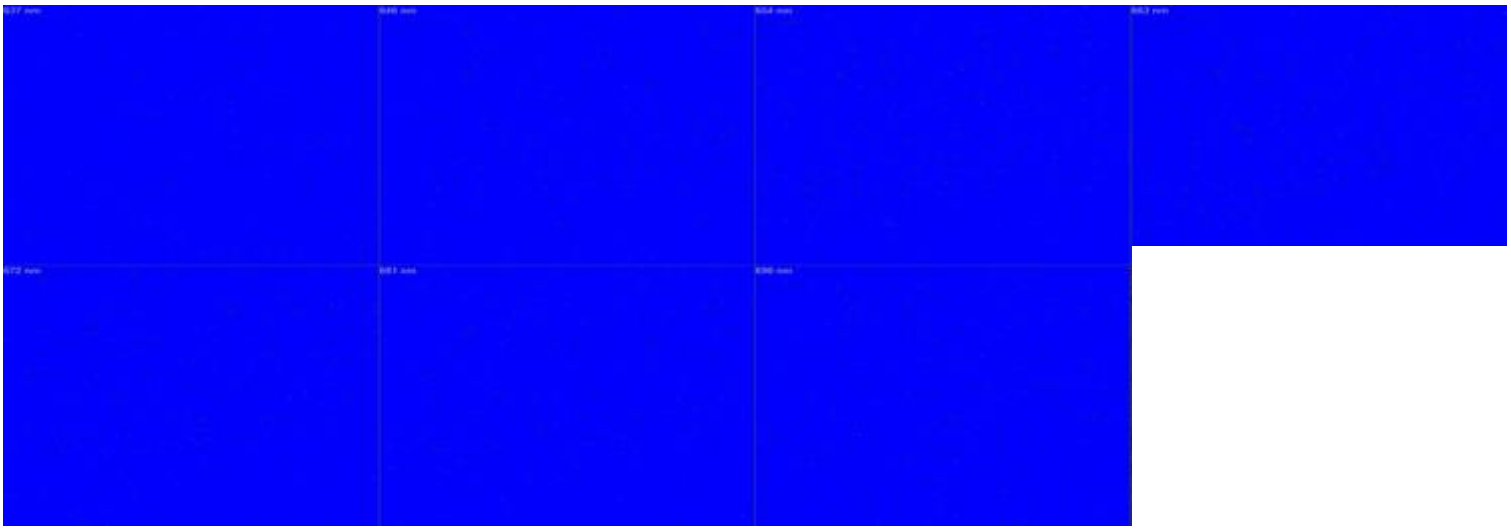

Figure 6: *AF detected using 514 nm laser in increments of 9 nm wavelengths.*

Synthesis scheme of 1-bromo-4-((2-(2-(vinyloxy) ethoxy) ethoxy) methyl) benzene (BM100):

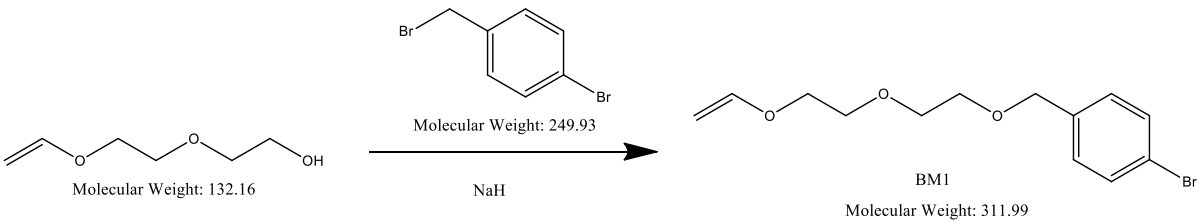

Scheme 1: *Synthesis of 1-bromo-4-((2-(2-(vinyloxy) ethoxy) ethoxy) methyl) benzene (BM100)*

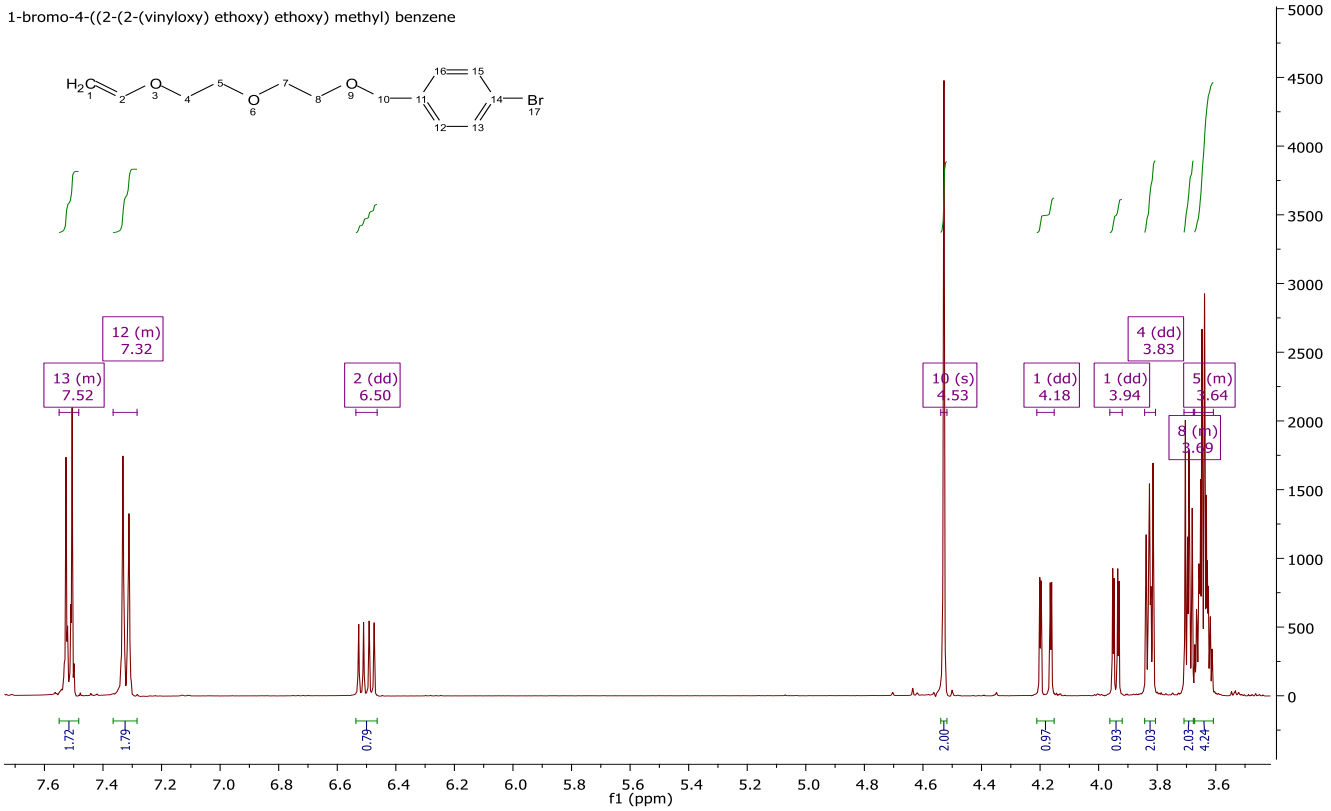

Figure 7: *^{1}H-NMR spectrum of BM100.*

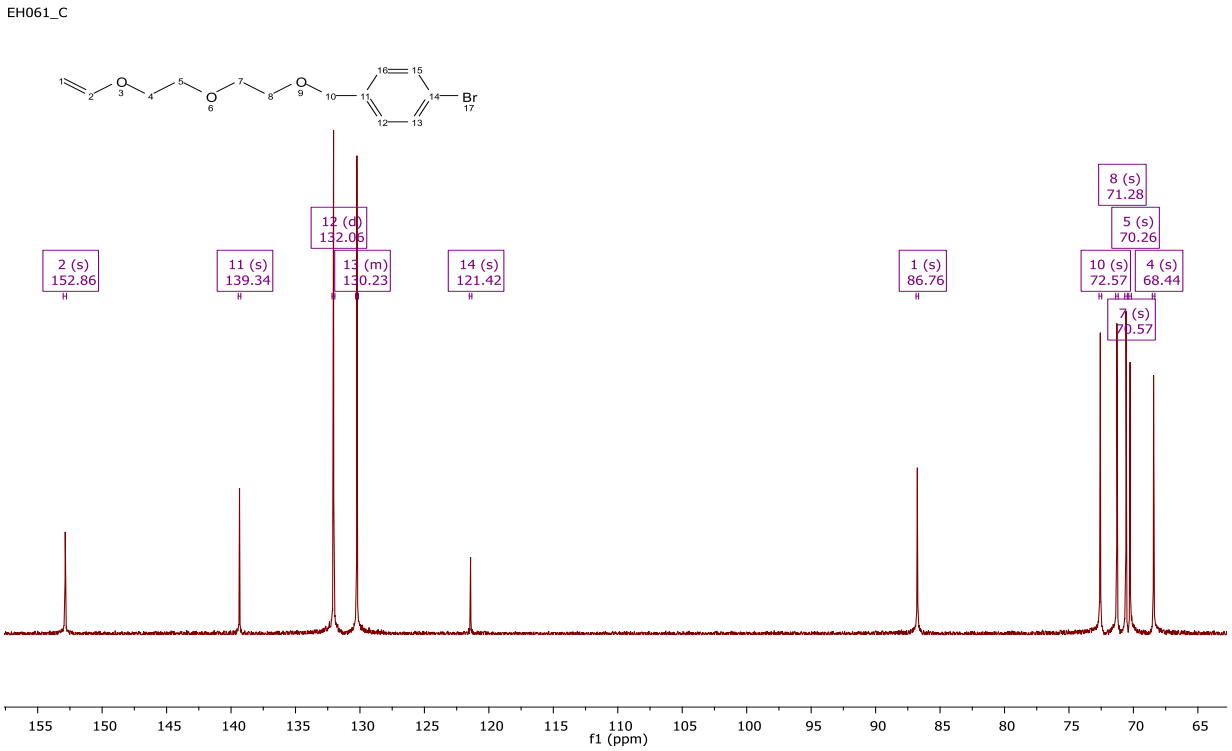

Figure 8: *^{13}C-NMR spectrum of BM100.*

Synthesis scheme of Lithium Triphenyl(4-((2-(2-vinyloxy)ethoxy)ethoxy)methyl)-phenyl)borate (TBVE):

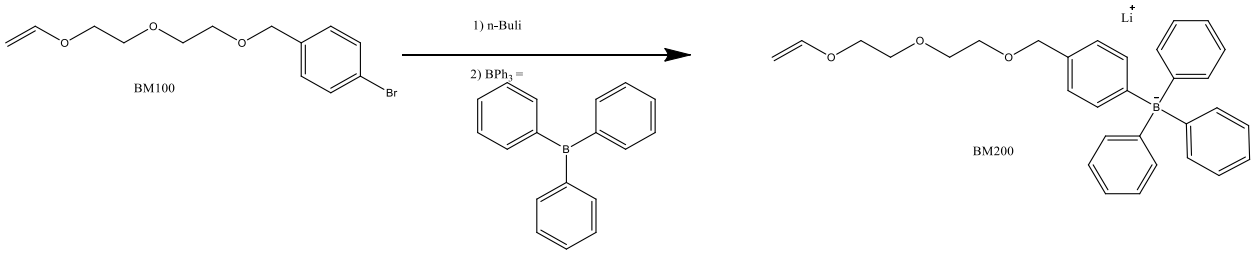

Scheme 2: *Synthesis of lithium triphenyl (4-((2-(2-vinyloxy) ethoxy) ethoxy) methyl)-phenyl) borate (TBVE) compound.*

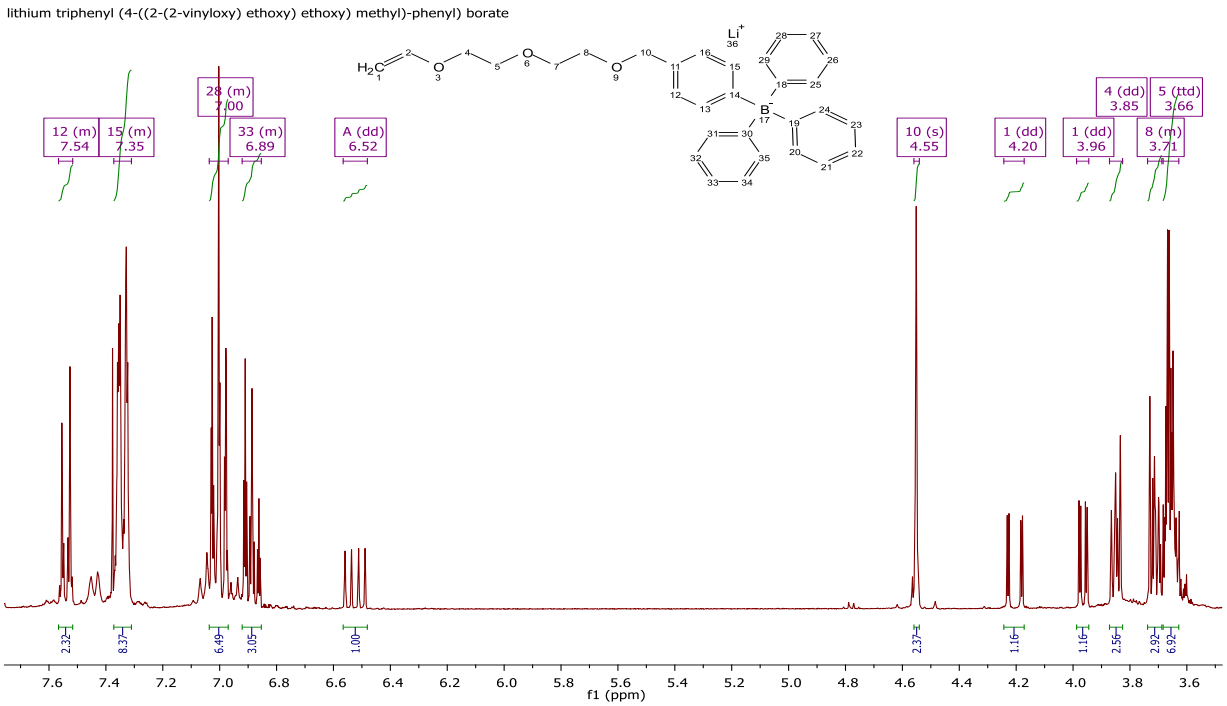

Figure 9: *^{1}H-NMR spectrum of TBVE.*

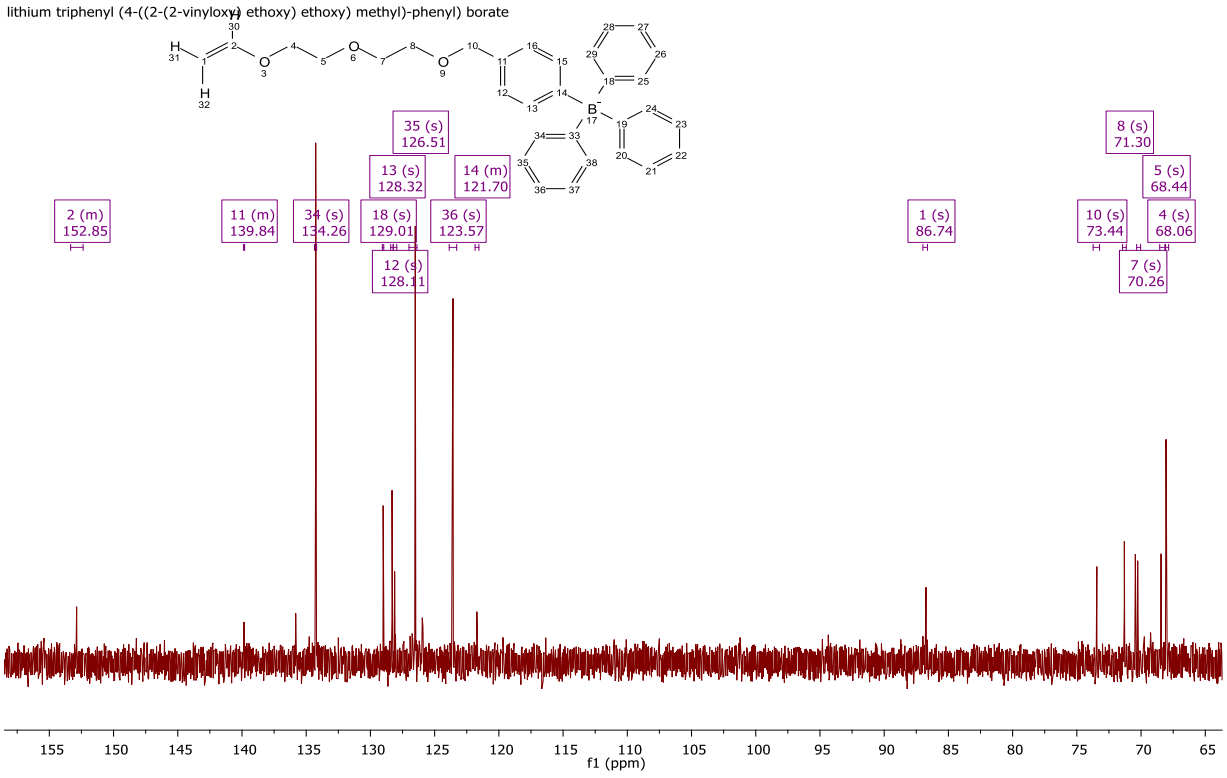

Figure 10: *^{1}H-NMR spectrum of TBVE.*

Elrika Harmzen-Pretorius